THE ASTROPHYSICAL JOURNAL

AN INTERNATIONAL REVIEW OF SPECTROSCOPY AND ASTRONOMICAL PHYSICS

VOLUME 105 MARCH 1947 NUMBER 2

A PHOTOELECTRIC STUDY OF THE ECLIPSING VARIABLE TX URSAE MAJORIS

C. M. HUFFER AND OLIN J. EGGEN

Washburn Observatory, University of Wisconsin

Received January 8, 1947

ABSTRACT

The eclipsing variable star, TX Ursae Majoris, was observed on 40 nights from 1935 to 1942 with the photoelectric photometer on the 15-inch refractor of the Washburn Observatory. A measure of precision of the observations is indicated by the probable error of a single normal of ± 0.0046 mag. The light-elements of Rügemer were used in the computation of the phases, with the amplitude of the sine term for the variation of the period reduced to 0.015 day. After rectification for small reflection and ellipticity effects, the Algol-type light-curve revealed minima of depths 2.00 and 0.032 mag. Anticipating the darkening coefficients as 0.4 and 0.6 for the B8 and gF2 components, a solution for the elements has been made. Because of the uncertainty of the presently available value for the mass ratio, no attempt has been made to proceed beyond "intermediate" elements.

The eclipsing binary, TX Ursae Majoris, was discovered independently in 1931 by H. Rügemer[1] and H. Schneller.[2] J. A. Pearce had found it in 1925 to be a spectroscopic binary with an amplitude in excess of 100 km/sec. Rügemer[3] later published the details of his photometric study, in which, with the use of the times of thirty-one minima, he found the light-elements to be

$$\text{Primary minimum} = \text{JD}2416426.784 + 3^{d}.0633175\,E + 0^{d}.021 \sin (0^{\circ}.0947\,E + 64^{\circ}.42) .$$

In 1940, Pearce[4] published an abstract containing the results of spectroscopic observations secured at Victoria over four different observational epochs of short duration during the preceding 15 years. Orbital elements derived for the separate seasons indicated that the line of apsides was advancing and that the remaining elements, e, V_0, and K were constant. The final results were:

$$e = 0.162 \pm 0.0043$$

$$\omega = 295^{\circ}.8 + 10^{\circ}.1\,(T - 1900) \pm 4^{\circ}.48 \pm 0^{\circ}.12$$

[1] *A.N.*, **242**, 178, 1931.

[2] *A.N.*, **242**, 179, 1931.

[3] *A.N.*, **257**, 349, 1935.

[4] *Pub. A.S.P.*, **52**, 287, 1940.

In 1938 J. A. O'Keefe[5] published the results of his photographic study, during which he had observed a secondary minimum of 0.05 mag. From the position of this secondary minimum he concluded that

$$e \cos \omega = 0.022 ,$$

which agreed well with Pearce's spectrographic result.

In 1942 Mrs. Gaposchkin[6] published a discussion of the period of TX Ursae Majoris which was based on the times of primary minima from Harvard photographs, and she was able to verify Rügemer's and Pearce's period for the motion of the line of apsides. In combining the Harvard observations of minima with an unpublished photoelectric light-curve determined by F. B. Wood, Mrs. Gaposchkin found the eccentricity to have the value of 0.015, greatly discordant with that given by Pearce. This small value is, however, confirmed by the present observations, being about the maximum allowable by the position of the secondary minimum.

In 1944, W. A. Hiltner[7] obtained 109 spectrograms of this system, including 11 at different phases within primary minimum. He assigned the spectral class B8 to the primary star and, with W. W. Morgan, classified the secondary, which Pearce has called "A3," as gF2. Table 1 contains Hiltner's and Pearce's final elements, with the ω of Pearce's

TABLE 1

SPECTROSCOPIC ELEMENTS OF TX URSAE MAJORIS

	Hiltner	Pearce
e	0.029± 0.018	0.162±0.0043
V_0	− 16.5 ± 0.91	−10.9 ±0.16 km/sec
K	51.8 ± 0.82	54.3 ±0.20 km/sec
ω	365°4 ±16°7	24°2 ±4°5

orbit as predicted from his expression for the apsidal advance. The discrepancy between the two values for the velocity of the center of mass is almost as serious as the difference in eccentricity. An attempt to force a circular solution through both sets of observations, for which purpose only 14 of the Victoria results were available,[8] produced the identical values for $V_0 = -15.6$ km/sec.

TX Ursae Majoris was observed over four seasons from 1935 to 1942 by the senior author, who used the photoelectric photometer of the Washburn Observatory. One comparison star was used throughout the observations, namely, HD 92787, visual magnitude 5.28, spectrum F0.

When the observations were grouped into normals, a typical Algol-type light-curve was evident. A harmonic analysis of the observations between minima yielded for the variation of light of the uneclipsed stars:

$$\begin{array}{llll} l = 1.0000 & - 0.0163 \cos \theta & - 0.0196 \cos^2 \theta . & \\ \pm 0.0007 & \pm 0.0025 & \pm 0.0046 & \text{(p.e.)} \end{array}$$

The constant of ellipticity is apparently quite small, and, as it is determined with relative uncertainty, it will be neglected for the present. The precision of the observations between minima is indicated by the probable error of a normal of unit weight, ±0.0044 mag., a satisfactory value in view of the relatively large scatter of the individual observa-

[5] *Harvard Bull.*, No. 908, 1938.

[6] *Harvard Bull.*, No. 916, 1942.

[7] *Ap. J.*, **101**, 108, 1945.

[8] *J.R.A.S. Canada*, **26**, 382, 1932.

tions. Tables 2 and 3 list the normal magnitudes. The reflected normals during primary minima are given in Table 3, where the first column gives the phase in decimals of a period, reckoned from mid-primary eclipse computed from the elements of Rügemer with 0.015 day as the amplitude of the sine term. The photoelectrically observed epochs of primary minima are given in Table 4. The second columns of Tables 2 and 3 list the observed differences in magnitude reduced to the magnitude at maximum light, while the third column of Table 3 contains the number of sets, of four observations each, which make up the normals.

TABLE 2

NORMAL MAGNITUDES BETWEEN MINIMA AND NEAR SECONDARY MINIMA

Between Minima			Secondary Minima		
Phase	Observed Δ Mag.	O−C	Phase	Observed Δ Mag.	O−C
0P169	0m011	−0m002	0P460	0m024	−0m008
.205	.007	+ .001	.481	.034	.000
.235	.004	+ .003	.488	.029	− .006
.274	− .013	− .010	.495	.032	− .003
.355	− .002	+ .001	.500	.044	+ .009
.415	− .009	− .009	.513	.039	+ .005
.582	.012	+ .008	0.526	0.032	−0.002
.613	.001	+ .003			
.704	− .006	− .002			
.804	.021	+ .013			
.862	.020	.000			
0.921	0.028	−0.004			

TABLE 3

REFLECTED NORMALS AT PRIMARY MINIMUM

Phase	Observed Δ Mag.	Rectified Δ Mag.	n	O−C	Phase	Observed Δ Mag.	Rectified Δ Mag.	n	O−C
0P0644	0m047	0m013	8	−0m003	0P0218	1m243	1m206	8	− m010
.0610	0.074	0.040	7	.000	.0196	1.362	1.324	8	.000
.0564	0.135	0.101	8	+ .009	.0177	1.456	1.418	7	+ .001
.0538	0.174	0.139	8	+ .005	.0162	1.528	1.490	8	− .005
.0509	0.221	0.186	8	− .002	.0146	1.620	1.582	7	+ .006
.0481	0.282	0.247	8	+ .001	.0131	1.694	1.658	7	− .010
.0455	0.340	0.304	7	− .004	.0118	1.756	1.718	8	+ .013
.0423	0.433	0.397	8	+ .003	.0105	1.808	1.770	7	+ .009
.0388	0.553	0.517	8	+ .018	.0090	1.825	1.817	8	− .004
.0353	0.656	0.619	8	− .002	.0076	1.907	1.868	8	+ .002
.0325	0.772	0.735	8	+ .008	.0060	1.953	1.915	9	+ .001
.0296	0.876	0.839	7	− .009	.0043	1.989	1.951	8	− .004
.0276	0.979	0.942	8	+ .007	.0027	2.017	1.979	8	+ .007
0.0243	1.114	1.086	8	− .002	0.0008	2.031	1.993	7	+0.001

The rectified depths of primary and secondary minima are 2.00 and 0.032 mag., respectively. The elements were derived with the aid of the method proposed by Z. Kopal[9] and with the use of the tables computed by V. Zessewich.[10] The spectrum of the primary

[9] *An Introduction to the Study of Eclipsing Variables* (Harvard University Press, 1946).

[10] *Bull. Astr. Inst. U.S.S.R. Acad. Sci.* No. 45, 1939; and No. 50, 1940.

component has been taken as B8, that of the secondary as gF2. At the effective wave length of 4500 A, the degree of darkening of the bright B8 star, which is eclipsed at primary minimum, should be in the vicinity of $u_1 = 0.40$, while the darkening coefficient of the F star has been assumed as $u_2 = 0.60$. With these values, together with an assumed ratio of radii k of 0.55, we find:

$$k = 0.55 \text{ (assumed)}, \qquad \alpha_0 = 0.932, \qquad p_0 = -0.785,$$

TABLE 4

PHOTOELECTRICALLY OBSERVED PRIMARY MINIMA

JD 242	E	O−C
7892.796	3743	+0^{d}002
7932.618	3756	.000
8278.772	3869	−0.001

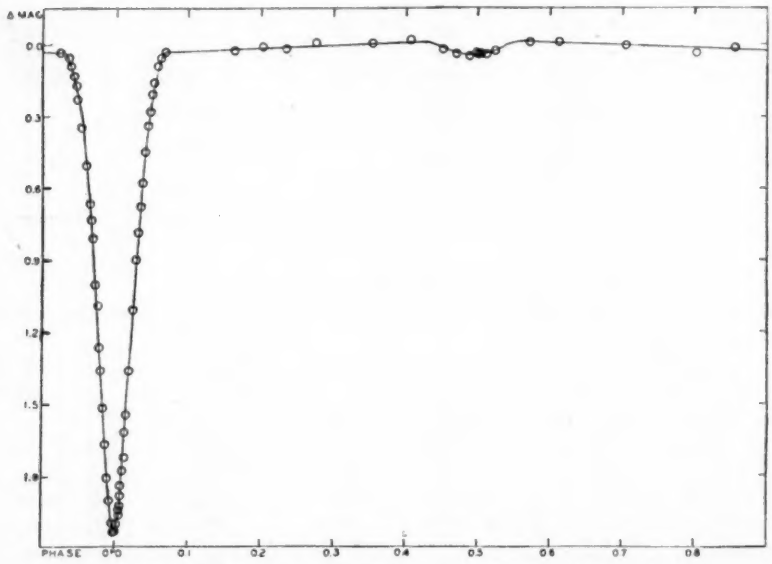

FIG. 1.—Photoelectric light-curve of TX Ursae Majoris

where α_0 and p_0 are, respectively, the fractional loss of light of the B8 star and the geometrical depth at the moment of maximum obscuration. Forming the "equations of condition" from the observed normals, as suggested by Kopal, and applying proper weights, the least-squares solution yielded $k = 0.558 \pm 0.018$. If we adopt this value, the geometrical elements are:

$$r_1 = 0.154 \pm 0.003 \qquad \frac{J_1}{J_2} = 30.9 \pm 2.3 \qquad L_2^* = 0.060 \pm 0.003$$

$$r_2 = 0.276 \pm 0.006 \qquad L_1 = 0.906 \pm 0.003$$

$$i = 80\overset{\circ}{.}9 \pm 0\overset{\circ}{.}4 \qquad L_2 = 0.094 \pm 0.003 \qquad \frac{J_1}{J_2^*} = 46.9 \pm 3.2$$

where the asterisk (*) denotes values freed of the reflection effect. The probable errors are from the least-squares solution and do not take account of the uncertainties of the loss of light at the two minima, values of which were taken directly from the rectified curve as $1 - \lambda_1 = 0.842$ and $1 - \lambda_2 = 0.028$.

The theoretical light-curve derived from these elements gives the residuals from the observed normals as shown in Tables 2 and 3. The probable error of a normal of unit weight during primary minimum is 0.0047 mag., which value compares favorably with that value for the normals between minima, 0.0044 mag., in view of the handicap imposed upon the photoelectric measures by the large decrease in magnitude.

From the spectrograms taken near primary eclipse, Pearce[11] has determined the slope of the velocity-curve of the secondary star and thus derived the mass ratio, $m_2/m_1 = 0.30$. Hiltner observed an abnormal behavior of the *Ca* II K line, which "cannot belong to either the principal spectrum of the secondary star or the spectrum of the primary star" and states: "Perhaps Pearce used this line when he classified the secondary star as A3." Hiltner concludes that the *Ca* II K line originates in the atmosphere of the F star; and, since the velocities measured from this line are of the same order of magnitude as the rotational velocity of the B8 star, lack of synchronism in the periods of rotation and revolution of the stars is indicated. The fact that these uncertainties would undoubtedly affect the adopted value for the mass ratio, together with consideration of the relatively large scatter of the photometric observations, makes it appear inadvisable to proceed beyond the "intermediate" elements derived above. The values given for the diametral and polar semi-axes in the summary of Table 5 were computed from the Roche

TABLE 5

PHOTOMETRIC ELEMENTS OF TX URSAE MAJORIS

Period	$P = 3^d0633715$
Ratio of radii of components	$k = 0.558 \pm 0.018$
Fractional loss of light of B8 star at mid-primary minimum	$a_0 = 0.929 \pm 0.003$
Inclination of the orbital plane	$i = 80°.9 \pm 0°.4$
Ratio of surface brightnesses of illuminated hemispheres	$J_1/J_2 = 30.9 \pm 3.2$
Ratio of surface brightnesses of dark hemispheres	$J_1/J_2 = 46.9 \pm 3.2$
Mass ratio	$m_1/m_2 = 3.3$
Semi-major axis of the relative orbit	$a_1+a_2 = 9.58\times10^6$ km

	Symbol	Bright Star	Faint Star
Spectrum		B8	gF2
Degree of limb darkening (assumed)	u	0.40	0.60
Longest semi-axis	a	0.154 ± 0.003	0.276 ± 0.008
Diametral semi-axis	b	0.154	0.250
Polar semi-axis	c	0.154	0.239
Fractional luminosity (freed from reflection)	L	0.906 ± 0.003	0.060 ± 0.003
Mass	m	$2.84\ \odot$	$0.86\odot$

model, utilizing Pearce's value for the mass ratio. This same mass ratio yields photometric ellipticities of 0.004 and 0.317 for the brighter and the fainter stars, respectively, leading to a theoretical value of 0.020 for the coefficient of the $\cos^2\theta$ term in the analysis of the light between minima. The observed reflection effect[12] indicates that the ratio of the temperature of the brighter to the fainter star is approximately 2 to 1, which is consistent with the observed spectral types within the uncertainties involved.

The more important constants of the system of TX Ursae Majoris, which have been derived or assumed in the present discussion, are collected in Table 5. It should be again mentioned that all constants depending upon the adopted mass ratio are affected by the uncertainties of the adopted value.

We are indebted to Dr. Joel Stebbins, who has critically examined the results, and to Dr. A. E. Whitford, who developed the photoelectric photometer.

[11] *Pub. A.A.S.*, **8**, 251, 1936.

[12] Z. Kopal, *Ann. New York Acad. Sci.*, **41**, 131, 1941.

SPECTROSCOPIC OBSERVATIONS OF RIGEL WITH HIGH DISPERSION*

ROSCOE F. SANFORD
Mount Wilson Observatory
Received December 16, 1946

ABSTRACT

Since 1937, fifty-nine high-dispersion spectrograms of Rigel have been obtained at Mount Wilson on fine-grain emulsion.

Velocities from the helium lines.—Velocities from the various helium lines differ systematically from one another. A mean helium velocity for each plate has been obtained by correcting the velocities from the individual lines by their mean residuals.

Systematic velocity differences.—The velocities from the lines of *Si* II, *Fe* II, *Mg* II, *N* II, *C* II (blue), and *Ne* I are consistent with one another; a mean from them is called an "I-velocity." Mean velocities from various other classes of lines differ from I-velocities by the following amounts: hydrogen, +5.8 ± 0.6 km/sec; *He* I, +3.8 ± 0.2 km/sec; *C* II (red), +4.9 ± 0.4; *Na* I (D1 and D2), +1.6 ± 0.4; *Ca* II (H and K), −1.2 ± 0.1. Which group yields the true systemic velocity is not known.

Velocity variations of Rigel.—The velocity variations yielded by any of these groups of lines are greater than the errors of measurement and are undoubtedly real, but they have not been fitted either to Plaskett's or to any other period. The I-velocities are strongly correlated with the helium velocities but not with the hydrogen velocities.

The H*α line.*—*Hα* in absorption is accompanied by shortward and longward emission components of varying intensities, which produce a variety of line profiles, thus preventing the use of the *Hα* absorption line for velocity determination.

Forty-five spectrograms of Rigel with fine-grain plates, with a dispersion of 2.9 A/mm in the blue and 5.8 A/mm in the red, have been obtained since 1937 at Mount Wilson by W. S. Adams and the writer. Fourteen others have a dispersion of 10 A/mm and 20 A/mm, respectively. All have been measured by the writer; a number which were also measured by Adams reveal no significant systematic difference. Velocities depend essentially upon the wave lengths of lines given in the "Multiplet Table of Astrophysical Interest," by C. E. Moore.[1] The largest number of lines measured upon a single plate was fifty-three; the smallest, six. Table 1 contains the velocities derived separately from various lines.

Accordant velocities were given by the lines of *Si* II, *Fe* II, *Mg* II, *N* II, *Ne* I, and *C* II (blue). Velocities derived from this group of lines are called "I-velocities." On the other hand, the lines of *H* I, *He* I, *Na* I, and *C* II (red) give velocities which differ systematically. The absorption lines, H and K, of *Ca* II also need special mention.

I-velocities.—The individual I-velocities have probable errors which average ±0.7 km/sec when derived from four to ten lines and ±0.5 when derived from more than ten lines. The mean for all the I-velocities is +17.7 km/sec, and the range is 13.4 km/sec for those velocities which depend upon six or more lines.

The hydrogen lines.—The probable errors of the velocities from the hydrogen lines from a single plate average ±1.1 km/sec for four to seven lines and ±0.7 km/sec for eight or more. There seem to be no systematic differences in the velocities from different hydrogen lines. The mean for all hydrogen-line velocities is +21.6 km/sec, and the range for velocities depending on six or more lines is 12.3 km/sec.

On twenty of the higher-dispersion spectrograms the velocities from no less than six hydrogen lines differ from the corresponding I-velocities by the mean value +5.8 ± 0.6 km/sec.

* *Contributions from the Mount Wilson Observatory, Carnegie Institution of Washington*, No. 729.

[1] *Contr. Princeton U. Obs.*, No. 20, Part II, 1945.

TABLE 1

VELOCITIES FROM VARIOUS ELEMENTS

Plate No. (Ce)	Julian Day	Kilometers per Second							Em. $H\alpha$ s/l
		I	Hydrogen	Helium	*Na*	C II (Red)	$H\alpha$	Sharp H and K	
1526....	2428838.021	+18.3 (7)*	+25.1 (5)	+20.3 (4)	.....	.....	.....	.....	.....
1823....	9211.988	17.2 (8)	17.1 (2)	24.3 (3)	.....	.....	.....	.....	.....
1898....	93.806	17.3 (8)	18.3 (2)	16.6 (3)	.....	.....	.....	.....	.....
1899....	93.846	16.5 (5)	11.3 (2)	20.7 (4)	.....	.....	.....	.....	.....
1988....	9362.638	17.2 (8)	18.7 (2)	21.1 (2)	.....	.....	.....	.....	.....
2134....	9537.030	15.3 (7)	27.7 (15)	15.9 (2)	.....	.....	.....	−16.8	.....
2172....	97.015	13.4 (8)	21.1 (4)	18.4 (3)	.....	.....	.....	.....	.....
2176....	99.931	22.4 (7)	27.9 (6)	24.3 (4)	.....	.....	.....	.....	.....
2212†...	9626.771	20.8 (8)	17.2 (12)	25.1 (7)	.....	.....	.....	.....	.....
2217†...	27.861	16.7 (7)	17.0 (8)	22.2 (3)	.....	.....	.....	.....	.....
2222....	28.810	15.4 (9)	18.2 (6)	20.1 (6)	.....	.....	.....	17.1	.....
2225....	29.786	16.2 (7)	22.7 (8)	21.6 (2)	.....	.....	.....	.....	.....
2226....	47.637	18.4 (8)	21.7 (11)	23.1 (7)	.....	.....	.....	14.9	.....
2231†...	48.591	21.7 (8)	25.8 (5)	22.1 (5)	.....	.....	.....	.....	.....
2238†...	48.881	23.0 (5)	20.9 (2)	26.8 (3)	.....	.....	.....	.....	.....
2250†...	57.726	25.7 (7)	27.3 (11)	31.0 (1)	.....	.....	.....	.....	.....
2257....	78.697	17.2 (10)	18.9 (7)	22.4 (6)	.....	.....	.....	15.0	.....
2262....	79.628	12.6 (5)	17.8 (4)	18.6 (3)	.....	.....	.....	16.6	
2270....	87.645	18.6 (10)	28.6 (8)	23.2 (7)	.....	.....	.....	.....	.....
2278....	9709.626	14.4 (7)	17.5 (13)	23.3 (2)	.....	.....	.....	16.2	.....
2298†...	13.684	13.2 (8)	17.4 (7)	22.5 (8)	.....	.....	.....	.....	.....
2435....	9916.960	23.6 (5)	25.5 (3)	28.5 (3)	.....	.....	.....	14.9	.....
2443....	19.034	15.6 (12)	25.1 (3)	19.7 (7)	.....	.....	.....	.....	.....
2445....	19.917	19.2 (7)	24.1 (5)	24.8 (2)	.....	.....	.....	13.9	.....
2618†...	2430275.052	20.0 (8)	23.5 (19)	23.4 (8)	.....	.....	.....	.....	.....
2639....	0301.819	13.3 (10)	26.2 (9)	17.1 (6)	.....	.....	.....	.....	.....
2664....	05.014	19.4 (3)	.....	23.6 (2)	+19.3	+24.6	.....	.....	<1
2668....	05.910	18.7 (10)	23.4 (13)	21.1 (7)	.....	.....	.....	.....	.....
2675....	09.044	12.3 (12)	21.1 (5)	15.0 (10)	.....	.....	.....	.....	.....
2681....	29.928	15.1 (3)	.....	21.0 (2)	19.1	19.4	+ 3.4	.....	>1
2684....	30.772	15.5 (2)	.....	21.7 (2)	19.4	27.6	+10.6	.....	1
2686....	31.806	16.8 (12)	16.4 (7)	22.1 (10)	21.4	22.4	+13.6	.....	1
2687†...	32.898	24.2 (2)	.....	29.0 (2)	.....	29.4	+22.5	.....	1
2690....	33.749	19.1 (11)	13.1 (1)	24.1 (4)	19.5	23.6	+ 8.9	.....	<1
2702....	63.757	13.7 (11)	20.2 (10)	18.5 (10)	.....	.....	+24.0	16.0	.....
2710....	66.768	14.8 (3)	.....	22.4 (2)	20.1	19.2	− 0.2	.....	>1
2711....	67.663	15.2 (12)	26.2 (11)	19.6 (10)	17.2	19.4	− 1.8	14.0	>1
2718†...	88.776	19.6 (2)	.....	25.5 (2)	.....	30.4	+13.3	.....	<1
2720†...	89.687	19.5 (3)	.....	16.0 (2)	.....	23.3	+ 8.2	.....	<1
2752†...	0448.619	15.4 (3)	.....	14.6 (2)	18.1	22.1	+14.6	.....	<1
2756....	49.642	13.5 (3)	.....	20.5 (2)	20.5	17.9	+15.4	.....	<1
2858....	0625.997	16.6 (14)	19.6 (3)	19.0 (6)	.....	24.9	+ 5.5	−17.4	<1
2864....	27.002	19.7 (11)	23.7 (4)	23.8 (4)	20.3	26.0	+ 3.4	.....	<1
2881....	58.026	20.2 (7)	20.4 (8)	24.2 (6)	.....	.....	.....	.....	.....
2887....	59.030	17.9 (3)	.....	25.1 (2)	18.1	24.7	− 1.8	.....	<1
2891....	59.941	16.5 (7)	.....	19.5 (2)	18.9	21.7	+ 2.6	.....	<1
2921....	88.950	21.5 (6)	28.1 (12)	26.2 (3)	.....	.....	.....	.....	>1
2944....	0772.613	16.5 (10)	26.6 (9)	20.4 (8)	20.2	21.6	+26.7	.....	>1
2951....	74.624	15.6 (9)	19.4 (9)	21.8 (5)	19.5	21.6	+ 6.8	.....	>1
2961....	0804.629	17.5 (7)	.....	21.7 (2)	19.7	20.1	+ 1.1	.....	<1
2964....	06.658	15.1 (9)	21.5 (9)	18.5 (8)	18.2	19.4	+13.4	.....	.....
2999†...	32.617	20.9 (6)	.....	27.2 (2)	22.4	24.4	+19.6	.....	.....
3665....	1432.812	23.8 (10)	28.5 (9)	25.5 (8)	.....	.....	.....	.....	.....
4113†...	1834.635	19.2 (18)	18.4 (20)	24.1 (11)	18.3	23.0	+ 5.0	.....	<1
4116†...	34.785	17.3 (11)	17.7 (19)	23.9 (10)	17.2	21.0	+ 6.0	.....	<1
4120....	35.628	17.6 (10)	19.3 (3)	23.0 (7)	19.4	22.6	+ 6.8	.....	<1
4121....	35.670	20.0 (7)	25.1 (9)	24.7 (2)	.....	22.5	+17.3	.....	<1
4123....	35.758	18.7 (6)	17.1 (2)	19.4 (6)	18.5	23.5	+ 8.9	.....	<1
4125....	35.851	+15.5 (6)	+26.0 (2)	+23.1 (9)	+15.0	+18.4	+ 9.0	.....	<1

* Figures in parentheses give the number of lines.

† Dispersion 10 and 20 A/mm in blue and red, respectively.

The *Hα* line is a broad absorption line which is usually distorted by shortward and longward emission components, either of which may be the stronger. Sometimes both may be so weak that the absorption line is little affected, or they may partially fill in the absorption line, although not reaching the intensity of the adjacent continuous spectrum. More often their intensities exceed that of the adjacent continuous spectrum. In

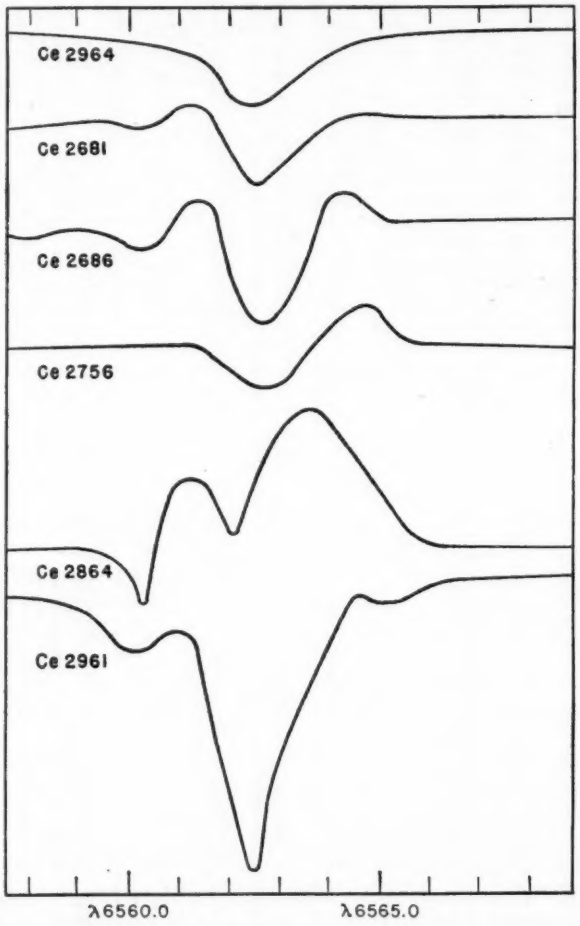

FIG. 1.—Smoothed microphotometer tracings of *Hα*, showing typical profiles

that case the components are separated by a relatively narrow absorption core, the intensity of the bottom of which may or may not exceed the intensity of the adjacent continuous spectrum. Such variable distortion of the *Hα* absorption line unfits it for radial-velocity determination. The last column in Table 1 indicates qualitatively, by the symbols $s/l = > 1, 1$, and < 1, whether the shortward or the longward emission component is the stronger. Figure 1 illustrates the types of profile which *Hα* may have. These profiles are from photometric tracings, with the plate grain smoothed out. They serve only to show the relations of emission components and accompanying absorption on a given plate; the variations from plate to plate are not comparable.

The velocities from the helium lines.—Various helium lines yield different velocities on the same plate. The residuals from the mean are consistent from plate to plate, their mean values being those given in Table 2.

When all lines had been corrected by means of Table 2, mean velocities for helium were derived (Table 1, fifth column). The probable errors for helium velocities on individual plates average ±0.7 km/sec for four to seven lines and ±0.55 km/sec for eight or more. Thirteen of these velocities depend upon six or more helium lines and average 3.8 ± 0.2 km/sec higher than the corresponding I-velocities. The mean of all the helium-line velocities is +22.0 km/sec; the range for the velocities based on six or more lines is 10.5 km/sec.

Unpublished measures by P. W. Merrill indicate that, for many B-type stars, D3 gives a radial velocity systematically higher than that derived from the red *Si* II lines. The mean differences between the velocities from individual helium lines and I-velocities can be derived from Table 1 by adding 3.8 km/sec to the quantities in the third column. The largest value, that for D3, λ 5876, amounts to +9.8 km/sec. The velocity residuals (Table 2) do not appear to be consistent with the Stark effect. In contrast with this result for the c-type star Rigel, Adams and Merrill conclude that the Stark effect is exhibited by the displacements of the helium lines in the spectrum of the subluminous B-type star τ Scorpii.[2] The residuals, however, do show a fair correlation with the laboratory line intensities, as in Figure 2, in which a line represents the points for the four triplet-D lines, λλ 5876, 4471, 4026, and 3820.

TABLE 2

VELOCITY RESIDUALS OF HELIUM LINES FROM THEIR MEAN

Multiplet	λ	Δ (Km/Sec)	Lab. Int.	Multiplet	λ	Δ (Km/Sec)	Lab. Int.
$^3P^\circ-{}^3D$ . .	3820	+0.7±0.5	5	$^1P^\circ-{}^1D$ . .	3926	0.0±1.1	1
	4026	+1.5±0.3	6		4009	−2.0±0.7	1
	4471	+2.5±0.4	7		4143	−2.8±1.0	2
	5876	+6.0±0.7	11		4387	−1.2±0.5	3
					6678	−0.3±0.6	6
$^3P^\circ-{}^3S$ . . .	3867	−0.7±0.7	3				
	4121	−1.6±0.7	4				

C II, λ 6578.03 and λ 6582.85.—The two *C* II lines in the red, λ 6578.03 and λ 6582.85, give velocities consistently higher than the corresponding I-velocities. There are thirteen spectrograms with both I-velocities (six or more lines) and velocities from these *C* II lines. The latter velocities exceed the former by the mean value +4.9 ± 0.4 km/sec. The reality of this difference is established by its small probable error. The velocities from the *C* II lines in the blue agree with the I-velocities. It would seem, therefore, that the laboratory wave lengths of the red and the blue lines of *C* II are not consistent or that the conditions in Rigel modify the wave lengths.

H and K lines of Ca *II.*—The H and K lines of *Ca* II yield velocities whose mean residual from the I-velocities is −1.2 ± 0.1 km/sec. Adams[3] had previously found from four spectrograms of Rigel that H and K yield a velocity of 6.8 km/sec less than that from hydrogen and helium. If, in my measurements, we combine the systematic differences of hydrogen and helium from the I-velocities and the similar differences of H and K, we get (+5.8 +3.8)/2 − (−1.2) km/sec, or +6.0 km/sec, in agreement with Adams.

[2] *Mt. W. Contr.*, No. 672; *Ap. J.*, **97**, 103, 1943.

[3] *Mt. W. Contr.*, No. 505; *Ap. J.*, **81**, 126, 1935.

When the spectrograms are wide and their grain and density excellent, very narrow, sharp components are present on the shortward sides of H and K. Eleven spectrograms yield a mean velocity of -15.7 ± 0.3 km/sec, the range being -13.9 to -17.4 km/sec. When these sharp components are not observed, they are presumably blended with the very strong stellar H and K lines but are too weak and narrow to alter the position of the stellar lines.

These sharp weak components of H and K and the velocity which they yield, -15.7 km/sec, are suggestive of the shortward interstellar components found by Adams[4] in the spectra of λ^1, ι, ϵ, σ, ζ, and κ Orionis, which yield a mean velocity of -15.3 km/sec. The velocities of the other components of H and K found by Adams for the aforementioned Orion stars would cause these components to be masked in the spectrum of Rigel by the strong stellar H and K.

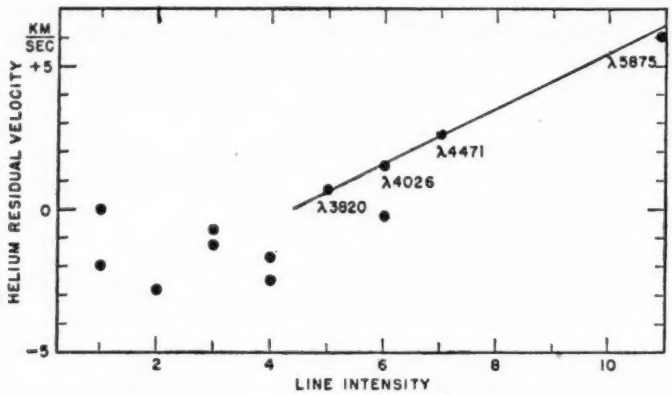

FIG. 2.—Mean velocity residuals of *He* lines, plotted against laboratory intensities. The straight line represents points for the four triplet D lines.

TABLE 3

RESIDUALS FROM THE I-VELOCITIES

Hydrogen	$+5.8 \pm 0.6$ km/sec
Helium	$+3.8 \pm 0.2$
C II (red)	$+4.9 \pm 0.4$
Na I (D1, D2)	$+1.6 \pm 0.4$
Ca II (H, K)	-1.2 ± 0.1

D-lines of Na *I*.—Velocities from the D-lines of *Na* I have a mean difference (*Na* I *minus* I-velocities) of $+1.6 \pm 0.4$ km/sec. It follows that sodium velocities would, in the mean, differ from hydrogen and helium velocities by $(+5.8 + 3.8)/2 - 1.6 = +3.2$ km/sec, whereas Adams obtained $+7.0$ km/sec from three spectrograms. This value, however, is decreased to $+5.9$ km/sec when derived from the wave lengths for D1 and D2, used in this paper.

Mean residuals of velocities of various types of lines from the I-velocities are summarized in Table 3. The ranges for the I-, hydrogen, and helium velocities are 13, 12, and 10, respectively—sufficiently large to indicate variability when individual probable errors are considered. However, while I-velocities correlate with helium velocities, they do not correlate with hydrogen velocities, as is evident from Figure 3. Therefore, there

[4] *Mt. W. Contr.*, No. 673; *Ap. J.*, 97, 105, 1943.

can be no simple period common to all three velocities. As a matter of fact, no period has been found which satisfies any one of the three.

From a large number of spectrograms made at Ottawa in 1908, J. S. Plaskett[5] obtained a velocity variation with a period of 21.90 days. Five velocities obtained at Lick fitted his curve, but those from Potsdam and Yerkes did not. Moreover, Plaskett's velocities of 1909 showed less amplitude than those of 1908. This earlier study by

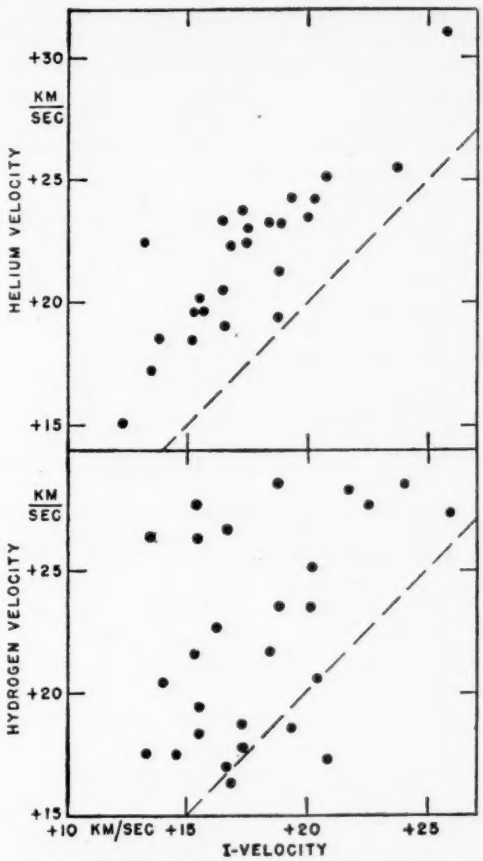

FIG. 3.—I-velocities correlated with *H* and *He* velocities

Plaskett and the results of this paper rule out simple periodicity for the velocity variations of Rigel.

Two other c-stars—α Cygni and χ^2 Orionis—have shown irregular variations in radial velocity. G. F. Paddock[6] has shown that the velocities of α Cyg display fluctuations whose maxima vary from 8 to 16 days (average, 12 days) and whose amplitudes vary from 3 to 11 km/sec (average, 5 km/sec). To demonstrate this, he had to obtain several spectrograms of α Cyg each night for long intervals. It is conceivable that Rigel might also display variations of this sort if sufficient concentrated observing could be done. This, however, is not feasible at Mount Wilson.

[5] *Ap. J.*, **30**, 26, 1909.

[6] *Lick Obs. Bull.*, **17**, 99, 1935.

The star χ^2 Ori also shows a velocity variation which exceeds errors of measurement but which has not been fitted to a satisfactory period, although many high-dispersion velocities have been obtained and studied at Mount Wilson and elsewhere.

It is evident that c-stars may have velocities with unquestioned variability. These velocities, however, are not periodic, at least in any simple way.

For Rigel the mean velocity from the I-group on all plates is +17.7 km/sec; from hydrogen, +21.6 km/sec; and from helium, +22.0 km/sec. Plaskett's value for the systemic velocity is +22.6 km/sec. Plaskett used only the three lines λλ 4340 (*Hγ*), 4471 (*He* I), and 4481 (*Mg* II). According to the systemic differences found from our spectrograms, these lines could be reduced to the I-velocities by the corrections −5.8, −6.3, and 0.0, respectively, or a mean correction of −4.0 km/sec. This would reduce his systemic velocity to +18.6 km/sec, agreeing with my mean for I-velocities. Or comparison may be made with my mean velocity for hydrogen by correcting λ 4471 and λ 4481 to conform to hydrogen. This changes his systemic velocity to +21.5, to be compared with my mean for hydrogen of +21.6 km/sec.

Rigel is a well-known visual binary star, the components of which have shown no certain change in relative position in more than a century since its discovery. Burnham[7] concluded from their common proper motion that the components form a physical pair. All three mean velocities of Rigel A, +17.7 km/sec (I-velocities), +21.6 km/sec (hydrogen velocities), and +22.0 km/sec (helium velocities) are within 3 km/sec of the value found by the writer for the systemic velocity, +19.1 km/sec, for the spectroscopic binary Rigel B.[8] Any one of the three mean velocities for Rigel A could conceivably accompany the systemic velocity of Rigel B if A and B formed a physical pair of reasonable masses, even with a period of many centuries. Therefore, the radial velocities of Rigel A and Rigel B are entirely compatible with Burnham's conclusions.

[7] *General Catalogue of Double Stars*, Part II, p. 411, 1906.

[8] *Mt. W. Contr.*, No. 661; *Ap. J.*, **95**, 421, 1942.

THE SPECTROSCOPIC ORBIT OF σ PISCIUM*

EMILIA PISANI BELSERENE
Lick Observatory and Rutherfurd Observatory
Received December 1, 1946

ABSTRACT

Observations of the spectroscopic binary, σ Piscium, with the Mills 3-prism spectroscope of the Lick Observatory lead to a period of 81.12 days. The spectra of both components are visible for a few days near one node but are blended during the rest of the period. Thirty-two observations near the node result in an orbit of unusually high eccentricity, $e = 0.898$.

The binary character of σ Piscium ($\alpha = 0^h57^m.3$; $\delta = +31°16'$, 1900; vis. mag., 5.46; sp., B9) was announced in 1918 by W. W. Campbell,[1] on the basis of a plate showing doubled lines, with the two components of approximately equal intensity and with a separation corresponding to a relative velocity of about 125 km/sec.

The star was put on the observing program of the Lick Observatory in 1941, with a view toward determining the period and spectroscopic orbit. The observations were made with the Mills 3-prism spectrograph (dispersion, 10 A/mm at λ 4500). Spectrograms, obtained throughout the fall of that year, led to inconclusive results as regards the period. Observation of the star was resumed in 1943, when the problem was suggested to the writer, and one hundred and sixteen plates were obtained at various intervals up to the fall of 1945.

In the usable region of the spectrum, there appear on most plates only two lines: λ 4481 *Mg* II, good, and λ 4549 *Fe* II + *Ti* II, weak, of which the former alone was measured. On thirty-three plates, lines of both spectra are visible, with the stronger component displaced toward the red in all cases. On the remaining eighty-three plates the lines of the two components are blended. The velocity of the blend was measured on forty of these plates and found to be constant within the limits of observational error. Columns 1–3 of Table 1 give, respectively, the date, Julian Day, and measured radial velocities of the two components of *Mg* II, or of the blend. All the measurements were made by the writer, who remeasured the early plates for the sake of uniformity.

The separation of the lines in the two spectra occurs at intervals of 81.12 days, a period which is well determined because of the 1918 observation. Since that observation, however, may have been on either the ascending or the descending branch of the velocity-curve, there are two possible periods, 81.116 or 81.126 days. If an allowance of 5 km/sec is made for accidental error in the measurement of that plate, the period of 81.12 days may be said to be correct to within 0.014 day.

The observations of separated lines show a steep rise and fall of radial velocity, a fact which indicates that the node is near periastron in an orbit of high eccentricity and that the longitude of periastron is near 0° or 180°. Since the two spectra remain blended at the other node, the semi-amplitudes of the velocity-curves are not available for use in the computation of the orbit. In an attempt to estimate the separation of the lines at that node by a study of the line profiles, as suggested by G. D. Shajn,[2] the spectrum in the vicinity of λ 4481 was traced with the Moll microphotometer of the Lick Observatory. Since the profiles of the two components were available from the plates on which the lines were observed separately, it was possible to compute the profile which the blended line should have for various separations. These calculated profiles were plotted

* *Contributions from the Lick Observatory*, Ser. II, No. 16.

[1] *Pub. A.S.P.*, **30**, 352, 1918.

[2] *Poulkovo Obs. Circ.*, No. 22, October, 1937.

TABLE 1

Date (1)	JD 2420000+ (2)	Velocity, *Mg* II (Km/Sec) (3)	Phase (Days) (4)	Weight (5)	O−C (Km/Sec) (6)	Sep. (Km/Sec) (7)	O−C (Km/Sec) (8)	Remarks (9)
1918 Oct. 31.....	1898.827	+ 74.0, − 55.2	.....	0.0, 0.0	.....	.....	.....	
1928 Oct. 18.....	5537.907	+ 7.5	69.880	1.0	− 2.9	.....	.....	
	2430000+							
1941 Sept. 9.....	0246.940	+ 7.9	73.953	1.0	− 2.5	.....	.....	
Sept. 10.....	0247.949	+ 6.4	74.962	1.0	− 4.0	.....	.....	
Sept. 12.....	0249.985	+14.6	76.998	1.0	+ 4.2	.....	.....	
Sept. 13.....	0251.025	+10.9	78.038	1.25	+ 0.5	.....	.....	
Sept. 15.....	0252.977	+10.2	79.990	0.0	.....	50	+ 6.2	Broad line
Sept. 17.....	0254.969	+ 67.1, − 46.8	0.862	0.6, 0.492	− 0.63, + 6.18	.....	.....	
Sept. 19.....	0256.829	+20.3	2.722	0.0	.....	30	−19.7	Broad line
Sept. 27.....	0264.826	+12.6	10.719	1.25	+ 2.2	.....	.....	
Sept. 28.....	0265.795	+15.8	11.688	1.25	+ 5.4	.....	.....	
Sept. 29.....	0266.731	+16.9	12.624	1.25	+ 6.5	.....	.....	
Sept. 29.....	0266.778	+11.1	12.671	1.25	+ 0.7	.....	.....	
Sept. 30.....	0267.993	+12.1	13.886	1.5	+ 1.7	.....	.....	
Oct. 1.....	0268.985	+12.0	14.878	1.5	+ 1.6	.....	.....	
Oct. 3.....	0270.915	+ 5.9	16.808	1.5	− 4.5	.....	.....	
Oct. 4.....	0271.989	+ 7.4	17.882	1.5	− 3.0	.....	.....	
Oct. 6.....	0273.981	+ 3.3	19.874	1.5	− 7.1	.....	.....	
Oct. 8.....	0275.982	+11.0	21.875	1.5	+ 0.6	.....	.....	
Oct. 9.....	0276.971	+14.5	22.864	1.5	+ 4.1	.....	.....	
Oct. 10.....	0277.945	+10.5	23.838	1.5	+ 0.1	.....	.....	
Oct. 14.....	0282.002	+14.3	27.895	1.25	+ 3.9	.....	.....	
Oct. 15.....	0282.998	+ 9.1	28.891	1.25	− 1.3	.....	.....	
Oct. 16.....	0284.731	+ 3.2	30.624	1.25	− 7.2	.....	.....	
Nov. 7.....	0305.800	+ 9.3	51.693	1.0	− 1.1	.....	.....	
Nov. 10.....	0308.874	+ 4.0	54.767	1.0	− 6.4	.....	.....	
Nov. 11.....	0309.896	+ 9.1	55.789	1.0	− 1.3	.....	.....	
Nov. 14.....	0312.757	+ 8.4	58.650	1.0	− 2.0	.....	.....	
1943 Dec. 7.....	1065.765	+ 90.6, − 75.9	0.458	0.9, 0.738	+ 0.02, + 2.34	.....	.....	Fair plate
Dec 8.....	1066.618	+ 59.2, − 33.5	1.311	0.56, 0.459	+ 5.98, + 3.44	80	−10.2	Poor plate
Dec. 8.....	1066.740	+ 56.2, − 47.8	1.433	0.6, 0.443	+ 5.76, −13.93	80	− 4.3	Secondary poor
1944 July 5.....	1276.941	+10.3	49.394	1.0	− 0.1	.....	.....	
July 10.....	1281.948	+21.1	54.401	1.0	+10.7	.....	.....	
July 13.....	1284.958	+17.9	57.411	1.0	+ 7.5	.....	.....	
July 19.....	1290.950	+ 8.7	63.403	1.0	+ 1.7	.....	.....	
July 20.....	1291.961	+10.9	64.414	1.0	+ 0.5	.....	.....	
July 22.....	1293.955	+ 5.5	66.408	1.0	− 4.9	.....	.....	
July 25.....	1296.957	+12.8	69.410	1.0	+ 2.4	.....	.....	

TABLE 1—*Continued*

TABLE 1—*Continued*

Date (1)	JD 2430000+ (2)	Velocity, *Mg* II (Km/Sec) (3)	Phase (Days) (4)	Weight (5)	O−C (Km/Sec) (6)	Sep. (Km/Sec) (7)	O−C (Km/Sec) (8)	Remarks (9)
1944 Aug. 4	1306.967	+12.2	79.420	0.0	.....	25	+ 2.9	Broad line
Aug. 6	1308.965	+ 97.2, − 86.6	0.298	1.0, 0.82	− 5.01, + 4.51	.....	.....	
Aug. 7	1309.968	+ 58.5, − 35.6	1.301	0.7, 0.574	+ 5.03, + 1.62	75	−15.7	
Aug. 8	1310.965	.....	2.298	.....	.....	60	+ 2.4	Not measured
Aug. 10	1312.939	.....	4.272	.....	.....	35	+ 2.7	Not measured
Oct. 25	1388.658	.....	79.991	.....	.....	55	+11.1	Not measured
Oct. 25	1388.721	.....	80.054	.....	.....	35	−12.6	Not measured
Oct. 25	1388.841	.....	80.174	.....	.....	60	+ 4.5	Not measured
Oct. 25	1388.889	.....	80.222	.....	.....	45	−14.4	Not measured
Oct. 26	1389.642	+ 94.6, − 85.0	80.975	1.0, 0.82	− 3.83, + 1.92	.....	.....	
Oct. 26	1389.721	+104.3, − 96.9	81.054	1.0, 0.82	− 1.52, − 1.80	.....	.....	
Oct. 26	1389.763	+104.7, −100.3	81.096	1.0, 0.82	− 4.03, − 1.99	.....	.....	
Oct. 26	1389.812	+113.1, − 95.2	0.025	1.0, 0.82	+ 2.16, + 5.56	.....	.....	
Oct. 26	1389.857	+115.9, −102.1	0.070	1.0, 0.82	+ 4.14, − 0.44	.....	.....	
Oct. 26	1389.910	+126.2, −105.1	0.123	0.7, 0.574	+14.91, − 3.95	.....	.....	Grainy
Oct. 26	1389.957	+107.2, − 99.7	0.170	1.0, 0.82	− 2.57, − 0.23	.....	.....	
Oct. 27	1390.658	+ 58.4, − 53.2	0.871	1.0, 0.82	− 8.94, − 0.65	.....	.....	
Oct. 27	1390.729	+ 55.0, − 53.3	0.942	0.9, 0.738	− 9.48, − 3.91	.....	.....	
Oct. 27	1390.809	+ 65.9, − 44.8	1.022	0.9, 0.738	+ 4.32, + 1.38	.....	.....	
Oct. 27	1390.908	+ 58.3, − 45.0	1.121	0.8, 0.656	− 0.08, − 2.35	.....	.....	
Oct. 29	1392.829	.....	3.042	.....	.....	45	+ 0.1	Not measured
1945 Sept. 14	1712.939	.....	79.792	.....	.....	25	− 9.4	Not measured
Sept. 14	1712.974	.....	79.827	.....	.....	40	+ 4.1	Not measured
Sept. 15	1713.750	+ 62.2, − 42.8	80.603	0.72, 0.590	+ 2.14, + 1.71	.....	.....	Poor plate
Sept. 15	1713.812	+ 68.9, − 46.2	80.665	0.81, 0.738	+ 3.62, + 4.08	.....	.....	Primary poor
Sept. 15	1713.864	+ 67.7, − 65.3	80.717	1.0, 0.738	− 2.45, − 9.64	.....	.....	Secondary poor
Sept. 15	1713.909	+ 72.7, − 57.1	80.762	1.0, 0.738	− 1.97, + 3.55	.....	.....	Secondary poor
Sept. 15	1713.955	+ 83.1, − 72.0	80.808	1.0, 0.82	+ 3.49, − 5.88	.....	.....	
Sept. 15	1714.007	+ 80.1, − 73.1	80.860	1.0, 0.82	− 5.36, − 0.51	.....	.....	
Sept. 16	1714.724	+ 87.6, − 79.5	0.457	1.0, 0.82	− 3.06, − 1.17	.....	.....	
Sept. 16	1714.768	+ 87.6, − 78.5	0.501	1.0, 0.82	+ 0.01, − 3.56	.....	.....	
Sept. 16	1714.801	+ 78.2, − 73.8	0.534	1.0, 0.82	− 7.17, − 1.32	.....	.....	
Sept. 16	1714.829	+ 89.7, − 68.1	0.562	1.0, 0.82	+ 6.14, + 2.38	.....	.....	
Sept. 16	1714.860	+ 82.8, − 65.0	0.593	1.0, 0.82	+ 1.20, + 3.31	.....	.....	
Sept. 16	1714.902	+ 86.4, − 67.8	0.635	1.0, 0.82	+ 7.31, − 2.26	.....	.....	
Sept. 16	1714.937	+ 85.6, − 58.6	0.670	1.0, 0.82	+ 8.50, + 4.74	.....	.....	
Sept. 16	1714.979	+ 71.8, − 63.0	0.712	1.0, 0.738	− 3.02, − 2.18	.....	.....	Secondary poor
Sept. 17	1715.783	+ 43.5, − 30.1	1.516	0.6, 0.492	− 5.26, + 1.91	.....	.....	

for every 0.05 A (=3.35 km/sec) up to 1.20 A and were compared with the observed profiles of the blended line. It was found that the widening is not appreciable for separations up to nearly 25 km/sec, and no values larger than this amount were observed except on plates immediately preceding and following the separation of the lines. For these plates the separations, estimated to the nearest 5 km/sec, are given in column 7 of Table 1.

In the absence of a knowledge of the semi-amplitudes, the standard methods of obtaining a preliminary orbit could not be used. The mean velocity of the blended *Mg* II line, however, was available as an approximation to the velocity of the system, and thirty-one velocities were used to obtain the mean. Because of the abundance of measures of this blend, it was deemed unnecessary to include weak plates or those with broad lines. The resulting mean velocity, a first approximation to the systemic velocity, is +10.5 km/sec. Observations of the blend that were used neither in this determination nor in the microphotometer work have been omitted from Table 1, since they contribute no important information.

When the observation of October 31, 1918, was omitted, because its position on the curve depended wholly on the choice of period, there were thirty-two observations available for the determination of the velocity-curves. Additional points, of lower weight, could have been included if the separations obtained from the line profiles had been used. Because of the possibility of a systematic difference between the two methods of measurement, however, it was deemed wiser to use only the observations of separated lines. These cover only 0.03 of the period, but they include a section of the velocity-curve which is sensitive to small changes in the orbit. By trial and error the preliminary elements shown in the accompanying tabulation were obtained. The conventional notation

$e = 0.90$	$K_1 = 54.83$ km/sec
$\omega_1 = 345°$	$K_2 = 60.65$ km/sec
$\omega_2 = 165°$	$\gamma = +10.5$ km/sec
$T =$ JD 2431308.66 days	

is used, and the subscript 1 refers to the component having the more intense spectral lines.

This provisional orbit formed the basis for a least-squares solution. Separate equations of condition in the form given by Lehmann-Filhés were written for each component and were weighted according to (*a*) the relative intensity of the lines, (*b*) the extent of blending of the lines, and (*c*) the quality of the lines as noted during measurement. In addition, thirty-one equations of the form

$$d\gamma = V - 10.5 ,$$

where V is the velocity of the blended line, were included. These equations received weights according to phase, with less weight assigned near the node of the preliminary orbit. The weights are tabulated in column 5 of Table 1, the remarks in column 9.

Corrected elements with their mean errors were obtained as shown in the accompanying tabulation.

$\gamma = +10.40 \pm 0.70$ km/sec	$T =$ JD 2431308.667 $\pm$ .025 days
$K_1 = 54.27 \pm 0.96$ km/sec	$M_2/M_1 = 0.9045$
$K_2 = 60.00 \pm 1.03$ km/sec	$a_1 \sin i = 26.6 \times 10^6$ km
$e = 0.898 \pm 0.002$	$a_2 \sin i = 29.5 \times 10^6$ km
$\omega_1 = 345°.2 \pm 2°.38$	$M_1 \sin^3 i = 0.56 \odot$
$\omega_2 = 165°.2 \pm 2°.38$	$M_2 \sin^3 i = 0.51 \odot$

The residuals of the thirty-two observations of separated lines, obtained from an ephemeris based on this orbit, are given in column 6 of Table 1, in the sense of Observed *minus* Computed. In no case do the residuals from the equations of condition differ from these by more than 0.12 km/sec. The residuals of the measured velocity of the blended *Mg* II line, obtained from the velocity of the system, are also given in column 6 of Table 1. The mean error of a single observation of unit weight is ± 4.5 km/sec. The use of the blended line in the determination of the velocity of the system is now seen to be justified, for, at maximum separation of the lines at the apastron node, the ephemeris velocities of the two components, referred to the center of mass, are -7.16 and $+7.91$ km/sec. The unweighted mean of these, $+0.4$ km/sec, is about one-tenth the mean error. When weighted according to the relative intensity of the lines, the mean becomes -0.4 km/sec.

The observed velocities are plotted against phase, reckoned from the epoch of periastron, as solid circles in Figure 1, together with the velocity-curves computed from the final orbit; the horizontal line represents the velocity of the system.

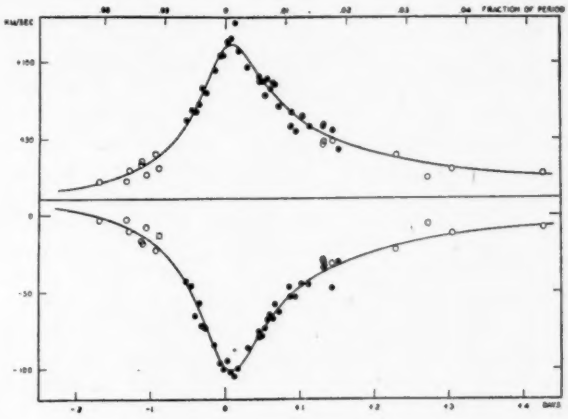

FIG. 1.—Velocity-curves of σ Piscium

The ephemeris based on the corrected orbit was further used to test the separations obtained from the line profiles. The residuals of the estimated separations from those computed from the orbit are given in column 8 of Table 1. By the use of the previously obtained mass-ratio and systemic velocity, the estimated separations can be expressed in terms of velocities of the two components. These velocities are shown as open circles in Figure 1. Although the agreement with the computed curve may be said to be fair, a systematic effect does seem to be present, in the sense that the estimated separations are smaller than those computed from the orbit.

The orbit is of somewhat unusual interest because of the large eccentricity, which is the highest known among spectroscopic binaries, although the orbit of β Arietis by H. Ludendorff,[3] with $e = 0.88$, is similar. The high eccentricity raises the interesting question of what happens during close approach at periastron and suggests examining the possibility of eclipse and of visual separation at apastron. If the stars are of average mass for their spectral type—say, 3 ⊙—i must be approximately 30°, and $a_1 + a_2$, therefore, is of the order of 100×10^6 km. For this mean value, the minimum separation could be as small as 10×10^6 km, or 15 solar radii.

[3] *Ap. J.*, **25**, 320, 1907.

Again, on the assumption that $i = 30°$, the projected distance between centers, at a phase corresponding to $v + \omega = 90°$, is about 13×10^6 km. Eclipse, therefore, is not possible unless the masses are abnormally small and the radii abnormally large.

The spectroscopic parallax of σ Piscium, as given by F. Schlesinger,[4] is 0".011. Corrected for duplicity, the parallax is 0".008. The maximum linear separation, if $i = 30°$, is under 200×10^6 km, which corresponds to an angular separation of less than 0".02, i.e., beyond the limit of visual separation with existing telescopes.

I wish to express my sincere gratitude to Dr. J. H. Moore, who suggested and guided the work; to Dr. G. F. Paddock, who gave freely of his time to obtain many of the spectrograms; and to Drs. M. Schwarzschild and R. J. Trumpler for their helpful suggestions.

[4] *General Catalogue of Stellar Parallaxes*, Yale University Observatory, 1935.

INTERPRETATION OF RADIO RADIATION FROM THE MILKY WAY

CHARLES HARD TOWNES
Bell Telephone Laboratories, Murray Hill, N.J.
Received December 20, 1946

ABSTRACT

The theory of emission of radio radiation by ionized interstellar gas is briefly discussed, and formulae are given for radiation intensity. Experimental measurements of radiation received from the Milky Way between 3×10^{10} and 9.5×10^{8} cycles per second are analyzed and compared with theory. It is shown that radiation from interstellar gas explains the observed radio radiation from the Milky Way if the density of electron gas is near 1 electron per cubic centimeter and its temperature is 100,000°–200,000° K. It appears difficult to explain such radiation, assuming the generally accepted conditions of density of 1 per cubic centimeter and temperature near 10,000° K.

Radio-frequency radiation originating outside the earth's atmosphere was first discovered by Jansky[1] at a frequency of 18 megacycles per second. Since then, Reber[2] and others[3,4] have measured the intensity of this radiation or "noise" at other frequencies and fixed its direction more exactly. Jansky[5] suggested that the radiation which he detected might have come from ionized gas in the Milky Way. Reber[6] made a rough calculation for such a mechanism, and Henyey and Keenan[7] first applied a more quantitative theory and showed that the magnitude of radio radiation from the Milky Way agrees approximately with the radiation that one might expect from free-electron collisions with protons in interstellar space. They assumed the accepted values of electron density of approximately 1 per cubic centimeter and temperature equal to 10,000° K.

This paper proposes to discuss briefly the theory of production of long-wave radiation by collisions between electrons and ions, to compare the available radio data with this theory, and to point out the high electron temperatures which are indicated.[8]

THEORY

Kramers[9] gave a classical derivation for continuous X-ray emission produced by bombarding nuclei with electrons. In doing so he obtained an expression which is also applicable to the radio-frequency radiation produced by collisions between electrons and hydrogen ions in interstellar space. By using Kramers' results and averaging over a Maxwellian velocity distribution as an approximation to the actual unknown electron velocity distribution, one can obtain the absorption coefficient γ per centimeter of ionized hydrogen for radiation of frequency ν.

$$\gamma = \frac{8 e^6}{3 \sqrt{2\pi} (kTm)^{3/2} c} \frac{n^2}{\nu^2} \log\left[\frac{(2kT)^{3/2}}{4.23 \pi \nu e^2 m^{1/2}}\right], \qquad (1)$$

[1] *Inst. Radio Engineers*, **20**, 1920, 1932.

[2] *Ap. J.*, **100**, 279, 1944.

[3] Friis and Feldman, *Inst. Radio Engineers*, **25**, 841, 1937.

[4] Hey, Philips, and Parsons, *Nature*, **157**, 296, 1946.

[5] *Inst. Radio Engineers*, **23**, 1158, 1935.

[6] *Inst. Radio Engineers*, **28**, 68, 1940.

[7] *Ap. J.*, **91**, 625, 1940.

[8] Townes, *Phys. Rev.*, **69**, 695, 1946.

[9] *Phil. Mag.*, **46**, 836, 1923.

where

n = Density of ions or electrons ,
e, m = Electronic charge and mass, respectively ,
k = Boltzmann's constant ,
T = Temperature corresponding to the electronic kinetic energy .

This expression is accurate when

$$\frac{kT}{2e^2n^{1/3}} \gg 1 \quad \text{and} \quad \frac{\pi\nu}{\sqrt{\frac{kT}{m}}\, n^{1/3}} \gg 1 .$$

If

$$\frac{\pi\nu}{\sqrt{\frac{kT}{m}}\, n^{1/3}} \ll 1 ,$$

then it may be shown that the expression for the absorption coefficient becomes

$$\gamma = \frac{8e^6}{3\sqrt{2\pi}\,(kTm)^{3/2}c}\,\frac{n^2}{\nu^2}\log\left\{\frac{kT}{1.64e^2n^{1/3}}\right\} . \tag{2}$$

For the discussion below, expression (1) will be used, since it is a reasonably good approximation for the conditions assumed. The numerical differences between it and expression (2) in the one or two cases where the latter might be preferred are quite small.

Gaunt,[10] Maue,[11] and Menzel and Pekeris[12] have given quantum-mechanical treatments. The results which they obtain and which were used by Henyey and Keenan[7] do not agree exactly in form with the formulae given above; but suitable modification in the approximations made in the quantum-mechanical treatment can be shown to yield essentially the same results as expressions (1) and (2).

From formula (1) the apparent temperature of the Milky Way, that is, the temperature of a black body which would radiate an equivalent amount of energy at frequency ν, is

$$T_a = T\{1 - e^{-\gamma S}\} = T\left(1 - e^{-10^{-2}\frac{n^2}{\nu^2 T^{3/2}}\left[19.7 - \log\frac{\nu}{(T)^{3/2}}\right]S}\right) , \tag{3}$$

where S is the extent of ionized gas in the direction of observation. For reasonable values $n = 1$, $T = 10{,}000°$, and $S = 60{,}000$ light-years in the long direction of the Milky Way, $\gamma S = 1$ for $\nu = 10^8$ cycles/sec. The Milky Way should then give maximum temperatures of approximately 10,000° for $\nu \ll 10^8$. For frequencies so great that the $\gamma S \ll 1$, we have

$$T_a \approx \frac{10^{-2}n^2}{\nu^2 T^{1/2}}\left(19.7 - \log\frac{\nu}{T^{3/2}}\right)S , \tag{4}$$

so that the apparent temperature is approximately inversely proportional to ν^2. Thus for high radio frequencies the radiation per unit area per unit solid angle per unit time per frequency interval is approximately independent of frequency, since the radiation power is

$$P = \frac{2k\nu^2 T_a}{c^2}\,\Delta\nu \text{ per square centimeter per steradian} . \tag{5}$$

[10] *Phil. Trans.*, A, **229**, 163, 1930.

[11] *Ann. d. Phys.*, **13**, 161, 1932.

[12] *M.N.*, **96**, 77, 1935.

RADIO DATA AND THEIR ANALYSIS

Actual radio measurements agree with the expectation that the radiation power is independent of frequency at high frequencies. They also agree with the expected variation with S, the path length through the Milky Way, as is well shown by the intensity contours of Reber and of Hey, Philips, and Parsons. Maximum temperatures at low frequencies are, however, considerably higher than expectations.

Table 1 gives radio measurements from a number of sources, expressed in terms of apparent temperature. These values have been reduced from the reported results, which are usually expressed in other terms. A discussion of their reduction is given below.

Table 1 also compares the measurements with two attempts to fit the results by formula (3). In each case a temperature T is assumed, and n is determined to fit Reber's measurement at 160 megacycles. The value of n so determined is consistent with other estimates[13] and probably more accurate than they are, if the radio radiation is produced by the mechanism discussed here.

TABLE 1

COMPARISON OF EXPERIMENTAL AND THEORETICAL VALUES FOR THE MAXIMUM APPARENT TEMPERATURE OF THE MILKY WAY

Observer	Frequency (Cycles/Sec)	Max. Apparent Temperature* (° K)	Max. Theoretical Apparent Temp. Assuming $n=$ 0.63/cc, $T=$ 10,000° K	Max. Theoretical Apparent Temp. Assuming $n=$ 1.1/cc, $T=$ 150,000° K
Dicke	3×10^{10}	<30	<5	<5
Reber	480×10^{6}	100–200	140	140
	160×10^{6}	1370	1370	1370
Hey, Philips, and Parsons	64×10^{6}	10,600	6000	9000
Jansky	18×10^{6}	92,000	10,000	84,000
Friis and Feldman	9.5×10^{6}	120,000	10,000	140,000

* Apparent temperature is the temperature of a black body which would radiate an equivalent amount of energy at the frequency of observation.

Dicke measured the temperature of interstellar space at microwave frequencies with a microwave radiometer described recently.[14] He has informed the writer that, since no detectable radiation was found, he concludes that the temperature must be less than 30° K. Southworth[15] also looked for radiation from the Milky Way at microwave frequencies and found none. His sensitivity was somewhat less than that of Dicke.

In discussing some of the other radio results, we shall use a fundamental thermodynamic relationship. An amplifier receives power equal to $kT\Delta\nu$ from a perfectly matched, lossless antenna, if T is the temperature of space surrounding the antenna, and $\Delta\nu$ is the frequency range or band width considered. This can be shown by examining the noise-power transmitted between two equal parallel-connected resistors, r_1 and r_2, at temperature T. Resistor r_1 delivers Johnson noise of power $kT\Delta\nu$ to r_2, and r_2 delivers an equal amount back to r_1. If r_2 is replaced by a matched, lossless antenna, r_1 must radiate into space power equal to $kT\Delta\nu$; and, if the surrounding space is at the same temperature, it receives $kT\Delta\nu$ to maintain thermal equilibrium. If reflections or losses are present in the antenna, the transmitted or received power is decreased accordingly.

[13] Dunham, *Proc. Amer. Phil. Soc.*, **81**, 277, 1939; see also n. 7.

[14] *Rev. Scientif. Instruments*, **17**, 268, 1946.

[15] *J. Franklin Inst.*, **239**, 285, 1945.

Reber's results at 160 megacycles are given in terms both of total power received and of radiation power per square centimeter per circular degree per frequency interval. To obtain the latter, he assumes that radiation of only one plane of polarization is received by the antenna, and he uses a beam width of $6° \times 8°$. If we compute the temperature from $kT\Delta\nu$, we obtain 1370° K. If we use his figures for power per square centimeter per circular degree per frequency interval and apply formula (5), the temperature is 5100° K. This latter figure was apparently used by Greenstein, Henyey, and Keenan[16] in their comparison of recent radio data with the theoretical curve given by Henyey and Keenan. The inconsistency between 1370° and 5100° must be explained either by an underestimation of the width of the main antenna lobe or by the presence of important minor lobes. Reber informs the writer that there is some possibility of error in the beam width $6° \times 8°$ which he assumed. If one uses the refraction pattern of a uniformly illuminated parabola of the size used by Reber, the expected beam is a cone, of diameter approximately 12°. Use of this beam width and formula (5) gives a temperature of approximately 2000°. It appears more correct to the author to make no assumptions about the antenna pattern and to take 1370° K as the average temperature seen by the antenna. This value should be good if transmission from the receiver through the antenna to space is perfect except for the 15 per cent loss in the mirror which was pointed out by Reber.

Reber's measurements at 480 megacycles have not yet been published, but he informs the writer that radiation energy is very nearly the same at this frequency as at 160 megacycles. On this basis, the apparent temperature is one-ninth that at 160 megacycles.

Hey, Philips, and Parsons[4] give results at 64 megacycles directly in units of radiation per unit area per unit solid angle per frequency interval, and in no other terms. The apparent temperature is then obtained from formula (5).

Jansky's measurements were not initially made on an absolute basis; but one of his later papers[17] enables us to obtain a fair value for absolute radiation power. Figures 3 and 5 of this later paper give the noise-power at the antenna terminals for two different antenna orientations as a function of time. The maxima of Figure 3 rise consistently to approximately 32.5 decibels below 1 micromicrowatt. Using the relationship discussed above, $P = kT\Delta\nu$, the power $10^{-15.25}$ watts with a band width of $\Delta\nu = 1586$ cycles, as measured by Jansky, corresponds to a temperature of 26,000°. However, Harper[18] gives a value 3.5 decibels for the power lost in the ground and antenna for an antenna of the same type as that used by Jansky. This raises the apparent temperature to 58,000°. In addition, the noise plotted against time in Jansky's Figure 3 is for an antenna direction which does not give maximum noise. The measurements of Figure 3, showing maxima at about 5:00 A.M. in January, 1937, for an antenna pointed N. 50°8′ E., correspond to this same direction at about 1:00 P.M. in the curves shown in his earlier paper[19] for September, 1932. These latter curves, showing radiation as a function of direction throughout the day, show peaks from 3:00 P.M. to 9:00 P.M., which are, on the average, 2 decibels higher than those at 1:00 P.M., corresponding to the January, 1937, measurements. Thus, assuming that the radiation intensity stayed constant during the five intervening years, the apparent temperature must be at least 92,000° at Jansky's 18-megacycle frequency. Several other corrections may be applied, most of which would increase the apparent temperature. They are difficult to estimate, however, and are probably not large. We shall take the radiation temperature measured by Jansky as 92,000°. This figure may well be too low but can hardly be more than 2 decibels too high.

[16] *Nature*, **157**, 805, 1946.

[17] *Inst. Radio Engineers*, **25**, 1517, 1937.

[18] *Rhombic Antenna Design*, p. 58, Van Nostrand, 1941.

[19] Jansky, *Inst. Radio Engineers*, **23**, 1158, 1935.

The data of Friis and Feldman[20] (Table VII of their paper) allow one to obtain the ratio of extra-terrestrial radio noise at 9.5 megacycles, using a narrow-beam antenna, to "thermal" noise when the antenna is replaced by a terminating resistance. The result is a ratio of 15.4-decibel maximum and 9.4-decibel minimum. Feldman informs the author that the so-called "thermal" noise of this paper was actually between 3 and 5 decibels above the theoretical thermal noise level $2\,kT_r$, where T_r is the temperature of the receiver, or approximately 300° K. The antennae used were of the same type as that used by Jansky, so that 3.5 decibels may be assumed lost in receiving. Thus the maximum noise from extra-terrestrial sources corresponds to a temperature of approximately $2T_r \times 10^{2.29} = 120{,}000°$. A single measurement is given at 18.6 megacycles, the temperature computed from it being 60,000°. Although this is not a maximum value, it substantiates Jansky's 92,000° result at approximately this frequency. The data of Friis and Feldman were taken incidentally to the study of an antenna system and consequently are sketchy. The direction from which noise was received is not well known, since the antenna had a number of lobes whose direction could be varied over a considerable angle. The results do show, however, that the apparent temperature at 9.5 megacycles is of the same order as that at 18 megacycles, both being extremely high.

Of course, the high temperatures obtained at low frequencies cannot be fitted with any assumption involving electron temperatures near 10,000°, as is generally supposed. The high-frequency results, as shown in Table 1, may be fitted with $T = 10{,}000°$. In order to fit the low-frequency data, an electron temperature near 150,000° must be assumed. This also fits the high-frequency measurements, giving a somewhat better fit for the 64-megacycle data, as shown in the table. Great consistency among the data cannot be expected, however, because of experimental errors and because most of the temperatures measured are averaged over different antenna beams rather than being the actual maxima for an infinitesimal beam width. Both temperatures may be said to give a perfectly satisfactory fit for the high frequencies.

It appears rather difficult to avoid a conclusion from the radio data that interstellar electrons have temperatures much greater than 10,000°. If one supposes that some mechanism other than these electrons is responsible for the radio-frequency radiation and that interstellar space is actually filled with electrons of density 1 per cubic centimeter and temperature 10,000°, then formula (1) gives an attenuation of e^{-1} for radiation of 9.5-megacycle frequency in a distance of 500 light-years. One must, then, look for a source of at least the lower-frequency radiation within a relatively short distance from the earth. Again, this source must produce radiation whose intensity increases rapidly with decreasing frequency, since the radiation energy received is approximately independent of frequency over a considerable range, although the absorption increases as $1/\nu^2$. Greenstein, Henyey, and Keenan[16] have pointed out a difficulty in attributing the source of this radiation to stars, as suggested by Pawsey, Payne-Scott, and McCready.[21] This same difficulty appears to prevent any explanation involving sources associated with the stars if our sun is to be regarded as a typical star. On the other hand, Hey, Parsons, and Philips[22] have recently found about 15 per cent variation with time of radiation intensity from the direction of Cygnus at 60 megacycles. Such a variation implies a small number of discrete sources of at least this component of the radiation and cannot be accounted for by the theory presented here.

The high temperatures indicated by radio data may be associated with the high temperature of the sun's corona, indicated by Edlén,[23] and supports the idea that the

[20] *Loc. cit.*

[21] *Nature*, **157**, 158, 1946.

[22] *Nature*, **158**, 234, 1946.

[23] Hunter, *Report on Progress in Phys., Phys. Soc.*, **9**, 101, 1942.

short-wave-length portions of the radiation in interstellar space may correspond to much higher temperatures than would be judged from the optical region.

Correlation of the variation of radiation intensity with direction and the dimensions and extent of our galaxy has not been attempted here. It appears to be fruitful and has received some attention from Reber and from Hey, Philips, and Parsons. It should be pointed out that the radiation maxima for all the measurements quoted were found in the direction from which maximum radiation is to be expected, with the exception of the data at 9.5 megacycles. In this case the direction from which radiation was detected is somewhat uncertain, and the measurement may not correspond to a true maximum.

The author has benefited from information and comment generously supplied by many of the experimenters in this field. That they have supplied much essential unpublished information will be obvious to the reader.

THE PHYSICS OF COSMIC GRAINS

FELIX CERNUSCHI
Harvard College Observatory
Received August 31, 1946

ABSTRACT

The present paper is primarily concerned with a critical analysis of existing theories on the formation of "cores" of condensation and crystals in interstellar space and with the growth (or lack of growth) of the cosmic grains and their electrical charges.

It appears very unlikely that the formation of cores of condensation and of the existing grains out of the interstellar gas is continuing under existing average conditions. As an alternative hypothesis to explain the origin of the cosmic grains, we suggest that they were formed in the early stages of the expansion of the universe when the critical conditions of saturation were realized.

We have applied, with certain modifications, the wave-mechanical theory for the interaction of gas particles with the surfaces of crystals developed by Lennard-Jones and his co-workers. The derived value for the accommodation coefficient for the cosmic gas on the cosmic grains is $\alpha < 0.35$. From this value it is found that the surface of a grain at 3° K produces a perturbation on the average velocity of a colliding atom with a speed corresponding to 10,000° K but that this perturbation is not strong enough to produce appreciable absorption. The escaping atoms will have, on the average, a velocity temperature greater than 6500° K. We conclude, therefore, that the cosmic grains cannot grow by an adsorption process.

An analysis of the probable electrical charges of the cosmic grains points to certain weak points in the theories of Jung and Spitzer. We arrive at the conclusion that the metallic cosmic grains would, in the *H* II region, have a positive electrical potential when the dilution coefficient, W, is greater than 10^{-12}, whereas for $W = 10^{-14}$ the potential is -0.7 volts. In the *H* I regions, which occupy 90 per cent of interstellar space, the electrical potential is probably $+0.8$ volts. Since at least a fraction of the cosmic grains are, in all probability, dielectric substances, we consider the probable electrical potentials also for this case. We conclude that they are positive, but small.

I. INTRODUCTION

It is well established that interstellar space is filled with gas and grains of matter.[1] The average density of gas in interstellar space is about 10^{-24} gm/cm^3; the predominant element is hydrogen. The average density of cosmic grains is about 10^{-26} gm/cm^3; in the densest dark nebulae this density may reach values of the order of 10^{-24} gm/cm^3 or even greater. The average diameter of the grains is of the order of magnitude of 10^{-5} cm. The temperature of the cosmic gas, caused by ionization from stellar light-quanta and collisions between electrons and atoms, is about 10,000° K. The temperature of the grains, which, on the average, contain a number of atoms of the order of 10^9, corresponds to the temperature of tiny black bodies in equilibrium with the diluted radiation of interstellar space and proves to be equal to 3° K.

The cosmic grains are supposed by many investigators to be metallic, i.e., of iron; but on this point there is no general agreement. Some authors have suggested that the grains may be dielectric crystals; there is the possibility of the presence of ice crystals in interstellar space, as was first suggested by Eddington. If all the cosmic grains were metallic, the percentage of metallic elements would be greater in interstellar space than the value to be expected from the known distribution of elements in the stars. Most probably there are cosmic grains of many different substances, with dielectric particles predominating.

B. Lindblad[2] assumes that, because of the extremely low temperatures of the grains,

[1] For a general background of the subject we refer to C. S. Beals, *Pop. Astr.*, **52**, 209, 1944, and to Lyman Spitzer, *Ap J.*, **93**, 369, 1941; **94**, 232, 1941; **95**, 329, 1942.

[2] *Nature*, **135**, 133, 1935.

every gas particle striking the surface of a cosmic grain is immediately frozen onto the surface of the grain and forever captured. On this assumption he arrives at the following formula for the mass of a typical cosmic grain as a function of the time:

$$m = 10^{36} (\delta t)^3 \qquad (t \text{ being measured in years}), \tag{1}$$

where δ is the gas density.

For $\delta = 10^{-26}$ gm/cm^3 and $t = 10^9$, the mass of the cosmic grain will be 10^{-15} gm, which is presumably the order of magnitude of the cosmic grains if one accepts an average density for these particles of about 5 gm/cm^3. For $\delta = 10^{-24}$ gm/cm^3, which seems like a more reasonable value for the gas density, one would obtain $m = 10^{-9}$ gm, to which corresponds a radius of 10^{-3} cm $< r < 10^{-2}$ cm, which would seem to be too large. According to Lindblad's theory, the mass of the grains would increase as the cube of δt. This has several consequences. If at some time in the past the average density was in excess of the present one by a factor of 10 (not unlikely on the basis of the expanding-universe hypothesis), the rate of growth would have been a thousand times as fast as it would be progressing now. Further, we note that our galaxy has presumably been more or less in its present stage for 3×10^9 years, thus providing an extra factor of 27 in the derived mass. Since considerations similar to these apply also to the different existing modifications of Lindblad's theory, we are led to conclude that the derived masses according to these theories are rather greater than the values suggested by direct observations.

Lindblad's theory has been modified and improved by several authors.[3] Van de Hulst[4] circumvents the difficulty of the too rapid growth of the grains by assuming that abundant hydrogen and helium do not stick to the surfaces of the grains but that all other elements do stick. The predicted particle sizes can then be obtained by a proper adjustment of the abundances of the elements present. This hypothesis cannot, however, be admitted without confirmation by laboratory experiments. Our theoretical considerations in Section IV indicate that this hypothesis is not correct.

A weak point in existing theories of growth is that they assume implicitly that each grain is built up by atoms of all kinds. It is hard to understand from the physical-chemical point of view how it would be possible to form such heterogeneous grains. Offhand, it would seem more likely for these grains to be either small crystals formed by the cooperation of atoms of only a few kinds or metallic drops.

Ter Haar[5] has developed a detailed theory for the formation of diatomic molecules in interstellar space. This theory, based on the study of the detailed processes involved, has been recently extended and improved by Kramers and Ter Haar.[6]

We shall present in Section II some critical remarks about the work of Kramers and Ter Haar. It will there be shown that the building-up of molecules with more and more atoms is not likely to yield an appreciable number of cores of condensation. In Section III we present evidence to show that the sticking of an atom to an interstellar particle as a consequence of a chance collision is probably also a rare phenomenon. We are, therefore, led to conclude that, under the conditions now prevailing in interstellar space, there is little likelihood of continued formation and growth of cosmic particles. Finally, in Section IV we examine critically the factors which determine the electrical charges of the cosmic grains.

[3] D. ter Haar, H. C. van de Hulst, J. H. Oort, and A. J. J. van Woerkom, *Nederl. Tijdschr. v. Natuurk.*, Vol. **10**, August, 1943.

[4] *Nederl. Tijdschr. v. Natuurk.*, **10**, 251, August, 1943.

[5] *Ap. J.*, **100**, 288, 1944.

[6] *Bull. Astr. Inst. Netherlands*, **10**, 139, 1946.

II. CRITICAL REMARKS ABOUT THE FORMATION OF CORES OF CONDENSATION IN INTERSTELLAR SPACE

In dealing with a gas in which the formation of molecules A_1A_2 can take place out of the atoms A_1 and A_2, we must remember that we may have two different elementary processes, one involving a three-particle collision: $A_1 + A_2 + A_3 = A_1A_2 + A_3'$; and another of a photochemical type: $A_1 + A_2 = A_1A_2 + h\nu$. We shall focus our attention on the latter, because it would provide for a greater amount of molecules at equilibrium with dilute radiation than would the first.

If m_1 and m_2 are the masses of the corresponding atoms, then w_1 and w_2 are the weights of the states of least internal energy of the atoms A_1 and A_2, respectively; and, if we designate by ϵ the energy necessary to break up a molecule in its lowest state into two free atoms at rest, then

$$\frac{\nu_1\nu_2}{\nu_{1,2}} = \left(\frac{2\pi m_1 m_2 k}{m_1 + m_2}\right)^{3/2} \frac{T^{3/2}\, e^{-\epsilon/kT}}{h^3} \frac{w_1 w_2}{b\,(T)}, \tag{2}$$

where the ν's represent the numbers of the corresponding particles per cubic centimeter.

We inquire, now, how equation (2) should be modified for the case of diluted radiation. If $T \to 0$ and if rotation is neglected, we have $b(T) \sim w_{1,2}$, the weight of the lowest state of the molecules in equilibrium with the diluted radiation. One has the following simple rule for the calculation of the number of molecules in equilibrium with diluted radiation. We apply relation (2), in which we write for a first approximation $b(T) = w_{1,2}$, and multiply the number thus obtained by the reciprocal of the dilution coefficient, α. Applying equation (2) to the case in which the atoms are H and C and the molecule CH and taking $w_1 = w_2 = w_{1,2} \sim 1$, we obtain for the number of molecules of CH in interstellar space,

$$\nu_{1,2} = \nu_1\nu_2\alpha^{-1}10^{-20}. \tag{3}$$

If we take concentrations (roughly according to the data of observation) of 1 H atom and 10^{-2} C atoms per cubic centimeter and use for the dilution coefficient $\alpha = 10^{-14}$, we obtain

$$\nu_{CH} \sim 10^{-8}/\text{cm}^3. \tag{4}$$

This value is in agreement with the one derived by Kramers and Ter Haar.

The obvious way to investigate the possibility of building up "cores of condensation" or small crystals from the cosmic gas under average present conditions is by generalizing the theory which has been given for the formation of diatomic molecules and to apply it to more complex molecules. If one uses similar considerations to determine the numbers of molecules per cubic centimeter of CH_2, CH_3, and CH_4 to be expected under equilibrium conditions in interstellar space, one obtains, to a first approximation,

$$\left.\begin{aligned} \nu_{CH_2} &\sim 10^{-6}\nu_{CH}\cdot\nu_H \sim \frac{10^{-14}}{\text{cm}^3}, \\ \nu_{CH_3} &\sim 10^{-6}\nu_{CH_2}\cdot\nu_H \sim \frac{10^{-20}}{\text{cm}^3}, \\ \text{and} \\ \nu_{CH_4} &\sim 10^{-6}\nu_{CH_3}\cdot\nu_H \sim \frac{10^{-26}}{\text{cm}^3}. \end{aligned}\right\} \tag{5}$$

Here we have taken $\nu_H \sim 1/\text{cm}^3$; $\nu_{CH_2} \sim \nu_{CH_2}^+$; $\nu_{CH_3} \sim \nu_{CH_3}^+$ and $\nu_{CH} \sim 10^{-8}/\text{cm}^3$. We have taken these molecules because they seem to be the ones with the greatest chances of being formed in interstellar space.

The average number of grains per cubic centimeter is of the order of

$$\frac{10^{-26}\ \frac{\text{gr}}{\text{cm}^3}}{10^{-15}\ \text{gr}} = \frac{10^{-11}}{\text{cm}^3}.$$

Comparing these equations, we see that the number of molecules with three atoms that we could expect under equilibrium conditions is only 0.1 per cent of the probable number of grains; the number of molecules with five atoms is too small by a factor of 10^{15}, compared to the number of grains actually observed. Consequently, it seems impossible to explain the formation of the cores of condensation through the building-up of molecules under equilibrium conditions.

It is well established now that the solar corona has a temperature of about 1,000,000° K. It seems reasonable that most of the stars have stellar coronas at a much higher temperature than the corresponding effective temperatures at the surfaces. The ultraviolet radiation from stellar coronas, novae, prominences, etc., despite the fact that the total amount of it may be small, may have an appreciable effect in the equilibrium temperature of interstellar gas and in the dissociation of molecules and evaporation from the cosmic grains.[7] This effect will tend to reduce the total amount of molecules that could exist at equilibrium in interstellar space, and, consequently, it reinforces our conclusions. The cosmic rays in a smaller degree would produce a similar effect.

In connection with the mechanism of formation of a molecule by the combination of two free atoms and the emission of radiation (to get rid of the excess of energy), we must keep in mind that processes of this type, called "chemi-luminescence," are known in liquids but have not been observed as yet in the gaseous state.[8] Consequently, it would be necessary to look for laboratory confirmation before we can be sure that this process applies to the interstellar gas. It is of interest to compare the number of *CH* molecules given by equation (4) with the value of 10^{-6} given by Dunham from observation. The computed number of *CH* molecules in equilibrium in interstellar space proves to be only 1 per cent of the value determined from observation. If further observational studies were to confirm Dunham's value, we should arrive at the conclusion that interstellar atoms and molecules are not yet in a state of equilibrium and that the molecules may be undergoing a process of disintegration rather than of integration. This would be so if most of the present interstellar molecules were the result of disintegration of more complex molecules or crystals.

In a private communication Swings has pointed out that, if one wishes to investigate the possible formation of cosmic grains around molecular condensation cores, special attention should be paid to H_2. Diatomic hydrogen molecules, while unobservable, are presumably more generally abundant than *CH*, *CN*, or CH^+ molecules. We note, however, that the hydrogen drops, even at the low temperature of 14° K, require a hydrogen molecular pressure of about 51 mm of mercury, which is of the order of 10^{16} higher than the average gas pressure in interstellar space.

In an unpublished report presented at the Copenhagen meeting of the International Astronomical Union, Swings points out that the theoretically computed abundances of *CH*, CH^+, and *CN* differ rather seriously from the abundances determined on the basis of observed intensities, if the assumption is made that the molecules are distributed uniformly in interstellar space. This discrepancy could be understood on the basis of the hypothesis of Merrill and Swings that the molecules are not uniformly distributed in space and that there may exist "circumstellar molecules." Another approach to the problem is through our suggestion that, because of the disintegration of grains and of complex

[7] The author is indebted to Dr. D. H. Menzel for this remark.

[8] Noddack, *Handb. d. Phys.*, **23**, 631, 1926; *International Tables*, **5**, 386, 1929; R. H. Fowler, *Statistical Mechanics* (2d ed., 1936), p. 742.

molecules into simpler ones and into atoms, molecules and atoms are not in equilibrium in interstellar space.

We turn, now, to another phase of Ter Haar's theory for the formation of cores of condensation, the part in which an attempt is made to account for the presence of the known cosmic grains, with about 10^9 atoms per grain. Ter Haar assumes that a quasi-stationary equilibrium exists, in which the number of grains containing a given number of atoms remains practically constant. On the basis of this assumption, Ter Haar[9] derives a relation for the maximum sizes of the cosmic grains. He assumes, further, that (*a*) the exhaustion of the cosmic gas is negligible and (*b*) in the condensation range one may neglect the terms representing the evaporation of atoms from the surface of the grain. Ter Haar derives from considerations of balance of energy for diluted radiation, the cosmic gas, and the grains of i-atoms the following relation[10] between the temperature corresponding to these grains and the number i:

$$T_i = \frac{83}{1 + \frac{1}{50} \log i}. \tag{6}$$

For a variety of reasons we do not feel inclined to accept Ter Haar's theory. Under his assumptions we are forced to admit the continuous growth of existing grains. The bigger the grain, the bigger should be its rate of growth. Under these conditions it does not seem permissible to use equations which are valid only in quasi-equilibrium states, and the theory does not seem self-consistent.

In connection with equation (6), Ter Haar does not consider the possibility of photo-evaporation. If one substitutes $i = 1$, one finds $T_i = T_g = 83°$ K, whereas the correct value should be 10,000° K (Ter Haar applies the equation for the case $i = 2$!), and for $i = 10^9$ (the average number of atoms per observed cosmic grain) we find $T = 59°$ K, instead of 3° K.

We shall, therefore, explore another approach to the problem. Following Fowler,[11] we can write, for the number of gaseous particles in equilibrium at a given temperature with the solid state, the following formula:

$$\bar{N} = \frac{f(T)}{k(T)}, \tag{7}$$

where $f(T)$ and $k(T)$ are the partition functions per particle in the gaseous and solid states, respectively. Substituting the corresponding expressions for these functions and remembering that $pV = \bar{N}kT$, one obtains, for the equilibrium pressure of the gas,

$$\log p = -\frac{\chi}{kT} + \frac{9T^3}{\theta^3} \int_0^{\theta/T} \log (1 - e^{-x})\, x^2 dx + \log \frac{(2\pi mkT)^{3/2}}{h^3} + \log kT, \tag{8}$$

where χ represents the difference of energy between the ground state of the crystal and a free particle in the gas at rest. We take as the zero energy level the one corresponding to the lowest possible state of the particle in the crystal; θ is the so-called Debye temperature.

We assume, now, that the crystal is in the lowest possible state of energy and that we may neglect the vibration energy of the crystal. If we take into account the effect of the dilution factor a, equation (8) can then be written to a first approximation (neglecting the integral in the second number of equation [8]) as

$$p = \frac{(2\pi mkT)^{3/2}}{h^3}\, e^{-\chi/kT} kT a. \tag{9}$$

[9] *Ap. J.*, **100**, 296, eq. (20), 1944. [10] *Op. cit.*, eq. (5), p. 290. [11] *Op. cit.*, p. 168.

The gas pressure in interstellar space, for $\rho \sim 10^{-24}$ gm/cm^3 and $T \sim 10{,}000°$ K, is of the order of 10^{-12} dynes/cm^3 $\sim 10^{-15}$ mm of mercury. If we apply equation 9 for the case of the interstellar gas with $a \sim 10^{-14}$, we obtain, for the value of the gas pressure at equilibrium within the crystal, $p \sim 10^{-3}$ dynes/cm^3, which is much greater than the actual gas pressure in interstellar space. This argument seems to indicate that the existing grains are undergoing a process of evaporation.

According to existing theories for the formation of drops or crystals,[12] the formation of a crystal is due to the simultaneous action of several atoms. Crystals are apparently not formed step by step, by successive additions of single atoms. Let us assume, for a first rough calculation, that there is 1 atom per cubic centimeter in interstellar space with an average velocity of about 10^6 cm/sec and that we consider cells with sides of about 10^{-8} cm; the average interval during which an atom remains in a given cell is, then, about 10^{-14} seconds. Therefore, there are 10^{31} separate instances in the time scale of the universe. The minimum condition for the formation of a crystal would seem to be that several atoms would find themselves simultaneously in one given cell. The probability that z different atoms meet in one elementary interval of time in any one of the 10^{24} cells existing per cubic centimeter is

$$P = (10^{-24})^z 10^{24} . \tag{10}$$

To obtain the average number of crystals per cubic centimeter formed during the past few billion years, one ought to multiply equation (10), first, by 10^{31} and then by a factor of the order of 10^{-8}, according to a rough estimate, to take into account the probability that the colliding atoms may lose the excess energy by photoemission. If one takes $z = 6$, certainly a rather low limit, one obtains, for the number of crystals per cubic centimeter,

$$N \sim 10^{-97} . \tag{11}$$

If we make the assumption that, to form a crystal, at least 6 atoms are required to find themselves by chance in a unit cell, then, even when neglecting photodissociation, we ought to expect 1 crystal in every 10^{97} cc, which is obviously a negligible frequency.

We wish to emphasize that, to have condensation, it is necessary to have the temperatures and pressures corresponding to the supersaturated vapors, which are given by relations of type (8) or (9). From our discussion it follows that the interstellar gas under existing average conditions is far from being in a saturated state. Oort[13] has pointed out that, in interstellar space, grains smaller than certain critical sizes will not have enough surface tension to prevent them from evaporating. But, to exceed the critical size in which the number of evaporated atoms is balanced by the number of condensed atoms, it will be necessary, if one assumes the growth of the grains step by step, to start with a grain of very small radius, which, however, would evaporate.

As an alternative hypothesis we suggest that the cosmic grains may be the result, not of an integration process of the cosmic gas in its present state but of a slow evaporation process of bigger grains, which are probably formed during the early stages of development of the universe.

Suppose that the initial temperature was high and that we start with a gaseous mixture of many different elements. If the pressure were to decrease gradually and if this were accompanied by a gradual dropping of the temperature, we ought to expect the formation of different molecules and then the formation of drops, each of atoms or molecules of one kind. A few elements might produce crystals when the corresponding condensation temperatures and pressures are reached. Since the temperatures and pressures corresponding to the supersaturated vapors are not the same for all elements or molec-

[12] Fowler, *op. cit.*, chap. xxi; F. Zwicky, *Proc. Nat. Acad.*, **17**, 524, 1931.

[13] J. H. Oort, *Nederl. Tijdschr. v. Natuurk.*, Vol. **10**, August, 1943.

ular combinations, these would not all condense simultaneously. The elements or molecules not yet condensed would continue to behave like a perfect gas, until they reached the corresponding critical conditions of condensation.

Let us now make the assumption that in the early stages of the expansion of the universe, and perhaps even in the present stage during the explosions of supernovae and possibly of some novae, there were ejected, from the interiors of the stars, large balls of very dense matter. Some of these stellar globes would expand at a very great velocity on account of their initially very high temperatures. They would cool rapidly on account of the work against the gravitational forces and the loss of energy by radiation. The saturation conditions for various atoms and molecules would be reached in a definite progression. The critical conditions for condensation can be calculated for the different substances by expressions similar to equation (8). According to these considerations, the grains would have been formed in an extremely short period of time, when the critical condensation conditions prevailed.

III. THE INTERACTION OF THE COSMIC GAS AND THE COSMIC GRAINS

To understand the present conditions and the future development of the grains, known to exist in interstellar space, it is important to study in detail the physics of the interaction between gaseous atoms and molecules and the surfaces of the grains under the conditions prevailing in interstellar space.

The processes of adsorption and re-evaporation are generally analyzed from the point of view of thermodynamics and statistical mechanics.[14] The results obtained from these methods are, in most cases, independent of the concrete description of the corresponding elementary mechanism. The mechanism is, however, very important in our cosmogonical problem, because we cannot be sure that there exists in interstellar space an equilibrium between the absorbed phase and the gaseous state.

Let

E_1 = Average energy of an adsorbed atom at the temperature T_1 of the solid

E_2 = Average energy of a gas atom at temperature T_2 ;

E_2' = Average energy of a gas particle when leaving the surface at temperature T_2' .

The so-called "accommodation coefficient"[15] is then defined by the relation (Fig. 1)

$$\alpha = \frac{T_2 - T_2'}{T_2 - T_1} = \frac{E_2 - E_2'}{E_2 - E_1}. \tag{12}$$

The theory that we shall present for the interaction of gas and grains in interstellar space is an application, with the necessary modifications, of the wave-mechanical theory of Lennard-Jones and collaborators.[16] The fundamental process can be visualized in the following way: A crystal is considered as an assembly of oscillators, which, according to

[14] J. W. McBain, *Sorption of Gases by Solids* (1932); Neil K. Adam, *The Physics and Chemistry of Surfaces* (1938); J. K. Roberts, *Some Problems in Adsorption* (1939); R. H. Fowler, *Proc. Cambridge Phil. Soc.*, **31**, 260, 1935, **32**, 144, 1936; Peierls, *Proc. Cambridge Phil. Soc.*, **32**, 471, 1936; Wang, *Proc. R. Soc.*, *A*, **161**, 127, 1937; F. Cernuschi, *Proc. Cambridge Phil. Soc.*, **34**, 392, 1938, and *C.R.*, **206**, 585, 1938.

[15] About the accommodation coefficient see, e.g., Zener, *Phys. Rev.*, **37**, 557, 1931, **40**, 178, 335, 1932; Jackson, *Proc. Cambridge Phil. Soc.*, **28**, 136, 1932; Jackson and Mott, *Proc. R. Soc.*, *A*, **137**, 703, 1932; Roberts, *Proc. R. Soc.*, *A*, **129**, 146, 1930, and **135**, 192, 1932.

[16] *Trans. Faraday Soc.*, **38**, 333, 1938; Lennard-Jones and Strachan, *Proc. R. Soc.*, *A*, **150**, 442, 1935; Strachan, *Proc. R. Soc.*, *A*, **150**, 456, 1935; Lennard-Jones and Devonshire, *Proc. R. Soc.*, *A*, **156**, 6 and 29, 1936; Devonshire, *Proc. R. Soc.*, *A*, **156**, 37, 1936; Lennard-Jones and Devonshire, *Proc. R. Soc.*, *A*, **158**, 242, 1937; Devonshire, *Proc. R. Soc.*, *A*, **158**, 269, 1937; Strachan, *Proc. R. Soc.*, *A*, **158**, 591, 1937.

the law of statistical equilibrium, have a definite distribution, for each temperature of the lattice, among all the possible states of vibration. At the low temperature of the cosmic grains ($T \sim 3°$ K), most of these oscillators presumably will be in the lowest state of energy. When a gas particle strikes the solid surface, it may give up part of its energy to the corresponding oscillator at the surface. In general, as for the case of interstellar space, the amount of energy absorbed by the oscillators is not enough to produce adsorption of the striking particle, and the particle will then leave the surface with a reduced kinetic energy. The study of the interaction of a gas particle with a solid surface (neglecting the possibility of diffusion) is the study of all the possible interchanges of energy between the striking particles and the lattice's oscillators and between these and the captured particles in the adsorbed phase. When the striking particles leave the surface without loss of energy, then we see from equation (12) that the accommodation coefficient $\alpha = 0$; we have $\alpha = 1$ if the gas particles are adsorbed by the surface. Lindblad admits implicitly that $\alpha = 1$, which, as we shall see, is not the case. In general,

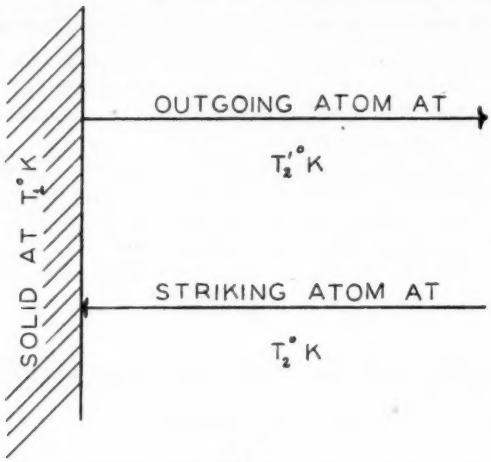

FIG. 1

under the conditions prevailing in interstellar space, $0 < \alpha < 1$; which means that the gas particles are not permanently adsorbed but leave the surface with reduced kinetic energy.

When a gas atom interacts with an oscillator in the ground state, as happens under interstellar conditions, the only possible interchange of energy is that in which the gas particle transfers energy to the oscillator; the smallest energy that the oscillator can take is $h\nu_{0,1}$, where $\nu_{0,1}$ is the frequency corresponding to the transition from the ground state to the first excited level. In general, the lattice oscillators have frequencies distributed over a range of from 0 to ν_m, where ν_m is the largest permissible frequency of the oscillators. This upper limit for the permissible frequencies results from the fact that a crystal containing N atoms can take, according to Debye's[17] theory, only the $3N$ lowest frequencies of a continuum with the same elastic properties as the actual crystal. Debye's theory was improved considerably by Born[18] and more recently by Blackmann;[19] but that upper frequency is not fundamentally modified.

The chances for the oscillators to derive energy from the kinetic energy of the striking atoms is greater for ordinary temperatures of the solid than for low temperatures. At

[17] *Ann d. Phys.*, **39**, 789, 1912.

[18] *Atom Theorie des festen Zustandes* (1923).

[19] *Proc. R. Soc., A*, **148**, 365, 384, 1934; **149**, 117, 126, 1935.

very low temperatures most of the oscillators will be in the ground state, and, to affect any one of them, it is necessary to transfer at least a minimum quantum, $h\nu_{0,1}$. Consequently, the number of different quanta which can be absorbed by the lattice is reduced as the temperature of the solid is lowered; and the interchange of energy between the striking particles and the solid surface becomes gradually less efficient.

We can now consider what most probably happens when very fast particles strike the surface of a crystal at a temperature near the absolute zero. The crystal would be quite rigid with nearly all its oscillators frozen in the lowest state of energy, and therefore the solid's surface would tend to act as a reflecting surface for the fast atoms colliding with it.

The rough picture which we have drawn of the elementary processes of interaction taking place in interstellar space shows clearly the great differences which exist between the phenomena in interstellar space and the so-called "condensation processes" in physics. It is incorrect to think in terms of condensation phenomena, as is done either explicitly or implicitly in most existing theories about the formation and growth of cosmic grains.

When the crystals are very small, as is the case in our problem, the permissible values of the frequencies are reduced to a small number; and, since the probability of absorption of energy by the lattice from the energy of the striking particles decreases as the number of different permissible frequencies goes down, we see that the probability for a colliding particle to be adsorbed by the surface will be smaller for a small crystal than for a large one. If we can prove for big crystals that they cannot grow by adsorption processes under the conditions prevailing in interstellar space, then it will be even more unlikely that the known small grains of matter will grow.

In the derivation of the formula for the accommodation coefficient, we are following the methods of Lennard-Jones and Strachan. We shall make use of a formula by Devonshire for the probability per collision that a colliding atom will obtain from the solid a quantum in a given frequency range. The resulting formula for the accommodation coefficient then is:

$$\left.\begin{aligned} \alpha = \frac{1}{k^2 T_2 (T_2 - T_1)} \int_0^{\nu_m} \frac{24\pi^4}{k^2} \frac{m^2}{M} \nu^4 \frac{(e^{h\nu/kT_1 - h\nu/kT_2} - 1)}{e^{h\nu/kT_1} - 1} d\nu \\ \times \int_0^{\infty} \frac{\sin h2\pi\mu \sin h2\pi\mu'}{(\cos h2\pi\mu - \cos h2\pi\mu')^2} e^{-E/kT_2} dE , \end{aligned}\right\} \quad (13)$$

where ν_m is again the Debye frequency; where m and M are the masses of the striking atom and of an atom of the crystal; and where

$$\mu = \frac{(2mE)^{1/2}}{kh} , \quad (14)$$

the primes referring to conditions after the collision.

So far we have not made any restrictions regarding the temperatures T_2 and T_1. In the past, most calculations have been restricted to the case in which the temperature of the solid is a little higher than the temperature of the gas—conditions characteristic for adsorption in electronic valves. For our problem we are more interested in the case in which the temperature of the gas, T_2, is much greater than the temperature of the solid, T_1. It is interesting to note that we finally obtain a formula very similar to the one given by Devonshire. We point this out to avoid the impression that we are applying a formula which was deduced for completely different conditions. In our case we have $T_2 > T_1$ and, consequently, $h\nu/kT_1 > h\nu/kT_2$. Therefore, we can write equation (13) in the form

$$\alpha = \frac{1}{k^2 T_2^2} \int_0^{\nu_m} \frac{24\pi^4}{k^2} \frac{m^2}{M} \nu^4 d\nu \int_0^{\infty} \frac{\sin h2\pi\mu \sin h2\pi\mu'}{(\cos h2\pi\mu - \cos h2\pi\mu'\pi)^2} e^{-E/kT_2} dE . \quad (15)$$

In the reduction of this formula we make use of the fact that

$$\mu\pi \gg 1$$

and that

$$E \gg h\nu .$$

If we write

$$\frac{\pi^2 m^{1/2}\nu}{kE^{1/2}2^{1/2}} = X = \frac{A\nu}{E^{1/2}}; \qquad A = \frac{\pi^2 m^{1/2}}{k2^{1/2}},$$

then the formula for a becomes

$$a = \frac{6\pi^4}{k^2 T_2^2 \nu_m^3} \frac{m^2}{Mk^2} \int_0^\infty dE \int_0^{A\nu_m/E^{1/2}} \frac{X^4}{\sin h^2 X} E^{5/2} e^{-E/kT_2} dX . \tag{16}$$

Taking the following numerical values: $\nu_m \sim 10^{13}$ sec^{-1}; $k \sim 10^8$ cm^{-1}; $m \sim 10^{-23}$ gm; $M \sim 10^{-22}$ gm; $h = 6.5 \times 10^{-27}$; and $k = 1.37 \times 10^{-16}$; using

$$\int_0^\infty E^{5/2} e^{-E/kT_2} dE = \tfrac{15}{8} (kT_2)^{7/2} \sqrt{\pi};$$

and making a graphical evaluation of the integral with respect to X, we obtain

$$a < 0.35 .$$

The true value of a will be smaller than this because frequencies in our small grains of matter, as we have pointed out previously, do not vary continuously between zero and ν_m. Consequently, the integral over X in equation (16) ought to be replaced by a summation over a finite number of frequencies. This will obviously reduce considerably the value of a. But, even when using $a = 0.35$, we learn from equation (12) that T_2', the average temperature of the atoms leaving the surface, will be

$$T_2' > 6500°K .$$

Therefore, the solid surfaces of the cosmic grains generally produce a marked perturbation on the average velocities of the colliding atoms. This perturbation is, however, not strong enough to produce adsorption in such a way as to make the grains grow at the expense of the cosmic gas under average physical conditions in interstellar space.

Now we shall consider what the total amount of adsorbed gas is that one may expect per unit area of cosmic grains at the conditions of interstellar space. Langmuir's adsorption isotherm was derived by Fowler[20] by methods of statistical mechanics and may be written in the following explicit form:

$$\frac{\theta}{1-\theta} = p \frac{h^3 v_s(T)}{(2\pi m)^{3/2} (kT)^{5/2}} \frac{e^{\epsilon_0/kT}}{b_g(T)}, \tag{17}$$

where θ is the fraction of the surface covered in the monolayer in equilibrium with the gas at pressure p; $v_s(T)$ is the partition function corresponding to the vibrations of an adsorbed gas particle in a definite "site"; $b_g(T)$ is the partition function for the rotations and vibrations of the free gas particles; and ϵ_0 is the energy difference between the lowest adsorbed state, which is taken as zero energy, and the lowest free state in the gas.

We have proved[21] that the isotherm (17) can be deduced as a particular case of the well-known equation of mass action. Consequently, we can use here an approach similar

[20] R. H. Fowler, *Proc. Cambridge Phil. Soc.*, **31**, 260, 1935.

[21] F. Cernuschi, *C.R.*, **206**, 585, 1938.

to that of Section II for the application of the mass-action equation to the formation of molecules in interstellar space under the action of diluted radiation. In interstellar space, the dilution coefficient, $a \sim 10^{-14}$. Furthermore, under interstellar conditions most of the adsorbed particles will be at their lowest possible state of energy (therefore, $v_s(T) \sim 1$); and, neglecting the rotation and vibrations of the gas particles ($b_g(T) \sim 1$), we may write equation (17) in the following way:

$$\frac{\theta}{1-\theta} = p \frac{h^3}{(2\pi m)^{3/2} (kT)^{5/2}} \frac{e^{\epsilon_0/kT}}{a}. \tag{18}$$

By substituting the corresponding numerical values for interstellar space ($2\pi m \sim 10^{-23}$; $p \sim 10^{-12}$ dyne/cm^2; $kT \sim 10^{-12}$; $a \sim 10^{-14}$; $\epsilon_0 \sim 10$ electron-volts) we obtain

$$\theta \sim 10^{-8}.$$

Since, per unit area, there are about 10^{16} sites for adsorbed particles, we see that we may expect 10^8 adsorbed particles per unit area of cosmic grains in equilibrium. On the average, 10^{-2} adsorbed particles would correspond to the surface of a cosmic grain with a radius of about 10^{-5} cm.

In conclusion, we wish to point out that some small amount of cosmic gas may be diffused inside the cosmic grains.[22] In some crystals there may be assumed to exist a series of "holes" of low potential energy, which are distributed periodically according to the lattice structure. These holes may be occupied by the gas particles by diffusion through the surface of the crystal. If one substitutes for the sites of low potential at the surface of a solid the holes in the interior of the crystal, then one can develop formulae similar to equations (17) and (18). Consequently, one might expect, at most, that the ratio of the occupied holes to the unoccupied ones would be of the order of 10^{-8}. If we assume that in certain crystalline structures there are 10^{20} holes per cubic centimeter, then we would expect, at most, 10^{12} diffused particles of the gas per cubic centimeter under equilibrium conditions. Small as is this amount of adsorbed and diffused gas, it is probably great enough to account for the production of gas in comets near the sun, on the assumption that they are an assembly of small solid particles.[23] We conclude, however, that it is very unlikely that the existing cosmic grains will grow by adsorption or by diffusion of atoms from the interstellar gas.

It would be very important if experiments on adsorption and accommodation coefficients were carried out in the laboratory under physical conditions similar to those found in interstellar space. In these experiments it would be necessary to use atomic beams of the elements existing in the interstellar gas and with average velocities corresponding to the temperatures of interstellar space. The target ought to be kept at a very low temperature through the use of liquid helium. In that way it would be possible to obtain experimental evidence about some of the processes taking place in interstellar space.

IV. THE ELECTRIC CHARGES OF THE COSMIC GRAINS

In the preceding section we studied the interaction of the cosmic gas and the cosmic grains on the assumption that the grains are electrically uncharged. If they were electrically charged, the conclusions might be different. If the cosmic grains were positively charged, the striking ions would be reflected even more strongly by the solid surface. If, on the other hand, they were negatively charged, the attraction between the positive ions and the grains would increase proportionally to the charge of the grain, and conse-

[22] See, e.g., Richard M. Barrer, *Diffusion in and through Solids* (1941); C. Smithells and R. H. Fowler, *Proc. R. Soc., A*, **160**, 38, 1937.

[23] See, e.g., B. A. Vorontsov-Velyaminov, *Astr. J. S. Union*, **22**, 317, 1945.

quently the rate of adsorption would also be increased. Therefore, the problem of the growth of the cosmic grains is directly related to the problem of their electrical charges.

The problem of the electrical charges has been investigated by Jung[24] and by Spitzer.[25] Jung arrived at the conclusion that the cosmic grains have, on the average, a positive potential of about 10 volts, whereas, according to Spitzer, the potential is a negative one of about 2.2 volts.

Jung's and Spitzer's theories refer to electric charges of metallic grains, e.g., of iron. We have already pointed out that in all probability most cosmic grains are built up of dielectric substances. This point is in need of clarification, for it may well be that in interstellar space we have a mixture of grains of dielectric substances and grains of metallic elements. We shall, therefore, consider, first, the case of metallic grains, also because this was the one studied by Jung and Spitzer; and then we shall present some considerations regarding the possible electric charges of dielectric grains.

It is well known from the photoelectric effect that, to remove an electron, it is necessary for an impinging photon to have an energy at least equal to the threshold potential of the solid. This potential in volts has the following values for some principal substances: aluminum, 2.5–3.6; gold, 4.82; carbon, 4.7; calcium, 2.7; potassium, 1.76–2.25; copper, 4.1–4.5; sodium, 1.90–2.46; lead, 3.5–4.1; iron, 4.72.[26] We shall take a value of 5 volts for the threshold potential in our calculations so as not to overestimate the influence of the photoelectric effect.

In Jung's calculations a number of assumptions are made that are in need of revision. He assumes, for example, that every quantum with a frequency equal to, or greater than, that corresponding to the threshold potential of 5 volts ($\nu_0 = 1.2 \times 10^{15}$; $\lambda_0 = 2500$ A) produces a photoelectron.

The highest yield which has been observed in the laboratory is for potassium, which, for the wave length corresponding to the selective maximum, emits 1 electron for every 14 quanta incident upon its surfaces.[27] For metals like platinum, aluminum, gold, and perhaps also iron, one obtains, on the average, 1 electron for every 1000 photons. These same metals and some others exhibit photoelectric yield-curves which increase regularly with increasing frequency. Consequently, we feel justified in assuming an average yielding coefficient of the order of 10^{-3} per average quantum greater than $h\nu_0$. With this correction the total number of photoelectrons per unit surface per unit time will be

$$N = \frac{8\pi a}{10^3 c^2} \int_{\nu_0}^{\infty} \frac{\nu^2 d\nu}{e^{h\nu/kT} - 1}. \tag{19}$$

Jung's calculation of the potential of the grains is made on the assumption that, under equilibrium conditions, the total number of striking electrons equals the total number of photoelectrons produced in the same time interval. This implies that every striking electron will be captured by the surface. The available laboratory evidence suggests that the assumption is correct for a high positive potential of the grain but that, for small positive, zero, and negative potentials, many striking electrons will be reflected; this would give to the photoelectrons a greater weight in the electrical balance. It appears reasonable to assume that, for small negative potentials, only 10 per cent of the striking electrons will be captured by the surface of a metallic grain.

With the above modifications we shall calculate from Jung's equations the potentials of the grains, separately for the regions of complete hydrogen ionization (H II) and for the regions where hydrogen is preponderantly neutral (H I).

[24] *Veröff. d. Sternw. Breslau*, No. 9, p. 426, 1938.

[25] *Ap. J.*, 93, 369, 1941.

[26] A. L. Hughes and L. A. Du Bridge, *Photoelectric Phenomena* (1932).

[27] *Ibid.*, p. 171.

In the *H* II regions the potential varies with the dilution coefficient. In the regions relatively near exciting stars, where $a > 10^{-12}$, the number of photoelectrons will be greater than the number of striking electrons, and, consequently, the grains (metallic or dielectric) will take a positive charge. For those parts of the *H* II regions in which $a < 10^{-12}$, the electric potential of the grains will be negative.

We can also calculate the probable potential in the regions for which $a = 10^{-14}$. We see that in this case we can neglect the photoelectric effect (as is assumed in Spitzer's theory) and we obtain

$$\phi \sim -0.7 \text{ volts} .$$

This value differs from the one given by Spitzer, because he considered that all striking electrons were captured.

According to Strömgren, the *H* II regions occupy, however, only 10 per cent of interstellar space. We now turn to the charges in *H* I regions, where all electrons come from elements other than hydrogen and where presumably $N_{el} \sim 10^{-3}$ and $N_p \sim 0$. It is also important to remember that cosmic grains are far more important in the *H* I regions where probably appear most of the dark nebulae. This point is not quite clear yet and needs further investigation.

For the *H* I regions we find

$$\phi \sim +0.8 \text{ volts} .$$

Consequently, in the regions of interstellar space where the cosmic grains are probably most abundant, we obtain a value of the electric potential of about +1 volt. Since in these regions most elements, with the notable exception of hydrogen, are ionized and since hydrogen probably cannot condense into drops in interstellar space, this positive charge reinforces the arguments of the preceding sections, viz., that most of the striking atoms will not stick to the surface of the cosmic grain.

Spitzer considers photoelectrons to be unimportant, and he assumes that the following mechanism determines the charges of the cosmic grains: Every electron or positive ion striking the surface of the grain is supposedly captured. Since the electrons are moving much faster than the positive ions, Spitzer supposes that in equilibrium the grain must have a negative potential sufficiently large to reduce the capture cross-section for the electrons and to increase the corresponding one for positive ions, in such a way that the number of electrons and positive ions striking the surface in unit time will be equal. Spitzer thus arrives at the result that a metallic cosmic grain will have a potential of −2.2 volts.

The influence of the photoelectric effect with all the restrictive factors is, however, not negligible everywhere in interstellar space. Spitzer's mechanism may have some validity for parts of interstellar space where the density of matter and the degree of ionization may be higher than average. Under these extreme conditions it would be possible to neglect the photoelectric effect. But even then most of the electrons striking a slightly negatively charged surface are not captured but reflected or diffracted. In this connection we may mention that Farnsworth[28] found, rather accidentally, that, when electrons of about 1 electron-volt or less strike a metallic surface which has an electric potential of −0.8 volts, 100 per cent reflection of the striking electrons will result. Probably some reflection is produced for a negative potential even smaller in absolute value. Consequently, the metallic cosmic grains, even in the densest regions of interstellar space with the highest degree of ionization, cannot have a negative electrical potential in excess of 1 volt. Besides that, when the potential is negative, the striking positive ions may become neutral before leaving the surface. Hence the effect of the collisions of positive ions will further tend to decrease the negative potential in absolute value.

[28] *Phys. Rev.*, **20**, Figs. 2 and 3 and p. 366, 1922.

At least a fraction of the cosmic grains are, in all probability, dielectric substances. We shall therefore inquire briefly into the possible electrical charges for dielectric cosmic grains.

The possible values for the energies of the free electrons in a crystalline lattice are given by bands of permitted energies separated by bands of forbidden energies. The electrons are distributed in each possible band of energy according to the Fermi-Dirac statistics. A. H. Wilson[29] has shown that, when the valency electrons completely fill up an allowed band and when the next allowed band is empty, it is impossible to set up a continuous current and the crystal is then an insulator. Consequently, in a solid dielectric all electrons are in the lowest permitted bands, and there are no holes left for new electrons. This is especially so when the dielectric is at a temperature near the absolute zero, as is the case in our problem. At ordinary temperatures some few electrons may jump to the next permitted band of energy. The energy gap between the last full energy band to the next empty one is about[30] 5 electron-volts. Consequently, if a solid dielectric is to get a negative charge at the very low temperatures of interstellar space, it would have to capture electrons with kinetic energies much greater than 5 electron-volts; therefore, the "captured" electrons would most probably escape.

The photoelectric effect operates also in dielectric crystals; but for these substances there are not many experimental data. In general, the threshold for the photoelectric effect in dielectric crystals is farther toward the ultraviolet.

We conclude that for dielectric cosmic grains one has to expect an electrical potential very near zero and probably slightly positive for the average physical conditions in interstellar space. Consequently, we have not found electrical potentials for the cosmic grains which would invalidate the conclusions of the preceding sections. Rather, we have found that the most probable values for the electrical potentials in interstellar space tend to reinforce the conclusions at which we have arrived.

The author is very pleased to express his deep gratitude to Dr. Bart J. Bok for very useful discussions on the subject; to Harvard College Observatory for the charming hospitality which he has always found there; and to the Guggenheim Foundation for the fellowship which permitted him to carry out the research on the physics of interstellar space.

[29] *Proc. R. Soc.*, *A*, **133**, 458, 1931; **134**, 277, 1931.

[30] F. Cernuschi, *Proc. Cambridge Phil. Soc.*, **32**, 278, 1936.

SMALL DARK NEBULAE

BART J. BOK AND EDITH F. REILLY
Harvard College Observatory
Received January 10, 1947

ABSTRACT

Attention is drawn to the small, round, dense dark nebulae with diameters varying between 5′ and 10′. We propose that these be named "globules." The region of Messier 8 abounds in globules. Published photographs show at least sixteen of them projected against the bright background of the diffuse nebula. At the derived distance of 1260 parsecs for Messier 8, the diameters of twelve of the sixteen observed globules are between 10,000 and 35,000 A.U. It is noteworthy that there is no evidence for globules in the region of the Orion nebula.

At least twenty of the dark objects in Barnard's lists are true globules. A preference is shown for the regions of Sagittarius and Ophiuchus and for the Scutum Cloud, but some isolated examples of large globules (with diameters of the order of 100,000 A.U.) are found in the anticenter region.

The estimated *minimum* absorptions for the small globules are 2–5 mag. The larger globules are more transparent (1 mag.).

In recent years several authors have drawn attention to the possibility of the formation of stars from condensations in the interstellar medium.[1] It is therefore necessary to survey the evidence for the presence in our galaxy of relatively small dark nebulae, since these probably represent the evolutionary stage just preceding the formation of a star.

In the early days of astronomical photography, Barnard drew attention to the prevalence of small dark objects, and his famous two lists of dark objects in the sky are still our best source in the field.[2] Since Barnard's days there have been published many excellent photographs of bright nebulae and of Milky Way regions, notably the Lick atlas[3] and the Ross-Calvert *Atlas*.[4] The new Schmidt cameras, with their short focal ratios and excellent definition and with scales comparable to those of the standard astrographic cameras, provide new opportunities for the search for, and detection of, small dark nebulae.

In connection with the possible evolutionary process referred to above, we are primarily interested in roundish, small dark nebulae. We shall omit here from consideration the wind-blown wisps of dark nebulosity that are seen in large numbers in many parts of the sky and shall concentrate our attention on the approximately circular or oval dark objects of small size. We shall for convenience refer to these as "globules."

Our search for globules has proceeded along two lines. We have examined with care the best available photographs of some of the well-known diffuse nebulae and listed the globules that can be seen projected against the luminous background. We have, further, examined a representative number of prints of the Milky Way photographs and marked on them the objects which satisfy our definition of a globule.

The first region to be investigated was that of Messier 8, a region for which an excellent photographic print is available in the Lick atlas. To guard against defects, this photograph was compared with other published photographs of this diffuse nebula,

[1] Spitzer, *Ap. J.*, **94**, 232, 1941; Whipple, *Ap. J.*, **104**, 1, 1946.

[2] *Ap. J.*, **49**, 1, 1919, and Barnard's *Photographic Atlas of Selected Regions of the Milky Way* (1927), Introd., p. 18.

[3] Moore, Mayall, and Chappell, *Astronomical Photographs Taken at the Lick Observatory.*

[4] *Atlas of the Northern Milky Way.*

notably a photograph by Duncan[5] and an original print of a plate taken by Struve and Elvey at the prime focus of the 82-inch reflector at McDonald Observatory.[6]

In 1908, Barnard[7] noted that there are "a number of very black, small, sharply defined spots or holes" among the markings of Messier 8. A similar observation was made by Duncan. The Lick photograph reveals the presence of twenty-three potential globules. Of these, sixteen are round and range in diameter from 6″ to 1′, and seven are irregular. The measured diameters of the sixteen true globules are distributed as shown in the accompanying tabulation. The dimensions of the irregular objects range from

Approx. Diam.	No.	Approx. Diam.	No.
0″–10″	1	30″–40″	1
10 –20	8	40 –50	1
20 –30	4	50 –60	1

6″ × 60″ and 12″ × 24″ to 60″ × 84″ and 36″ × 216″. Some of these are of an oval shape, with small dark streamers extending from them.

Since the globules are seen projected against the diffuse nebula, Messier 8, their distances must all be smaller than that of the diffuse nebula. The distance of Messier 8 can be determined with a fair degree of accuracy, since we have, apparently associated with the nebula, the galactic cluster NGC 6530. This region has recently been the subject of a careful study by Wallenquist,[8] who obtains $m - M = 11.00$ as the value for the distance modulus, uncorrected for absorption. This value for the distance modulus agrees well with that of 11.05 for the two stars of spectral class Oe5 and B0, which, according to Hubble,[9] are most likely to be responsible for the emission nebula.

To derive the probable distance, we must first apply a correction for absorption. Four stars in the region are in the list of Stebbins, Huffer, and Whitford,[10] and we find from the observed excesses that the total photographic absorption for $m - M = 11.0$ equals 0.6 mag. The derived distance of Messier 8 is then 1260 parsecs, corrected for absorption.

The globules viewed against Messier 8 are, therefore, at the maximum distance of 1260 parsecs. The *maximum* linear diameters of the globules can, therefore, be computed on the assumption that 1″ = 1260 A.U. We find, then, that the maximum diameters of the globules viewed against Messier 8 range from 7000 to 80,000 A.U., with twelve of the sixteen globules having diameters between 10,000 and 35,000 A.U.

The evidence for other large bright nebulae shows that the population of globules viewed against the luminous background of Messier 8 is unusually large. The Trifid nebula, which is a close neighbor of Messier 8, shows, for example, at the most, only three or four objects that could be called globules, and in other parts of the sky globules seem almost totally absent. The Orion nebula is apparently free from superimposed globules, which is all the more surprising since there is plenty of obscuring matter associated with it. Another instance of a bright nebula without globules is the delicate California nebula in Perseus.

The emission nebula near η Carinae is also rich in globules. The general appearance is very much like that of Messier 8. At least a dozen globules can be recognized on a plate taken with the 60-inch Rockefeller reflector of the Boyden Station.

In our further search for globules, we have examined the dark objects in Barnard's lists.[2] It is not a simple matter to draw the line between true globules and minor condensations in dark lanes or in regions of variable obscuration. From an inspection of the beautiful prints in Barnard's *Atlas* and in the Ross-Calvert *Atlas* we find, however, at least twenty unmistakable globules.

[5] *Ap. J.*, **51**, 5, 1920.

[6] See Bok and Bok, *The Milky Way*, Fig. 65

[7] *A.N.*, **177**, 234, 1908.

[8] *Uppsala Ann.*, Vol. 1, No. 3, 1940.

[9] *Ap. J.*, **56**, 184, 1922.

[10] *Ap. J.*, **91**, 20, 1940.

The regions of the star clouds in Sagittarius and Ophiuchus are rich in clearly marked globules. Plate 21 in the Barnard *Atlas* shows numerous objects that stand out against the bright stellar background. Barnard 68, 69, 70, and 255 (in the region near θ Ophiuchi) appear very similar in character to the globules in Messier 8. If one assumes that they are at the distance of the near-by dark nebulae in Ophiuchus, one finds diameters of the order of 30,000 A.U. for some of the best-defined objects. They seem to occur at the rate of one per square degree in the regions where the star density is sufficient to show them by contrast to the background.

A few exceedingly small and distinct globules are seen projected against the Scutum Cloud. It is unlikely that the linear diameter of Barnard 117 or 118 is much in excess of 20,000 A.U. About half-a-dozen globules can be recognized in this section.

The situation in Cygnus and Cepheus is of interest, since in this transition region there are indications for the presence of a few round dark holes, such as Barnard 350. The stellar background is, however, not sufficiently dense in this section to show the globules as clearly as for the Sagittarius-Ophiuchus section. A few globule-like dark spots are seen projected against the North America nebula, but these are more generally hazy and not nearly so distinct as the globules seen projected against Messier 8.

In Perseus, Auriga, and Gemini the stellar background is too thin to permit the detection of many globules. Only the larger objects cover sufficiently large areas to be detectable. Barnard 34 in Auriga, 201 in Perseus, and 227 in Gemini are among the clearest "dark holes" in the anticenter region. Their diameters are large, 10′–20′, which, in all probability, means that the corresponding linear diameters are of the order of 100,000 A.U. or more.

It is not a simple matter to measure the total photographic absorptions produced by the globules. The small ones, seen projected against diffuse nebulae, show no stars shining through them; and the best that we can do is to estimate a ***minimum*** absorption by comparing the surface brightness in the globule with that in the outer parts of the diffuse nebula. Because of possible overlying bright nebulosities, this represents, at best, a minimum estimate for the absorption, which, for the globules with diameters of 10,000–35,000 A.U., proves to be between 2 and 5 mag.

For some of the larger globules, absorptions can be estimated with greater accuracy, since stars shine through them in considerable numbers. Stoddard[11] has made star counts according to photographic and photovisual magnitudes for four large globules in Barnard's list, Barnard 34, 201, 226, and 227. He finds the average total photographic absorptions to be of the order of 1 mag. Star counts on plates taken with the Harvard Jewett-Schmidt telescope confirm this estimate. It is worth noting that these four objects are all in the anticenter section of the Milky Way and that their minimum diameters are of the order of 100,000 A.U.

The cosmological status of the globules was considered in a paper presented at the Harvard Observatory Centennial Symposium on Interstellar Matter (December, 1946). The globules are interesting objects, which deserve further study by the powerful Schmidt telescopes now being put into operation. Every one of them merits further careful study with the largest available reflecting telescopes. Star counts in blue, red, and infrared light should be supplemented with measurements of surface brightness for the globules and for neighboring "unobscured" areas of comparable size.

[11] *Ap. J.*, **102**, 267, 1945.

THE ECLIPSING SYSTEM UX MONOCEROTIS

SERGEI GAPOSCHKIN
Harvard College Observatory
Received January 9, 1947

ABSTRACT

The eclipsing system UX Monocerotis has been studied on 32 spectrograms of the McDonald Observatory and on 1389 photographic patrol plates of the Harvard Observatory. The spectra of classes A7p and G2p exhibit several quite unusual phenomena with respect to change of lines, especially those of *H* and *Ca* II. The orbits of the two components were determined, and the spectroscopic elements from the metallic lines are: $K_A = 68.0$ km/sec; $K_G = 66.5$ km/sec; $e = 0.08$; $\omega = 316°$; $(a_A + a_G) \sin i = 10.92 \times 10^6$ km $= 15.71 \odot$; and $(m_A + m_G) \sin^3 i = 1.47 \odot$. The velocities of the *H* and *Ca* II lines show about twice as large an amplitude. The photographic light-curve exhibits two minima, one total and deep, the other shallow. The elements are: Min = JD2427536.506 + 5.904604 E; Max = $8^m.71$; $m_1 = 9^m.74$; $m_2 = 8^m.75$; $k = 0.30$; $r_G = 0.283$; $r_A = 0.085$; $i = 88°.6$; $e = 0.3$?; $L_A = 0.69$; the ratio of surface brightnesses is 17.3 for the uniform solution. The combination of the spectroscopic and photometric elements gives the radii as 1.34 ⊙ and 4.46 ⊙ and the masses as 0.73 ⊙ and 0.74 ⊙ for the A7 and G2 components, respectively.

INTRODUCTION

The relatively little-known eclipsing variable UX Monocerotis is an interesting system: it has an extensive atmosphere, probably around both components, both of which are visible and measurable in size, mass, and luminosity—a completeness rare among the unusual eclipsing variables. It is not a supergiant system and has the relatively short period of 5.9 days. Some new results on this system are given in the present paper.

SPECTROSCOPIC OBSERVATIONS

During my stay at the McDonald Observatory in December, 1944, I obtained 32 spectrograms of UX Monocerotis with the quartz spectrograph attached to the 82-inch mirror in the Cassegrain focus. Table 1 gives a summary of the material.

All plates were measured by the author only once and were reduced by Mrs. Payne-Gaposchkin. The velocities show considerable scattering, as is seen from Figure 1. The spectrum shows a large number of metallic lines, together with *H*, and all display changes from cycle to cycle, especially those of *H* and *Ca* II. Dr. Wyse[1] has classified the two spectra on low-dispersion spectrograms as A5 and dG1p, and my estimation on the Yerkes system is A7p and G2p. Since the spectra have many lines in common and the orbital velocities are not large, it is difficult to disentangle the individual velocities. In Table 3, I have summarized the material on individual velocities (from Table 2) in four groups. The division into negative and positive velocities has been made more or less arbitrarily. The values in parentheses indicate the numbers of individual velocities in each mean. In deriving the spectroscopic elements, I used the final grouping of velocities given in Table 4. The method of Lehmann-Fihlés was used in deriving the elements. Table 5 gives the results.

As is seen from Figures 1, 2, and 3, the velocities of *H* and *Ca* II exhibit at least twice as large an amplitude as the other lines; in addition, the center of gravity for the *H* lines seems to be shifted (a small shift between the two metallic orbits seems also to be indicated). The *H* velocities have been omitted in obtaining the dimensions of the components.

[1] *Lick Obs. Bull.*, No. 464, p. 39, 1934.

Among the unusual characteristics of the spectrum, we select the following ones:

1. *H* and *Ca* II have about twice as great a range in velocity, in the same orbital period, and show a constant shift of their center of gravity relative to that of the system.

2. The *H* lines are usually double at both elongations, at $\varphi = 0^{p}.8$ when the A7 star approaches, and at $\varphi = 0^{p}.3$ when the G2 star approaches.

3. At both elongations the violet component in the double lines of $H\delta$ and $H\gamma$ is much the stronger. For $H\gamma$ this tendency is less conspicuous, and for *Ca* II it is often reversed.

TABLE 1

SPECTROGRAMS FOR UX MONOCEROTIS

No.	JD	Phase (φ_0)	Exposure Time (Minutes)	Remarks
1	31430^{d}.922	0^{p}.119*	60	Beginning of secondary minimum
2	430.959	.125	50	Beginning of secondary minimum
3	432.896	.453	45	
4	432.924	.458	45	
5	432.956	.463	45	
6	432.986	.469	40	
7	433.019	.474	44	
8	437.922	.304	46	
9	438.867	.465	46	
10	439.805	.623	30	End of primary minimum
11	439.978	.653	34	End of primary minimum
12	440.803	.792	32	
13	440.950	.817	30	
14	441.823	.965	30	
15	442.838	.137	52	Within secondary minimum
16	443.826	.304	28	
17	443.999	.334	33	
18	444.828	.474	50	
19	444.996	.503	40	Beginning of primary minimum
20	445.688	.620	60	End of primary minimum
21	446.004	.673	40	
22	446.853	.871	30	
23	447.830	.982	30	
24	448.830	.152	40	
25	453.825	.998	60	
26	455.829	.336	67	Hurricane, 52 miles/hour
27	456.780	.498	40	
28	456.974	.531	40	Within primary minimum
29	457.000	.536	39	Within primary minimum
30	457.028	.540	40	Totality
31	458.760	.834	39	
32	458.806	0.841	40	

* Computed with $\varphi_0 = 1/P$ (JD − 2400000).

4. The *H* lines are single around the secondary minimum and before the primary. They gradually disappear or greatly diminish in intensity during the primary minimum, indicating that they are chiefly associated with the A7 component.

5. At the secondary minimum, when the A7 star is in front, these single lines are very broad (about 400 km), of uniform intensity within the line, and very square and strong—indeed, stronger than at any other time.

6. During both minima $H\beta$ is in emission, in both cases on the red side.

Several spectrograms are reproduced in Figure 5 through the courtesy of the Yerkes Observatory.

TABLE 2

RADIAL VELOCITIES (KM/SEC)

No.	JD	φ	*Ti* II λ 3900	*Ti* II λ 3913	*Fe* II λ 4395	*Fe* II λ 4444	*Fe* II λ 4533	*Fe* II λ 4233	*Fe* II λ 4351	*Mg* II λ 4481	*Ca* I λ 4227	*Ca* II λ 3933	*Hζ* λ 3889	*Hδ* λ 4101	*Hγ* λ 4340	*Fe* I λ 4005	*Fe* I λ 4045	*Fe* I λ 4063	*Fe* I λ 4144	*Fe* I λ 4325	*Fe* I λ 4383
20...	31445^{d}638	0.620	.....	− 15	.....	− 81	− 9	− 25	− 3	− 23	+ 17	− 51	.....	−16	− 59	.....	+ 22	.....	.....	− 16	+ 26
10...	439.805	.623	− 34	+ 18	.....	− 5	0	+ 4	+ 5	+ 23	+ 10, −100	− 42	.....	− 6	− 29	.....	+ 10	.....	− 6	+ 6	+ 58
11...	439.978	.653	.....	− 42	.....	− 13	.....	+ 15::	+20	− 10	+ 20	− 39	−43	− 9	− 41	.....	+ 32	.....	.....	+ 48	+ 15
21...	446.004	.673	.....	.....	.....	− 14	.....	− 79	+12	− 2	− 59	− 63	.....	−12	− 9	.....	.....	.....	.....	.....	+104
12...	440.803	.792	.....	.....	.....	.....	.....	.....	.....	.....	.....	−142	.....	−124, + 99	−147, +116	+135	+ 81	.....	.....	.....	+119
13...	440.950	.817	.....	.....	.....	.....	−180, +130	.....	.....	.....	.....	−197	−184, +125	−230, +110	−235, + 45	+119	+ 55	.....	+28	.....	+ 88
22...	446.853	.817	.....	.....	.....	− 65	.....	.....	+70	.....	+ 60	−237, + 35	.....	−243, + 99	−234, +123	.....	−231, +7	.....	.....	.....	+ 84
31...	458.760	.834	.....	− 69	.....	+ 15	.....	− 14	+93	.....	+ 35	− 97	−128, +139	−159, + 96	−132, +147	+ 87	+ 39	.....	+59	+ 6	+108
32...	458.806	.841	− 44	− 51	.....	+ 11	− 50	+ 22	+58	+ 64	+ 32	− 81	.....	−126, + 42	− 78, + 52	+ 75	+ 25	.....	+31	+ 3	+ 72
14...	441.823	.965	−102	− 84	.....	− 69	.....	− 68	.....	+ 18	+ 10	−109	−152, + 8	−317, − 39	−405, − 36	+116	− 13	.....	.....	.....	+ 69
23...	447.830	.982	.....	−156, 31	.....	.....	.....	+ 40	+66	.....	− 37	−255, − 60	.....	−257, + 48	−302, + 14	.....	− 39	.....	.....	.....	+ 15
25...	453.825	.998	.....	.....	.....	− 5	−101	− 18	+48	+ 35	− 26	− 94	.....	−167, − 26	−116	.....	− 3	.....	+49	.....	+ 30
1....	430.922	.119	− 59	− 33:	−67	− 37	− 77	− 92?	−73	− 50	−102	−297, +69	.....	−230, + 72	−325, + 56	− 73	− 74	−98	−51	− 65	+ 19
2....	430.959	.125	Fuzzy	Fuzzy	−74	− 25	− 26	.....	−52	− 55	−102	− 69	.....	− 86	−135	− 71	− 33	−46	−42	− 65	+ 6
15...	442.838	.137	− 56	.....	.....	−101	+ 29	− 39	−26	.....	− 77	−252, +115	.....	−280, + 72	−314, + 67	+ 20	.....	.....	.....	.....	+ 3
24...	448.830	.152	.....	.....	.....	− 89	.....	− 3	−68, 1	− 47	−105	+ 1	.....	− 67	−120	+ 4	−102	.....	−37	− 96	+ 6
8....	437.922	.304	.....	+ 91:	.....	.....	.....	+ 78	.....	.....	− 70	+ 99	− 75:, +136	−113, +119	−120, +135	+ 1:	− 68	.....	.....	.....	.....
16...	443.826	.304	.....	.....	.....	.....	.....	+ 58	.....	.....	− 55	−179, +115	−167, +130	−150, +153	−181, +120	− 59	−137	.....	.....	.....	.....
17...	443.999	.334	.....	.....	.....	.....	.....	.....	.....	− 10	− 55	+ 96	.....	−129, +180	−177, +197	.....	− 88	.....	.....	.....	.....
26...	455.824	.336	.....	.....	.....	.....	+ 25	?	+20	+ 80	− 70	+121:	.....	+48	+ 63	− 49	− 36	.....	.....	.....	+ 61
3....	432.896	.453	+ 84	+100	+78	+136	+ 21	+102	+89	+ 39	− 73	+ 57	.....	+16	− 13	+ 11	− 39:	+86:	.....	− 55	+ 84
4....	432.924	.458	+ 76	+ 73	.....	.....	.....	+116	+66	.....	−123	+ 69	.....	+11	− 21	− 5	− 75	.....	.....	− 98	+ 35
5....	432.956	.463	.....	.....	.....	.....	+102	+138	+24	.....	− 91	+ 60	.....	+ 8	− 21	.....	.....	.....	.....	+135	.....
9....	438.867	.465	.....	.....	.....	.....	.....	+106	.....	.....	+ 6:	+ 50	+14	+31	− 2	.....	.....	.....	.....	.....	.....
6....	432.986	.469	.....	.....	.....	.....	− 13	+ 73	+46	+ 72	− 41	+115	.....	+68	− 6	.....	− 19	.....	+37:	− 80	+108
7....	433.019	.474	.....	.....	.....	.....	.....	+ 80	+16	+ 18	− 23	+ 16	.....	+58	− 24	− 65:	+ 16::	.....	−71	− 65	+ 45
18...	444.828	.474	+ 28:	.....	.....	.....	.....	.....	.....	.....	.....	+ 60	.....	− 6	− 24	.....	.....	.....	.....	− 24	.....
27...	456.780	.498	.....	.....	.....	.....	.....	?	.....	.....	− 48	+ 90	.....	+34	.....	+ 33	− 23	.....	.....	.....	.....
19...	444.996	.503	.....	.....	.....	.....	.....	.....	.....	.....	− 34	+ 51	.....	− 9	− 9, −169	.....	− 39	.....	.....	− 77	+ 26
28...	456.974	.531	.....	.....	.....	− 5	.....	.....	− 1	.....	− 80	.....	.....	+21	− 6	.....	.....	.....	.....	− 42	+ 22
29...	457.000	.536	.....	.....	.....	− 53	.....	.....	+ 1	.....	−115	.....	.....	−33	− 59	.....	.....	.....	.....	− 65	− 24
30...	457.028	0.540	.....	.....	.....	.....	.....	.....	.....	.....	−109	.....	.....	.....	− 71	.....	.....	.....	.....	− 88	− 72

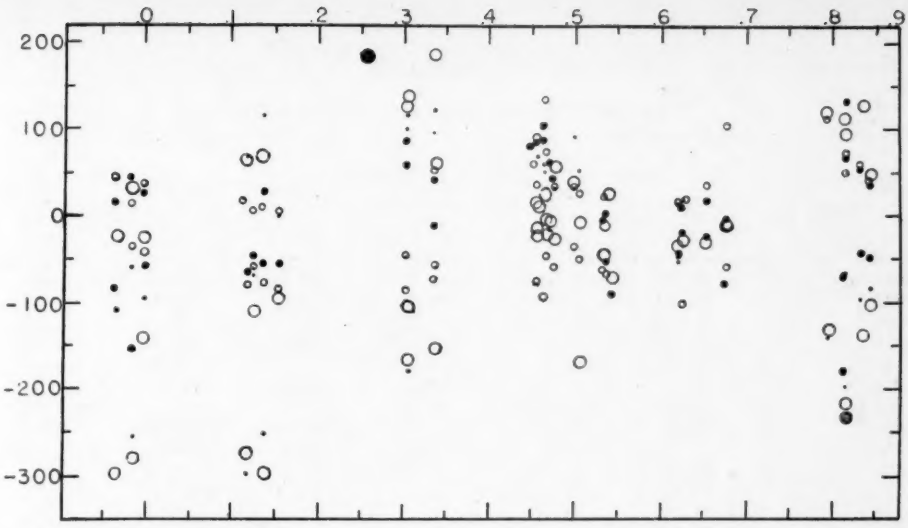

FIG. 1.—Individual velocities of UX Monocerotis. *Large dots*, high-excitation lines; *small circles*, low-excitation lines; *large circles*, *H* lines; *small dots*, *Ca* II lines.

TABLE 3

RADIAL VELOCITIES IN GROUPS (KM/SEC)

Phase	Ionized Metals		Neutral Metals		*Ca* II		Hydrogen	
0P119	− 61.0(8)	.....	− 77.2(6)	+ 19	−297	+ 69	−277.5(2)	+ 64.0(2)
.125	− 46.4(5)	.....	− 59.7(6)	+ 6	− 69	.....	−110.5(2)	.....
.137	− 55.5(4)	+ 29	− 77	+ 11.5(2)	−252	+115	−297.0(2)	+ 69.5(2)
.152	− 51.8(4)	.....	− 85.0(4)	+ 5.0(2)	.....	+ 1	− 93.5(2)	.....
.304	.....	+ 84.5(2)	− 44.3(3)	.....	.....	+ 99	−102.7(3)	+130.0(3)
.304	.....	+ 58.0	− 83.7(3)	.....	−179	+115	−166.0(3)	+134.3(3)
.334	− 10	.....	− 71.5(2)	.....	.....	+ 96	−153.0(2)	+188.5(2)
.336	.....	+ 41.7(3)	− 58.3(3)	+ 61	.....	+121	.....	+ 55.5(2)
.453	.....	+ 81.1(8)	− 55.7(3)	+ 60.3(3)	.....	+ 57	− 13	+ 16
.458	.....	+ 82.8(4)	− 75.2(4)	+ 35	.....	+ 69	− 21	+ 11
.463	.....	+ 88.0(3)	− 91	+135	.....	+ 60	− 21	+ 18
.465	.....	+106	.....	+ 6	.....	+ 50	− 2	+ 22.5(2)
.469	− 13	+ 63.7(3)	− 46.7(3)	+ 72.5(2)	.....	+115	− 6	+ 68
.474	.....	+ 38.0(4)	− 49.6(5)	+ 30.5(2)	.....	+ 38.0(2)	− 18.0(3)	+ 58
.498	.....	.....	− 35.5(2)	+ 33	.....	+ 90	.....	+ 34
.503	.....	.....	− 50.0(3)	+ 26	.....	+ 51	−169	− 9.0(2)
.531	− 3.0(2)	.....	− 61.0(2)	+ 22	.....	.....	− 6	+ 21
.536	− 53	1	− 68.0(3)	.....	.....	.....	− 46.0(2)	.....
.540	.....	.....	− 89.7(3)	.....	.....	.....	− 71	.....
.620	− 42.0(6)	.....	.....	+ 12.2(4)	.....	+ 51	− 37.5(2)	.....
.623	− 19.5(2)	+ 10.0(5)	−100	+ 15.6(5)	− 42	.....	− 17.5(2)	.....
.653	− 21.7(3)	+ 17.5(2)	.....	+ 28.8(4)	− 39	.....	− 31.0(3)	.....
.673	− 79	− 1.3(3)	− 59	+104	− 63	.....	− 10.5(2)	.....
.792	.....	.....	.....	+111.7(3)	−142	.....	−135.5(2)	+107.5(2)
.817	−180	+130	.....	+ 72.5(4)	−197	.....	−216.3(3)	+ 93.3(3)
.817	− 65	+ 70	−231	+ 50.3(3)	−237	+ 35	−238.5(2)	+111.0(2)
.834	− 41.5(2)	+ 54.0(2)	.....	+ 55.7(6)	− 97	.....	−139.7(3)	+127.3(3)
.841	− 48.3(3)	+ 37.4(5)	.....	+ 41.2(5)	− 81	.....	−102.0(2)	+ 47.0(2)
.965	− 80.7(4)	+ 18	.....	+ 45.4(4)	−109	.....	−291.3(3)	+ 22.3(3)
.982	−156	+ 45.4(3)	− 38.0(2)	+ 15	−255	− 60	−279.5(2)	+ 31.0(2)
0.998	− 59.5(2)	+ 26.0(3)	− 39.5(2)	+ 14.5(2)	− 94	.....	−141.5(2)	− 26

TABLE 4

FINAL GROUPING OF THE VELOCITIES (KM/SEC)

PHASE	METALS		HYDROGEN		*Ca* II	
	A7	G2	A7	G2?	A7	G2?
0P965	− 80.7(4)	+ 40.0(5)	−291.3(3)	− 22.3(3)	−109(1)	.....
.982	− 77.3(3)	+ 38.0(4)	−279.5(2)	+ 31(2)	−255(1)	− 60(1)
.998	− 30.6(5)	+ 40.5(4)	−141.5(2)	− 26(1)	− 94(1)	.....
.119	− 67.9(14)	+ 19(1)	−277.5(2)	+ 64(2)	−297(1)	+ 69(1)
.125	− 53.7(11)	+ 6(1)	−110.5(2)	.....	− 69(1)	.....
.137	− 59.8(5)	+ 17.3(3)	−297(2)	+ 69.5(2)	−252(1)	+115(1)
.152	− 77.7(7)	+ 2.3(3)	− 93.5(2)	.....	.....	+ 1(1)
.304	− 57(4)	− 77.8(5)	+132.2(6)	−134.4(6)	+108(2)	−179(1)
.334	.....	− 51(3)	+188.5(2)	−153(2)	+ 96(1)	.....
.336	+ 46.5(4)	− 58.3(3)	+ 55.5(2)	.....	+121(1)	.....
.453	+ 75.5(11)	− 55.7(3)	+ 16	− 13	+57(1)	.....
.458	+ 73.2(5)	− 75.2(4)	+ 11	− 21	+ 69(1)	.....
.466	+ 85.2(11)	− 48.6(5)	+ 32.8(3)	− 9.7(3)	+ 75(3)	.....
.474	+ 35.5(6)	− 49.6(5)	+ 58	− 18.0(3)	+ 38	.....
.498	+ 33(1)	− 35.5(2)	+ 34	.....	+ 90	.....
.503	+ 26(1)	− 50(3)	+169	− 9(2)	+ 51	.....
.531	+ 22(1)	− 32(4)	+ 21	− 6	.....	.....
.536	+ 1(1)	− 64.2(4)	.....	− 46(2)	.....	.....
.540	.....	− 89.7(3)	.....	− 71(1)	.....	.....
.622	− 40.3(10)	+ 14(13)	− 27.5(4)	.....	− 46.5(2)	.....
.653	− 21.7(3)	+ 25.0(6)	− 31(3)	.....	− 39	.....
.673	− 69(2)	+ 25(4)	− 10.5(2)	.....	− 63(1)	.....
.792	.....	+111.7(3)	−135.5(2)	+107.5(2)	−142(1)	.....
.817	−158.7(3)	+ 71.2(9)	−225.2(5)	+101(5)	−217(2)	+ 35(1)
.834	− 41.5(2)	+ 55.2(8)	−139.7(3)	+127.3(3)	− 97(1)	.....
0.841	− 48.3(3)	+ 39.3(10)	−102(2)	+ 47(2)	− 81(1)	.....

TABLE 5

SPECTROSCOPIC ELEMENTS

A7 Component	G2 Component	The System
$V_{max}=64$ km/sec	+55 km/sec	$K_A=68.0$ km/sec
$V_{min}=-72$	−78	$K_G=66.5$
$V_0=-23$	− 3	$e=0.08$
		$\omega=316°$
		$(a_A+a_G)\sin i=10.92\times10^6$ km
		$(m_A+m_G)\sin^3 i=1.47\ \odot$

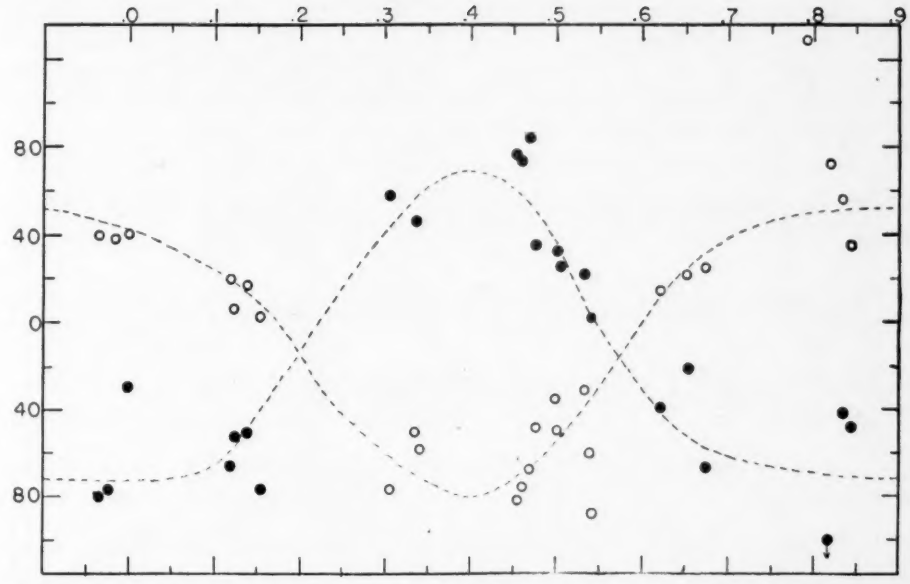

FIG. 2.—Orbital velocities of A7 (*dots*) and G2 (*open circles*) stars. *Abscissa*, phase in periods; ***ordinate***, radial velocity.

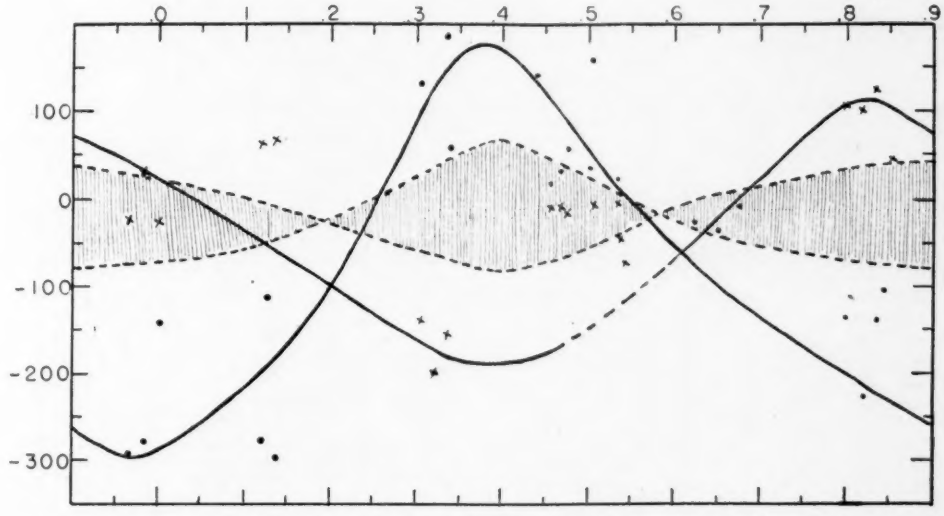

FIG. 3.—Hydrogen velocities of UX Monocerotis. The striped area represents the velocities for the metallic lines.

PHOTOMETRIC INVESTIGATION

The existing Harvard patrol plates were used, and 1389 photographic observations were obtained by the author. The published period has been investigated, and a small correction has been found; the new period is $5^d.904604$. In Table 6 are tabulated the minima which were used for checking the period.

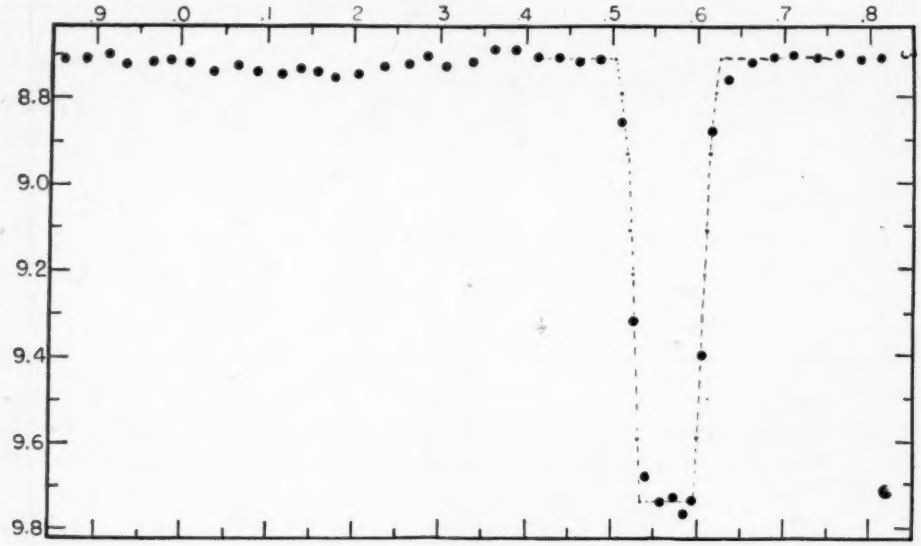

FIG. 4.—Photographic light-curve of UX Monocerotis (1389 observations)

TABLE 6

MINIMA OF UX MONOCEROTIS

JD	Est.	JD	Est.	JD	Est.
$15762^d.636$	−1	$20072^d.843$	−1	$27459^d.694$	0
16943.544	0	078.881	0	530.540	+4
17681.575	+4	096.867	0	536.552	0
705.534	+2	238.517	0	548.229	+4
18000.577	+2	769.841	+1	753.632	+2
006.576	−1	775.858	−1	765.600	+2
295.786	0	21720.500	0	855.527	−1
307.778	0	22375.708	+2	197.667	+2
602.864	−1	23054.768	0	28197.722	0
19429.673	0	816.750	+4	221.587	+1
429.720	+3	25304.664	0	29248.751	0
777.747	+2	599.752	0	331.555	+2
795.708	+1	599.834	−1	337.561	+5
801.678	0	26343.780	0	349.318	+2
801.721	+2	27046.557	+2	717.537	+3

The photographic magnitudes of the comparison stars were determined on four plates with reference to Selected Area No. 124. In Table 7 the adopted magnitudes of the comparison stars are given. All observations were reduced by the formula: $\varphi_0 = P^{-1}$ (JD − 2400000), and the mean light-curve is given in Table 8.

The observational properties of the light-curve are as follows: (1) The principal minimum is well defined and is total; (2) the photometric orbit is eccentric; (3) there is no

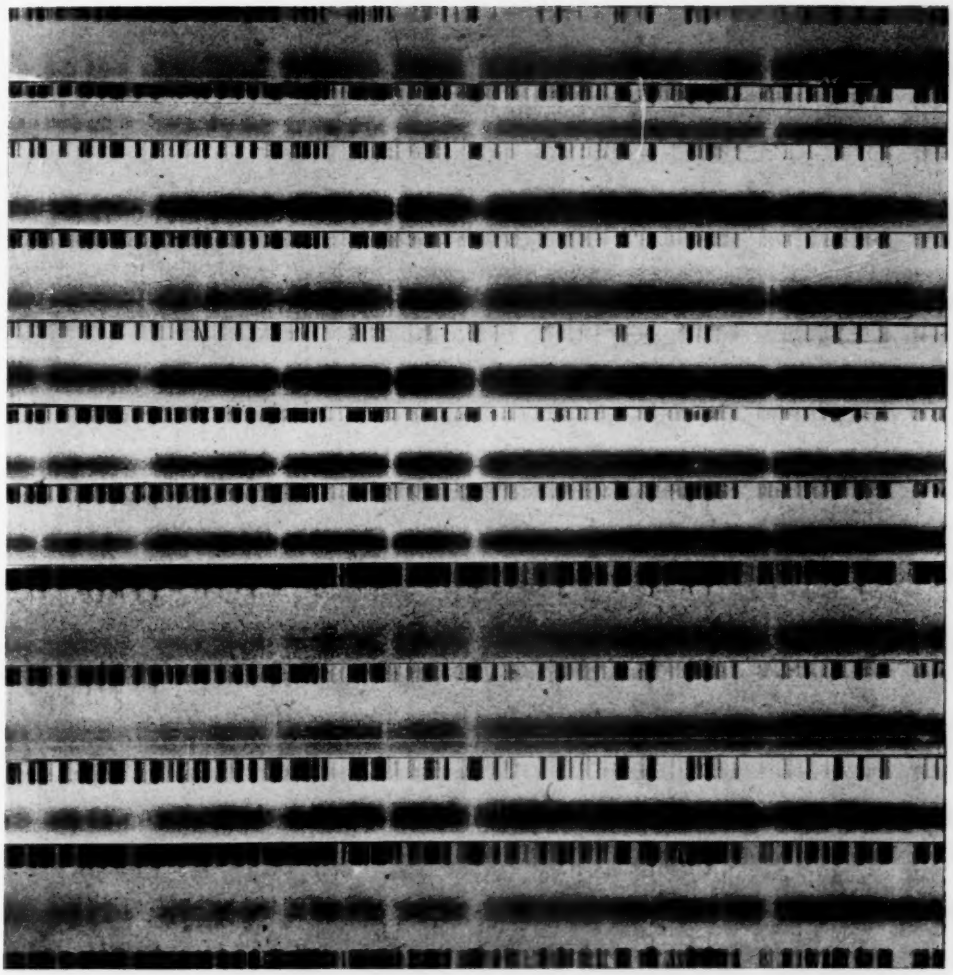

FIG. 5.—Spectra of UX Monocerotis

Phase*	Position	Date	Remarks
0P125	Secondary minimum	Dec. 6	Lines are square and single
.137	Secondary minimum	Dec. 18	Lines are square and single
.304	Elongation, G2 approaches	Dec. 13	Duplicity of the lines
.304	Elongation, G2 approaches	Dec. 19	Duplicity of a double line is reversed
.465	Well before the primary minimum	Dec. 14	No double lines
.474	Well before the primary minimum	Dec. 17	No double lines
.623	End of the eclipse	Dec. 15	Single lines
.673	Well out of the eclipse	Dec. 21	Single lines
.817	Elongation, A7 approaches	Dec. 16	Lines are double, $H\gamma$ is weak
.965	Elongation, A7 approaches	Dec. 17	Ratio in double lines different from that of $\varphi = 817$
0.998	Well before the secondary minimum	Dec. 29	Lines square and single

* The phase of the primary minimum is 0P565, that of the secondary, 0P150.

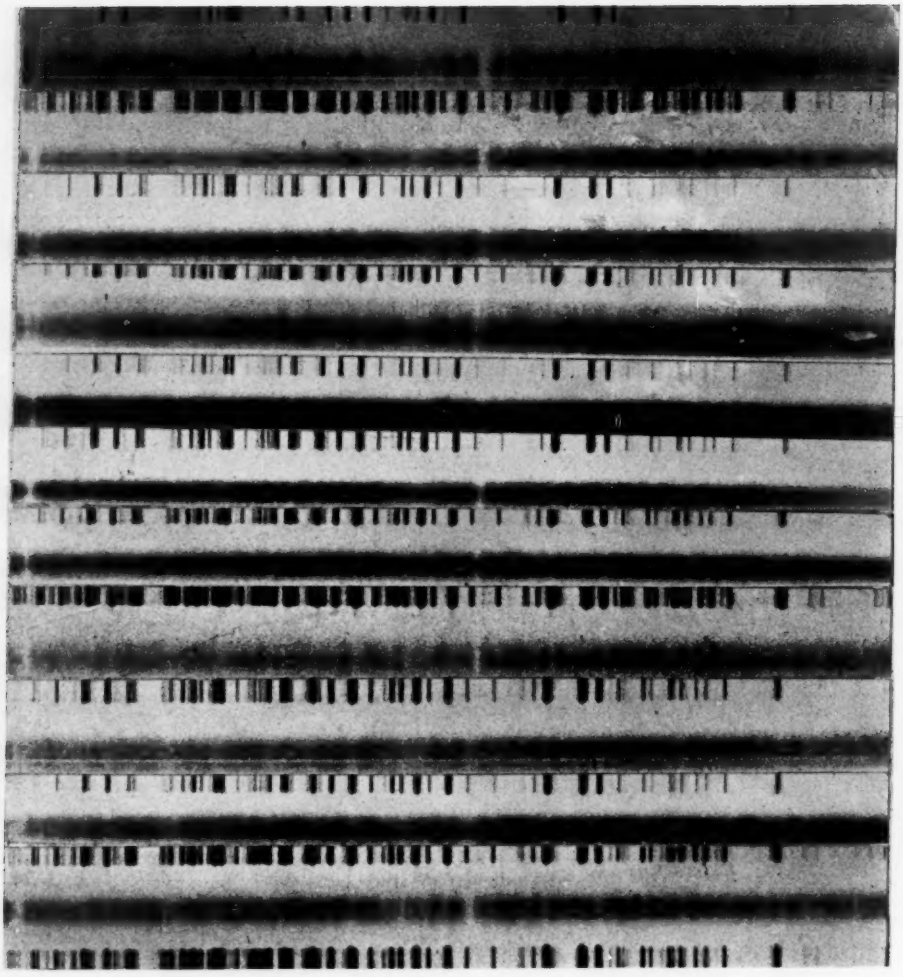

FIG. 5.—*Continued*

(or a very small) ellipticity; (4) the secondary minimum is shallow and seems to be much wider than the primary; (5) Max = $8^m.71$, $m_1 = 9^m.74$, $m_2 = 8^m.75$, $1 - \lambda_1 = 0.6127$, $1 - \lambda_2 = 0.0273$. In Table 9 are the basic data for computing the relative elements in accordance with the method of Scharbe.

Now, plotting $\sin^2 \varphi$ as abscissa against l as ordinate, we find, after two trials, the three values of $\sin^2 \varphi$ for $a = 0.1$, 0.5, and 0.9 to be 0.1144, 0.0770, and 0.0488, which give a function $f(k)$ equal to 0.0701, from which follows the ratio of radii 0.30, in full agreement with the depths of minima for the uniform solution. Scharbe's two constants, A and B, are 0.0070 and 12.50, respectively. Thus, $\cot^2 i = 0.00056$ ($i = 88°.6$).

TABLE 7

COMPARISON STARS FOR UX MONOCEROTIS

Star	IPg	Scale	Star	IPg	Scale
BD−7°2264 ($7^m.3$)	$8^m.15$:	+14	BD−6°2395 ($9^m.2$)	$9^m.63$	0
−6°2402 (8.7)	8.84	+ 6	−7°2287 (8.7)	10.02	− 4

TABLE 8

MEAN LIGHT-CURVE FOR UX MONOCEROTIS

Phase φ_0	IPg	No.	Phase φ_0	IPg	No.	Phase φ_0	IPg	No.	Phase φ_0	IPg	No.
$0^P.009$.....	$8^m.72$	29	$0^P.287$.....	$8^m.70$	40	$0^P.541$.....	$9^m.68$	23	$0^P.736$.....	$8^m.71$	27
.038.....	8.74	22	.309.....	8.73	36	.558.....	9.74	10	.762.....	8.70	53
.063.....	8.73	39	.337.....	8.72	36	.570.....	9.73	11	.788.....	8.71	29
.086.....	8.74	45	.362.....	8.69	51	.584.....	9.77	13	.812.....	8.71	30
.115.....	8.75	33	.388.....	8.69	32	.593.....	9.74	12	.840.....	8.70	38
.136.....	8.74	35	.411.....	8.71	30	.605.....	9.40	13	.862.....	8.71	35
.161.....	8.75	39	.437.....	8.71	35	.615.....	8.88	26	.886.....	8.71	35
.186.....	8.74	34	.460.....	8.72	37	.637.....	8.76	35	.913.....	8.70	31
.214.....	8.75	40	.486.....	8.71	36	.661.....	8.72	40	.934.....	8.73	29
.236.....	8.73	34	.511.....	8.86	27	.687.....	8.71	35	.966.....	8.72	47
0.261.....	8.72	27	0.525.....	9.32	16	0.712.....	8.70	31	0.988.....	8.72	33

The solution for the darkened limb of the A7 component was less satisfactory. A similar uniform solution was computed by Mrs. Shapley[2] in 1928 ($k = 0.42$ and $i = 88°.8$), though she used a photographic light-curve with fewer observations and with a deeper primary minimum, which was the result of a less standardized magnitude scale than that used here.

In Table 10 the computed light-curve is given for seven points within the primary minimum. The probable error of a normal point is between $0^m.025$ and $0^m.015$. There is no visual light-curve known to the author. On account of the striking spectroscopic peculiarities, one would expect an effect of the thick atmosphere to appear in this system. In Table 11 a summary of the results is given.

DISCUSSION

With respect to the spectroscopic peculiarities, the system UX Monocerotis presents an entirely new and unsolved problem among the eclipsing variables. Though we know of more than a dozen eclipsing systems which display the existence of extensive gaseous

[2] I. Woods and M. B. Shapley, *Harvard Bull.*, No. 854, p. 6, 1928.

masses around the components, none of them has shown such puzzling phenomena as the square contours of the *H* lines, the appearance of emission at both minima, and the apparent existence of at least two centers of orbital velocity for each component.

It is natural that we should discuss the system in an astrophysical sense, not confining ourselves to purely geometrical properties. There are now seven systems known which

TABLE 9

BASIC DATA FOR UX MONOCEROTIS

IPg	Phase	$\sin^2\varphi$	Δm	l	IPg	Phase	$\sin^2\varphi$	Δm	l
8^m72.....	0^P895*	0.3757	0^m01	0.991	9^m77.....	0^P019	0.0142	1^m06	0.377
8.71.....	.921	.2268	0.00	1.000	9.74.....	.028	.0306	1.03	0.387
8.86.....	.946	.1108	0.15	0.871	9.40.....	.040	.0619	0.69	0.530
9.32.....	.960	.0619	0.61	0.570	8.88.....	.050	.0955	0.17	0.855
9.68.....	.976	.0226	0.97	0.409	8.76.....	.072	.1911	0.05	0.955
9.74.....	.993	.0019	1.03	0.387	8.72.....	.096	.3218	0.01	0.991
9.73.....	0.005	0.0010	1.02	0.391	8.71.....	0.122	0.4811	0.00	1.000

* Computed from φ and $\varphi_0 = 0^P565$.

TABLE 10

COMPUTED LIGHT-CURVE FOR UX MONOCEROTIS

a	Φ	$\Phi-A$	$\sin^2\varphi$	φ	m
0.0.....	1.690	1.683	0.1346	0^P060	8^m71
0.1.....	1.437	1.430	.1144	.055	8.79
0.3.....	1.172	1.165	.0932	.049	8.93
0.5.....	0.970	0.963	.0770	.045	9.11
0.6.....	0.879	0.872	.0698	.043	9.21
0.9.....	0.617	0.610	.0488	.035	9.51
1.0.....	0.490	0.483	0.0386	0.031	9.74

TABLE 11

THE SYSTEM OF UX MONOCEROTIS

Spectroscopic Elements	Photometric Elements	Absolute Dimensions
$(a_1+a_2)\sin i = 15.71\ \odot$	$P = 5^d904604$	$R_G = 4.46\ \odot$
$(m_1+m_2)\sin^3 i = 1.47\ \odot$	$r_G = 0.283$	$R_A = 1.34\ \odot$
$e = 0.08$	$r_A = 0.085$	$m_A = 0.73\ \odot$
$\omega = 316°$	$k = 0.30$	$m_G = 0.74\ \odot$
$Sp_2 = A7p$	$i = 88.6$	
$Sp_1 = G2p$	$L_A = 0.61$	

are especially conspicuous for their astrophysical peculiarities. These are the two Wolf-Rayet eclipsing variables, V 444 Cygni (two spectra, the minima are shallow) and HV 11086 (one spectrum, shallow minima); the supergiants, υ Sagittarii, β Lyrae, and RY Scuti; and the two giants, SX and RX Cassiopeiae. Except for the two Wolf-Rayet stars, the rest represent systems with large components and long periods. It is interesting that the Wolf-Rayet systems, which have deep atmospheres, do not show any drastic changes in spectrum from cycle to cycle comparable to those in UX Monocerotis. The

system υ Sagittarii shows extraordinary spectral characteristics, but photometrically it is a very difficult star, the period being too long and the minima too shallow for continuous study. The systems RY Scuti and β Lyrae show high ellipticities of the components, and the latter are almost in contact. The only system which has a similar light-curve and spectral class is SX Cassiopeiae, but it has a period of 36 days.

This paper concludes a series of investigations which originated in connection with my visit to the McDonald Observatory in Texas. More than one hundred and fifty spectrograms were obtained for six eclipsing systems and a few individual stars. Three eclipsing systems—AS Eridani, RX Geminorum, and RY Geminorum—showed only one spectroscopic orbit. The other three—RT Andromedae, UV Leonis, and UX Monocerotis—are double-lined spectroscopic binaries. The great efficiency of the McDonald equipment and the generous scientific help of Dr. Struve and his staff are gratefully acknowledged.

LUMINOSITY FUNCTIONS OF THE BRIGHTER STARS*

JOHN W. ABRAMS[1]
Van Vleck Observatory, Wesleyan University
Received December 10, 1946

ABSTRACT

Luminosity functions are calculated for the giant and the supergiant ranges. Two methods are employed: the first, a modification of Strömberg's v-component method, and the second, a combined τ- and v-component method designed to eliminate spurious supergiants. The data are specially selected in order to obtain a maximum of supergiants and hence better resolution in the higher luminosities. Three rough groupings are made according to spectral type.

The supergiants appear well defined and clearly separated from the giants. In the F0–G0 spectral group an additional maximum appears to be present for the shorter-period ($P\sim10$ days) cepheids.

I. INTRODUCTION

In an extensive series of papers, G. Strömberg[2] developed and applied a method for determining the luminosity distribution of stars brighter than a given apparent magnitude from radial velocities and from τ- and v-components of proper motions. This method is of greater refinement than any which preceded it; however, it still admits of further refinements designed to increase the resolution in the luminosity function. Some of these improvements were pointed out by Oort[3] and by Öpik.[4] With the availability of more accurate data, it seemed that the application of a more refined method would be of value, particularly in the case of supergiants, because of the present uncertainty of their luminosity distribution and of the value of this knowledge in the analysis of star counts.

The great distances which separate us from the supergiants preclude the determination of trigonometric parallaxes for these stars, and their parallaxes are, perforce, found mainly from statistical treatments. Of the two statistical methods used by Strömberg, the one based upon parallactic velocities is to be preferred because it depends to a lesser degree upon a complete knowledge of the distribution of peculiar velocities and of their correlation with absolute magnitude.

The observational material (see Sec. VI) was divided into three groups according to spectral type. These groups, loosely called "A," "F," and "K," contained stars within the *Henry Draper* limits B8–A5, F0–G0, and G5–K5, respectively. Stars earlier than B8 were omitted because for them it would be necessary to use smaller subdivisions of spectral class and fainter stars would have to be included to obtain a sufficient number for statistical study. Stars later than K5 were not considered because of the small number available.

In order to obtain maximum resolving-power in the region of the supergiants, it was decided to make the faint limit of apparent magnitude as bright as possible without too seriously restricting the number of available stars. This limit was, therefore, set at $4^m.5$ visual for the A and K groups, and $5^m.0$ visual for the F group. This naturally served to enhance the ratio of supergiant to other stars. To increase this ratio further, as well as to secure greater homogeneity of material, the region of the sky from which the stars

* *Contributions from the Lick Observatory*, Ser. II, No. 17.

[1] Lick Observatory Fellow, 1938–1939.

[2] *Mt. W. Contr.*, Nos. 395, 396, 410, 411, 418, 430, 440, 442, 554; *Ap. J.*, **71**, 163, 175, 1930; **72**, 111, 117, 1930; **73**, 40, 110, 342, 1931; **75**, 115, 1932; **84**, 412, 1936.

[3] *Bull. Astr. Inst. Netherlands*, **6**, 289, 1932.

[4] *Harvard Circ.*, No. 381.

were selected was restricted to a belt 60° wide, centered on the galactic plane. Finally, to obtain better resolution in the supergiant range, a method of "reduced" τ-components was developed that excluded large τ-components and eliminated stars which possess small v-components but for which the total proper motion is not small. It was felt that the combination of these factors of selection would place our present knowledge of the supergiants upon a more firm basis.

II. OUTLINE OF METHOD

Let

μ_v = v-component of proper motion ;

t_{p_v} = Peculiar v tangential velocity, i.e., the component of the tangential velocity in the direction of the solar motion ;

V_0 = Solar velocity = 19.65 km/sec (adopted) ;

λ = Angular distance to antapex ;

p = Parallax .

Now

$$\frac{4.74}{p}\,\mu_v = V_0 \sin \lambda + t_{p_v}, \tag{1}$$

and

$$M = m + 5 + 5 \log p\ , \tag{2}$$

where M and m are the visual absolute and apparent magnitudes, respectively, and interstellar light-absorption is neglected. Equation (1) has been developed more fully by Strömberg.[5]

By elimination of the logarithmic form of equation (2) and the substitution of p from equation (2) into equation (1), we get

$$\frac{47.4}{\sin \lambda}\,\mu_v 10^{m/5} = \left(V_0 + \frac{t_{p_v}}{\sin \lambda}\right) 10^{M/5}. \tag{3}$$

Equation (3) is transformed into the form

$$x = yz \tag{3'}$$

by the introduction of the three auxiliary variables,

$$\left.\begin{aligned} x &= \frac{47.4}{\sin \lambda}\,\mu_v 10^{m/5}, \\ y &= V_0 + \frac{t_{p_v}}{\sin \lambda}, \\ z &= 10^{M/5}. \end{aligned}\right\} \tag{4}$$

A consideration of equation (3′) shows that each of the three variables is of different nature: x contains only known observable quantities and can be computed for each star individually; y contains, besides the known solar velocity, the peculiar tangential velocity whose distribution can be established statistically from radial-velocity observations; and z contains the desired unknown, M. It may also be noted that x and y should not be used when sin λ is small; accordingly, the regions within 20° from the apex and antapex

[5] *Mt. W. Contr.*, No. 410; *Ap. J.*, **72**, 111, 1930.

were not used. Because y is known only statistically from its frequency function, our entire problem becomes a statistical one involving the relations between the frequency functions of the variables x, y, and z.

In the case of equation (3′), we have

$$\Phi(x)\,\Delta x = \Delta x \int_0^\infty \chi(y)\,\Psi(z)\,\frac{dz}{z}; \qquad y = \frac{x}{z}, \tag{5}$$

where $\Phi(x)$, $\chi(y)$, and $\Psi(z)$ are the relative frequency functions of these variables when y and x are not correlated. This is not strictly applicable here, because of the correlation between M and space velocity; thus, strictly, $\chi(y)$ varies with z. This correlation will be taken into account later.

While equation (5) admits of solution by numerical integration, it does require logarithmic interpolation in the $\chi(y)$, with consequent computational difficulties. A simplification is readily made by noting that x and y must always be of the same sign because of the essentially positive nature of z. Therefore, if we consider positive and negative values of x separately, we can adopt a logarithmic form for the parameters themselves and can eliminate our logarithmic interpolation. The results obtained by considering positive and negative x separately can then be combined for inspection. Mathematically, this can be done as follows:

when $x < 0$:

$$\left.\begin{aligned} A' &= \log(-x) \\ B' &= \log(-y) \\ C &= \log(z) = \frac{M}{5} \end{aligned}\right\} \tag{6}$$

when $x > 0$:

$$\left.\begin{aligned} A &= \log(x) \\ B &= \log(y) \\ C &= \log(z) = \frac{M}{5} \end{aligned}\right\} \tag{7}$$

Equation (3′) thereby assumes the forms

$$\left.\begin{aligned} A &= B + C, \quad \text{for} \quad x > 0, \\ A' &= B' + C, \quad \text{for} \quad x < 0; \end{aligned}\right\} \tag{8}$$

and the relations between the frequency functions of these new parameters become

$$\Phi_1(A)\,\Delta A = \Delta A \int_{-\infty}^{+\infty} \chi_1(B)\,\Psi_1(C)\,dC, \qquad B = A - C, \tag{9a}$$

and

$$\Phi_2(A')\,\Delta A' = \Delta A' \int_{-8}^{+\infty} \chi_2(B')\,\Psi_1(C)\,dC, \qquad B' = A' - C. \tag{9b}$$

Of the terms appearing in equations (9a) and (9b), $\Phi_1(A)$ and $\Phi_2(A')$ are directly calculable; $\chi_1(B)$ and $\chi_2(B')$ can be obtained from radial velocities; and $\Psi_1(C)$ possesses a linear relationship to the desired luminosity function. If $L(M)$ is the absolute frequency function representing a distribution of luminosities, i.e., the number of stars whose absolute magnitudes fall in the interval $M - \frac{1}{2}$ to $M + \frac{1}{2}$, then

$$L(M) = \frac{N}{5}\Psi_1(C), \tag{10}$$

where N = total number of stars in the group.

In practice, a trial-and-error solution was made for equations (9*a*) and (9*b*) to yield a preliminary value of $L(M)$. This was next used as a basis for a second solution, in which the correlation between y and z, or between B and C, was taken into account. Dwarf stars were not included in the statistical solution, and their absolute magnitudes were found from trigonometric parallaxes.

III. DISTRIBUTION OF SPACE VELOCITIES

Although it was recognized that the only type of velocity distribution which would be entirely satisfactory would be one derived for the stars under consideration, sufficient data were not available in each spectral class to obtain a good solution for all nine parameters of the velocity ellipsoid. Therefore, the less variable parameters were assumed, and a conditioned least-squares solution was made for the remainder.

It was assumed that:

(*a*) V_0 = Solar velocity = 19.65 km/sec;

(*b*) α_0, δ_0 = Co-ordinates of the solar apex, $\alpha_0 = 18^h$, $\delta_0 = +34°$;

(*c*) For the directions of the principal axes of the ellipsoid, the xy-plane is the galactic plane, with the x-axis pointing toward galactic longitude 340°.

TABLE 1

CONSTANTS OF THE VELOCITY ELLIPSOIDS

Group *HD* Sp. Cl.	No. Stars	σ_x	σ_y	σ_z	Limiting m	Limits of M
A (B8–A5)	114	18.5	6.5	5.0	4.5	None
F (F0–G0)	129	23.1	12.1	12.1	5.0	$M<3.5$
K (G5–K5)	169	24.2	11.1	11.1	4.5	$M<3.0$

In the case of the F and K stars, the further assumption was made that $\sigma_y = \sigma_z$, i.e., the y- and z-axes of the ellipsoid were equal. Use was then made of the well-known expression[6] connecting the velocity dispersion in a particular direction with known direction cosines L, M, and N, with the dispersions along the principal axes of the velocity ellipsoid; namely,

$$\sigma^2 = L^2\sigma_x^2 + M^2\sigma_y^2 + N^2\sigma_z^2 . \qquad (11)$$

In practice this was applied as follows: Since only stars within 30° of the galactic plane were to be considered, the sky was divided into three belts, each 20° wide, with the middle belt centered on the galactic equator. Each belt was then split into twelve equal regions, 30° in length, thereby dividing the regions under consideration into thirty-six areas. Within each of these areas the dispersion in the peculiar radial velocities was computed, the peculiar radial velocities having been previously obtained from the observed radial velocities by removing the solar-motion component. The thirty-six observed dispersions in the peculiar radial velocities yielded thirty-six condition equations of the form of equation (11). These equations were weighted according to the number of stars in the area, and a least-squares solution was made to determine σ_x, σ_y, and σ_z. The results are shown in Table 1.

[6] C. W. L. Charlier, *The Motion and Distribution of the Stars* ("Memoirs of the University of California," Vol. 7 [1926]), p. 48.

In the case of the A stars, the least-squares solution yielded an imaginary value for σ_z, but an approximate value of 5.0 was then obtained from a consideration of the τ-components. The K stars were treated somewhat differently, and two velocity ellipsoids were employed to take into account the high-velocity stars; the procedure is described in the next section. The value given here is for the normal ellipsoid. The limiting values of M were determined from trigonometric parallaxes.

IV. HIGH-VELOCITY STARS

The asymmetric distribution of the high-velocity stars makes it difficult to attempt to express the velocity distribution of a group which includes such stars by means of a single analytic distribution function. In order to obtain a distribution function which would accurately express this characteristic of stellar motions, it would be necessary to employ a series of ellipsoids of different dispersions, whose centers should lie along the line of direction of the drift and whose displacements should vary with their dispersions according to the parabolic rule of Strömberg.[7] To adopt such a law as a basis for actual computation is fraught with difficulties, for we do not know the individual stars which belong to each distribution. In this work it was decided to represent this phenomenon, at least to a first approximation, if necessary, by the superposition of two ellipsoidal distribution laws, a normal ellipsoid (i.e., $V_0 = 19.65$ km/sec), and a high-velocity ellipsoid. The criterion for the necessity of employing this second ellipsoid was to be an observed excess of large peculiar radial velocities above the number predicted on the basis of the ellipsoid computed from all stars. Only in the case of the K stars was this excess considered significant. Although a similar treatment might be considered necessary for the F stars, it did not appear to be called for by the above criterion. A further factor was the smaller number of stars in this latter group.

The determination of the characteristics of the second ellipsoid was undertaken as follows: A preliminary ellipsoid was computed according to the method of the preceding section, but with the exclusion of all stars whose peculiar radial velocities exceeded 60 km/sec. From this preliminary ellipsoid a computed value of the dispersion in radial velocities was derived for each of the thirty-six areas. All stars whose peculiar radial velocities exceeded 2σ for their respective areas were removed. From the remaining stars a second least-squares solution was made for the dispersions along the axes of an ellipsoid, in the same manner as before. The dispersions obtained by this method, σ_r, the so-called "reduced" dispersions, can be related to the ordinary dispersion, σ, expected from a normal frequency law, by the relation

$$\sigma = 1.2924\sigma_r . \tag{12}$$

The advantage of computing the ellipsoid in this fashion lies in the fact that we have decreased the number of stars belonging to the high-velocity ellipsoid, which otherwise would have tended to introduce an error in the values of the axes. The constants of this ellipsoid are given in Table 1.

This ellipsoid was then adopted as representing the stars of normal velocity, and the excess in high velocities was attributed to the high-velocity distribution. From a consideration of this excess, a solution was made by trial and error to obtain a high-velocity ellipsoid with sufficient stars attributed to it to reproduce the observed number and dispersion of high-velocity stars. The values adopted were

$$V_H = \text{Asymmetric velocity} = 35 \text{ km/sec} ,$$

$$\sigma_x = 72 \text{ km/sec} ,$$

and

$$\sigma_y = \sigma_z = 36 \text{ km/sec} .$$

Sixteen per cent of the stars belonged to the high-velocity group.

[7] *Mt. W. Contr.*, No. 293; *Ap. J.*, **61**, 363, 1925.

This adopted distribution was found to be in excellent agreement not only with the radial-velocity distribution but also with the number of positive and negative v-components and with the distributions of the τ-components. The method of comparison will be shown in a later section.

V. DISTRIBUTION OF THE TANGENTIAL VELOCITIES IN THE v-DIRECTION

After the expressions for the velocity distributions had been obtained, it was necessary to derive from them the distribution function of t_{p_v}, or $\chi(t_{p_v})$. As this function varies throughout the sky, it was necessarily computed for each of the thirty-six areas. Our immediate interest, however, lies in the determination of the $\chi(y)$, where $y = V_0 + t_{p_v}/\sin\lambda$. This was obtained from the $\chi(t_{p_v})$ by dividing the dispersion in each area by $\sqrt{\sin\lambda}$ for that area; in this manner the dispersion characterizing the normal distribution of $t_{p_v}/\sqrt{\sin\lambda}$ was found in that area. This normal frequency distribution was then expressed as an absolute frequency function, whose summation equaled the number of stars found in the area. Next, these absolute functions were summed over the sky—except for the regions within 20° of the apex or antapex—and the result was expressed as a relative frequency function. From this mean composite function, the $\chi(y)$ was obtained by shifting the origin by V_0.

At this point it was possible to obtain a second check upon the adopted distributions, because the number of stars with $(V_0 + [t_{p_v}/\sin\lambda]) > 0$ should equal those with $\mu_v > 0$ after correction for observational errors. This check was introduced as a necessary condition for the adoption of a distribution.

With $\chi(y)$, known, $\chi_i(B)$ was found from

$$\left.\begin{aligned} \frac{1}{\text{Mod.}}\, y\chi(y) &= \chi_1(B), \qquad y > 0, \\ \frac{1}{\text{Mod.}}\,(-y)\,\chi(-y) &= \chi_2(B'), \qquad y < 0. \end{aligned}\right\} \tag{13}$$

and

The expressions $\chi_1(B)$ and $\chi_2(B')$ were tabulated for each spectral group.

VI. SOURCES OF DATA

1. *Radial velocities.*—The radial velocities were obtained from Moore's *General Catalogue of Radial Velocities*[8] and thus were expressed on the system of the Mills spectrograph, as was the solar velocity.

2. *Magnitudes.*—The magnitudes were taken from the catalogue of visual magnitudes by Mrs. Payne-Gaposchkin.[9] All A and K stars brighter than $4^m.50$ and all F stars brighter than $5^m.00$ were used. Inasmuch as this catalogue is not complete, a check was made through other catalogues to insure completeness. All magnitudes, however, were reduced to the scale of the above-mentioned catalogue. In the case of double stars, a combined magnitude was used if the stars would not show a separation of 1″ at 10,000 parsecs.

3. *Co-ordinates.*—The α_{1900} and δ_{1900} were taken from Moore's *Radial Velocity Catalogue* and Schlesinger's *Catalogue of Bright Stars*.[10] They were converted into galactic coordinates by means of Ohlsson's tables.[11] They were also used to determine the angular distance from the antapex, and the position angle of the antapex from Smart's charts.[12]

[8] *Pub. Lick Obs.*, Vol. 18, 1932.

[9] *Harvard Obs. Mim.*, Ser. III, Nos. 1 and 2.

[10] Yale University Observatory, 1930.

[11] *Annals of the Observatory of Lund*, No. 3, 1932.

[12] *Charts Giving the Angular Distance of Stars from, and the Position Angles Relative to, the Ant-apex of the Solar Motion*, London: Royal Astronomical Society, 1923.

4. *Proper motions.*—The expressions μ_α^* and μ_δ'' were obtained from Boss's *General Catalogue.*[13] They were reduced to 1900.

5. *Spectral type.*—The *Henry Draper* classification was used throughout, except where a mean spectrum type corresponding approximately to the composite spectrum was employed to combine binaries.

6. *Trigonometric parallaxes.*—The trigonometric parallaxes which were used to eliminate the dwarf stars in groups F and K were obtained from Schlesinger's *General Catalogue of Stellar Parallaxes,*[14] and the Yale Observatory *Transactions,* Volume **8**. Professor Schlesinger also very kindly supplied the writer with additional parallaxes.

7. *Star clusters.*—Individual members of small-diameter clusters should be excluded from a study of this type, because of the influence of the similarity of their motions on the velocity ellipsoids. Accordingly, stars in the Pleiades and in the Taurus cluster were removed.

VII. DWARF STARS AND CEPHEID VARIABLES

Because of the bright value of the limiting apparent magnitude, very few dwarfs were among the acceptable stars. Furthermore, their luminosity distribution could be better determined by trigonometric methods than by statistical ones. Hence F stars with $M > 3^m5$ and K stars with $M > 3^m0$ were excluded from the statistical discussion. The $L(M)$ for these stars was determined by trigonometric parallaxes. This imposed a boundary condition of continuity on the $L(M)$ as determined from the integral equation.

Variable stars were included in the statistical study in order to give a better correspondence to an observable function. Cepheid variables, however, offered an analogous situation to the dwarfs, inasmuch as their absolute magnitudes could be determined from the period-luminosity curve. Hence they, too, were excluded from the statistical discussion but were added later in the final adopted $L(M)$.

VIII. TREATMENT OF DATA AND SOLUTION OF THE INTEGRAL EQUATIONS

The τ- and υ-components of the proper motion were computed principally by means of a mechanical device built to facilitate this operation. After the values of μ_υ had been obtained, they were corrected for galactic rotation. With the corrected values of μ_υ, x was computed for each star, and the values were arranged in the form of a frequency function, $\Phi(x)$. This frequency function was corrected for errors in the proper motions and converted to the logarithmic form, according to the following formulae:

$$\left.\begin{aligned} \Phi_1(A) &= \frac{1}{\text{Mod.}} x\Phi(x), \qquad x > 0, \\ \text{and} \qquad \Phi_2(A') &= \frac{1}{\text{Mod.}} (-x)\,\Phi(-x), \qquad x < 0. \end{aligned}\right\} \tag{14}$$

The $\Phi_1(A)$ and $\Phi_2(A')$ thus computed were used in the solutions of the integral equations.

As we have seen before, the luminosity function can be obtained by a simultaneous solution of the two integral equations (9*a*) and (9*b*). In these equations it is to be noted that the unknown function $\Psi_1(C)$ is located under the integral sign. Of the two equations, (9*a*) is considerably more important than (9*b*), because of the larger number of stars to which it applies. It was therefore solved first, and the result was checked by equation (9*b*), which served only to yield minor adjustments.

Equations (9*a*) and (9*b*) lent themselves readily to solution by trial and error. An assumption for $\Psi_1(C)$ was made, its values for successive intervals of C multiplied by the values of $\chi_1(B)$, $B = A - C$, and the product was numerically integrated. The computed $\Phi_1(A)$ so obtained could be compared with the $\Phi_1(A)$ as observed. By inspection of lead-

[13] Carnegie Institution of Washington, 1936.

[14] Second printing, Yale University Observatory, 1935.

ing terms, the assumed $\Psi_1(C)$ was altered until the computed $\Phi_1(A)$ agreed with the observed function. The $\Psi_1(C)$ was then placed in equation (9*b*), and the process was repeated.

When a satisfactory solution for $\Psi_1(C)$ was eventually obtained, the computed values of $\Phi_1(A)$ and $\Phi_2(A')$ were transformed into a single frequency function of x, $\Phi(x)$. This computed $\Phi(x)$ was then compared with the observed $\Phi(x)$. The comparison of linear functions was decidedly superior to the comparison of logarithmic ones, because it permitted clear perception of just how the adopted luminosity function would reproduce a linear function of the observed proper motions. Illustrations of the comparisons and agreements are given in Figures 1–3. Finally, the luminosity functions, $L(M)$, derived from $\Psi_1(C)$, were used as a basis for the τ-component method and for further refinements.

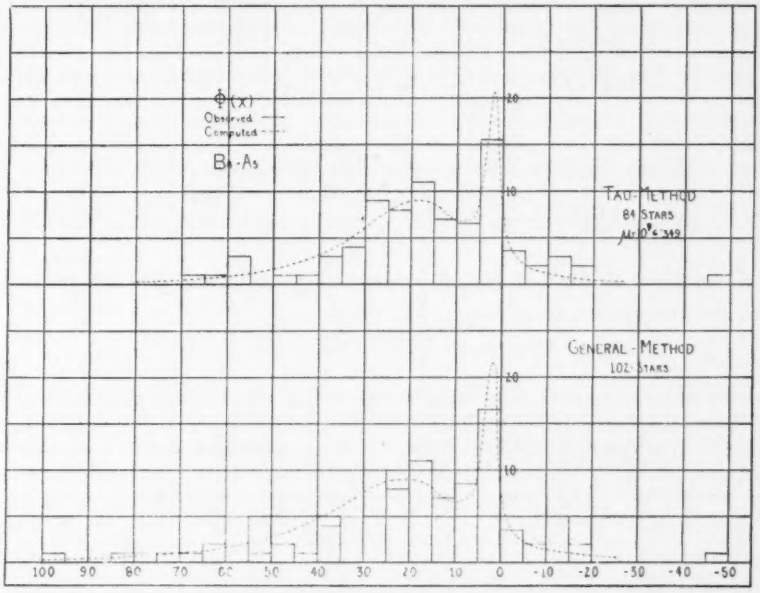

FIG. 1.—Comparison of observed $\Phi(x)$ with computed (B8–A5 stars). The ordinates are numbers of stars, and the abscissae values of $x = \dfrac{47.4}{\sin \lambda}\, \mu_v\, 10^{\frac{m}{5}}$.

IX. τ-COMPONENT METHOD

The purpose of this method was to eliminate from consideration as possible supergiants those stars which accidentally possess small v-components. This was accomplished by removing that 20 per cent or so of the stars which had the largest reduced τ-components ($\mu_\tau\, 10^{m/5}$). Obviously, such a selection should distort the luminosity distribution by removing stars of lower luminosity. This effect was a desired one, for, by increasing the percentage of high-luminosity stars, a more accurate knowledge of their characteristics could be obtained.

The effect of this distortion on the luminosity function was calculable from a study of the tangential motions in the τ-direction after a preliminary value of the luminosity function was known. The following procedure was used. Let

$L(M)$ = Preliminary value of the luminosity function obtained as in the preceding section,

and

$L'(M)$ = The luminosity distribution obtained from the selected data with stars of large reduced τ-components removed.

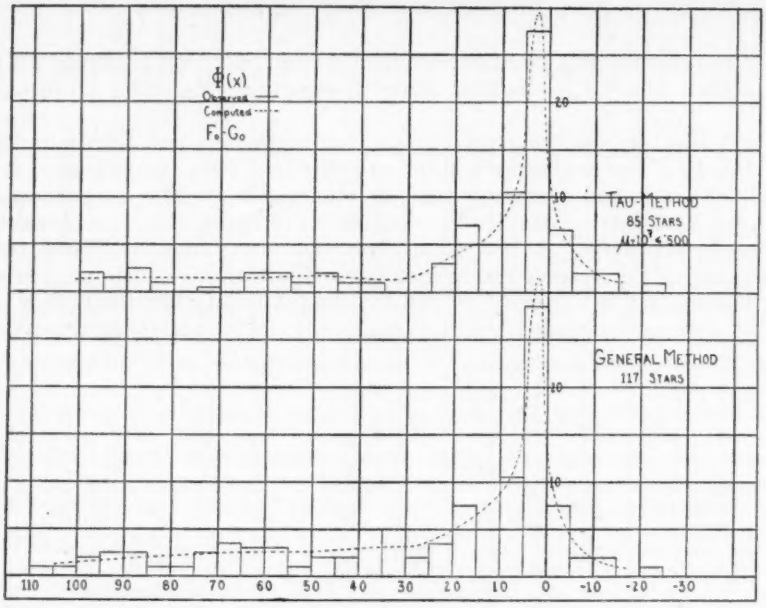

FIG. 2.—Comparison of observed $\Phi(x)$ with computed (F0–G0 stars). The ordinates are numbers of stars, and the abscissae values of $x = \dfrac{47.4}{\sin \lambda}\, \mu_v\, 10^{\frac{m}{5}}$.

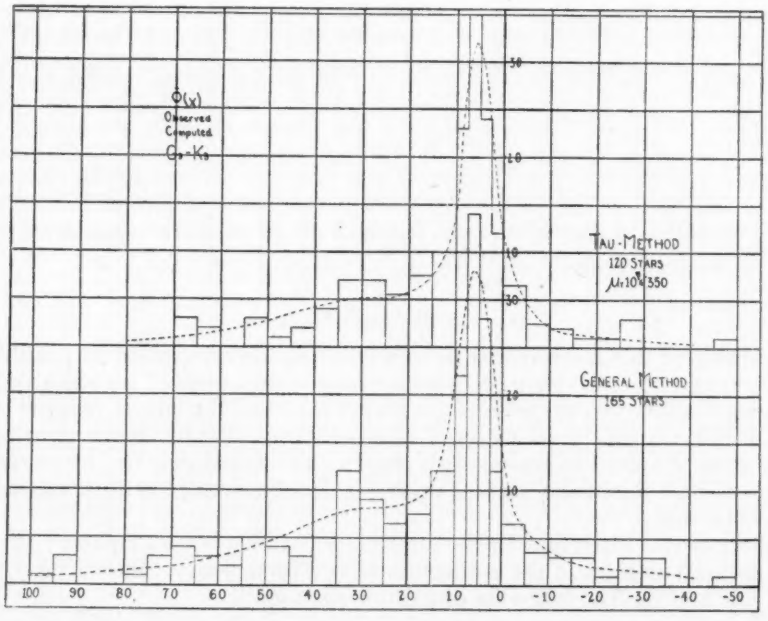

FIG. 3.—Comparison of observed $\Phi(x)$ with computed (G5–K5 stars). The ordinates are numbers of stars, and the abscissae values of $x = \dfrac{47.4}{\sin \lambda}\, \mu_v\, 10^{\frac{m}{5}}$.

Then let $i(M)$ be the so-called incompleteness factor, defined by

$$L(M) = i(M)\, L'(M). \tag{15}$$

By an analogous method to that used for the v-components, we have:

$$t_\tau 10^{M/5} = 47.4\,(\mu_\tau 10^{m/5}). \tag{16}$$

Thus we see that when a maximum limit for $\mu_\tau 10^{m/5}$ is set, a corresponding maximum is set for $t_\tau\, 10^{M/5}$. From this can be computed the maximum allowable value of t_τ for each absolute magnitude. Then, if we have the relative frequency function of the tangential τ-velocities, $\Theta(t_\tau)$, $i(M)$ can be obtained from

$$\frac{1}{i(M)} = \int_0^{t_{\tau_{\max}}} \Theta(t_\tau)\, dt_\tau\,; \tag{17}$$

$\Theta(t_\tau)$ was obtained from the velocity ellipsoids in a manner similar to that used in computing $\chi(t_{p_v})$.

This method permitted the evaluation of $i(M)$ theoretically, but it was deemed advisable at this point to compare it with observation, and for this purpose the preliminary luminosity function was employed, as follows:

If $L(M)$ and $\Theta(t_\tau)$ are reasonably accurate, the following relation should hold:

$$\left.\begin{aligned} &\int_M L(M) \left[\int_{t_{\tau_{\max}}}^{\infty} \Theta(t_\tau)\, dt_\tau\right] dM \\ &\qquad = \text{No. of stars with } \mu_\tau 10^{m/5} \text{ greater than } (\mu_\tau 10^{m/5})_{\max}\,, \end{aligned}\right\} \tag{18}$$

where $L(M)$ is an absolute frequency function. Agreement with this relation was made a necessary condition for the adoption of any velocity distribution. After suitable values of $i(M)$ had been obtained, the integral equations (9*a*) and (9*b*) were set up and solved. The solutions were undertaken as before, except that $\Psi_1(C)$ yielded $L'(M)$ instead of $L(M)$. The latter was obtained from the former by equation (15).

The $L(M)$ determined by this method was compared with that found from the preceding method. The final adopted $L(M)$ was a mean between the two methods, with greater weight given to the latter method in the range of higher luminosities and less weight for the remainder of the curve.

X. VARIATION OF VELOCITY WITH M

From the manner in which $\chi(t_{p_v})$ and $\Theta(t_\tau)$ were determined, it is clear that they represent some sort of a mean value for all absolute magnitudes. However, since it is known from observation that the velocity dispersion decreases with increasing luminosity, allowance for this effect is possible, although such an empirical correction could be applied only to the F and K spectral groups, because there is little information concerning the velocity dispersion of supergiants.

The luminosity distribution, $L(M)$, obtained from the mean velocity function, showed the stars to be arranged in well-defined absolute-magnitude groups. Hence, instead of assuming $\chi(B)$ to vary continuously with C, a separate distribution function was used for each group. The relative number of stars in each group was taken from the previously determined $L(M)$. The space velocities of the stars in a given spectral division were thus assumed to be represented by the superposition of several ellipsoidal distribution laws, each applying to one of the luminosity groups. As the absolute magnitudes of the individual stars are not known, the dispersions of the different ellipsoids had to be obtained by trial and error, so that their superposition would fit the observed distribution of

radial velocities. The weights used in different areas also had to take into account the greater galactic concentration of the supergiants.

With the new velocity-distribution laws, each of the integral equations became of the form

$$\left.\begin{aligned}\Phi(A)\,\Delta A = \Delta A \int_{-\infty}^{C_I} \chi_I(B)\,\Psi(C)\,dC \\ + \Delta A \int_{C_I}^{C_{II}} \chi_{II}(B)\,\Psi(C)\,dC + \ldots\ldots, \qquad B = A - C,\end{aligned}\right\} \tag{19}$$

where $\chi_i(B)$ was the distribution function valid over the integration interval in C, i.e., over the appropriate range in M. The dispersions obtained for the different ellipsoids are given in Table 2.

TABLE 2

RELATION BETWEEN VELOCITY ELLIPSOIDS AND ABSOLUTE MAGNITUDES

Spectral Group	Range in M	σ_x	σ_y, σ_z
F.....	$-\infty$ to -3.125	12.1	12.1
	-3.125 to 0.0	22.0	12.1
	0.0 to $+3.5$	28.0	12.1
K.....	$M<-1.25$	11.1	11.1
	$M>-1.25$	27.0	11.1*

* To this distribution was added the asymmetric high-velocity ellipsoid.

The velocity distributions of Table 2 were used to make another determination of $\Psi(C)$ by both the general and the τ-component methods. It was found that, although they did not greatly alter the values of $L(M)$, they did improve markedly the fit between the observed and the computed values of $\Phi(x)$. The results of the application of this correction are shown in Figures 1–6.

XI. ABSORPTION

As the data were selected on the basis of apparent magnitudes, they consequently are affected by the absorption of light in interstellar space. How this entered may be seen by a reconsideration of the fundamental equations of the method: equation (1) is unaltered, but equation (2) is no longer valid.

If we assume a uniform absorption for the limited volume of space within which our stars are situated, equation (2) becomes

$$M = m + 5 + 5 \log p - a r\,, \tag{2'}$$

where

a = Absorption in mag/kpc .

and

r = Distance in kiloparsecs .

From equations (1) and (2′) we get

$$\frac{47.4}{\sin \lambda}\,\mu_v 10^{m/5} = \left(V_0 + \frac{l_{p_v}}{\sin \lambda}\right) 10^{(M+ar)/5}. \tag{3a}$$

Now if x and y remain as before, then, in order for equation (3′) to remain of the same form as before, we must define a new z by

$$z' = 10^{(M+ar)/5} . \tag{4'}$$

From equation (4′) we see that, in reality, we have solved for $L(M + ar)$ instead of for $L(M)$.

If all stars were of the same apparent magnitude, $L(M + ar)$ would be only a function of M, and the distribution law of M could be derived from that of z'. Although this equality of apparent magnitude is not fulfilled, most of the stars lie in a fairly small magnitude range, and a correction based on their mean magnitude should be good to the first order. By elimination of the few stars brighter than $2^m.5$, the mean magnitude $\bar{m}$ was obtained for the remainder. With this mean magnitude considered to apply to all the stars, each $M + ar$ was reduced to its corresponding M from:

$$M + a\bar{r} = \bar{m} + 5 - 5\,\overline{\log r} . \tag{20}$$

The assumption was then made that $\overline{\log r}$ did not differ greatly from $\log \bar{r}$, which was justifiable over the range used and to the required degree of approximation. Equation (20) thus became

$$M + a\bar{r} = \bar{m} + 5 - 5 \log \bar{r} . \tag{21}$$

As $\bar{m}$ was known, $\bar{r}$ was found from this equation for every given value of $(M + a\bar{r})$. By taking a equal to $0^m.5$/kpc., values of M were obtained which correspond to each value of $(M + a\bar{r})$.

This correction of the luminosity function then merely required an adjustment of the abscissae in $L(M + ar)$, which was readily made. While this method will overcorrect the bright stars and undercorrect the faint ones, the discrepancy will not be serious.

XII. SUMMARY OF RESULTS

The values of $L(M)$ obtained directly from the solution of the integral equations were adjusted to include dwarfs and cepheids and were corrected for absorption. The adjusted values of $L(M)$ are given in Table 3 and shown graphically in Figures 4–6.

Because of the different methods of selection and spectral groupings employed, it is difficult to compare the results of this method with those of other determinations. They are, however, in fair agreement with the values given by Öpik[15] and by Strömberg.[16]

A rough comparison was made with the results of R. E. Wilson's[17] work on the c-stars. It was found that approximately twice as many supergiant stars were predicted by this method as were predicted by him as c-stars. This seems to indicate that, although c-characteristics appear to be associated with some supergiants, they are not a necessary attribute of these stars.

It is also of interest to compare the absolute magnitudes of the peaks of the luminosity-curves determined by this method with the mean absolute magnitudes for supergiants determined elsewhere. The comparison is given in Table 4.

The agreement between the various methods is fairly satisfactory. Further support for these results is provided by P. van Rhijn's work on the O and B stars.[18]

The features of $L(M)$ found by this method are, in general, the expected ones, with the exception of the low luminosity found for F giants and the maximum found between

[15] *Loc. cit.*

[16] *Loc. cit.*

[17] *Mt. W. Contr.*, No. 643; *Ap. J.*, **93**, 379, 1941.

[18] *Pub. Kapteyn Astr. Lab.*, No. 51, 1946.

TABLE 3

ADOPTED VALUES OF $L(M)$

M	A Stars	F Stars*	K Stars	M	A Stars	F Stars*	K Stars
−7.5	0.1	.....	.....		1.1	4.1	.....
−7.0	0.3	.....	.....	−1.0	5.2	1.2	.....
	1.2	0.4	.....		14.0	0.6	1.8
−6.0	2.2	0.8	.....	0.0	25.1	1.2	83.8
	3.1	3.0	.....		24.4	4.2	25.3
−5.0	3.8	4.7	.....	+1.0	9.2	8.6	1.1
	3.6	5.2	.....		3.2	14.8	.....
−4.0	2.4	1.7	.....	+2.0	0.9	9.2	0.2
	1.2	0.8 (0.6)	8.5			3.1	0.8
−3.0	0.5	2.5	43.2	+3.0	.....	2.6	.....
	0.1	4.2 (2.6)	0.2	+3.5	.....	.....	.....
−2.0	0.3	3.7 (1.3)	.....				

* The number of F stars has been reduced to the number brighter than apparent magnitude 4.5. Cepheid variables are shown in parentheses.

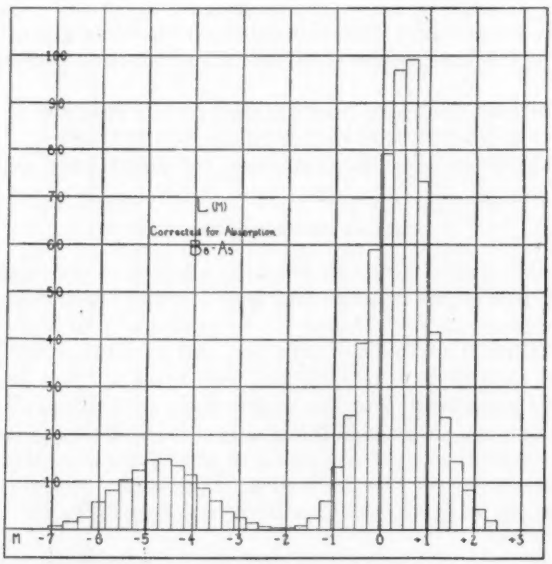

FIG. 4.—The luminosity distribution for (B8–A5) stars as a relative frequency function. The ordinates are relative numbers of stars, and the abscissae are values of the absolute magnitude, M.

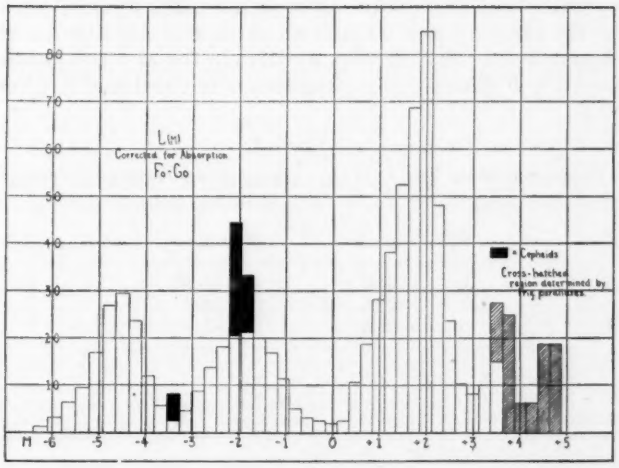

FIG. 5.—The luminosity distribution for (F0–G0) stars as a relative frequency function. The ordinates are relative numbers of stars, and the abscissae are values of the absolute magnitude, M. Cepheid variables, whose absolute magnitudes were determined from the period-luminosity-curve, are shown in solid black. Dwarfs, whose luminosities were determined by trigonometric parallaxes, are shown cross-hatched.

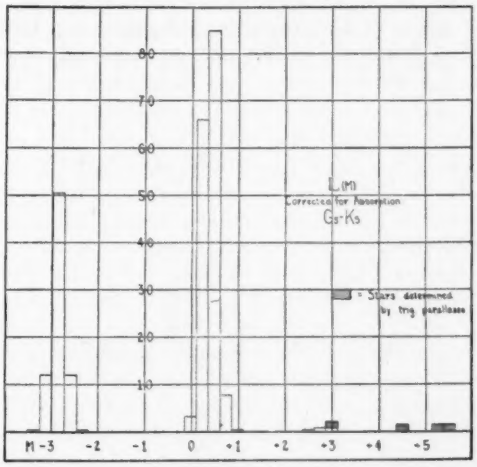

FIG. 6.—The luminosity distribution for (G5–K5) stars as a relative frequency function. The ordinates are relative numbers of stars, and the abscissae are values of the absolute magnitude, M.

the F giants and the supergiants. The position found for the maximum of the F giants may easily be a statistical fluctuation, inasmuch as this method loses some of its resolving-power in the range of lower luminosities. It may also be due partly to the inability to take into account the high-velocity stars in this spectral group. The maximum appearing between the F giants and supergiants is of considerable interest. It was previously suggested by Öpik's[19] work, as well as by the luminosity distributions found in galactic clusters. The fact that this maximum can be extended to include the cepheid variables is most interesting.

TABLE 4

COMPARISON OF PEAK MAGNITUDES WITH OTHER METHODS

Spectral Type	Peak *M*	*M* (Wilson*)	*M* (Greenstein†)
A	−4.8	−4.8	−5.4
F	4.5, −1.8	4.1	5.1
K	−2.9	−2.3	−3.5

* *Mt. W. Contr.*, No. 643; *Ap. J.*, **93**, 379, 1941.

† *Proc. Nat. Acad. Sci.*, **26**, 263, 1940. The figures quoted above were not taken directly from Greenstein's paper but have been derived from it to apply to the spectral groupings used here. The systematic difference is due in part to Greenstein's use of a visual absorption coefficient of 0m93/kpc.

I should like to express my appreciation to Professor R. J. Trumpler, who suggested this problem, for his friendly advice and invaluable suggestions. I am also indebted to the Regents of the University of California for the grant of a Lick Observatory Fellowship, during my tenure of which the major part of this study was made.

[19] *Loc cit.*

A STUDY OF THE SPECTRUM VARIABLES OF TYPE A

ARMIN J. DEUTSCH
Yerkes Observatory
Received November 16, 1946

ABSTRACT

The periods of variation have been found for the five spectrum variables BD−18°3789, BD+33°1008, π Boo(A), χ Ser, and γ Ari(S); the last three named have been newly discovered. Other new spectrum variables described are 78 Vir, 56 Ari, and 45 Her. Reproductions of spectrograms are given which illustrate the variation. The companions of the spectrum variables π Boo(A) and 17 Com(A) have been found to be metallic-line stars. A catalogue of spectrum variables has been compiled, which gives the gross spectroscopic characteristics of all such stars now known. The phase relations among lines originating from different elements have been discussed and found to differ from star to star. The luminosities and colors of the A0p stars correspond approximately to type B8. In general, the peculiar A stars appear to be appreciably bluer than normal stars of equivalent spectral type and to lie about 1 mag. above the main sequence.

I. INTRODUCTION

The spectrum variables of type A are those A stars of constant brightness (within, say, one-tenth of a magnitude) whose spectra contain absorption lines which vary in intensity or appearance but which do not show the c-characteristic. The problem of the spectrum variables appears to be closely related to the larger problem of the classification of the A stars. The wide diversity of spectra encountered among stars of this type has been frequently remarked, and it has now been well established[1] that the spectra of type A cannot be arranged in the two-dimensional array which suffices for the classification of earlier and later types. It is probably of profound significance that in only two well-delimited regions of the spectral sequence does the two-dimensional array become inadequate: among the stars of type A, where the hydrogen lines dominate the spectrum, and among the stars of very late type, where the molecular bands are dominant.

An understanding of the physical conditions which produce this hitherto unexplained diversity of spectra may be expected to come from a study of the most anomalous cases, such as the "silicon" and "strontium" stars of the *Henry Draper Catalogue*. The physical parameters which characterize the atmospheres of these stars are known to be those which produce spectrum variability in a number of cases, and it seems not unlikely that a better knowledge of this phenomenon will lead to the solution of the wider problems involved in the interpretation of the spectra of type A.

Two approaches to the problem suggest themselves. One is a program of detailed study of the brightest members of the class: spectroscopic investigations, under the highest possible dispersion, of the nature and identification of the absorption lines and of the changes in radial velocity which may be present, together with photometric and spectrophotometric studies of the continuum and the changes which may occur in it. The other approach is a survey of as many spectrum variables as can be found, with the ultimate object of determining in what respects they are alike and in what respects unlike and with the hope of being able eventually to isolate the relevant physical factors which produce the extremely complex phenomena observed in detail.

The first type of investigation is typified by the work of O. Struve and P. Swings[2] on α^2 Canum Venaticorum. The only other spectrum variables which have been studied in any detail are ϵ Ursae Majoris, most recently by J. W. Swensson;[3] BD−18°3789, by

[1] W. W. Morgan, *Pub. Yerkes Obs.*, Vol. 7, Part III, 1934.

[2] *Ap. J.*, **98**, 361, 1943.

[3] *Ap. J.*, **99**, 258, 1944.

W. W. Morgan;[4] and 73 Draconis, also by Morgan.[5] The second type of investigation has recently been rather neglected. Accordingly, it has seemed desirable to undertake a systematic search for new representatives of the class of spectrum variables.

A file of the peculiar A stars in the *Draper Catalogue*, compiled by Morgan, was consulted. From it an observing list was prepared which comprises all the peculiar A stars brighter than magnitude 6.0 and accessible at the Yerkes Observatory. The list also includes a few stars recognized by Morgan or others as having peculiar spectra, although not so noted in the *Draper Catalogue*. The list comprises sixty-one stars in all.

It is my purpose to find which of these sixty-one stars are spectrum variables and which are not; to describe the gross characteristics of the variation in each case where it is found; and to find the period of variation, if it be periodic, in each such case. The present paper is in the nature of a report on the progress made in this program, which is as yet far from completed.

II. THE OBSERVATIONAL MATERIAL

I have used a one-prism spectrograph attached to the 40-inch refractor of the Yerkes Observatory. A total of 83 observations have been made with a 6-inch camera and 269 observations with a 12-inch camera, during the interval from September, 1945, to August, 1946. An "observation" comprises one or more spectrograms (usually two), taken consecutively, of a single star. The 6-inch camera gives a dispersion of about 125 A/mm at $H\gamma$ and was employed to give a spectrogram of good definition between λ 3900 and λ 4500; the spectrograms measure about 8.2 mm from $H\beta$ to $H8$ and were widened at the telescope to a width of 0.6 mm. The slit width was 0.25 mm, which projects to 0.039 mm, or 4.8 A, on the plate. The exposure time was about 4 minutes for a star of magnitude 5.0; a second, longer exposure was frequently given, to be sure of sufficient density in the region below $H\epsilon$. The 12-inch camera gives a dispersion of about 60 A/mm at $H\gamma$ and gives good definition over the same region as is covered by the 6-inch camera; the spectrograms measure 17 mm from $H\beta$ to $H8$ and were usually widened at the telescope to a width of 1.5 mm. The slit width was 0.096 mm, or 0.029 mm = 1.8 A on the plate. The exposure time was about 15 minutes for a star of magnitude 5.0 or longer to get the region of K sufficiently dense. In order to facilitate the direct comparison of two spectrograms by superposing the plates, emulsions together, and juxtaposing the spectra, the usual comparison exposures were not impressed beside the stellar spectra. However, one comparison exposure on a neon lamp was impressed on each plate as a check against poor focusing.

The emulsion used was Eastman 103*a*-O, and all plates were developed in Eastman D-19 developer. Special care was taken to keep the plates of comparable density and contrast. The distribution of density in the continuum, however, depends sensitively upon the guiding; this effect is apparent in the reproductions given below.

In addition to the plates taken by myself, reference will be made to plates taken by other observers with the Bruce spectrograph attached to the 40-inch refractor. These plates were taken with two different 600-mm cameras and have a dispersion of about 30 A/mm at λ 4500. Most of the plates were taken for radial-velocity determinations; a variety of emulsions was used. The Bruce plates will be distinguished by the letters "IB" and "IR," respectively, depending upon which camera was used. Reference will also be made to plates taken at the McDonald Observatory with the Cassegrain spectrograph and 82-inch reflector. Those plates taken with two quartz prisms and the 500-mm camera have a dispersion of 55 A/mm at $H\gamma$ and will be designated by the letters "CQ." Plates taken with two glass prisms and the same camera have a dispersion of 28 A/mm at $H\gamma$ and will be designated by the letters "CG." My own plates will be designated by the letter "α" if taken with the 6-inch camera and by the letter "β" if taken with the 12-inch camera. All the enlargements given below were made from β plates.

[4] *Ap. J.*, **74**, 24, 1931.

[5] *Ap. J.*, **77**, 77, 1933.

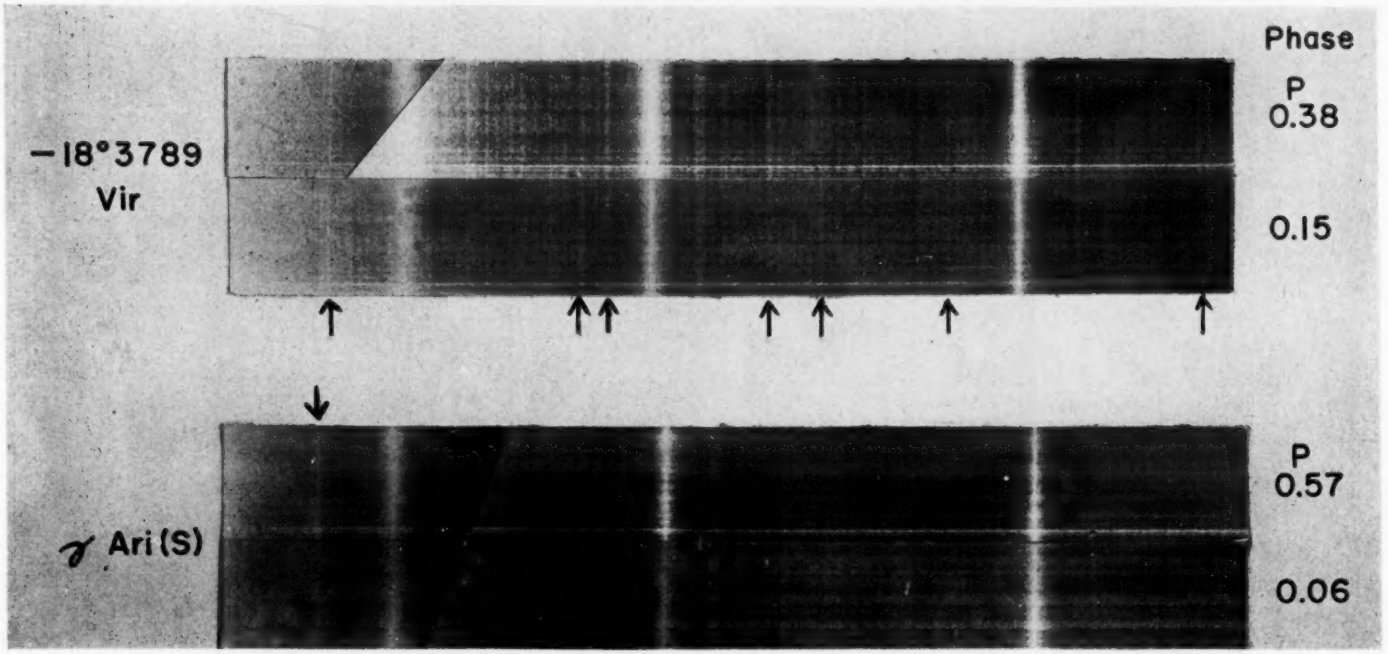

FIG. 1.—Intensity variations in two spectrum variables. In the spectra of −18°3789 Vir, the lines marked are, from left to right, *Ca* II K, λ 4063 (unidentified), λ 4078 (*Sr* II + *Cr* II), *Cr* II 4171, *Eu* II, 4205, λ 4290 (unidentified), and *Mg* II 4481. In the spectra of γ Ari (S), *Ca* II K is marked.

III. OBSERVATIONS OF EIGHTEEN SPECTRUM VARIABLES

1. *BD−18°3789 Virginis = HD 125248.*—The star BD−18°3789 Virginis is classified A0p in the *Henry Draper Catalogue*, with the remark that λ 4128 and λ 4131 are strong. The spectrum bears some resemblance to that of α^2 CVn but is richer under moderate dispersion. The *Si* II doublet at λλ 4128–4131 is somewhat stronger in α^2 CVn, and the lines of *Cr* II are weaker.

Large changes in the intensities of absorption lines in the spectrum of BD−18°3789 were discovered by W. W. Morgan,[3] who found that the lines of *Eu* II exhibited periodic changes in strength, while those of *Cr* II varied in the opposite sense. An unidentified line at λ 4296 was found to vary with *Eu* II, and *Cr* I 4254 was found to vary with *Cr* II. Possible changes in the lines of *H* and *Mg* II were also noted.

Examination of 13 β plates and 25 CQ plates taken during 1944–1945 confirms the very large changes which occur in the lines of *Eu* II and *Cr* II. The elements of variation are found to be

$$Eu \text{ II maximum} = Cr \text{ II minimum} = \text{JD } 2430143.07 + 9.295\,E;$$

TABLE 1

CRITERIA FOR ESTIMATES OF LINE INTENSITIES IN SPECTRUM OF BD−18°3789 VIR

Criterion	Definition	Scale
I	λ 3930/λ 3933	1, λ 3930 < < λ 3933; 4, λ 3930 = λ 3933; 6, λ 3930 > λ 3933
II	λ 4063/λ 4078	1, λ 4063 < < λ 4078; 4, λ 4063 = λ 4078; 7, λ 4063 > > λ 4078
III	λ 4205/λ 4233	1, λ 4205 < < λ 4233; 4, λ 4205 = λ 4233; 7, λ 4205 > > λ 4233
IV	λ 4481	1, λ 4481 invisible; 7, λ 4481 strongest
V	0.2(2A+2B+C)	1.0–6.6
VI	Morgan's estimates	1.2–6.7 (see text)

and other variable lines have the same period. The lines *Ca* II K and *Mg* II 4481 vary with *Cr* II, and so do lines at λλ 4078, 4161, 4215, and 4290. The first three of these lines are probably due mainly to *Sr* II, although *Cr* II contributes to λ 4078 and λ 4215. The line λ 4290 is due partly to *Cr* I; the relative weakness of the other two strong components of the *Cr* I resonance multiplet at λ 4254 and λ 4275 makes it appear probable that there is another important contributor to λ 4290. The variation of the unidentified line at λ 4296 with *Eu* II is confirmed, and a very strong unidentified line at λ 4063 is found to vary in the same sense. Lines of *Si* II and *Fe* II probably vary with *Cr* II. Representative β plates are reproduced in Figure 1.

In order to derive the period of variation, estimates of line strength were made as given in Table 2. It was found convenient to employ one or more different criteria for different sets of plates; the criteria listed in Table 2 are defined in Table 1. Criterion VI was derived from Morgan's estimates[6] of λ 4205 and λ 4558 by inverting his scale for λ 4558, applying appropriate scale factors, and adding. It should be understood that, when a ratio is given as the criterion, the notation is only symbolic, so that when criterion I is given as 6, for example, the notation does not mean that λ 3930 is six times as strong as λ 3933. In Figure 2 there is plotted for each of 53 plates the spectral characteristic according to the criterion of highest number given in Table 2.

The true form of the variation-curves can be better inferred from Figure 3, in which single criteria are plotted separately for the CQ plates only and which therefore present a more nearly homogeneous set of data. The curves for criteria I, II, and III agree in

[6] *Ibid.*, p. 27.

TABLE 2

OBSERVATIONS OF BD−18°3789 VIR = HD 125248

	Plate	JD 2400000.00+	Phase* P	Spectral Characteristics					
				Criterion					
				I	II	III	IV	V	VI
IR	8774	25309.94	0.029	.....	.....	6	.....	.....	.....
	8786	25310.84	.125	.....	.....	6	.....	.....	.....
	8797	25323.88	.528	.....	.....	1	.....	.....	.....
	9595	26355.98	.566	.....	.....	.....	.....	.....	1.5
	9601	26357.98	.781	.....	.....	.....	.....	.....	5.5
	9606	26358.97	.890	.....	.....	.....	.....	.....	6.0
	9618	26366.98	.750	.....	.....	.....	.....	.....	4.1
	9621	26367.95	.855	.....	.....	.....	.....	.....	6.7
	9628	26375.94	.715	.....	.....	.....	.....	.....	3.2
	9634	26377.97	.932	.....	.....	.....	.....	.....	3.9
	9643	26381.93	.358	.....	.....	.....	.....	.....	1.2
	9648	26386.93	.895	.....	.....	.....	.....	.....	5.9
	10515	27107.97	.469	.....	.....	1	.....	.....	.....
	10925	27457.96	.122	.....	.....	5	.....	.....	.....
	12081	28244.91	.787	.....	.....	5	.....	.....	.....
CQ	806	30126.74	.243	1	1	1	.....	1.0	.....
	819	30133.77	.000	3	6	7	2	5.0	.....
	823	30134.74	.104	3	6	7	3	5.0	.....
	830	30135.72	.210	2	3	4	4	2.8	.....
	831	30139.68	.636	1	1	1	4	1.0	.....
	832	30140.63	.739	1	2	2	3	1.6	.....
	835	30141.62	.845	2	5	3	4	3.4	.....
	836	30141.68	.851	2	6	2	3	3.6	.....
	837	30142.75	.965	5	7	5	2	5.8	.....
	838	30143.75	.073	6	6	7	2	6.2	.....
	839	30144.71	.176	4	5	3	3	4.2	.....
	840	30144.78	.184	3	6	6	4	4.8	.....
	900	30205.61	.729	1	1	1	.....	1.0	.....
	1288	30381.98	.703	1	1	.....	.....	1.0	.....
	1289	30382.01	.707	1	2	1	7	1.4	.....
	1290	30382.04	.710	1	2	1	6	1.4	.....
	1307	30384.01	.922	5	6	5	2	5.4	.....
	1319	30385.02	.030	3	6	7	1	5.0	.....
	2161	30897.66	.182	3	5	6	6	4.4	.....
	2168	30898.65	.289	2	3	2	6	2.4	.....
	2173	30899.67	.399	1	1	1	6	1.0	.....
	2180	30900.64	.503	1	1	1	7	1.0	.....
	2187	30902.64	.718	1	1	1	7	1.0	.....
	2193	30903.66	.829	3	5	5	5	4.2	.....
	2199	30904.61	.930	5	6	.....	.....	5.5	.....
β	42	31919.83	.151	.....	5.5	.....	.....	.....	.....
	45	31921.72	.354	.....	3.0	.....	.....	.....	.....
	46	31922.82	.474	.....	2.0	.....	.....	.....	.....
	48	31936.67	.966	.....	6.5	.....	.....	.....	.....
	50	31937.66	.070	.....	6.0	.....	.....	.....	.....
	51	31937.82	.087	.....	5.5	.....	.....	.....	.....
	62	31969.74	.521	.....	1.0	.....	.....	.....	.....
	65	31975.70	.163	.....	5.5	.....	.....	.....	.....
	70	31996.65	.417	.....	1.0	.....	.....	.....	.....
	72	31998.61	.626	.....	1.0	.....	.....	.....	.....
	76	32003.62	.167	.....	5.0	.....	.....	.....	.....
	78	32005.61	.381	.....	2.0	.....	.....	.....	.....
	82	32007.61	0.596	.....	1.0	.....	.....	.....	.....

* *Eu* II maximum = Phase 0 = JD 2430143.07 + 9.295 E.

the main, and there are probably no significant differences among them. The curve for the mean criterion, V, is somewhat smoother than the others, as was to be expected. All the curves indicate an abrupt change in the spectrum near phases $0^{p}.2$ and $0^{p}.8$ after *Eu* II maximum. There appears to be a real difference in the forms of the two extremes, the minima being in all cases very flat while the maxima are rather more rounded. In the cases of criteria I, II, and III the true ratios of equivalent widths vary enormously, and there is a tendency to assign the extreme value which the scale of estimation admits whenever the true ratios differ greatly from unity. That this effect is at work is suggested by the fact that the true ratios deviate most from unity when criteria I, II, and III are at their minima, and that is just where the flatness is most pronounced. In an attempt to assess the importance of this effect, the plates at minimum phases have been intercompared, but no differences were found which were related to phase. It is concluded that the almost rectangular minimum is probably real, although possibly exaggerated by the method of estimation, and that the variation is certainly anharmonic. This point may be further clarified by actual microphotometry of the changing lines, and the writer hopes to undertake this in the near future.

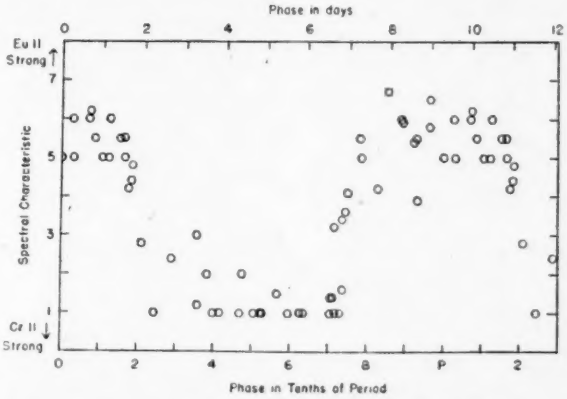

FIG. 2.—Variation of line intensities in the spectrum of BD−18°3789. Each point represents a single plate. The phases have been calculated from the elements, Phase = 0 at JD 2430143.07 + 9.295 E.

The object BD−18°3789 is situated so far south that plates cannot be obtained which are separated by more than 6 hours on a single night. The periods near 1 day which are reciprocal to the adopted period[7] have been investigated, and the curves so derived show appreciably greater scatter. However, the possibility that the period is actually very nearly 1 day cannot be entirely eliminated until the elements are checked at another longitude.

2. *BD+33°1008 Aurigae = HD 34452.*—The *Draper* type of this star is A0p, the noted peculiarity being the strength of *Si* II 4128–4131. These lines are stronger than in any other spectrum which I have observed. Other marked peculiarities include lines in the positions of *Sr* II 4078 and *C* II 4267, an unidentified line of moderate strength at λ 4057, and strong unidentified lines at λλ 3955, 3992, and 4200. The last three lines occur together in a number of the peculiar A stars and may well have a common origin. The strength of *Ca* II K is appropriate to a normal spectrum of type B9. The spectrum does not resemble closely that of any other known spectrum variable. Representative spectrograms are shown in Figure 4.

A further peculiarity is the appearance of a strong line at λ 4026 and another, weaker

[7] O. Struve, *Pop. Astr.*, **36**, 411, 1928.

line at λ 4471, both undoubtedly due to *He* I. Miss C. Westgate[8] discovered that these two lines varied in strength, and she suspected certain other lines of changing. Thirteen β plates confirm the changes in the lines of *He* I and reveal that *Ca* II K changes with *He* I and that λ 4481 of *Mg* II and λ 4267 probably vary in the same sense. The lines λλ 3955, 3992, 4200, and 4057, and probably *Fe* II 4233, change in the opposite sense.

From the 13 β plates and from 27 CQ plates taken during 1944 it has been found that the elements of variation are

$$He \text{ I maximum} = \text{JD } 2431334.90 + 2.4660\,E;$$

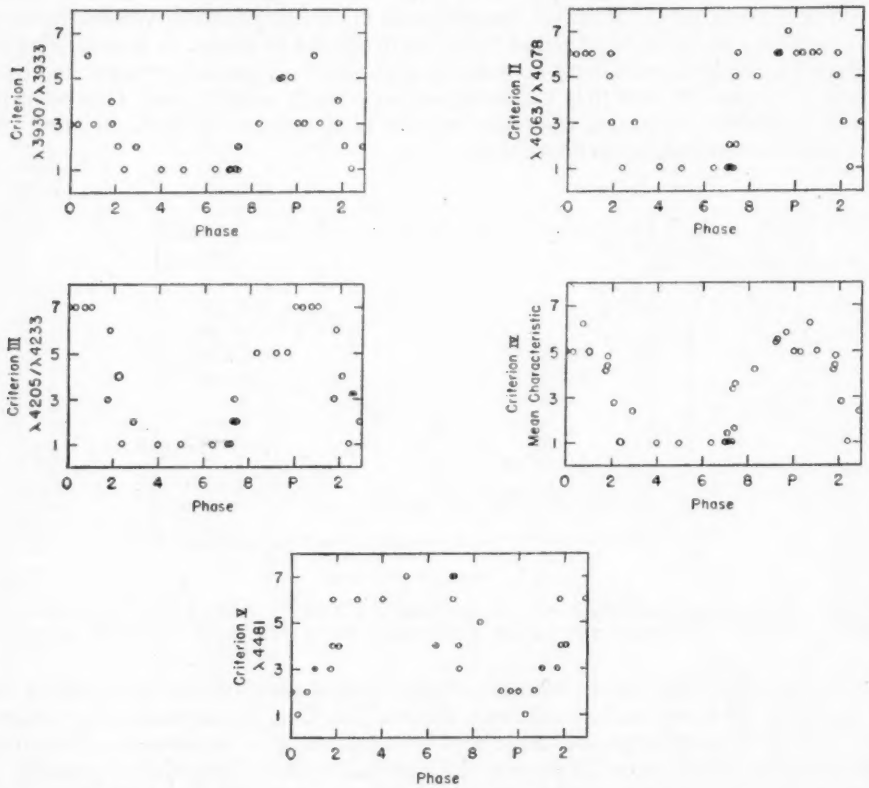

FIG. 3.—Variation of line intensities in the spectrum of BD−18°3789. Each point represents a single CQ plate. The phases have been calculated from the elements, Phase = 0 at JD 2430143.07 + 9.295 E.

the periods near 1 day have been eliminated. Figure 5 shows the variations of the *He* I lines with phase; the estimates on which it is based are given in Table 3, and the criteria used are defined at the foot of the table. The curve of variation is definitely asymmetrical, with the decline of the *He* I lines appreciably steeper than their rise and with the minimum flatter and broader than the maximum.

3. *π Bootis(A) = HD 129174, and α Andromedae = HD 358.*—The star π Boo is classified A0 in the *Draper Catalogue* and is a visual binary. In the spectrum of component A, peculiar lines of moderate strength are present at λλ 3944, 3984, 4137, 4171, 4179,

[8] *Ap. J.*, **77**, 227, 1933.

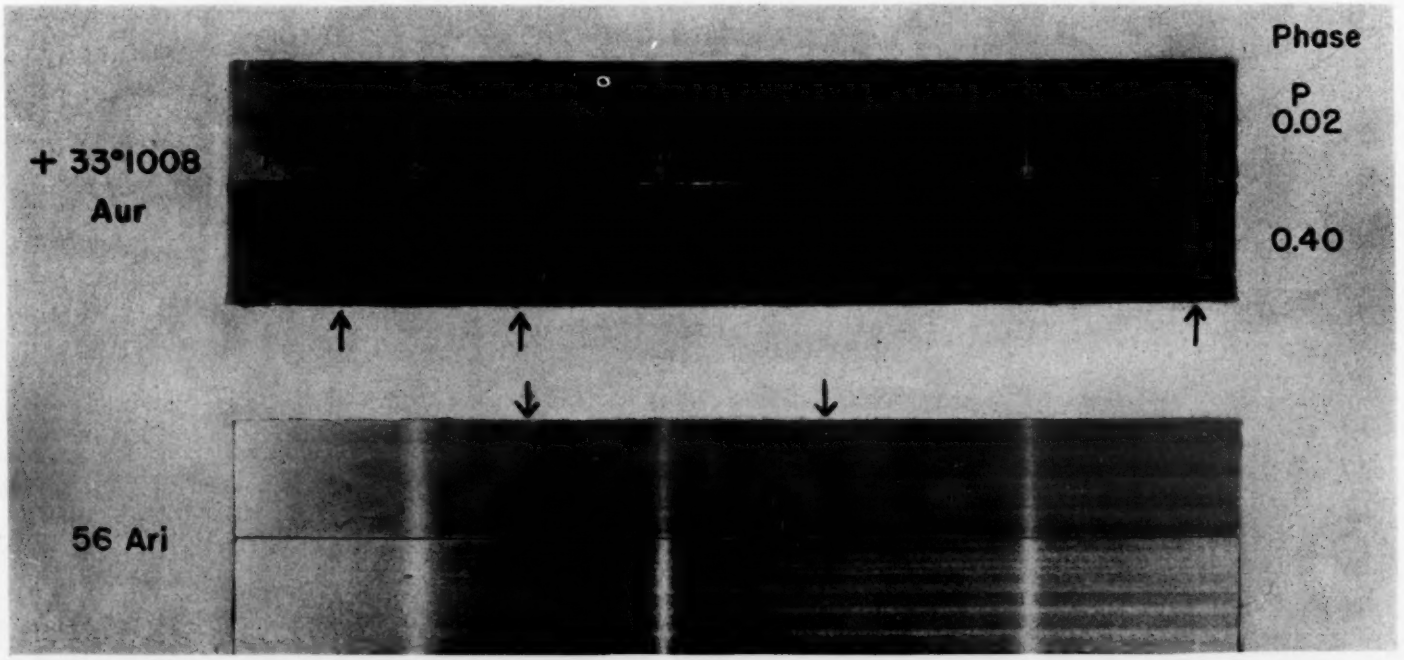

FIG. 4.—Intensity variations in two spectrum variables. In the spectra of +33°1008 Aur, the lines marked are *Ca* II K, *He* I 4026, and *He* I 4471. In the spectra of 56 Ari, the lines marked are *He* I 4026 and λ 4200 (unidentified).

4206, 4253, and 4282.[9] Morgan[10] has pointed out the close resemblance of the spectrum to that of α And, in which all these lines except λ 3984 are the same strength as in π Boo(A). The line λ 3984 is appreciably stronger in π Boo(A), and so is *Ca* II K. Representative spectrograms are shown in Figure 6.

From 9 β plates it is found that the K line in π Boo(A) suffers large changes in intensity. Other lines which change with K are λ 4137 and probably λλ 3944, 3984, and 4282; lines which change in the opposite sense are λ 4253 and probably λ 4206. The *Si* II doublet at λλ 4128–4131 is possibly less distinctly resolved when K is strong, suggesting the emergence of *Eu* II 4129; however, the β plates show none of the other strong *Eu* II lines.

The β plates were too few to permit the derivation of the period of variation; hence an attempt was made to accomplish this by referring to the Yerkes file of IB and IR plates

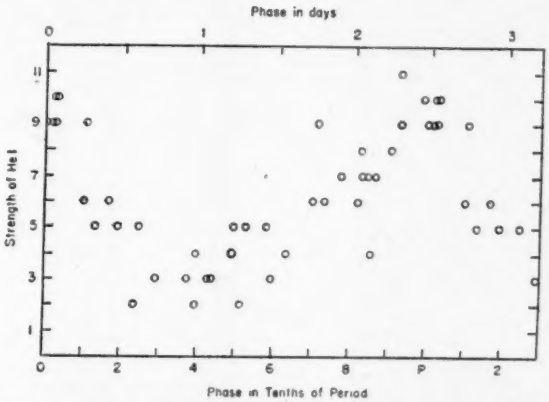

FIG. 5.—Intensity variation of λλ 4026 and 4471 of *He* I in the spectrum of BD+33°1008. Each point represents a single plate. The phases have been calculated from the elements, Phase = 0 at JD 2431334.90 + 2.4660 E.

taken at intervals between 1917 and 1932. These plates are poorly suited to the estimation of line intensities, for they differ greatly among themselves in density, contrast, and quality. Nevertheless, what seem to be real differences appear from plate to plate in the strengths of certain lines in the region best exposed, and most conspicuously at λ 4206. Accordingly, two independent estimates of the strength of this feature were made on each of 38 plates, and from the mean estimates the elements of variation were derived. These are

$$\lambda\ 4206\ \text{maximum} = \text{JD}\ 2421391.45 + 2.2445\ \text{E};$$

the periods reciprocal to the adopted one have been eliminated. The estimates are given in Table 4, and the scale of estimation is noted at the foot of the table. The curve of variation is given in Figure 7.

The scatter in Figure 7 is large, as was to be expected from the nonuniformity of the plates used, but the estimates seem to indicate a real variation with the adopted period. However, the variations in the K line exhibited by the β plates appear to be incompatible with this period. It is not impossible that K varies with a period different from

[9] In the spectrum of κ Cancri, which closely resembles that of π Boo(A), Struve has identified (*Ap. J.*, 99, 220, 1944) these lines as follows: λ 3944, *Mn* II; λ 3984, *Fe* I + *Cr* I; λ 4137, *Mn* II; λ 4171, *Ti* II; λ 4179, *Fe* II; λ 4206, *Mn* II; λ 4253, *Cr* II + *Mn* II; λ 4282, *Mn* II.

[10] *Ap. J.*, **73**, 104, 1931.

that of λ 4206, but it is considered more probable that the period derived from the Bruce plates is illusory. A new series of spectrograms suitable for the estimation of line intensities will be required to resolve the problem; meanwhile, the period of 2.2445 days will be tentatively adopted.

TABLE 3

OBSERVATIONS OF BD+33°1008 AUR = HD 34452

PLATE	JD 2430000.00+	PHASE* P	STRENGTH OF *He* I		
			Criteria†		
			I	II	III
CQ 3686	1334.98	0.032	6	4	10
3697	1335.98	.438	1	2	3
3770	1352.88	.292	2	1	3
3775	1353.92	.714	5	4	9
3781	1354.87	.101	3	3	6
3786	1355.84	.495	2	3	5
3790	1356.85	.905	3	5	8
3802	1361.85	.929	6	3	9
3814	1363.82	.730	3	3	6
3826	1364.82	.134	3	2	5
3846	1367.87	.373	2	1	3
3865	1369.00	.831	5	2	7
3877	1369.83	.166	5	1	6
3881	1370.00	.236	1	1	2
3882	1370.02	.244	2	3	5
3894	1370.84	.525	3	2	5
3919	1373.81	.775	4	3	7
3923	1374.02	.864	4	3	7
3934	1374.83	.191	2	3	5
3938	1375.83	.596	2	1	3
3954	1376.87	.016	6	3	9
3971	1378.02	.486	2	2	4
3983	1378.84	.819	3	3	6
4007	1380.85	.632	2	2	4
4011	1381.02	.701	4	2	6
4022	1381.76	.000	5	4	9
4023	1381.82	.024	5	4	9
β 2	1724.79	.105	6	3	9
3	1732.91	.397	3	1	4
4	1738.94	.844	3	4	7
29	1863.67	.425	2	1	3
43	1920.61	.515	1	1	2
44	1921.63	.929	6	5	11
47	1936.58	.989	5	5	10
50	1937.58	.397	1	1	2
53	1941.59	.020	6	4	10
56	1948.58	.855	2	2	4
90	2021.88	.580	2	3	5
93	2023.89	.397	2	2	4
99	2029.89	0.826	4	4	8

* *He* I maximum = Phase 0 = JD 2431334.90 + 2.4660 E.

† Criteria:
I: λ 4026/λ 4078. 1, λ 4026 << λ 4078; 4, λ 4026 = λ 4078; 6, λ 4026 > λ 4078.
II: λ 4471. 1, λ 4471 invisible; 5, λ 4471 strongest.
III: I + II.

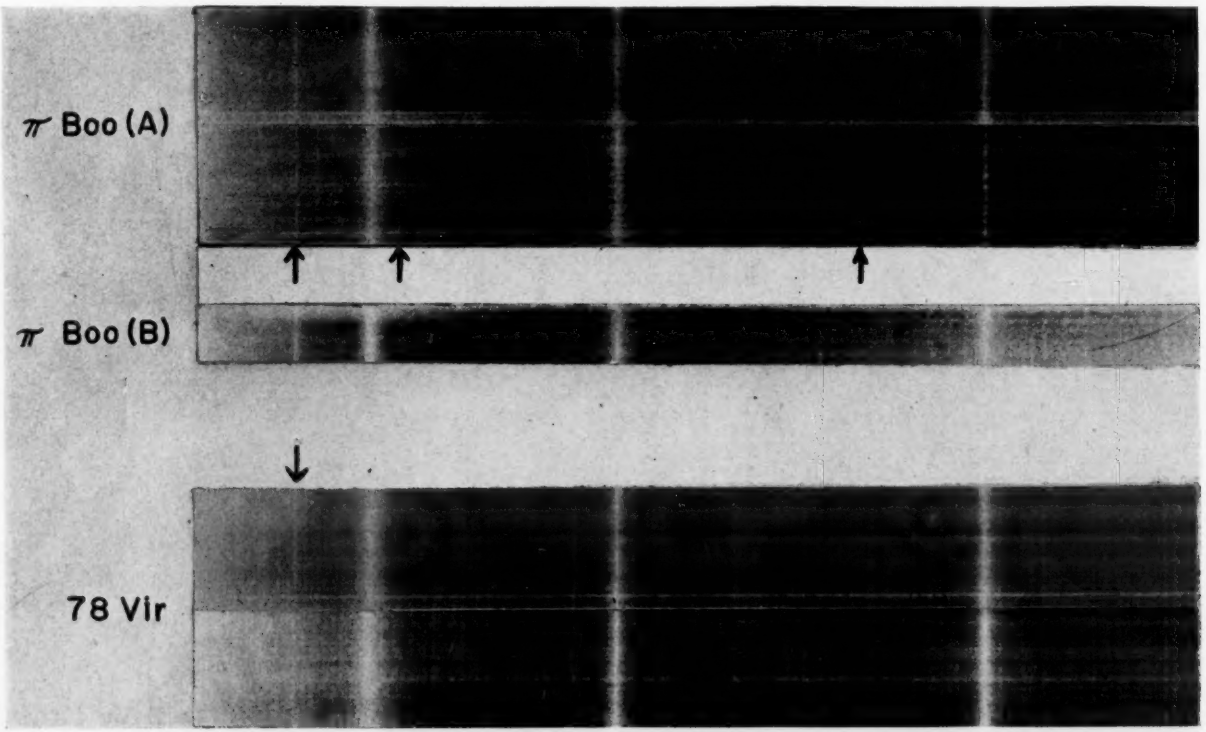

FIG. 6.—Intensity variations in two spectrum variables. In the spectra of π Boo (A), the lines marked are *Ca* II K, λ 3992 (unidentified), and *Mn* II 4253. The object π Boo (B) is a metallic-line star; the K line is much too weak for the lines of *Fe* I, *Mn* I, and *Ca* I. In the spectra of 78 Vir the K line is marked. The broad absorption feature at K in the lowest spectrogram is best seen by viewing the reproduction at arm's length.

While the period of variation remains uncertain, there can be little doubt that the variation is real and periodic. It is significant that N. Lockyer and F. E. Baxandall[11] and, later, P. Guthnick[12] found slight changes in the spectrum of α And; unfortunately, these writers have not given the wave lengths of the changing lines. In the spectrum of the same star, Ludendorff[13] has noted changes in the appearance of *Mg* II 4481 and *Hγ*.

TABLE 4

OBSERVATIONS OF π BOO(A) = HD 129174

Plate	JD 2420000.00+	Phase* *P*	Strength† of λ 4206		
			1st Estimate	2d Estimate	Mean
IB 4034	0565.78	0.237	2	1	1.5
4043	0566.99	.775	3	2	2.5
4047	0569.95	.094	2	2	2.0
4095	0593.70	.677	3	2	2.5
4122	0607.79	.951	4	3	3.5
4145	0628.71	.272	3	1	2.0
4168	0657.61	.151	1	1	1.0
4754	1239.99	.619	1	1	1.0
4778	1251.94	.942	3	3	3.0
4786	1254.00	.859	3	2	2.5
4793	1258.99	.085	3	1	2.0
4820	1279.90	.400	1	1	1.0
4828	1281.91	.294	2	1	1.5
4832	1283.86	.165	4	2	3.0
4835	1286.98	.557	2	3	2.5
4840	1309.80	.721	4	3	3.5
4848	1311.83	.628	2	2	2.0
4850	1314.96	.022	4	4	4.0
4861	1325.76	.834	2	2	2.0
4868	1328.75	.165	2	2	2.0
4877	1342.73	.392	1	3	2.0
4898	1358.77	.539	2	2	2.0
4917	1365.66	.610	1	1	1.0
4935	1391.60	.165	3	4	3.5
4949	1409.61	.192	3	3	3.0
5440	1983.92	.067	2	3	2.5
5466	2018.49	.468	1	1	1.0
5475	2028.80	.063	3	3	3.0
5489	2049.73	.388	1	1	1.0
5502	2076.68	.393	2	2	2.0
5505	2088.59	.699	3	3	3.0
5509	2091.64	.058	4	4	4.0
5513	2102.70	.869	4	4	4.0
5547	2161.62	.236	1	0	0.5
5556	2168.62	.456	1	1	1.0
6149	2777.74	.739	2	1	1.5
IR 10097	6811.65	.982	4	4	4.0
10115	6825.73	0.254	4	3	3.5

* *Mn* II maximum = Phase 0 = JD 2421391.45 + 2.2445 E.

† 0, λ 4206 invisible; 4, λ 4206 strongest.

[11] *Proc. R. Soc.*, A, **77**, 550, 1906.

[12] *A.N.*, **245**, 228, 1932.

[13] *A.N.*, **176**, 327, 1907.

Kohl[14] has confirmed these changes and has also found that K varies; he suspected changes in a number of other lines, particularly λ 4026 and λ 4471 of *He* I and λ 3984. I have only three β plates of α And, and these seem to indicate that variation is present, notably in λ 3984 and λ 4137.

In the case of α And, Baxandall[15] pointed out a number of coincidences with lines in the spark spectrum of manganese and concluded that, among the stronger peculiar lines, those at λλ 3944, 4137, 4206, 4253, and 4282 were due to "proto-manganese." Large differences in relative intensity between star and spark were noted and ascribed to excitation effects. Morgan has subsequently discussed[10] the spectra of the stars like α And and has concluded that most of the peculiar lines are due to an ionized state of manganese. The four strongest lines of the multiplet *Mn* II $a^5F - z^5D$ agree in position with star lines, two of which are λ 4206 and λ 4253.

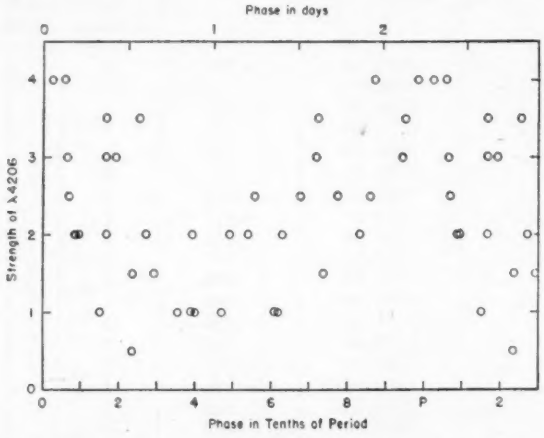

FIG. 7.—Intensity variation of *Mn* II 4206 in the spectrum of π Boo (A). Each point represents a single plate. The phases have been calculated from the (provisional) elements, Phase = 0 at JD 2421391.45 + 2.2445 E.

There can be no doubt that *Mn* II accounts in part for the peculiarities of the spectra of stars like α And. However, Miss C. E. Moore's revised *Multiplet Table*[16] gives no lines in the spectrum of *Mn* II which could account for λ 3944, λ 4137, or λ 4282. Of these lines, the second varies out of phase with *Mn* II 4253, and the other two probably do the same. Since we know of no case in which lines originating from a given ion vary out of phase with one another, the evidence from the variation is that λλ 3944, 4137, and 4282 probably do not originate from *Mn* II. It appears that a satisfactory discussion of the peculiar lines in the spectra of stars like α And must wait upon a more complete term analysis of *Mn* II than is available at the present time.

The star π Boo(B) is 0.87 mag. fainter than A and 5″.8 distant in position angle 105°. The position angle is increasing slowly; and Aitken[17] states that the pair is probably a physical one, although the proper motions are widely divergent: 0″.016 in 82°.8 for A, and 0″.020 in 287°.8 for B.[18] F. Leonard[19] gives the spectral type of B (= HD 129175) as A5.

[14] *A.N.*, **262**, 469, 1937.

[15] *M.N.*, **74**, 250, 1914.

[16] A *Multiplet Table of Astrophysical Interest* ("Contr. Princeton U. Obs.," No. 20 [1945]).

[17] *New General Catalogue of Double Stars* (Washington: Carnegie Institution of Washington, 1932).

[18] Dr. G. P. Kuiper writes: "The pair is definitely a physical one; the large difference between the Boss motions is spurious, as is obvious from the micrometer measures."

[19] *Lick Obs. Bull.*, **10**, 169, 1923.

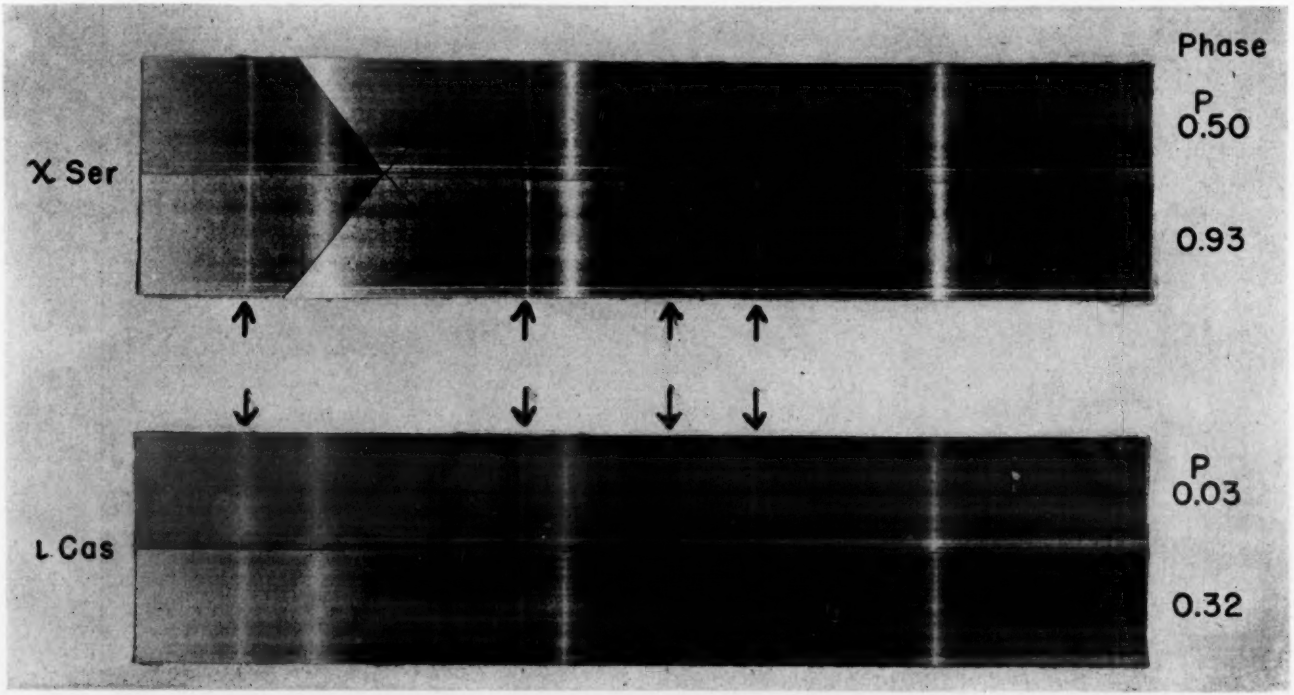

FIG. 8.—Intensity variations in two spectrum variables. In the spectra of χ Ser, the lines marked are *Ca* II K, *Sr* II 4078, λ 4161 (*Sr* II?), and *Sr* II 4215. In the spectra of ι Cas, the same lines are marked. Note that K varies in phase with the other variable lines in ι Cas, and out of phase in χ Ser.

A β plate, reproduced in Figure 6, shows that it is a typical metallic-line star, with the K line indicating a type of A2 while the other metallic lines correspond to A7 or F0. This association of a spectrum variable with a metallic-line star is particularly interesting; it is observed also in the case of the chromium-europium star, 17 Comae (*q.v.*).

It is necessary to add that spectrograms of either component of π Boo are probably contaminated to some small extent by the light of the other. That the contamination cannot be sufficient, however, to produce the changes observed in the spectrum of A is readily concluded from an inspection of Figure 6.

4. χ *Serpentis* = *HD 140160.*—The spectrum of χ Serpentis closely resembles that of ι Cassiopeiae. Its *Draper* classification is A0p, the noted peculiarity being the strength of λ 4078. This line, with λ 4215, becomes considerably stronger than in ι Cas; K is always much weaker than in ι Cas; and lines at λ 4422 and λ 4489 are weaker than in ι Cas. Representative spectrograms are reproduced in Figure 8.

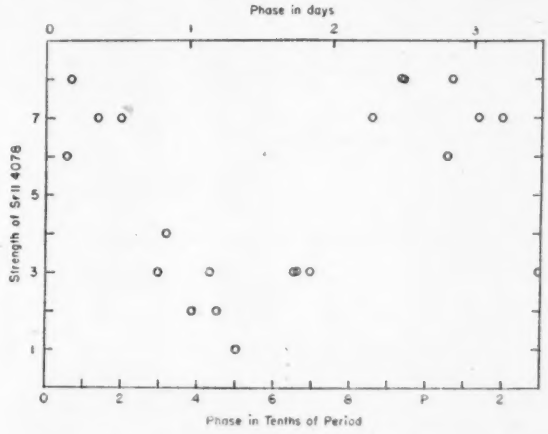

FIG. 9.—Intensity variation of *Sr* II 4078 in the spectrum of χ Ser. Each point represents a single plate. The phases have been calculated from the elements, Phase = 0 at JD 2432003.85 + 2.675 E.

From a study of 16 β plates, it is found that λ 4078 and λ 4215 exhibit large variations in intensity. The elements of variation are

$$Sr \text{ II maximum} = \text{JD } 2432003.85 + 2.675 \text{ E};$$

the periods reciprocal to the adopted one have not been eliminated. The curve of variation is indicated in Figure 9; it is based upon the estimates given in Table 5. These estimates were made by intercomparison of the β plates, which were arranged in order of increasing strength of λ 4078 and then assigned the numbers given in the table. The plates are too few to establish conclusively the nature of the variation-curve, but the present evidence indicates that it is very nearly harmonic.

Unidentified lines at λ 4161 and λ 4290 vary strongly in phase with the resonance doublet of *Sr* II, and K varies in the opposite sense. The amplitude of the variation in λ 4078 and λ 4215 is much greater than in ι Cas, and the amplitude of the variation in K is much less. It is remarkable that in ι Cas the lines of *Sr* II and *Ca* II vary together, while in χ Ser they change out of phase with each other.

5. γ *Arietis* (*S*) = *HD 11503.*—This star is classified A0p in the *Draper Catalogue*, with the remark that the *Si* II doublet at $\lambda\lambda$ 4128–4131 is strong. Guthnick[20] subsequent-

[20] *Sitz. Preuss. Akad. Wiss. Berlin*, No. 29, 1931.

ly called attention to the peculiarities of the spectrum and implied that he suspected it of varying. Morgan[21] has identified *Eu* II 4205 in the spectrum. There is a close resemblance to the spectrum of BD−18°3789 at *Cr* II maximum, except that the lines of *Cr* II are somewhat stronger in the latter star. Representative spectrograms are reproduced in Figure 1.

TABLE 5

OBSERVATIONS OF χ SER=HD 140160

Plate	JD 2430000.00+	Phase* *P*	Strength of Sr II	Plate	JD 2430000.00+	Phase* *P*	Strength of Sr II
β 51.....	1937.83	0.318	4	β 82....	2007.72	.450	2
65.....	1975.76	.501	1	85....	2009.73	.198	7
68.....	1992.76	.854	7	88....	2021.64	.651	3
70.....	1996.61	.296	3	92....	2023.73	.430	3
72.....	1998.64	.052	6	94....	2025.61	.135	7
76.....	2003.69	.937	8	96....	2027.73	.929	8
78.....	2005.70	.693	3	98....	2029.68	.660	3
81.....	2006.79	.064	8	100....	2031.63	0.386	2

* *Sr* II maximum = Phase 0 = JD 2432003.85 + 2.675 E.

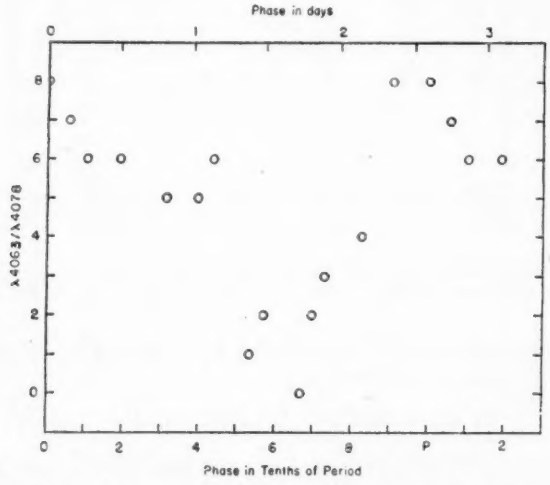

FIG. 10.—Intensity variation of the blends at λ 4063 and λ 4078 in the spectrum of γ Ari (S). Each point represents a single plate. The phases have been calculated from the (provisional) elements, Phase = 0 at JD 2431782.5 + 2.607 E.

Examination of 14 β plates reveals that at least some of the features which change in BD−18°3789 are also variable in γ Ari (S). Except in the case of the K line, the changes are of much smaller amplitude in the latter star, and the phase relations appear to differ between the two stars. On each of the β plates, the ratio λ 4063/λ 4078 has been estimated twice; the estimates are given in Table 6, and they are plotted in Figure 10, according to the elements

$$Ca\ \text{II minimum} = Cr\ \text{II minimum} = \text{JD } 2431782.5 + 2.607\ \text{E}\ .$$

[21] *Ap. J.* **75**, 53, 1932.

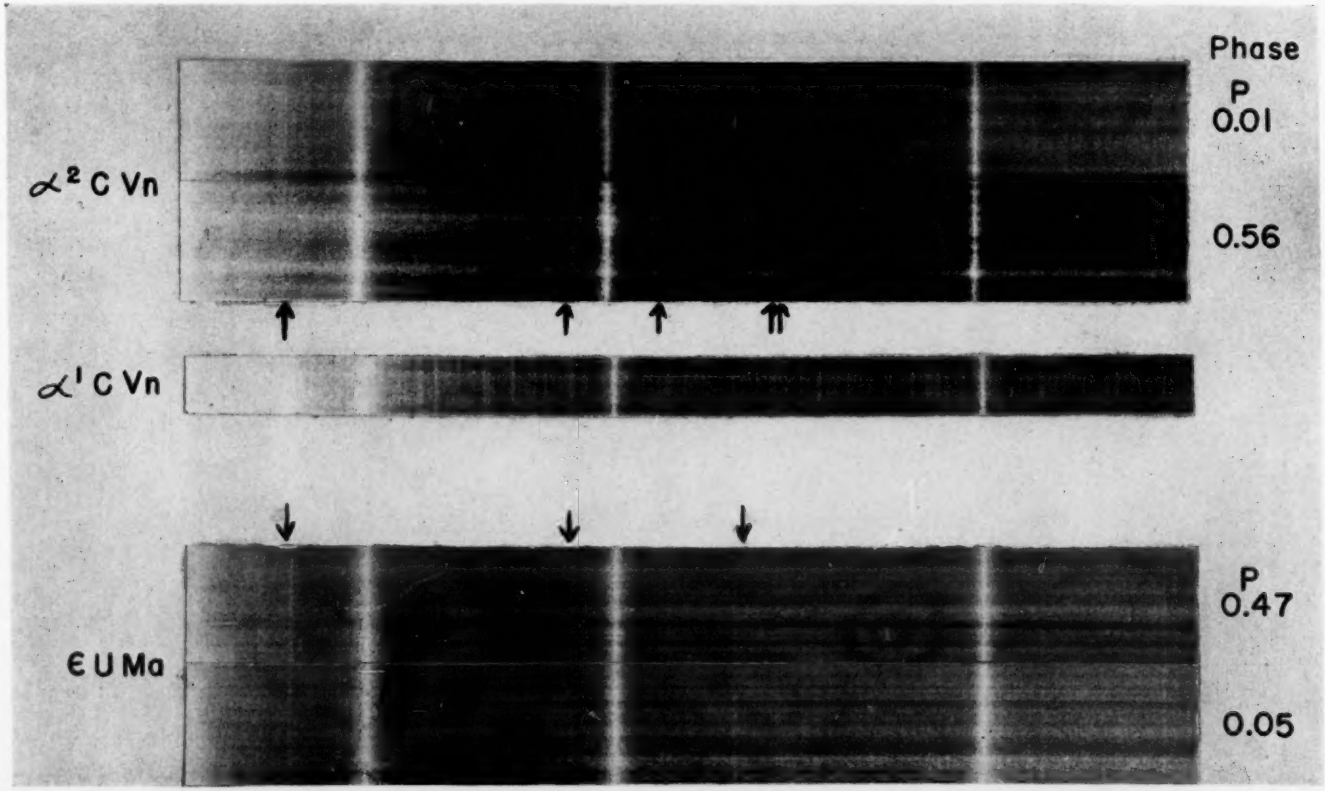

FIG. 11.—Intensity variations in two spectrum variables. In the spectra of α^2 CVn, the lines marked are *Ca* II K, λ 4078 (*Sr* II + *Cr* II), λλ 4128–31 (*Si* II + *Eu* II), λ 4200 (unidentified), and *Eu* II 4205. α^1 CVn is of type F5 IV. In the spectrum of ε UMa, the lines marked are *Ca* II K, *Cr* II 4078, and λ 4179 (*Fe* II + *Cr* II).

The periods reciprocal to the adopted one have been eliminated; however, these elements are based on a small number of plates and require confirmation. There are too few plates to permit conclusions regarding the form of the variation-curve.

The star γ Ari (N) (= HD 11502) is 8″ distant in position angle 0°. Its spectrum is of type B9V and appears to be normal, although Guthnick[20] regards the K line as weak and excessively broad. The brightness of γ Ari (N) is 0.08 mag. greater than that of its peculiar companion, but the image configuration of the binary on the slit-jaws is such that there can be no question of the contamination of the spectrum of one component by the light of the other.

The two components of γ Ari have common proper motion and undoubtedly form a physical system.

6. ι *Cassiopeiae* = *HD 15089.*—The *Draper* type is A5p, and the lines of *Sr* II and *Cr* II are strong. The K line has been found[22] to change its intensity by an amount equivalent to a change in type from about A2 to F0. The period of variation is 1.740 days, and

TABLE 6

OBSERVATIONS OF γ ARI (S) = HD 11503

Plate	JD 2430000.00+	Phase* P	λ 4063/λ 4078			Phase	JD 2430000.00+	Phase* P	λ 4063/λ 4078		
			1st Estimate	2d Estimate	Mean				1st Estimate	2d Estimate	Mean
β 10.....	1784.65	0.825	2	2	4	β 69.....	1992.88	0.698	1	1	2
17.....	1836.54	.729	2	1	3	74.....	1098.89	.000	4	4	8
28.....	1863.59	.103	.....	3	6:	77.....	2003.85	.905	4	4	8
32.....	1869.56	.395	2	3	5	79.....	2005.84	.666	0	0	0
34.....	1871.63	.188	3	3	6	81.....	2006.85	.058	3	4	7
35.....	1872.53	.534	1	0	1	83.....	2007.84	.437	3	3	6
36.....	1874.56	0.314	2	3	5	92.....	2023.82	0.568	1	1	2

* *Cr* II minimum = Phase 0 = JD 2431782.5 + 2.607 E.

the resonance doublet of *Sr* II changes in phase with K. Examination of 10 β plates and 14 α plates confirms the published period, which is probably correct to within 0.001 day. From the β plates and from four CG plates taken in January, 1946, it is found that λλ 4133, 4161, 4199, 4423, and 4431 change with K; only λ 4179 among the stronger lines appears to vary in the opposite sense. A number of other lines probably vary with K, notably λ 4290 and the lines of *Cr* II. The CG plates show no trace of *Eu* II 4205. The lines of *Fe* II are quite strong, especially λ 4233; *Fe* I is present but weak. Representative spectrograms are shown in Figure 8.

7. *78 Virginis* = *HD 118022.*—The *Draper* classification of this star is A2p, with the remark that λλ 4128–4131 are strong and that the spectrum resembles that of θ' Microscopii. Except for a much weaker K line, the spectrum is very similar to that of ι Cas. The latter star does not show the lines of *Eu* II, however, and these are definitely present in 78 Vir, as Morgan[21] has already shown. The lines of *Cr* II are also rather stronger in 78 Vir, as are *Fe* II 4233, and λ 4290 and λ 4423. The last-named line becomes very strong in 73 Draconis, which also resembles 78 Vir but is distinctly later in type.

Three β plates show changes in the spectrum of 78 Vir, the most pronounced variation being at *Ca* II K. When the K line is weak, it appears superposed over a diffuse absorption feature about 8A wide. This feature was first pointed out[23] by Morgan and his col-

[22] Deutsch, *Ap. J.*, **103**, 99, 1946.

[23] *An Atlas of Stellar Spectra* (Chicago: University of Chicago Press, 1943), p. 18.

laborators; it is not present when K is strong. The lines of *Cr* II and *Sr* II probably vary out of phase with K. The period of variation is unknown. The spectral changes are illustrated in Figure 6.

8. *56 Arietis = HD 19832.*—The star 56 Ari is especially interesting for the reason that it is the only known spectrum variable that has poor lines on plates of moderate dispersion. The *Draper* type is A0p, the peculiarity being a feature at λ 4129. From 10 β plates it is found that other peculiarities are *He* I 4026, which varies from complete invisibility to an intensity appropriate to type B8, and the unidentified lines at λλ 3955, 3992, and 4200, which seem to be stronger when λ 4206 is absent. The feature at λ 4129 also varies, probably in phase with the unidentified lines, and a very weak line in the position of *Cr* II 4078 probably changes in the same sense. The K line is extraordinarily weak. The period of variation is unknown; there is some evidence that it may be much shorter than that of any other known spectrum variable. Representative spectrograms are shown in Figure 4. The spectrum of BD+3°2867 Vir closely resembles that of 56 Ari.

9. *45 Herculis = HD 151525.*—The *Draper* type is A0p, with λλ 4128–4131 noted. The spectrum closely resembles that of ε UMa, except that *Mn* I 4030–4034 do not appear. From 6 β plates it is established that *Ca* II K varies and that *Mg* II 4481 probably varies with K, while the lines of *Cr* II probably vary in the opposite sense. The amplitude of variation appears to be somewhat smaller than in ε UMa; the period is unknown.

10. *49 Cancri = HD 74521.*—The *Draper* type is A0p, and a resemblance to the spectrum of α Doradus is noted. The spectrum also resembles that of α^2CVn, but K is much stronger. Other differences are in the *Si* II doublet λλ 4128–4131, in λ 4078 and λ 4215 of *Sr* II, and in *Fe* II 4233, all of which are appreciably stronger than in α^2 CVn. The line *Eu* II is present, as noted by Morgan.[21] Three β plates do not reveal the changes in λ 4205 and λ 4215 reported by Morgan;[24] however, the number of plates is too small for conclusions to be drawn.

11. *17 Comae = HD 108662.*—The *Draper* type is A0p, and the spectrum is almost identical with that of 78 Vir. Morgan has reported[25] variations in certain lines of *Cr* II and *Sr* II. Four β plates reveal no certain changes, but this evidence is inconclusive.

A companion with common proper motion is 145″ distant in position angle 250°. This star is HD 108651, type A3, magnitude 6.69. A CQ plate taken by J. L. Greenstein in May, 1942, exhibits a spectrum of type about F2, but with the K line only as strong as in type A2. Certain other anomalies appear to be present in the spectrum.

12. *21 Comae = HD 108945.*—The *Draper* type is A3p, and the spectrum is nearly identical with that of ι Cas at *Ca* II minimum. Morgan[25] has reported variations in λ 4215. A study of 11 β plates suggests that most or all of the features which change in ι Cas are variable in this spectrum, but the changes are of much smaller amplitude and are not conclusively established by the β plates.

13. *ε Ursae Majoris = HD 112185.*—The *Draper* type is AOp, the noted peculiarities being the weakness of K and the strength of *Si* II 4128–4131. Six β plates reveal changes in K which conform to the period given by Guthnick.[26] Pronounced changes in the opposite sense occur in the lines of *Cr* II. Representative spectrograms are shown in Figure 11.

14. *α^2 Canum Venaticorum = HD 112413.*—The most exhaustively studied[1] of the spectrum variables, α^2 CVn is of type A0p; λλ 4128–4131 are strong. Six β plates exhibit changes which conform to the elements determined by Miss G. Farnsworth.[27] The most pronounced changes occur in λ 3930 and λ 4205 of *Eu* II and in *Ca* II K, which varies with *Eu* II; in *Cr* II 4078, *Fe* II 4233, and an unidentified line at λ 4200, all of which vary out of phase with *Eu* II.

[24] *Ap. J.*, **76**, 315, 1932.

[25] *Ibid.*, p. 275.

[26] *Sitz. Preuss. Akad. Berlin*, No. 19, p. 13, 1934.

[27] *Ap. J.*, **76**, 313, 1932.

The star α^1 CVn, of magnitude 5.39, is 20″ distant in position angle 228°. Leonard[19] gives its spectral type as F2; a recent β plate indicates that its classification on the MKK system is F5 IV. The star is probably a spectroscopic binary of small range. Spectrograms of α^1 and α^2 CVn are reproduced in Figure 11.

15. ω *Ophiuchi* = *HD 148898*.—The *Draper* type is F0, but the spectrum is nearly identical with that of ι Cas (A5p) except for λ 4078 and λ 4215 of *Sr* II, which are always stronger in the latter star. The K line has the same strength as in ι Cas at *Ca* II maximum. Morgan[24] has reported changes in λ 4215. Six β plates strongly suggest that this line varies and that changes also occur in K, λ 4137, and some other lines as well.

16. *21 Aquilae* = *HD 179761*.—The spectrum is of type B8. Morgan[25,28] has reported variations in the intensity and appearance of λ 4121 and λ 4471 of *He* I. Four β plates reveal no definite changes, but this evidence is inconclusive.

17 γ *Equulei* = *HD 201601*.—The *Draper* type is F0p, the peculiarity noted being the strength of *Sr* II 4078. This line and the other component of the resonance doublet, at λ 4215, are stronger in γ Equ than in any of the known spectrum variables. The lines of *Cr* II are somewhat weaker than in the peculiar stars of earlier type, and *Eu* II is stronger. The spectrum resembles that of β Coronae Borealis, which has recently been studied under high dispersion by W. A. Hiltner.[29] Morgan[24] has reported changes in *Cr* II 4558; three β plates reveal no changes, but the number of plates is far too small to establish nonvariability.

IV. CATALOGUE OF SPECTRUM VARIABLES

It seems desirable at this time to compile a first catalogue of spectrum variables which will summarize the present state of knowledge concerning the gross spectroscopic characteristics of these stars. Table 7 is such a compilation. It lists twenty stars, of types B8–F0, in which changes in the absorption lines have been observed.

The first six columns are self-explanatory; the positions and magnitudes are those of Schlesinger's *Bright Star Catalogue*. The seventh column gives the strongest peculiar features which distinguish each spectrum. The symbols have the following significance:

Cr means that λ 4078 and λ 4171 of *Cr* II are strong;
Eu means that λ 3930 and λ 4205 of *Eu* II are strong;
Mn means that λ 4206 and λ 4253 of *Mn* II are strong;
Si means that λ 4128 and λ 4131 of *Si* II are strong;
Sr means that λ 4078 and λ 4215 of *Sr* II are strong;
λ 4137 means that λλ 3944, 4137, and 4282 are strong;
λ 4200 means that λλ 3955, 3992, and 4200 are strong.

It is assumed that *Cr* II is the principal contributor to λ 4078 in spectra where *Cr* II 4171 is strong but λ 4215 is weak or absent; where λ 4215 is strong, λ 4078 is attributed mainly to *Sr* II.

The eighth and ninth columns give the lines which vary. Since all the lines of a given ion appear always to vary together, it is sufficient merely to name the ion which is the source of variable lines of known origin. Unidentified lines are indicated by their wave lengths. The variable lines are grouped into two classes: I, those which vary in phase with *Ca* II K, and II, those which vary out of phase with K. Where the variation of K has not been observed, this classification is, of course, ambiguous. Lines whose variation requires further verification are inclosed in parentheses; these have probably been too liberally employed, and I should estimate that more than 80 per cent of the lines so distinguished are truly variable. The elements of variation are compiled. The periods are probably correct to within two units in the last decimal place; exceptions are the periods distinguished by parentheses, which require further verification.

[28] *Ap. J.*, **77**, 226, 1933.

[29] *Ap. J.*, **102**, 438, 1945.

TABLE 7

A FIRST CATALOGUE OF SPECTRUM VARIABLES

No.	Star	R.A. 1900	Decl. 1900	Mag. Vis.	HD		Peculiar Features	Lines of Class I (Lines Which Vary with K)	Lines of Class II (Lines Which Vary Opposite K)	Elements of Variation		
					Number	Type				Phase	Epoch (J.D.)	Period
1..	α And	0^h03^m2	+28° 32′	2.15	358	A0p	*Mn*, λ 4137	.....	.....	.....	.....	.....
2..	γ Ari (S)	1 48.0	+18 48	4.83	11503	A0p	*Cr, Eu, Si*	*Ca* II, λ 4161; (*Cr* II),(*Mg* II)	(*Eu* II), λλ (4063), (4179)	*Cr* II min.	2431782.5	(2^d.607)
3..	ι Cas	2 20.8	+66 57	4.59	15089	A5p	*Sr, Cr*	*Ca* II, *Sr* II, λλ 4133, 4161, 4423, 4431; (*Cr* II), (λ 4290)	(λ 4179)	*Ca* II max.	2431700.1	1.740
4..	56 Ari	3 06.3	+26 53	5.65	19832	A0p	*Si*?, λ 4200	λ 4200; λλ (3955), (3992), (4129)	*He* I	*He* I max.	2432227.55	2.563
5..	+33°1008	5 12.4	+33 39	5.39	34452	A0p	*Si*, λ 4200	*Ca* II, *He* I; (*C* II), (*Mg* II)	λλ 3955, 3992, 4057, 4200; (*Fe* II)	*He* I max.	2431334.90	2.4660
6..	θ Aur	5 52.9	+37 12	2.71	40312	A0p	*Si*	(*Cr* II), (*Cr* I), (*Sr* II)	.....	.....	.....	.....
7..	49 Cnc	8 39.3	+10 27	5.58	74521	A0p	*Si, Cr, Eu*	(*Eu* II), (*Sr* II)	.....	.....	.....	.....
8..	17 Com	12 23.9	+26 28	5.38	108662	A0p	*Cr, Eu*	(*Cr* II), (*Sr* II)	.....	.....	.....	.....
9..	21 Com	12 26.0	+25 07	5.39	108945	A3p	*Sr, Cr*	(*Sr* II)	.....	.....	.....	.....
10..	ε UMa	12 49.6	+56 30	1.68	112185	A0p	*Cr, Eu*	*Ca* II	*Cr* II, *Cr* I, *Fe* II, *Fe* I, *Mn* II, *Mn* I; (*Sr* II), (*Ti* II), (*Ni* II), (*Si* II), (*O* I)	*Ca* II min.	2426437.01	5.0887
11..	α^2 CVn	12 51.4	+38 51	2.90	112413	A0p	*Si, Cr, Eu*	*Ca* II, *Ti* II, *Mn* II, *Sr* II, *Eu* II, *Gd* II, *Dy* II, *Ce* II, *Pr* II, *Nd* II, *Sm* II, *Fe* I, *Ni* I; (*Cr* I)	*Cr* II, λ 4200; (*Fe* II)	*Eu* II max.	2419869.720	5.46939

TABLE 7—*Continued*

No.	Star	R.A. 1900	Decl. 1900	Mag. Vis.	HD Number	HD Type	Peculiar Features	Lines of Class I (Lines Which Vary with K)	Lines of Class II (Lines Which Vary Opposite K)	Elements of Variation: Phase	Epoch (J.D.)	Period
12..	78 Vir	13h29m1	+ 4°10′	4.93	118022	A2p	*Sr, Cr, Eu*	*Ca* II	(*Cr* II), (*Sr* II)	.....	.....	.....
13..	−18°3789	14 13.1	−18 15	5.74	125248	A0p	*Cr, Eu*	*Ca* II, *Cr* II, *Mg* II, λ 4161, λ 4290; (*Sr* II), (*Fe* II), (*Si* II), (*Cr* I)	*Eu* II, λ 4063, λ 4296	*Eu* II max.	2430143.07	9.295
14..	π Boo(A)	14 36.0	+16 51	4.94	129174	A0	*Mn*, λ 4137	*Ca* II, λ 4137; λλ (3944), (3984), (4282)	λ 4253; (λ 4206)	*Mn* II max.	2421391.45	(2.2445)
15..	χ Ser	15 37.1	+13 10	5.26	140160	A0p	*Sr, Cr*	*Ca* II	*Sr* II, λ 4161, λ 4290	*Sr* II max.	2432003.85	2.675
16..	ω Oph	16 26.2	−21 15	4.57	148898	F0	*Sr, Cr*	(*Ca* II), (*Sr* II)	.....	.....	.....	.....
17..	45 Her	16 42.8	+ 5 26	5.28	151525	A0p	*Cr*	*Ca* II, (*Mg* II)	(*Cr* II)	.....	.....	.....
18..	21 Aql	19 08.7	+ 2 07	5.10	179761	B8	.....	(*He* I)	.....	.....	.....	.....
19..	73 Dra	20 32.8	+74 37	5.18	196502	A2p	*Sr, Cr, Eu*	*Eu* II, *Ti* II; (λ 4423)	.....	*Eu* II max.	2430678.22	20.27
20..	γ Equ	21 05.5	+ 9 44	4.76	201601	F0p	*Sr, Eu*	(*Cr* II)	.....	.....	.....	.....

NOTES FOR TABLE 7

1. Sp.bin., P = 96d7; 10.8 mag. (var?) comp., 80″, 280°.
2. 4.75 mag. comp., A0, 8″, 0°, c.p.m.
3. 6.8 mag. comp., F6, 2″, 250°; 8.0 mag. comp., G4, 7″, 111°.
4. From Yerkes and Perkins (1946–47) plates.
6. 7.5 mag. comp., 3″, 330°.
8. 6.7 mag. comp., A-met-l., 145″, 250°, c.p.m.
10. Sp.bin.?, P = 4y15; in Ursa cluster.
11. 5.39 mag. comp., F5 IV, 20″, 228°, Sp.bin., c.p.m.
12. In Ursa cluster.
14. 5.81 mag. comp., A-met.-l., 6″, 105°.
15. In Ursa cluster.
20. 11 mag. comp., 2″, 270°.

Inspection of the table shows that the periods appear to be uncorrelated with other characteristics. The variable lines are seen usually to include those strong lines which mark the spectrum as peculiar, except in the case of *Si* II, which usually does not vary.

Table 8 sets forth the phase relations among lines of different ions in each of the stars in Table 7. Included are all lines or sets of lines which are found to vary in three or more of the stars. The stars are arranged approximately in order of increasing effective excitation, according to the system elucidated by Morgan.[30] The columns are arranged in order of increasing ionization potential. The notation is the same as in Table 7. The table in-

TABLE 8*

PHASE RELATIONS AMONG VARIABLE LINES IN SPECTRUM VARIABLES

Source	*Cr* I	*Sr* II	*Eu* II	*Ca* II	*Ti* II	*Mg* II	*Mn* II	*Fe* II	*Cr* II	*He* I	λ 4161	λ 4200	λ 4290
I.P. (e.v.)	6.7	11.0	11.2	11.8	13.6	15.0	15.6	16.2	16.6	24.5	.....	.....	.....
21 Aql	.....	.....	.....	.....	.....	.....	.....	.....	.....	.....	.....	.....	.....
56 Ari	.....	.....	.....	.....	.....	.....	.....	.....	.....	II	.....	I	.....
+33°1008	.....	.....	.....	I	.....	(I)	.....	(II)	.....	I	.....	II	.....
α And	.....	.....	.....	.....	.....	.....	.....	.....	.....	.....	.....	.....	.....
π Boo (A)	.....	.....	.....	I	.....	.....	II	.....	.....	.....	.....	.....	.....
θ Aur	(I)	(I)	.....	.....	.....	.....	.....	.....	(I)	.....	.....	.....	.....
45 Her	.....	.....	.....	I	.....	(I)	.....	.....	(II)	.....	.....	.....	.....
ε UMa	II	(II)	.....	I	(II)	.....	II	II	II	.....	.....	.....	.....
α^2 CVn	(I)	I	I	I	I	.....	I	(II)	II	.....	.....	II	.....
49 Cnc	.....	(I)	(I)	.....	.....	.....	.....	.....	.....	.....	.....	.....	.....
17 Com	.....	(I)	.....	.....	.....	.....	.....	.....	(I)	.....	.....	.....	.....
78 Vir	.....	(II)	.....	I	.....	.....	.....	(II)	(II)	.....	.....	.....	.....
γ Ari(S)	.....	.....	(II)	I	.....	(I)	.....	(II)	(I)	.....	I	.....	.....
−18°3789	(I)	(I)	II	1	.....	I	.....	(I)	I	.....	I	.....	I
21 Com	.....	(I)	.....	.....	.....	.....	.....	.....	.....	.....	.....	.....	.....
ι Cas	.....	I	.....	I	.....	.....	.....	(II)	(I)	.....	I	.....	(I)
ω Oph	.....	(I)	.....	(I)	.....	.....	.....	.....	.....	.....	.....	.....	.....
73 Dra	.....	.....	I	.....	I	.....	.....	.....	.....	.....	.....	.....	.....
χ Ser	.....	II	.....	I	.....	.....	.....	.....	.....	.....	II	.....	II
γ Equ	.....	.....	.....	.....	.....	.....	.....	.....	(I)	.....	.....	.....	.....

* Lines of class I vary with K; lines of class II vary opposite K. The classification is ambiguous in spectra where the variation of K has not been observed. Parentheses indicate that the variation requires verification.

dicates six well-established cases in which the phase relations differ from star to star among lines of pairs of ions. These cases are as follows:

1. In α^2 CVn, *Eu* II and *Ca* II vary in phase; in BD−18°3789, they vary out of phase.
2. In ι Cas and α^2 CVn, *Sr* II and *Ca* II vary in phase; in χ Ser, they vary out of phase.
3. In BD−18°3789, *Ca* II and *Cr* II vary in phase; in ε UMa and α^2 CVn, they vary out of phase.
4. In α^2 CVn, *Ca* II and *Mn* II vary in phase; in π Boo(A) they vary out of phase.
5. In ι Cas, *Ca* II and λ 4161 vary in phase; in χ Ser, they vary out of phase.
6. In ε UMa, *Cr* II and *Mn* II vary in phase; in α^2 CVn, they vary out of phase.

Table 8 suggests that in each star all lines originating from atoms or ions having ionization potentials within certain limits vary together, while lines originating from atoms or ions of lower or higher ionization potential vary in the opposite sense Thus, in α^2 CVn, the lines of class I originate from atoms or ions having ionization potentials less than 16 volts, and those of class II originate from atoms or ions having ionization potentials

[30] *Ap. J.*, **77**, 330, 1933.

greater than 16 volts. Two exceptions appear in the table. The first is BD+33°1008; but here the rule would be preserved if it were assumed that the unidentified line at λ 4200 has a source of ionization potential between 16 and 24 volts. The second exception is γ Ari (S), and this can be reconciled with the proposed rule only if the observations are in error.

V. LUMINOSITIES AND COLORS

A careful comparison of the spectra of the known spectrum variables with the spectra of other peculiar stars on the observing list fails to reveal any criterion, except the variability itself, by which they can be distinguished. There are a number of cases in which the spectrum of a star not known to vary matches almost identically, at some phase, that of one which does vary (e.g., 10 Aql and ι Cas). It is to be expected that continued observation will reveal many new cases of variability among such spectra, and it is by no means impossible that all the peculiar A stars will eventually prove to be spectrum variables of greater or smaller amplitude.

In view of the spectroscopic identity of the variable and (apparently) nonvariable peculiar A stars, it appears legitimate to discuss their luminosities and colors together. The data are very meager at best, and the admission of all peculiar A stars alleviates this deficiency in an important degree.

1. *Luminosities.*—The peculiar A stars generally exhibit less strongly winged hydrogen lines than do main-sequence stars of the same spectral type. The effect is not large, but it appears to be real. The application of the other usual luminosity criteria in the discussion of peculiar stars later than type A2 is probably not legitimate, since some of the lines involved are those which mark the spectrum as peculiar.

The distances probably most accurately known are those of ε UMa, χ Ser, and 78 Vir, which are assumed to be members of the Ursa cluster. Smart's recent discussion[31] give absolute magnitudes of −0.32 for ε UMa (A0p), +0.41 for χ Ser (A0p), and +0.47 for 78 Vir (A2p). The corresponding mean absolute magnitudes are +0.81 ± 0.41 for nine cluster stars of (normal) type A0 and +1.51 ± 0.42 for seven cluster stars of (normal) type A2. The errors indicated are average residuals for single stars. It follows that ε UMa and 78 Vir, at least, probably lie appreciably above the main sequence. Moreover, the effective excitation in the spectrum of χ Ser corresponds to a type certainly later than A0, so that this star, too, must lie above the main sequence.

The two spectrum variables in the Coma cluster present a similar case, if somewhat less convincing. According to Trumpler's value[32] of the parallax (0".012), 17 Com (A0p) has an absolute magnitude of +0.83, and 21 Com (A3p) of +0.84. The effective excitation in both spectra is definitely later than in type A0, so that both these stars probably lie at least slightly above the main sequence.

Among all the peculiar stars on the observing list, there are thirteen for which Schlesinger[33] gives a trigonometrical parallax of 0".020 or greater. These stars are listed with their parallaxes, according to Schlesinger, in Table 9. The first four columns require no explanation; the fifth column gives the absolute magnitude, $M(p)$, derived from the magnitude and parallax. The probable error given is $2.17\ \Delta p/p$, where p is the parallax and Δp its probable error. The use of this formula is not strictly legitimate here because of the large values of $\Delta p/p$, but it provides a useful approximation. The sixth column gives the difference between the absolute magnitude of the fifth column and the absolute magnitude, M_0, of a main-sequence star of corresponding spectral type. The values of M_0 have been taken from Trumpler's work.[32]

It is readily seen that a normal distribution of the errors in p produces a skew distribution of the errors in $M(p)$ such that $M(p)$ is probably too faint. Since this is the case,

[31] *M.N.*, **99**, 448, 710, 1939.

[32] *Lick Obs. Bull.*, **14**, 157, 1930.

[33] *General Catalogue of Parallaxes* (2d ed.; Lancaster, Pa., 1935).

the difference $M(p) - M_0$ is probably too great. Moreover, since this is true for each star, it is also true of the weighted mean, $\overline{M(p) - M_0}$. Using weights proportional to the inverse squares of the probable errors of M_0, we thus find that $\overline{M(p) - M_0} = -0.56 \pm 0.14$ (p.e.), i.e., on the average these stars probably lie more than half a magnitude above the main sequence.

The arbitrary exclusion from the table of all measured parallaxes less than 0".020 introduces an error which arises from the circumstance that parallaxes whose true values are less than this limit but whose measured values exceed it are included, while those whose true values exceed the limit but whose measured values fall below it are excluded. The effect of this cutoff error will be seen, however, to include stars whose $M(p)$ is too faint and to exclude those whose $M(p)$ is too bright. We may therefore regard 0.5 mag. as a kind of lower limit of the distance from the main sequence upward to the peculiar stars.

TABLE 9

TRIGONOMETRICAL PARALLAXES AND ABSOLUTE MAGNITUDES OF PECULIAR STARS

Star	HD Type	m	Trigonometrical Parallax (p)	$M(p)$	$M(p)-M_0$	Corrected Parallax
β Tau.....	B8	1.78	0".022±0".007	−1.51±0.69	−1.3	0".055±0".017
α And.....	A0p	2.15	.024± .005	−0.95±0.45	−1.8	.043± .009
+73°2743.....	A0p	5.38	.023± .009	+2.19±0.85	+1.3	.181± .071
μ Lep.....	A0p	3.30	.021± .007	−0.09±0.72	−1.0	.063± .021
θ Aur.....	A0p	2.71	.021± .006	−0.68±0.62	−1.7	.048± .014
α^2 CVn.....	A0p	2.90	.025± .005	−0.11±0.43	−1.0	.063± .013
ω Her.....	A0p	4.53	.033± .006	+2.12±0.39	+1.2	.175± .032
108 Aqr.....	A0p	5.32	.020± .010	+1.83±1.08	+0.9	.153± .077
κ Psc.....	A2p	4.94	.035± .006	+2.66±0.37	+1.0	.156± .027
ι Cas.....	A5p	4.59	.022± .009	+1.30±0.89	−1.0	.063± .026
ω Oph.....	F0	4.57	.033± .008	+2.16±0.53	−0.7	.071± .017
γ Equ.....	F0p	4.76	.022± .006	+1.47±0.59	−1.4	.052± .014
β CrB.....	F0p	3.72	0.033±0.005	+1.31±0.33	−1.6	0.048±0.007

Since there appears to be no systematic change of $M(p) - M_0$ with spectral type, we may now proceed on the assumption that $M - M_0$ is a constant for the peculiar stars. Consider the case of two stars whose spectral types and measured parallaxes are identical but whose apparent magnitudes differ appreciably. If we assume that the $M(p)$ of the brighter star is correct, then the true parallax of the fainter star must be much less than its measured value. However, if we assume that the $M(p)$ of the fainter star is correct, then the true parallax of the brighter must be much greater than its measured value. It is readily shown that the first alternative has an appreciably greater a priori probability than the second and that selection effects operate in the same sense. We must therefore weight most heavily the stars of brighter apparent magnitude. This can be achieved by correcting all the parallaxes to the values for which $m = M_0$. The seventh column of Table 9 gives these corrected parallaxes with their probable errors. If we now take the weighted mean of these, we find that $\bar{p} = 0".057 \pm 0".004$ (p.e.); the corresponding value of $M - M_0$ is then found to be -1.22 ± 0.15 (p.e.). From the manner in which this value is derived, it follows that we may regard it as a kind of upper limit to the distance from the main sequence upward to the peculiar stars.

The most serious weakness in this argument would seem to be the uncertainty of the *Draper* types, which are very probably not correct for some of the stars. It is unlikely, however, that the classification errors are sufficiently systematic to produce the whole effect which is found. We therefore conclude that the peculiar stars, as a group, lie about 1 mag. above the main sequence.

2. *Colors.*—Reference has been made to the catalogue of color indices compiled by Öpik[34] from various published determinations. The catalogue gives colors for 654 stars. The scale is slightly more extended than the Harvard scale. Each color is given a weight by Öpik; he states that the unit of weight corresponds to a probable error of ± 0.06 mag.

The colors of the twenty stars on the observing list which are given by Öpik are collected in Table 10, together with their weights. The letter "c" in the weight column indicates that the components of a visual binary have been measured together. The stars are arranged approximately in order of increasing effective excitation.[30] Table 11 gives the relation between *Draper* type and color deduced by Öpik from the whole material of his catalogue.

TABLE 10

COLORS OF PECULIAR A STARS (AFTER ÖPIK)

Star	C.I.	Wt.	HD	Star	C.I.	Wt.	HD
+3°2867	−0.25	2	A0p	ϵ UMa	−0.14	7	A0p
α And	− .23	5	A0p	α^2 CVn	− .29	5	A0p
π Boo	− .26	2c	A0	γ Ari	− .39	2c	A0p
β Tau	− .23	5	B8	κ Psc	− .14	3	A2p
κ Cnc	− .18	4	B8	ω Her	− .16	3	A0p
υ Her	− .21	3	B9	52 Her	− .09	2	A2p
ϕ Her	− .24	4	B9p	78 Vir	− .12	4	A2p
11 Ori	− .20	3	B9	ι Cas	+ .01	2	A5p
θ Aur	− .15	5	A0p	73 Dra	− .10	2	A2p
ϕ Dra	−0.22	2	A0p	χ Ser	+0.06	3	A0p

TABLE 11

RELATION BETWEEN DRAPER TYPE AND COLOR (AFTER ÖPIK)

	HD TYPE								
	B3	B5	B8	B9	A0	A2	A3	A5	F0
C.I.	−0.27	−0.24	−0.20	−0.17	−0.11	−0.03	+0.05	+0.06	+0.16

If we reject the colors of π Boo and γ Ari (in which cases the components were measured together), we find that the weighted mean color index of the eight remaining A0p stars in Table 11 is −0.18, which corresponds to type B9. This value for the mean color is somewhat reduced if we exclude χ Ser, which is obviously of lower excitation than the other A0p stars. The weighted mean of the remaining seven A0p stars then is −0.20, which corresponds to type B8. Still excepting χ Ser, we see, further, that every one of the A0p stars has a bluer color than the normal A0 star. Similarly, each of the four A2p stars is bluer than the normal A2 star, and ι Cas is bluer than the normal A5 star.

Notwithstanding the low weight of some of these colors, the evidence must be regarded as conclusive that the peculiar A stars, as a group, are bluer than the normal A stars of equivalent spectral type. There remains, however, the possibility that the bluer colors may not reflect higher color temperatures but may be due only to the weakening, already mentioned, of the Balmer lines in the blue and violet. That this is not the case is indicated by the Greenwich gradients[35] of five of the stars in Table 10. These are α And,

[34] *Pub. Obs. U. Tartu* (Dorpat), **27**, 3, 1929.

[35] *M.N.*, **100**, 189, 1940.

-0.10; θ Aur, -0.05; ϵ UMa, -0.05; α^2 CVn, -0.06; and π Boo, $+0.06$. The gradients are measured relative to the mean of nine A0 stars, and their probable error is given as ± 0.02. In the case of π Boo, the components were measured together, so that its gradient can be rejected. The remaining four gradients all indicate color temperatures significantly higher than in a normal A0 star.

Additional evidence for the excessive blueness of the peculiar A stars is provided by the photoelectric colors which Stebbins and Whitford have given[36] for two peculiar stars. One is α^2 CVn, for which the V − I index is -2.12; the other is 108 Aquarii, for which V − I = -2.11. Both these stars are of type A0p. The mean color index for A0 stars is given as -1.80, and for B5 stars as -2.24. The base-line for the V − I indices is so long that these deviations from normal color cannot possibly be attributed to a luminosity weakening of the hydrogen lines.

In conclusion, we may note that the normal stars of type B8 are about 1 mag. brighter than the normal stars of type A0. It is therefore highly suggestive that the A0p stars, as a group, are also about 1 mag. brighter than the A0 stars and have colors corresponding to type B8. One is tempted to regard an A0p star as an object having the gross characteristics of a B8 star, but one in whose atmosphere some unknown mechanism suppresses the lines of helium and enhances those of hydrogen and of one or more of the ions whose lines mark the spectrum as peculiar: *Si* II, *Sr* II, *Cr* II, *Mn* II, and the rare earths.

I wish to acknowledge the kind assistance of Dr. W. W. Morgan, who has largely directed the course of this investigation. I am also indebted to Dr. O. Struve for his permission to refer to many spectrograms in the files of the Yerkes and McDonald Observatories; to Dr. J. L. Greenstein for the CG plates of ι Cas and for the CQ plate of 17 Com (B); and to Dr. G. P. Kuiper for illuminating discussions on the subject of the absolute magnitudes of the peculiar stars. Grateful acknowledgment is also made to my wife, who has given much help in the preparation of the manuscript and illustrations.

[36] *Ap.J.*, **102**, 318, 1945.

STELLAR MODELS WITH CONVECTION AND WITH DISCONTINUITY OF THE MEAN MOLECULAR WEIGHT

P. LEDOUX
Yerkes Observatory
Received December 9, 1946

ABSTRACT

In this paper the effect of a discontinuity in the mean molecular weight, μ, in stellar models is examined. The case when such a discontinuity occurs in the envelope ($r/R < \frac{1}{2}$ and $m[r] \simeq M$) is first considered. And it is shown that, in general, a discontinuity in μ produces convective instability in a small zone past the place where the discontinuity occurs. The resulting turbulence will cause mixing, and the star will rapidly adjust itself to a neighboring stable state, in which the interior region of higher μ and the exterior region of lower μ are separated by a transition region in which μ varies according to the law $\mu \propto P^{7/5}$. It is further shown that the time required for such a readjustment is very small, compared to the time in which a discontinuity in μ can be established.

The case in which the discontinuity in μ occurs in the deep interior is next examined. It appears that, even here, a pure discontinuity of μ will, in general, be smoothed out and a transition zone of variable μ established. The law of variation of μ in this transition zone follows the law $\mu \propto m(r)P^{7/5}$. Owing to the presence of the factor $m(r)$, the importance of the transition zone is greater when the change in μ occurs in the deep interior.

Finally, stellar models are constructed which consist of convective cores and radiative envelopes with assigned mean molecular weights μ_i and μ_e, respectively, separated by transition zones of variable μ (also in radiative equilibrium). It is shown that these models satisfy *all* the conditions of the problem and, further, that they do not differ greatly in their physical properties from models constructed with point-source envelopes fitted directly to convective cores without regard to the continuity of the luminosity at the interface. However, up to a certain point their interpretation as a sequence of evolution is easier.

1. *Introduction.*—Stellar models in which the mean molecular weight, μ, takes different values in different parts of the star have been discussed on a number of occasions in recent years. The most important physical context in which the problem arises is in connection with the expected increase in the mean molecular weight in the convective regions in the interior, consequent to the gradual impoverishment of hydrogen by the continued operation of the carbon cycle.[1] F. Hoyle and R. A. Lyttleton[2] have also considered the possibility that accretion of interstellar hydrogen might lead to a discontinuity of μ in the outer parts of a star also. Particularly in this latter case, these authors conclude from a discussion of the conditions to be satisfied at an interface, where μ jumps discontinuously from a value μ_e in the outer part to a value μ_i in the interior, that the ratio μ_i/μ_e cannot exceed a certain limiting value ($\simeq 1.53$); and they further infer from this that when μ_i/μ_e exceeds this critical value, developments of a dynamical nature must take place, with large-scale currents setting in; they even envisage the possibility of nonstatic atmospheres arising in this way. However, a detailed examination of this problem undertaken in §§ 3–5 reveals that these conclusions are without any real foundations.

Again it appears that there are also numerous misunderstandings regarding the problem considered by Schönberg and Chandrasekhar (*op. cit*). The discontinuity in μ assumed by these writers at the place r_c, where the radiative gradient becomes unstable, is a simplification of a mathematical nature which cannot, of course, be realized in practice. It is apparent that, even if a discontinuity should be artificially introduced at a given instant, we should expect that the "corners" will be smoothed by mixing at the

[1] M. Schönberg and S. Chandrasekhar, *Ap. J.*, **96**, 161, 1942; see also M. Harrison, *Ap. J.*, **100**, 343 1944; **103**, 193, 1945; **105**, 322, 1947.

[2] *M.N.*, **102**, 218, 1942.

interface. Indeed, it might even be argued by some that large-scale currents of the nature expected in rotating stars will prevent any appreciable inhomogeneities from arising in the chemical composition of a star. However, we shall not consider this latter possibility and shall restrict ourselves to those processes of mixing which may be expected in a star in hydrostatic equilibrium. There are, then, two types of processes to be considered: mixing (or sedimentation) consequent to thermal or similar diffusion and mixing by turbulent eddies when these exist in virtue of a prevailing superadiabatic gradient. It would seem that the former, as an agency in bringing about or smoothing existing differences of chemical composition, is very inefficient.[3] We are, therefore, left with mixing only in regions where convection exists or in regions where convection is set up in consequence of a difference of μ in neighboring regions; in the latter case, we may expect the mixing to cease, once an appropriate redistribution has been effected. And, since turbulent eddies are known from meteorological experience to be very efficient as an agency for mixing, we shall restrict ourselves to this mechanism alone in our further considerations. One consequence which follows on these assumptions is that μ will have a constant value in the (Cowling) convective core and that the variation of μ outside this region must be steep. This is the justification for the assumption of a discontinuous μ made in the investigation we have referred to. However, we shall show in this paper how it is possible to avoid the strictly nonphysical assumption of a mathematical discontinuity in μ by deriving the variation of μ which will result in the outer radiative regions in consequence of turbulence having once existed.

2. *Preliminary considerations.*—It is well known that, for stars of normal masses, radiation pressure as a factor in the equation of hydrostatic equilibrium can be ignored, and the equations of the problem are

$$\frac{dP}{dr} = -\frac{Gm(r)\rho}{r^2}, \tag{1}$$

$$\frac{dT}{dr} = -\frac{3\kappa\rho}{16\pi acT^3}\frac{L(r)}{r^2}, \tag{2}$$

or

$$\frac{d\log T}{d\log P} = \frac{3\kappa_0\mu(1-X^2)}{16\pi acG\Re}\frac{L(r)}{m(r)}\frac{P^2}{T^{8.5}}, \tag{3}$$

where we have used Kramer's law of opacity,

$$\kappa = \kappa_0(1-X^2)\rho T^{-3.5}. \tag{3'}$$

In the foregoing equations, X is the abundance of hydrogen. To the same order of approximation, the mean molecular weight is given by

$$\mu = \frac{2}{1+3X}. \tag{4}$$

Further, we have

$$P = \frac{\Re\rho T}{\mu} \tag{5}$$

and

$$dL(r) = 4\pi\rho\epsilon r^2 dr, \tag{6}$$

where ϵ is the rate of generation of energy and

$$dm(r) = 4\pi\rho r^2 dr. \tag{7}$$

[3] S. Chapman, *M.N.*, **82**, 292, 1922.

In a region where μ is a constant, the condition of convective stability resulting from the requirement that a small parcel of matter displaced adiabatically upward (downward) becomes heavier (lighter) than the surrounding medium is

$$\frac{d \log T}{d \log P} \leqslant \frac{2}{5}, \tag{8}$$

if the ratio of specific heats, γ, is taken to be $\frac{5}{3}$, as for a monatomic gas.

In a region where μ varies (owing to a real spatial difference in chemical composition and not to the variation of physical conditions), we must take into account the fact that μ remains constant during the displacement of a small element, and the condition of stability becomes

$$\frac{d \log T}{d \log P} \leqslant \frac{2}{5} + \frac{d \log \mu}{d \log P}. \tag{9}$$

Now, if μ varies from a value μ_e in the outer part to a value $\mu_i = \mu_e + \Delta\mu$ in the inner part across a spherical shell of thickness Δr between the two parts, then in this region of varying μ, equations (1)–(7) will continue to be valid, whatever the value of the ratio $\Delta\mu/\Delta r$. Equations (1) and (7) require that $\Delta m(r)$ and ΔP be proportional to Δr, while from equation (5) it follows that one of the ratios $\Delta\rho/\Delta r$ or $\Delta T/\Delta r$ must be of the same order of magnitude as $\Delta\mu/\Delta r$. L. Gratton[4] argues in favor of taking $\Delta T/\Delta r$ proportional to $\Delta\mu/\Delta r$. But, by equation (2), this would make $L(r)$ depend, in that region, on the steepness of the variation of μ, which is physically inadmissible; and ΔT, like $\Delta m(r)$ and ΔP, should be proportional to Δr. Passing to the limit of a discontinuity in μ, we obtain the usual boundary conditions, namely, that $m(r)$, P, and T are continuous across the interface, while ρ has a discontinuity related to that of μ by

$$\frac{\rho_i}{\rho_e} = \frac{\mu_i}{\mu_e}. \tag{10}$$

These are the boundary conditions used by Schönberg and others in their investigations.

As ΔT and ΔP are proportional to Δr, while $\Delta\mu$ is independent of it, condition (9) shows that such a region of variation of μ will become extremely stable with respect to convection as Δr decreases.

By equation (6) $L(r)$ also should be continuous across the interface. It is this condition that Hoyle and Lyttleton[2] have taken explicitly into account in their investigation of the external layers of a star. Recently,[4] they have extended their discussion to the deep interior, considering especially the case in which the discontinuity of μ occurs at the boundary of the convective core. They consider that, since, by definition, convection should stop at the boundary of the core, the transfer of energy on both sides of the interface should be governed by equation (2), and the continuity of $L(r)$ at the interface would require, according to equation (3), that

$$(n_e + 1)\,\mu_e\,(1 - X_e^2) = (n_i + 1)\,\mu_i\,(1 - X_i^2), \tag{11}$$

where we have introduced the effective polytropic index n,

$$(n + 1) = \frac{d \log P}{d \log T}. \tag{12}$$

[4] Dr. Gratton's original paper is not accessible to the author, but, through the kindness of Dr. Chandrasekhar, the author has seen some correspondence in which Dr. Gratton has stated his argument. Similarly, the author has also had the opportunity of seeing a manuscript of a paper by Hoyle and Lyttleton on the same subject.

Hoyle and Lyttleton point out that condition (11) is incompatible with the procedure generally adopted in fixing the boundary of the convective core ($n_i = \frac{3}{2}$) where the radiative solution for the point-source envelope becomes unstable ($n_e = \frac{3}{2}$), except in the case in which there is no change of composition across the interface ($\mu_i = \mu_e$). Furthermore, condition (11) implies a limitation for the possible variation of μ, just as in the external layers. Thus, when μ_i is different from μ_e, Hoyle and Lyttleton propose to replace the condition of the continuity of n across the interface by condition (11), whenever it can be satisfied. However, we shall show (§§ 5, 6) that condition (11), even when it is satisfied for $n_i = \frac{3}{2}$, does not, in itself, tell us anything as to the existence or otherwise of a convective region past the interface. Also, the limit formally set by equation (11) on the magnitude of the variation of μ can be violated in the interior of the star just as in the external layers without endangering its equilibrium. In fact, we shall show (§§ 5, 6), contrary to the views expressed by Hoyle and Lyttleton, that for any assigned value of μ_i/μ_e equilibrium configurations can be found which will be compatible with all the conditions of the problem, including the condition of the continuity of $L(r)$ and the stability criteria (8) and (9). But it may be said, even here, that these detailed considerations confirm what may indeed be expected, on general grounds—that a satisfactory first approximation is obtained by insuring the continuity of n across the interface and ignoring condition (11). Thus a stellar model, constructed with the usual boundary conditions of continuity of n and discontinuity of ρ at the interface, where μ is discontinuous, will violate condition (11). The consequence of this violation is that more energy is leaving the external side of the interface than is brought to its internal side by radiation alone. But it is well known that, in the convective parts of the star, turbulence is very effective as a means for transporting energy,[5] so that only a very slight superadiabatic gradient extending to the surface of the convective core would be sufficient to compensate for this. Thus, if we suppose, for example, that the two kinds of material composing the external and the internal regions cannot mix at all (or that they are separated by a perfectly conducting membrane of negligible mass), a finite pressure, p_c, due to turbulence will be applied to the base of the external part, and it should be taken into account in the equations of fit. However, just like the very slight degree of superadiabasy necessary, this pressure will be very small compared to P, so that the external solution to be chosen will not be very different from the one corresponding to the ordinary fitting or, on the other picture, the membrane between the two parts need sustain only very small stresses.

In reality, some mixing will take place at the interface, and we shall see how it leads to a stable state free of any difficulties arising from condition (11).

3. *The solution for a discontinuity of μ in the external layers.*—In the external layers of a star, M and L can be considered as constants, and equations (1) and (3) reduce to

$$\frac{dP}{dr} = -\frac{GM}{r^2}\rho \tag{13}$$

and

$$\frac{1}{T}\frac{dT}{dr} = C(1 - X^2)\mu\frac{P^2}{T^{8.5}}\frac{1}{P}\frac{dP}{dr}, \tag{14}$$

where

$$C = \frac{3\kappa_0}{16\pi a c G \Re}\frac{L}{M}. \tag{15}$$

If we use equation (14), the conditions of stability (8) and (9) become, respectively,

$$C(1 - X^2)\mu\frac{P^2}{T^{8.5}} \leqslant \frac{2}{5} \tag{16}$$

and

$$C(1 - X^2)\mu\frac{P^2}{T^{8.5}} - \frac{d\log\mu}{d\log P} \leqslant \frac{2}{5}. \tag{17}$$

[5] Cf., e.g., Cowling, *M.N.*, **96**, 51–52, 1935.

First, we shall assume that a discontinuity of μ occurs at $r = r_c$ (say).

The solution for T in the external part ($r_c \leqslant r \leqslant R$) is well known[6] and can be written in the form

$$T_e = \frac{GM\mu_e}{4.25\Re}\left[\frac{1}{r} - \frac{1}{R}\right]. \tag{18}$$

The other variables are related to T by

$$C(1 - X_e^2)\,\mu_e P_e^2 = \frac{1}{4.25} T_e^{3.5}, \tag{19}$$

or

$$\frac{P_e}{P_{ec}} = \left(\frac{T_e}{T_{ec}}\right)^{4.25} \quad \text{and} \quad \frac{\rho_e}{\rho_{ec}} = \left(\frac{T_e}{T_{ec}}\right)^{3.25}. \tag{20}$$

Obviously, condition (16) is satisfied, and the radiative equilibrium is stable in that region.

In the inner part, close enough to the interface, L and M can still be considered as constant, and the solution can still be obtained by integrating equation (14). After determining the constant of integration by the continuity of P and T at the interface, which requires that P_{ic} and T_{ic} satisfy equation (19), we have

$$C(1 - X_i^2)\,\mu_i \frac{P_i^2}{2} = \frac{T_i^{8.5}}{8.5}\left[1 - \left(\frac{T_{ic}}{T_i}\right)^{8.5}\left(1 - \frac{1 - X_i^2}{1 - X_e^2}\frac{\mu_i}{\mu_e}\right)\right]. \tag{21}$$

Introducing the value of $P_i^2/T_i^{8.5}$ from equation (21) in equation (14) and replacing dP/dr by its value (13), we obtain

$$\frac{dT_i}{dr} = -\frac{1}{4.25}\frac{GM\mu_i}{\Re r^2}\left[1 - \left(\frac{T_{ic}}{T_i}\right)^{8.5}\left(1 - \frac{(1 - X_i^2)\,\mu_i}{(1 - X_e^2)\,\mu_e}\right)\right]. \tag{22}$$

When we write

$$y = \frac{T_i}{T_{ic}}, \quad r = \frac{1}{x}, \quad \alpha = \frac{1}{4.25}\frac{GM\mu_i}{\Re T_{ic}} = \frac{\mu_i}{\mu_e}\frac{Rr_c}{R - r_c}, \quad \beta = -\left(1 - \frac{1 - X_i^2}{1 - X_e^2}\frac{\mu_i}{\mu_e}\right), \tag{22'}$$

equation (22) becomes

$$\frac{dy}{dx} = \alpha\left(1 + \frac{\beta}{y^{8.5}}\right). \tag{23}$$

To obtain the exact solution of equation (23) is rather cumbersome, but, as we shall need it only in the immediate vicinity of the interface, where y is very close to 1, we can use a suitable approximation. Thus, if we wish to evaluate y as a function of x, we can integrate equation (23) by the method of successive approximations. In the second approximation we find

$$\left.\begin{aligned}\frac{T_i}{T_{ic}} = 1 + \frac{\mu_i}{\mu_e}\frac{Rr_c}{R - r_c}\left(\frac{1}{r} - \frac{1}{r_c}\right) \\ + \frac{\beta}{7.5\,(1+\beta)}\left\{1 - \frac{1}{\left[(1+\beta)\frac{\mu_i}{\mu_e}\frac{Rr_c}{R - r_c}\left(\frac{1}{r} - \frac{1}{r_c}\right) + 1\right]}\right\}.\end{aligned}\right\} \tag{24}$$

On the other hand, if we wish to evaluate x as a function of y, it is more convenient to write $y = 1 + z$ in equation (23); and, limiting ourselves to the second-order terms in the development of $(1 + z)^{8.5}$, we find

$$\alpha\,dx = \frac{dz}{1 + \beta\,[1 - 8.5z + 40.375z^2]}. \tag{25}$$

[6] Cf. S. Chandrasekhar, *Introduction to the Study of Stellar Structure*, p. 300.

Finally, we may explicitly note that, in the solution of the problem that we have presented, ρ has a discontinuity at $r = r_c$ in accordance with equation (10).

We have now all that is necessary to study the stability of the radiative solution in the neighborhood of the interface. Since we have integrated equations (13) and (14) exactly, the continuity of L at the interface has, of course, been insured.

We have already seen that the radiative equilibrium is stable in the external part of the star. To investigate its stability in the internal part, near the interface, we introduce the value of $P_i^2/T_i^{8.5}$ given by equation (21), into condition (16), and we find

$$\frac{1}{4.25}\left[1-\left(\frac{T_{ic}}{T_i}\right)^{8.5}\left(1-\frac{1-X_i^2}{1-X_e^2}\frac{\mu_i}{\mu_e}\right)\right] \leqslant \frac{2}{5}. \tag{26}$$

At the interface, $T_i = T_{ic}$, and condition (26) for stability reduces to

$$\frac{1}{4.25}\left(\frac{1-X_i^2}{1-X_e^2}\frac{\mu_i}{\mu_e}\right) \leqslant \frac{2}{5}; \tag{27}$$

and when this is taken with the equality sign, it is equivalent to condition (11) of Hoyle and Lyttleton. Now if the values of μ_i and μ_e are such that

$$\left(\frac{1-X_e^2}{1-X_i^2}\right)\frac{\mu_e}{\mu_i} < \frac{5}{8.5} = 0.588, \tag{27'}$$

the radiative equilibrium will be unstable on the internal side of the interface. However, as we leave the interface, $(T_{ic}/T_i)^{8.5}$ decreases so rapidly that, after we have gone only a little distance, condition (26) will again be satisfied. We can, accordingly, expect that the extent of the unstable region resulting from the violation of equation (27) will be very small indeed.

On the other hand, as we have already seen, a discontinuity of μ (with $\mu_i > \mu_e$) is going to provide a very effective barrier to convection. Thus we must expect that the energy available for convection on the internal side of the interface will soon be used up by the mixing of two narrow regions on both sides of the interface.

As an example, let us take $\mu_e = 1$, $X_e = \frac{1}{3}$, and $\mu_i = 2$, $X_i = 0$, and suppose that the discontinuity of μ occurs at $r_c = 0.9R$. In that case, using condition (26) and equations (21) and (5), we find that the unstable region extends to the point where P, T, and ρ have the values

$$P_i^* = 1.1616P_{ic}; \qquad T_i^* = 1.0706T_{ic}; \qquad \text{and} \qquad \rho_i^* = 1.0850\rho_{ic}. \tag{28}$$

Introducing into equation (25) the numerical value of β corresponding to this case and integrating, we get

$$r_c - r^* = 0.01812\,\frac{r_c}{R}(R - r_c), \tag{29}$$

so that the extent of the unstable region is of the order of 1–2 per cent of the external region. In the particular case considered ($r_c = 0.9R$),

$$r^* = 0.89834R. \tag{30}$$

To compute the mass Δm_i of the unstable region, we can assume that ρ is constant in it and equal to ρ_{ic}, so that, using equations (18), (20), and (10), we can write the ratio of Δm_i to the mass M_e of the external part as

$$\frac{\Delta m_i}{M_e} = \frac{\mu_i}{\mu_e}\left(\frac{1}{\xi_c}-1\right)^{3.25}\frac{(\xi_c^3 - \xi^{*3})}{3f(0,\,\xi_c)}, \tag{31}$$

where $\xi = r/R$ and $f(0, \xi_c)$ is the function tabulated by S. Chandrasekhar.[7] In our example, with the value 0.000014 of $f(0, 0.9)$ given by S. Chandrasekhar, formula (31) gives $\Delta m_i/M_e = 0.153$.

The solutions T/T_{ec}, P/P_{ec}, and ρ/ρ_{ec} in the vicinity of the interface are represented in Figure 1 (*full curves*).

4. *Energy available in the unstable region and resulting motion and mixing.*—Consider, next, an element of matter of unit mass situated at the base of the unstable region. If a

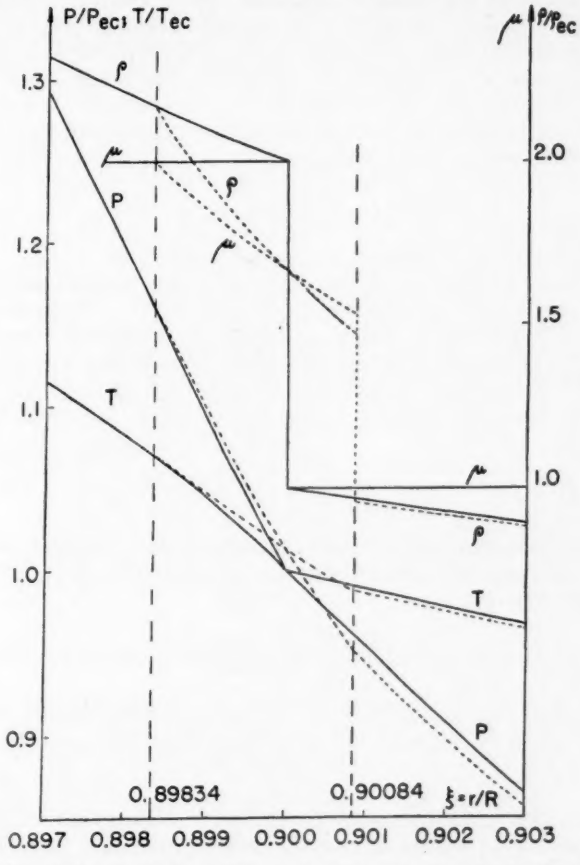

FIG. 1.—Distribution of the physical conditions at a discontinuity of μ in the stable (*dotted curves*) and unstable states (*full curves*).

small adiabatic displacement outward is given to it, its speed outward will increase all through the unstable region. Neglecting friction, we can express its kinetic energy, on reaching the interface, in the form

$$\tfrac{1}{2} v^2 = \frac{P_{ic}}{\rho_{ic}} \int_{(P_i^*/P_{ic})}^{1} \left[\left(\frac{\rho_{ic}}{\rho_i} \right) - \left(\frac{\rho_{ic}}{\rho_{ad}} \right) \right] d \left(\frac{P_i}{P_{ic}} \right), \tag{32}$$

where

$$\rho_{ad} = \rho_i^* \left(\frac{P_i}{P_i^*} \right)^{3/5} = \rho_{ic} \left(\frac{\rho_i^*}{\rho_{ic}} \right) \left(\frac{P_{ic}}{P_i^*} \right)^{3/5} \left(\frac{P_i}{P_{ic}} \right)^{3/5}. \tag{33}$$

[7] *Op. cit.*, p. 302.

For the example studied in § 3, the values of the different constant ratios in equation (33) have been given, and the values of ρ_i/ρ_{ic} and P_i/P_{ic} can be obtained from the solutions given there or can be taken directly from Figure 1. Evaluating the integral, we find that

$$\tfrac{1}{2}v^2 = 0.000405\frac{P_{ic}}{\rho_{ic}} = 2.7\times 10^{-4}\,(n\tfrac{3}{2}kT_{ic})\,, \tag{34}$$

where n is the number of the particles contained in the element considered. Equation (34) shows that the available energy in the unstable region is very small, compared to the internal energy of that region, which is itself a small quantity. It is, therefore, difficult to see how any large-scale motion can result from the instability in the small region bordering on r_c.

An elementary computation also shows that the time required by a small element to go across the unstable region is of the order of

$$\Delta t \simeq \frac{10^2}{\sqrt{\bar{\rho}}} \text{ seconds}\,, \tag{35}$$

where $\bar{\rho}$ is the mean density, in grams, of the star considered.

Now a rising element of gas will arrive at the interface with a finite kinetic energy of the order of magnitude given by expression (34). Using the corresponding equation (32) and the relation (20) between ρ_e and P_e, it is easy to determine the pressure P_e^0 corresponding to the level ξ^0 in the external part where that kinetic energy will be used up. We find $P_e^0 = 0.9996\,P_{ec}$ and $\xi^0 = 0.90001$. If we denote by Δm_e the mass of the layer comprised between ξ_c and ξ^0, its ratio to the mass Δm_i of the unstable region is of the order of

$$\frac{\Delta m_e}{\Delta m_i} \simeq \frac{\rho_{ec}}{\rho_{ic}}\frac{\xi^0-\xi_c}{\xi_c-\xi^*} = 0.0027\,. \tag{36}$$

If we now consider a downward motion, a small element initially at the internal side of the interface will stop somewhere between the points ξ^* and ξ_s, where the following relations hold, respectively,

$$\frac{1}{T_i^*}\frac{dT_i^*}{dr} = \frac{2}{5}\frac{1}{P_i^*}\frac{dP_i^*}{dr} \tag{37}$$

and

$$\frac{P_{is}}{P_{ic}} = \left(\frac{T_{is}}{T_{ic}}\right)^{5/2}. \tag{38}$$

From our discussion in the preceding paragraph it follows that, when μ is assumed to change discontinuously at a point in violation of condition (27), turbulence in a small region surrounding that point will immediately result. This resulting turbulence will lead to a small amount of mixing of the internal and the external parts. And if, as we shall show, a neighboring stable state can be reached in consequence of this turbulence, it is not really relevant to our problem to describe in detail the exact changes which will lead to that stable state. However, in a general way, it is apparent that the first step will be a mixing of two regions whose masses are of the order of Δm_e and Δm_i with the formation of an intermediate region of mass $a\Delta m_e + b\Delta m_i$ and mean molecular weight

$$\mu_m \simeq \mu_i\left\{1-\left(\frac{\mu_i}{\mu_e}-1\right)\frac{a\Delta m_e}{b\Delta m_i}\right\},$$

where a and b are two constants of order unity. In the example considered, $\mu_m = 1.995$ if $a = b = 1$. The radiative solutions for these regions, characterized, respectively, by μ_i, μ_m, and μ_e, can be obtained and the radiative instability at each interface examined.

It will again be seen that, in the intermediate part, there will be a small region around the points defined by the corresponding relations (38) and (37) which will be little affected by mixing at this stage, and the extent of the region affected in the internal part will again be determined by the same analogous relations. The changes in μ which will result from the corresponding mixing can be estimated as before, and the process can be continued a step further. In this manner a stable state can be reached, and the time required to attain it can be estimated as follows:

At a given stage the time required for a single "turnover" of the unstable regions may be taken to be of the same order as that given by equation (35). A hundred such turnovers would probably be more than sufficient to mix the relevant regions thoroughly. If a thousand such steps are necessary to bring the regions to a stable state, a total time of the order of $1/\sqrt{\bar{\rho}}$ years will be required. For all reasonable values of $\bar{\rho}$ this is such a short time, as compared to the time required for the building-up of an appreciable discontinuity of μ (either by exhaustion of hydrogen, by nuclear reactions, or by accretion of interstellar hydrogen) that we can safely consider that the readjustment takes place practically instantaneously!

5. *Final state of equilibrium.*—What we have said in § 4 of the detailed manner in which a stable state will be reached is sufficient to show that at each step there will be a number of small regions (equal to the number of discontinuities of μ), each little affected by the subsequent mixing and comprised between points ξ^* and ξ_*, where the relations corresponding to (37) and (38) are satisfied. As the number of discontinuities in μ increases, these two points, ξ^* and ξ_*, in each region of constant μ will tend to come closer and closer. At the limit, where the variation of μ can be considered as continuous, relations (37) and (38) will hold at each point, so that, if we denote by a suffix t the values of the variables in that region, we have

$$\frac{1}{T_t}\frac{dT_t}{dr}=\frac{2}{5}\frac{1}{P_t}\frac{dP_t}{dr} \tag{39}$$

and

$$\frac{P_t}{P_{tc}}=\left(\frac{T_t}{T_{tc}}\right)^{5/2}, \tag{40}$$

where the suffix c here refers to the values of the variables at the exterior limit of the region of variable μ.

If we assume that this intermediate region of variable μ is also in radiative equilibrium, equation (14) should hold in it; and, comparing it with equation (39), we obtain

$$C(1-X_t^2)\,\mu_t=\frac{P_t^2}{T_t^{8.5}}=\frac{2}{5}, \tag{41}$$

or, using equation (40),

$$(1-X_t^2)\,\mu_t=\frac{2}{5C}\frac{T_{tc}^{8.5}}{P_{tc}^2}\left(\frac{P_t}{P_{tc}}\right)^{7/5}. \tag{42}$$

With equation (41), condition (17) for the stability of the radiative equilibrium in that region reduces to

$$\frac{d\log\mu_t}{d\log P}\gtrless 0. \tag{43}$$

But, according to equation (42), μ_t, in fact, increases with P, so that condition (43) is satisfied and our assumption about the stability of radiative equilibrium in that region is confirmed. This transition region of variable μ will be limited by the fact that when μ_t

has been reduced to a certain value, μ_{tc}, such that equation (27) with $\mu_i = \mu_{tc}$ is verified with the sign of equality, the discontinuity of μ is no longer able to render the radiative equilibrium unstable. If $\mu_e = 1$, $X_e = \frac{1}{3}$, we find that μ_{tc} and X_{tc} must have the values $X_{tc} = 0.1031$ and $\mu_{tc} = 1.528$. These are, of course, equivalent to the limiting values of Hoyle and Lyttleton.

When μ_t varies from its value 1.528 to its value 2, $(1 - X_t^2)$ varies from 0.99 to 1; and in a first approximation we can neglect this factor, so that equation (42) immediately gives the variation of μ in the form

$$\frac{\mu_t}{\mu_{tc}} = \left(\frac{P_t}{P_{tc}}\right)^{7/5}. \tag{44}$$

From equations (5) and (40), we obtain

$$\frac{\rho_t}{\rho_{tc}} = \left(\frac{P_t}{P_{tc}}\right)^{2}. \tag{45}$$

The integration of equation (13) then gives

$$1 - \frac{P_{tc}}{P_t} = \frac{GM\mu_{tc}}{\Re T_t}\left(\frac{1}{r} - \frac{1}{r_c}\right). \tag{46}$$

The solution allowing for the variation of the factor $(1 - X_t^2)$ in this transition region can, of course, be obtained by eliminating X_t between equations (4) and (42) and then proceeding as above. But we shall not consider such refinements here.

In the external part ($\mu = \mu_e$), the solution is the same as before, and it is, of course, stable.

In the internal part ($\mu = \mu_i$), integrating equation (14) and taking into account the fact that all the variables must be continuous at the interface, r^*, where the variation of μ_t ceases, we obtain

$$C(1 - X_i^2)\,\mu_i \frac{P_i^2}{2} = \frac{T_i^{8.5}}{8.5}\left[1 + 0.7\left(\frac{T_i^*}{T_i}\right)^{8.5}\right]. \tag{47}$$

The gradient of temperature in this region can be expressed in the form

$$\frac{dT_i}{dr} = -\frac{\mu_i GM}{4.25\Re}\left[1 + 0.7\left(\frac{T_i^*}{T_i}\right)^{8.5}\right]\frac{1}{r^2}. \tag{48}$$

Using the value of $P_i^2/T_i^{8.5}$ given by equation (47), the criterion of stability (16) can be written

$$\frac{2}{5} - \frac{1.4}{8.5}\left[1 - \left(\frac{T_i^*}{T_i}\right)^{8.5}\right] \leqslant \frac{2}{5}; \tag{49}$$

and we see that this condition is just satisfied with the sign of equality at the interface. As we go further inside, $(T_i^*/T_i)^{8.5}$ decreases, and the requirement (49) will be met with the sign of inequality. Thus we can picture the star in its final state as being composed of the three parts we have described, all of which are in stable radiative equilibrium.

It may be noted that when μ_e and μ_i are given, the extent of the intermediate region, where μ varies continuously, is determinate, for, μ_e being known, equation (27) taken with the sign of equality can be solved for μ_{tc} and, by equations (44) and (46), we have

$$\frac{r_c}{R} - \frac{r^*}{R} = \left[1 - \left(\frac{\mu_{tc}}{\mu_i}\right)^{5/7}\right]\frac{\mu_e}{\mu_{tc}}\,\frac{1}{4.25}\,\frac{r^*}{R}\left(1 - \frac{r_c}{R}\right), \tag{50}$$

since T_{tc} must be equal to T_{ec} and its value can be obtained from equation (18).

Thus, if we choose the values of μ_i, μ_e, and r_c, the solution is completely determined in the envelope, and the problem of fitting it to a central part without singularity can be solved in the usual way. We shall not concern ourselves here with the actual mass-luminosity radius relation appropriate for these models, except to point out that the relevant relation will be practically the same whether we consider the change in μ as taking place discontinuously and ignore the effect of the small convective unstable region just interior to the interface, or whether we treat it more rigorously with the introduction of a transition region of variable μ. We shall illustrate this numerically for the example we have considered.

Suppose that the general problem has been solved for the case in which μ has been assumed to change discontinuously from its value μ_e to μ_i at $r_c = 0.9R$ and that the configuration has a mass M, luminosity L, and radius R. The effect of the instability in the small region interior to r_c will, of course, be that the star will rapidly evolve toward the state with a transition region of variable μ as we have already described. During such an adjustment, the total mass will, of course, remain constant; and, to the extent that the energy sources are in the deep interior, the luminosity will also remain constant. What will happen then is that the radius will change slightly. To estimate the extent of this change in R which will result from the redistribution of μ, we shall consider a second configuration with the same luminosity, in which the inner limit r^* of the transition region is at the same place at which the convectively unstable region in the first configuration ends. We shall further assume that the temperatures in the two configurations are also the same at the two points mentioned. Under these conditions, the solutions interior to r^* in the two configurations will be identical. And if the problem for the interior on the approximate assumption of a discontinuous μ has been solved for the first configuration, the problem can be considered as solved for the second configuration as well. On the other hand, for $r > r^*$ we can express the temperature T in the two configurations considered in terms of the radius r and the parameter T^*. And, since r^* and T^* have been assumed to be the same, we can eliminate the temperature from the relations appropriate for the two models applied at the end of the external regions ($\mu = 1$). In this way we obtain a relation between the radii R and R' of the two configurations and the value $r_c = 0.9R$ and r_c', which defines the outer extent of the transition region in the second configuration. Equation (50) provides another relation, so that we can solve for both r_c' and R'. We get

$$r_c' = 0.900844R \qquad \text{and} \qquad R' = 0.999734R\,.$$

The last relation shows that, for all practical purposes, R can be considered as unchanged.

If we should now integrate equation (7) from r^* outward in both configurations, we should find that the masses of the external parts are not quite the same. But, remembering the order of magnitude of the external mass and comparing the new distribution of density (*dashed curve* in Fig. 1) with the old one, it is evident that the difference, as compared to the total mass, cannot be greater than one part in 10^6. In other words, the masses will be the same to a precision even higher than that in which the numerical integrations are generally carried out for the interior!

Thus, contrary to what Hoyle and Lyttleton have said, with a discontinuity of μ in the external layers not satisfying condition (27), we can always construct a stable state of equilibrium very near the one obtained by ignoring this condition altogether. And, as we have further seen, the final stable state will be reached in a relatively short time by turbulent mixing of a very narrow zone, which has the effect essentially only of "smoothing" the discontinuity. No large-scale motions of the kind imagined by Hoyle and Lyttleton can intervene.

So far we have treated only one example, where $\mu_i = 2$ and $\mu_e = 1$, but it is apparent that the conclusions will remain valid for all reasonable discontinuity of μ. When the pressure of radiation is not negligible, the algebra becomes somewhat more complicated,

but, unless it becomes a very large part of the total pressure, it does not introduce any further novel features.

6. *Discontinuity of μ in the interior of the star.*—We shall limit ourselves again to the case in which the pressure of radiation is negligible. But, in contrast to our earlier discussion, we must allow for the variation of $m(r)$, and an analytical treatment becomes impossible. However, the use of an effective polytropic index, as defined by equation (12), and of the homology invariant variables,[8]

$$U = \frac{4\pi\rho r^3}{m(r)} = \frac{d \log m(r)}{d \log (r)} \tag{51}$$

and

$$V = \frac{2}{5}\frac{Gm(r)\rho}{rP} = -\frac{2}{5}\frac{d \log P}{d \log r}, \tag{52}$$

simplifies the discussion considerably. The use of these variables is suggested since, in the fitting-together of two solutions, the continuity of U and V automatically implies the continuity of $m(r)$, P, and T across the interface. If different values of μ are assumed in the different regions, then it is the continuity of U/μ and V/μ across the interface which should be required. Since the generation of energy is strongly concentrated toward the center, the distribution of physical conditions in an extensive region of the star from the surface inward is given by a point-source solution. For a given total mass M, we have a whole family of such solutions, which can be arranged and discussed in the (U, V)-plane very much in the same way as the polytropic solutions corresponding to a given index n.[9]

The differential equations for the variations of U, V, and n along a point-source solution can be obtained easily from definitions (12), (51), and (52) and from equations (3) and (7). They are

$$\frac{d \log U}{d \log r} = 3 - U - \frac{5}{2}\frac{n}{n+1}V - \frac{5}{2}V\frac{d \log \mu}{d \log P}, \tag{53}$$

$$\frac{d \log V}{d \log r} = U + \frac{5}{2}\frac{1}{n+1}V - 1 - \frac{5}{2}V\frac{d \log \mu}{d \log P}, \tag{54}$$

and

$$\frac{d \log (n+1)}{d \log r} = U - \frac{5}{2}\left(\frac{6.5 - 2n}{n+1}\right)V + \frac{5}{2}V\frac{d \log \mu (1 - X^2)}{d \log P}. \tag{55}$$

If μ is constant, these equations reduce to

$$\frac{d \log U}{d \log r} = 3 - U - \frac{5}{2}\frac{n}{n+1}V, \tag{56}$$

$$\frac{d \log V}{d \log r} = U + \frac{5}{2}\frac{1}{n+1}V - 1, \tag{57}$$

and

$$\frac{d \log (n+1)}{d \log r} = U - \frac{5}{2}\left(\frac{6.5 - 2n}{n+1}\right)V. \tag{58}$$

Suppose that we go toward the center of a star along one of the point-source solutions labeled by a Q and that we arrive at a point r_c, where μ jumps from its value μ_e to a value

[8] Cf. Chandrasekhar, *op. cit.*, p. 352.

[9] I am indebted to Dr. S. Chandrasekhar for allowing me the use of his tabulation of the functions U and V for a whole family of point-source solutions. In Dr. Chandrasekhar's tabulations the point-source solutions have all been conveniently reduced in a standard system of nondimensional variables (cf. Mrs. Harrison, *Ap. J.*, **103**, 193, 1946, particularly eqs. [23]–[27]).

μ_i. At this point the effective polytropic index will have a certain value n_e and, by condition (11) of Hoyle and Lyttleton, we can determine the value of n_i. Let us assume, first, that the discontinuity of μ and the value of n_e are such that $n_i = \frac{3}{2}$. Now suppose that the conditions of fit to a polytropic solution $E_{3/2}$ are satisfied at r_c (i.e., that in the $[U, V]$-plane, the point of co-ordinates $\mu_i\, U_c/\mu_e\ \mu_i\, V_c/\mu_e$ lies on $E_{3/2}$). There is no loss of generality in making this assumption, since it is always possible to find such a point r_c on any of the point-source solutions. However, the fact that n_i is equal to $\frac{3}{2}$ just on the internal side of the interface does not mean that this is the starting-point of a convective region.

To examine the stability of the radiative gradient in the region interior to r_c, we let $n = n_i = \frac{3}{2}$ in equation (58) and obtain for the variation of n just past the interface the equation

$$\frac{d \log (n+1)}{d \log r} = U - \tfrac{7}{2} V\,. \tag{59}$$

Thus, if the representation of the point r_c in the (U, V)-plane falls above the line

$$2U - 7V = 0\,, \tag{60}$$

n increases again above its value $\frac{3}{2}$ as we leave the interface toward the interior, and the radiative gradient continues to be stable. It may be noted, however, that the radiative solution which we should use to extend our solution past the discontinuity of μ need not belong to the usual point-source solutions, since in this case P, ρ, and T need not tend simultaneously to zero at some value of r.

It is now seen that line (60) lies very close to the locus of the points on the radiative solutions where n becomes equal to $\frac{3}{2}$. Since it is only between the line (60) and the locus of the points $n = \frac{3}{2}$ $(\mu_i > \mu_e)$ that condition (11) of Hoyle and Lyttleton can lead to a fitting with a convective core, it is evident that the models obtained in this way cannot differ very much from the one fitted at the points $n = \frac{3}{2}$. However, condition (11) has the further consequence that, since on any of the point-source solutions n_e will remain very close to $\frac{3}{2}$ in the region where the fit to a convective core is possible, the only permissible discontinuities of μ at the interface with a convective core are going to be very small (cf. eq. [11]). In fact, all the resulting models would be very close to Cowling's solution $(\mu_i = \mu_e)$.

We have considered the case in which the discontinuity of μ is such that n_i according to condition (11) is just equal to $\frac{3}{2}$. But, since n_e has its maximum value (3.25) in the external layers, n_i will always be smaller than $\frac{3}{2}$, say, $(\frac{3}{2} - \epsilon)$, no matter where the discontinuity takes place, provided that $\mu_i/\mu_e > 1.53$. The variation of n on the internal side of the interface will then be given by

$$\frac{d \log (n+1)}{d \log r} = U - \frac{17.5 + 10\epsilon}{5 - 2\epsilon}\, V\,. \tag{61}$$

As ϵ increases, the region of the (U, V)-plane, where dn/dr is negative, increases also; and, although n_i becomes smaller than $\frac{3}{2}$ just at the interface, it will start increasing after that, and in many cases radiative equilibrium will soon re-establish itself. The situation is therefore very similar to what we have described under analogous conditions in the stellar envelope $(r/R > \frac{1}{2})$. We may accordingly expect that, in our present context also, there will be a rapid readjustment to a transition region, in which μ will vary. To determine the law of variation of μ in the resulting transition region we argue as follows:

For any given point, r_c, the maximum discontinuity in μ which is compatible with the stability of the radiative gradient $(n_i = \frac{3}{2})$ just past the interface will be given by condition (11) with the equality sign. If μ remains constant after crossing the interface and if we should be above line (60), n_i will start increasing again for decreasing r. Indeed, ac-

cording to equations (58), (51), and (52), the increase in n_i which will take place when r decreases by Δr will be given by

$$\tfrac{2}{5}\Delta n_i = (U - 3.5V)\frac{\Delta r}{r_c} = \Delta \log m(r) + \tfrac{7}{5}\Delta \log P . \tag{62}$$

At $r = r_c - \Delta r$, therefore, $n_i = \frac{3}{2} + \Delta n_i > \frac{3}{2}$, and we can again have a small discontinuity of μ of amount $\Delta\mu$, which will reduce $n_e = \frac{3}{2} + \Delta n_i$ to $\frac{3}{2}$ again, according to condition (11). Using condition (11), we obtain the following relation between Δn_i and $\Delta\mu$

$$\frac{\Delta\mu}{\mu} = \tfrac{2}{5}\Delta n \tag{63}$$

if we neglect the factor $(1 - X^2)$; as we have already seen in our earlier discussion in §§ 4 and 5, the factor $(1 - X^2)$ has only a very small influence on the final results. Using relation (62), we find that equation (63) becomes

$$\frac{\Delta\mu}{\mu} = \Delta \log m(r) + \tfrac{7}{5}\Delta \log P . \tag{64}$$

We can repeat this process until we have reached the pre assigned value μ_i for the core. Making the various steps Δr smaller and smaller, we shall obtain, in the limit $\Delta r = 0$, a region throughout which

$$n_i = \tfrac{3}{2} . \tag{65}$$

Further in this region, μ will vary continuously accordingly to the law

$$\mu = C_1 m(r) P^{7/5} . \tag{66}$$

According to equation (65), we also have

$$T = C_2 P^{2/5} . \tag{67}$$

Apart from the factor $m(r)$ (the variation of which cannot be neglected in our present context), relations (66) and (67) are the same as those obtained in § 5 (eqs. [40] and [44]) by considering in detail the process of mixing.

The differential equations (53) and (54) for U and V in the transition region of variable μ are therefore (cf. eq. [66])

$$\frac{d \log U}{d \log r} = 3 - 5V \tag{68}$$

and

$$\frac{d \log V}{d \log r} = 2U - \tfrac{5}{2}V - 1 . \tag{69}$$

Combining these two equations, we have

$$\frac{dV}{dU} = \frac{V}{U}\frac{2U - \frac{5}{2}V - 1}{3 - 5V} . \tag{70}$$

The general nature of the solutions of equation (70) can be readily pictured by drawing the system of isoclinical curves in the (U, V)-plane, along which dV/dU is constant. These isoclinical curves are a series of hyperbolas and are shown in Figure 2. The short lines (of constant slope) drawn across each curve represent the directions in which the solutions of equation (70) will cross this curve. From the arrangement of the isoclinical curves in Figure 2, it is seen that the solution-curves of equation (70) spiral around the

point $U = 1.25$ and $V = 0.6$; at this point both the numerator and the denominator of the quantity on the right-hand side of equation (70) vanish. This singular point of equation (70) corresponds to the following singular solution of equations (1)–(7) when relations (66) and (67) are satisfied:

$$P = C_1 r^{-3/2}, \quad \rho = C_2 r^{-7/4}, \quad T = C_3 r^{-3/5},$$
$$\mu = C_4 r^{-17/20}, \quad \text{and} \quad m(r) = C_5 r^{5/4};$$

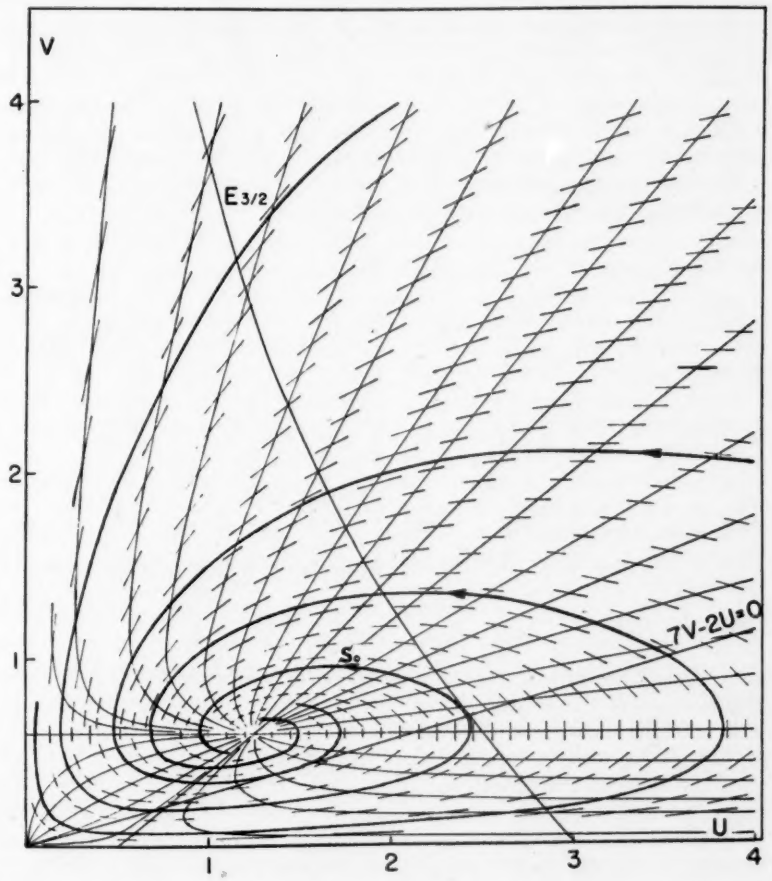

FIG. 2.—General run of the spiral solutions in a region where μ varies continuously according to the law $\mu \propto m(r)P^{7/5}$.

here C_1, C_2, etc., are constants. All the other solutions asymptotically tend to this singular solution as we approach the surface ($r \to \infty$, $m[r] \to \infty$), and along them the radius increases in the direction indicated by the arrows.

Along any one of the spiral solutions we have (cf. eq. [66])

$$\frac{d \log \mu}{d \log P} = U - \tfrac{7}{2} V. \tag{71}$$

Thus μ increases with decreasing r above line (60); while below this line μ decreases with decreasing r. According to the criterion of stability (9) and equation (67), we conclude

that the radiative gradient will be unstable below the line (60), and therefore these portions of the spiral solutions should not be used in physical models.

We shall now show how, with the help of the solutions sketched in Figure 2, we can construct stellar models in which μ is assigned certain values for the envelope ($\mu = \mu_e$) and the core ($\mu = \mu_i$) with possible transition zones in which μ is variable according to law (66). Suppose, now, that the region of $\mu = \mu_e$ (point-source solution) extends down to $r = r_c$, where $U = U_c$ and $V = V_c$. At this point (U_c, V_c), μ can jump to a value μ_t given by condition (11) with $n_i = \frac{3}{2}$. If that point is above the line (60), μ can then continue to increase according to equation (66). We must now follow, in the sense of decreasing r, the spiral solution starting at the point ($[\mu_t/\mu_e]U_c$, $[\mu_t/\mu_e]V_c$), until μ reaches its value μ_i, say, at the point (U^*, V^*). As we continue the solution further, μ must remain constant. If the point (U^*, V^*) is still above line (60), then we must continue with a radiative solution which ultimately will become unstable deeper in the star, owing to the concentration of energy sources. When this occurs, the solution should be continued by an $E_{3/2}$ solution, and the conditions of fit there will permit us to fix the point-source solution to be used in the external part of the star.

TABLE 1

$\mu_i/\mu_e(\mu_e=1)$	μ_t/μ_e	m_e/M	r_e/R	m_t/M	r_t/R	HARRISON*	
						m_c/M	r_c/R
Cowling 1	.....	0.150	0.171	.....	.....	0.150	0.171
1.055	.....	.168	.171	.....	.....	.143	.161
1.147	1.144	.189	.164	0.206	0.170	.131	.146
1.248	1.206	.181	.150	.230	.165	.119	.132
1.483	1.276	.154	.117	.240	.143	.095	.108
1.8	1.315	.123	.086	.230	.116	.083	.091
2.0	1.320	0.104	0.072	0.214	0.103	0.081	0.087

* *Ap. J.*, **100**, 343, 1944.

The case of immediate physical interest is, however, one in which the convective core starts just at the end of the transition region of variable μ, since it is in the convective core that the principal change in the chemical composition occurs. Further in the convective core μ must be uniform on account of mixing. In this case, since n must decrease at the end of the zone of transition, the point (U^*, V^*), where μ reaches its value μ_i, must lie under or on line (60). On the other hand, we have seen that we can use the spiral solutions only above this line. Thus the only spiral solution which will lead to a convective core starting at the end of the zone of transition is the one which intersects $E_{3/2}$ at the same point as the straight line (60). It can be shown that at this point the spiral solution and $E_{3/2}$ have the same tangent. This particular spiral solution is shown in Figure 2. Using this solution S_0 tangential to $E_{3/2}$, we constructed a few models composed of a point-source envelope followed by a region of transition which ends in a convective core. For a given change of $\mu(\mu_e, \mu_i)$ we must find on one of the point-source solutions a point U_c, V_c, n_c, such that its co-ordinates, multiplied by μ_t/μ_e (where μ_t is given by condition [11] of Hoyle and Lyttleton with $n_e = n_c$, $n_i = \frac{3}{2}$), represent a point on the spiral solution S_0. Furthermore, as we go along that solution (decreasing r), μ increases from its value μ_t, and it should just reach the value μ_i at the point of contact with $E_{3/2}$. In general, for given μ_e and μ_i, we shall have to interpolate between the various point-source solutions. It is, therefore, more convenient to start from a particular point-source solution and determine the corresponding variation of μ which permits us to fit it to a

convective core with a transition zone. It is in this way that the results given in Table 1 were obtained. The mass and radius of the convective core are denoted by m_c and r_c and those of the convective core, plus the zone of transition, by m_t and r_t. It will be noted that the second model has no zone of transition, and it corresponds to the case where the condition of Hoyle and Lyttleton leads directly to a solution. In fact, the corresponding discontinuity of μ is already close to the maximum compatible with this condition alone.

In the last two columns we have given the masses and radii of the convective cores derived by Schönberg and Chandrasekhar (*op. cit*) and Mrs. Harrison[10] in their discussion of the "generalized Cowling model." As we have already stated, in the discussions carried out by these writers μ, was assumed to jump discontinuously from μ_e to μ_i at the surface of the convective core, with a corresponding discontinuity of density. It will be seen that the general sense of the evolution derived by these writers is in general agreement with our more rigorous treatment of the same problem.

Finally, we may note that for the model $\mu_i/\mu_e = 2$, we find $L = 2.78L$ (Cowling's model) and $R = 2.57R$ (Cowling's model). They are somewhat greater than those obtained by M. Schönberg and S. Chandrasekhar, who found $L = 1.41L$ (Cowling's model) and $R = 1.65R$ (Cowling's model). The central condensation is also greater, and the ratio $\rho_c/\bar{\rho}$ becomes equal to 390 instead of 179. But the differences between the two models become less for smaller ratios of μ_i/μ_e.

It is seen from Table 1 that if we wish to regard these models as a sequence of evolution, the mass of the convective core starts by increasing. But, as soon as the chemical composition has been altered appreciably, its mass decreases rapidly, while the mass m_t varies more slowly and goes on increasing for some time. We can imagine that by turbulent mixing at the interface, material which has lost part of its hydrogen in the convective core is continually being drawn into more external regions. However, as the exhaustion of hydrogen in the internal region proceeds, it is seen that we reach a stage when μ_i/μ_e is of the order of 1.5, at which the mass m_t reaches a maximum. At this point, the fraction of the total hydrogen content of the star which has been used is still small, of the order of 15 per cent if we start with $\mu_i = \mu_e = 1$. However, since the mass of the external part $(M - m_t)$, where $\mu = \mu_e = 1$, cannot increase, there are difficulties in following the evolution beyond this stage. But it should be remembered that there are many other points which remain to be investigated in this connection. In particular, for these models due to the special position of the center and the vanishing of the gravitational acceleration here, even a slight amount of dissipation may be sufficient to create a small finite zone where the exhausted hydrogen is not replenished fast enough. If that should be the case, we may expect that an isothermal core will start forming at the center even before the hydrogen is fully exhausted in the whole convective core. And, once the formation of an isothermal core has been initiated, it will grow continually at the expense of the convective region owing to the fringe in radiative equilibrium which will always surround it. We shall not, however, continue this discussion here.[11]

It is a pleasure to acknowledge the many interesting discussions which I had with Dr. Chandrasekhar in the course of this investigation.

[10] *Ap. J.*, **100**, 343, 1944.

[11] In this connection see M. Harrison, *Ap. J.*, **105**, 322, 1947, where the solutions of the "generalized Cowling model," together with solutions of models with isothermal cores, are displayed. It should, however, be remarked that the existence of the transition zone is not included in this discussion.

STELLAR MODELS WITH ISOTHERMAL CORES AND POINT-SOURCE ENVELOPES

MARJORIE HALL HARRISON
Yerkes Observatory
Received January 1, 1947

ABSTRACT

Stellar models, consisting of isothermal cores and point-source envelopes, are considered, in which the ratio of the mean molecular weight in the core to the mean molecular weight in the envelope varies from 1 to 2. It is found that the upper and lower limit of the mass and radius of the core is a decreasing function of μ_c/μ_e. The evolution of main-sequence stars consequent to the burning of hydrogen in the central regions is also examined.

1. *Introduction.*—The construction of stellar models formed by an isothermal core surrounded by a point-source envelope was discussed by L. R. Henrich and S. Chandrasekhar[1] and by M. Schönberg and S. Chandrasekhar[2] for two values of the ratio μ_c/μ_e, namely, $\mu_c/\mu_e = 1$ and $\mu_c/\mu_e = 2$. It is now proposed to determine the effect of intermediate values on the fraction of the mass and radius inclosed in the convective core, the total radius and luminosity of the configuration, and the ratio of the central to the mean density.

2. *The equations of the models.*—The equation of state of the isothermal core with negligible radiation pressure is

$$P = K_2 \rho \,, \tag{1}$$

where

$$K_2 = \frac{k}{\mu H} T \,. \tag{2}$$

With the foregoing equation of state, the equation of equilibrium,

$$\frac{1}{r^2} \frac{d}{dr} \left(\frac{r^2}{\rho} \frac{dP}{dr} \right) = -4\pi G \rho \,, \tag{3}$$

can be reduced to the form

$$\frac{1}{\eta^2} \frac{d}{d\eta} \left(\eta^2 \frac{d\phi}{d\eta} \right) = e^{-\phi} \,, \tag{4}$$

where

$$r = \beta \eta \,; \qquad \rho = \lambda_2 e^{-\phi} \,; \qquad \beta = \left[\frac{K_2}{4\pi G \lambda_2} \right]^{1/2} \,, \tag{5}$$

and λ_2 is an arbitrary constant.

The mass of the material inclosed up to a radius η is given by

$$M(\eta) = 4\pi \beta^3 \lambda_2 \eta^2 \frac{d\phi}{d\eta} \,. \tag{6}$$

The equations of equilibrium for the point-source envelope are used in the standard form given in a recent paper.[3]

[1] *Ap. J.*, **94**, 525, 1941.

[2] *Ap. J.*, **96**, 161, 1942.

[3] Harrison, *Ap. J.*, **103**, 196, 1946.

3. *The equations of fit.*—Let the interface occur at $\xi = \xi_i$ and $\eta = \eta_i$. Our equations of fit then are

$$-\tfrac{2}{5}M\frac{\xi^2}{\sigma}\frac{d(\sigma\theta)}{d\xi} = 4\pi\beta^3\lambda_2\eta^2\frac{d\phi}{d\eta}, \tag{7}$$

$$R\xi = \beta\eta\,, \tag{8}$$

$$\rho_0\sigma = \lambda_2 e^{-\phi}x\,, \tag{9}$$

and

$$\frac{k}{\mu H}\rho_0 T_0\sigma\theta = \frac{k}{\mu H}T\lambda_2 e^{-\phi}, \tag{10}$$

where, in equation (9)

$$x = \frac{\rho_{\text{env}}}{\rho_{\text{core}}} \simeq \frac{\mu_{\text{env}}}{\mu_{\text{core}}}. \tag{11}$$

This system of equations can be reduced to one involving only two homology invariant combinations of σ, θ, and their derivatives σ', θ', and ξ. If we raise equation (8) to the third power, multiply by equation (9), and divide by equation (7), we are left with

$$-\frac{5}{2}\frac{\sigma^2\xi}{(\sigma\theta)'} = \frac{\eta e^{-\phi}}{\phi'}x\,, \tag{12}$$

which we re-write in the form

$$-\frac{5}{2}\frac{\sigma^2\xi}{(\sigma\theta)'} = u(\xi) = U(\eta) = \frac{\eta e^{-\phi}}{\phi'}x\,. \tag{13}$$

When we divide equation (7) by equation (10), multiply by equation (9), and divide by equation (8), we have

$$-\frac{2}{5}\frac{(\sigma\theta)'}{\sigma\theta}\xi = \tfrac{3}{5}\eta\phi' x\,, \tag{14}$$

which we re-write in the form

$$-\frac{2}{5}\frac{(\sigma\theta)'}{\sigma\theta}\xi = v(\xi) = V(\eta) = \tfrac{3}{5}\eta\phi' x\,. \tag{15}$$

4. *The construction of the models.*—Our fitting conditions are those which are usually used, namely, that the mass, radius, and pressure are continuous at the interface; and we have also made allowance for the difference in the mean molecular weights of the core and envelope by making the density discontinuous at the interface (cf. eq. [11]). The physical characteristics of the models are determined by the method used in the previous investigation with the same two sets of integrations of the point-source envelope.[4]

5. *The physical characteristics of the models.*—From equation (15) we readily obtain the formula for the radius R,

$$R = \tau\frac{\mu_c H}{k}\frac{GM}{T_c}, \tag{16}$$

where

$$\tau = \frac{1}{v_i}\frac{2}{5}\frac{\psi_i}{\xi_i}\frac{\mu_e}{\mu_c}. \tag{17}$$

The variation of R will thus be governed only by the factor $\tau\mu_c$ if T_c is assumed to remain constant. This factor is tabulated in Table 1.

[4] Harrison, *op. cit.*, p. 198.

TABLE 1

PHYSICAL CHARACTERISTICS OF THE COMPOSITE MODEL FOR VARIOUS VALUES OF x

$Q\times10^3$	ξ_i	ψ_i	$\tau\mu_c$	$\frac{L_0}{(\tau\mu_c)^{\frac{1}{2}}}\times10^{-25}$	$\rho_g/\bar{\rho}\times10^{-2}$
			(a) $x=1$		
1.410....	0.1591	0.1777	0.7743	0.8863	0.805
1.547....	.1612	.1937	0.7802	0.9681	0.977
1.776....	.1660	.2315	0.7857	1.108	1.14
1.947....	.1674	.2491	0.7936	1.209	1.31
2.451....	.1673	.2857	0.8181	1.498	1.84
2.750....	.1656	.3001	0.8381	1.662	5.35
3.086....	.1622	.3144	0.8626	1.837	6.47
3.885....	.1588	.3426	0.9124	2.249	7.81
6.157....	.1445	.3673	1.025	3.362	8.79
8.698....	.1224	.3682	1.199	4.391	27.6
8.698....	.0867	.2716*	1.496	3.931	552
6.157....	.0919	.2341*	1.355	2.924	190×10
6.157....	0.1074	0.2720*	1.239	3.058	287×10^3
			(b) $x=1/1.2$		
1.547....	0.1214	0.1111	0.8920	0.9053	0.991
1.776....	.1250	.1390	0.9078	1.031	1.31
1.947....	.1264	.1540	0.9193	1.122	1.51
2.451....	.1268	.1851	0.9589	1.384	2.15
2.750....	.1260	.2000	0.9829	1.535	2.60
3.086....	.1237	.2146	1.016	1.693	3.30
3.885....	.1193	.2380	1.079	2.069	5.07
6.157....	.1061	.2685	1.243	3.053	13.2
8.698....	0.0860	0.2702	1.500	3.926	53.4
			(c) $x=1/1.4$		
1.776....	0.1032	0.1023	0.984	0.990	1.66
1.947....	.1040	.1139	1.002	1.075	1.93
2.451....	.1036	.1394	1.056	1.319	2.86
2.750....	.1023	.1515	1.089	1.457	3.56
3.086....	.0999	.1614	1.130	1.606	4.47
3.885....	.0948	.1832	1.216	1.948	7.82
3.885....	.0596	.1251*	1.497	1.756	180×10
3.885....	0.0703	0.1401*	1.401	1.815	106×10^3
			(d) $x=1/1.6$		
1.776....	0.0896	0.0838	1.036	0.964	2.11
1.947....	.0897	.0932	1.060	1.045	2.53
2.451....	.0883	.1149	1.127	1.277	4.00
2.750....	.0867	.1251	1.169	1.406	5.20
3.086....	.0835	.1350	1.225	1.542	7.25
3.885....	.0769	.1503	1.341	1.855	14.5
3.885....	.0520	.1160*	1.585	1.706	520
3.086....	.0536	.0972*	1.463	1.410	166×10
3.086....	0.0624	0.1064*	1.378	1.454	958×10^2

*This intersection corresponds to one for which ψ_i has already reached its maximum and thus is not a physically reliable solution.

TABLE 1—*Continued*

$Q\times10^3$	ξ_i	ψ_i	$\tau\mu_c$	$\frac{L_0}{(\tau\mu_c)^{\frac{1}{2}}}\times10^{-25}$	$\rho_c/\bar{\rho}\times10^{-2}$
	(*e*) $x=1/1.8$				
1.947....	0.0795	0.0811	1.106	1.024	3.36
2.451....	.0770	.0998	1.189	1.243	5.82
2.750....	.0738	.1072	1.250	1.360	8.16
3.086....	.0705	.1164	1.313	1.489	12.8
3.086....	.0484	.0924*	1.516	1.386	451
2.750....	.0485	.0813*	1.458	1.260	111×10
2.451....	.0509	.0747*	1.378	1.155	247×10
2.451....	0.0569	0.0793*	1.324	1.178	258×10²
	(*f*) $x=1/2$				
1.776....	0.0720	0.0654	1.115	0.930	3.57
1.947....	.0714	.0730	1.149	1.004	4.54
2.451....	.0677	.0893	1.247	1.213	9.01
2.750....	.0638	.0955	1.319	1.324	14.3
3.086....	.0569	.1006	1.429	1.427	36.3
3.086....	.0501	.0940*	1.498	1.394	105
2.750....	.0454	.0790*	1.493	1.244	360
2.451....	0.0454	0.0712*	1.442	1.128	698

For a homologous family of stellar configurations based on Kramers' law of opacity, the luminosity is given by a formula of the form

$$L=\frac{L_0}{Q\mu^{7.5}}\frac{M^{5.5}}{R^{0.5}}\mu_e^{7.5}\times1.809\times10^{-28}, \tag{18}$$

where Q is a parameter defined as in a previous paper[5] and L_0 can be determined from the particular value of Q which satisfies the equations of fit. Combining equations (17) and (18), we have

$$L=\frac{L_0}{(\tau\mu_c)^{0.5}}\left(\frac{k}{GH}\right)^{0.5}\frac{1}{Q\mu^{7.5}}T_c^{0.5}M^5\mu_e^{7.5}\times1.809\times10^{-28}. \tag{19}$$

It is clear from equation (19) that, if the central temperature is assumed constant, the variation in the luminosity will be governed by the factor $L_0(\tau\mu_c)^{-0.5}$; this factor is tabulated in Table 1.

The ratio of the mean to the central density is also readily found from equations (5) and (6),

$$\frac{\rho_c}{\bar{\rho}}=\frac{\psi_i\eta_i}{3\xi_i^3\phi_i'}. \tag{20}$$

This quantity is also tabulated in Table 1.

6. *Conclusions.*—The curves in Figure 1 illustrate the variation of the radius and luminosity of a star for different values of μ_c/μ_e and constant central temperature for the composite model and the generalized Cowling model.[6] The upper and lower figures on each curve are ψ_i and ξ_i, respectively. It is clear from an inspection of the curves that

[5] *Ibid.*, p. 196.

[6] Harrison, *Ap. J.*, 96, 343, 1944.

the upper and lower limit of the mass and radius of the core is a decreasing function of μ_c/μ_e; the maximum value is reached for $\mu_c/\mu_e = 1$ and the minimum value for $\mu_c/\mu_e = 2$.

By using Figure 1 we can trace the evolution of main-sequence stars. During the relatively early stages of the evolution of a star, as a result of hydrogen combustion in the center, there will be either the formation of an isothermal core or a shrinkage of the convective core. In the latter case the evolution would take place along the curve for the generalized Cowling model (also shown in Fig. 1) in the direction of decreas-

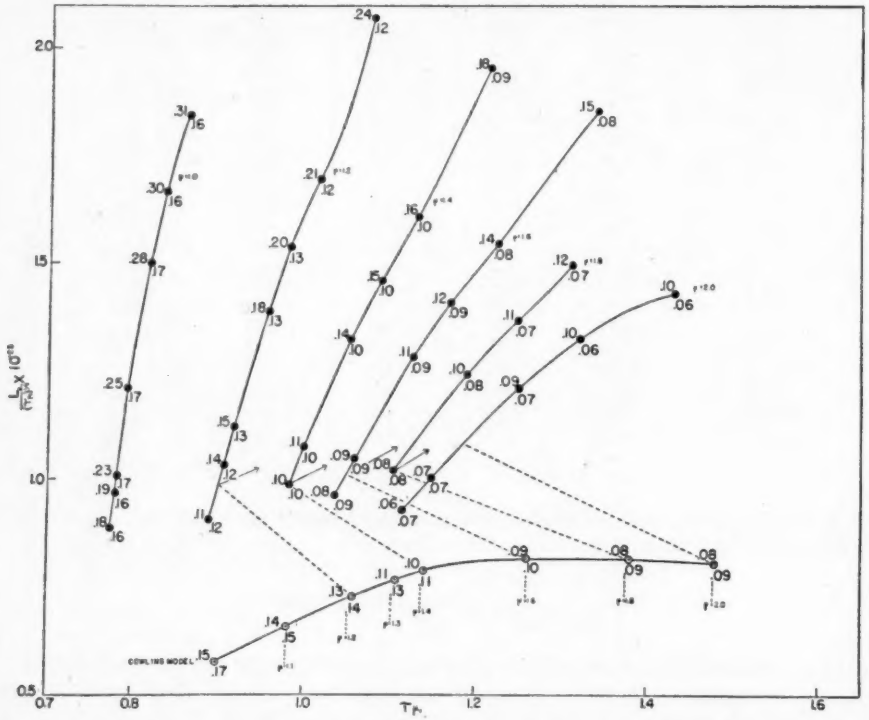

Fig. 1.—The curves illustrate the variation in the luminosity for constant central temperature as a function of the radius for stellar models with isothermal cores and point-source envelopes and the generalized Cowling model. The dotted lines and arrows trace the evolution of main-sequence stars.

ing ψ_i and increasing μ_c/μ_e. The growth of an isothermal core at the center would slow down, and finally stop, convection when the fraction of the stellar mass inside it exceeded a value depending on μ_c/μ_e as shown at the lower end of each curve (●). The transition from one model to another would take place somewhat along the dotted lines as shown in the figure; this transition can take place only at points on the isothermal curves where the mass of the core is equal to the mass of the core of the generalized Cowling model. In the course of the evolution the radius slowly contracts, thus giving rise to an increase in the luminosity which is necessary for the transition. The evolution then continues along a sequence formed by isothermal cores surrounded by point-source envelopes evolving across these curves in the direction of increasing μ_i.

I wish to express my sincere thanks to Dr. S. Chandrasekhar for suggesting this problem and for many helpful discussions and criticisms.

ON THE BROADENING OF NEUTRAL HELIUM LINES IN STELLAR SPECTRA

MARGARET K. KROGDAHL
Yerkes Observatory and Evanston, Illinois
Received January 10, 1947

ABSTRACT

The broadening of helium lines in early-type stellar spectra is considered here from the point of view of the direct interactions between a proton and a helium atom which were calculated in earlier papers. The theory of such broadening is discussed with a view toward determining, in terms of the physical conditions in the stellar atmosphere, whether it may be expected to be predominantly of the Lorentz-Weisskopf type or of the statistical, or Holtsmark, type. The results of this discussion are applied to the calculation of the broadening of several helium lines for the case of τ Scorpii. It is found that for most of these lines the broadening due to direct interactions is largely of the collisional type and, further, that such a theory appears to be capable of accounting for the equivalent widths within the uncertainties of the observations.

I. REMARKS ON THE PROBLEM OF LINE BROADENING

1. *Introduction.*—The problem of the pressure broadening of helium lines in early-type stellar spectra has been discussed at length by several authors, including Struve, Foster and Douglas, Verweij, and Unsöld.[1] Despite the fact that it was pointed out by Struve as early as 1938 that collisional broadening by ions might play a role in this connection (in particular, with regard to the "filling-in" of the space between λ 4470 and λ 4471), most of the subsequent treatments have been primarily concerned with what might be termed the "statistical" Stark effect, arising from the electric fields present in the atmosphere. However, as has been mentioned in connection with a related problem,[2] the electric fields acting upon absorbing atoms in a stellar atmosphere are caused by the neighboring charged particles, which, moreover, because of the high temperatures, are in a continual state of motion with respect to the absorbing atoms. Considerations such as this suggest that it would also be of interest to discuss the formation of the helium lines in terms of the direct interactions between a helium atom and a neighboring charged particle—specifically, a proton.[3]

2. *On the pressure broadening of spectral lines.*—As has been pointed out in the recent discussions of pressure broadening, the problem can be considered from two points of view. We have, on the one hand, the collision-broadening theory of Lorentz and Weisskopf, in which the time dependence of the perturbation is the principal factor. The wave train of the optical atom is considered to be "interrupted" by collisions with interacting particles; and the resultant intensity distribution, as a function of the pressure and temperature, is obtained from the Fourier analysis of such wave trains. On the other hand, there is the statistical theory originally due to Holtsmark, based on the existence of a direct correspondence between the perturbation and the emitted frequency, the resulting intensity distribution being simply a consequence of the probability with which any given perturbation takes place. It is clear that, in the limiting case of no relative velocity

[1] For an account of some of these investigations see A. Unsöld, *Physik der Sternatmosphären* (Berlin, 1938), § 73; also Struve, *Observatory*, **61**, 53, 1938. More recent papers are those of Foster and Douglas, *M.N.*, **99**, 150, 1939; Verweij, *Proc. Neth. Acad.*, **43**, 1000, 1940; and Unsöld, *Zs. f. Ap.*, **23**, 75, 1944.

[2] Krogdahl, *Ap. J.*, **100**, 333, 1944, and **102**, 64, 1945.

[3] Because of the enormous hydrogen abundance and the high temperatures, protons and electrons will be by far the most numerous charged particles. It is not immediately clear, however, that broadening by electrons can be discussed by the present methods, whose quantum-mechanical justification depends upon the validity of the Franck-Condon principle and the smallness of the De Broglie wave length of the perturbing particles.

between atom and perturber, we should be correct in applying the latter theory.[4] As is well known, however, when there is a relative motion, the central portion of the resulting line is governed by the collision-broadening theory, while the statistical theory must be applied when one considers the wings. Estimates have been made in various ways of the relative ranges of applicability of the two theories.[5]

It is thus apparent that, in order to apply correctly the direct interactions in a calculation of the collisional and/or statistical broadening of any stellar line, it is necessary, first of all, to be able to state the relative importance of the two processes in terms of the fundamental physical properties of the atmosphere, that is, the temperature and the pressure. A simple theory which shows how it is possible to do this and which, at the same time, furnishes a single convenient formula giving the intensity at any point in the line has been developed by Burkhardt.[6] This calculation, which is an attempt to extend the work started by Lenz,[7] is made on the basis of the classical theory; and it may further be noted that it was not intended as anything more than a preliminary theory.

In actual fact, of course, to speak of such matters as the relative importance of collisional and statistical broadening and the "boundary" between them is rather artificial. Ideally, what is needed is a theory which considers the effect of frequency perturbations upon the formation of lines quite generally, without making the very special assumptions which lead to the so-called "limiting" cases. In particular, such a theory should derive these concepts as limiting forms of the general contour and improve our understanding of them rather than try to superpose limiting cases or "smear" one type of distribution over the other. A theory such as this is what was attempted by Lenz, and only very recently extended by Lindholm,[8] who makes a Fourier analysis of the emission frequency with respect to the collision time.

However, inasmuch as the use of concepts like "collision broadening" and "statistical broadening" has proved fruitful in many problems,[9] it is felt that to continue along such lines is sufficiently good for a preliminary study of the broadening of the helium lines. This is especially true in view of other uncertainties in the problem which are unavoidable at this stage (for example, in the observed data, f-values, etc.). Accordingly, in the following section the essential features of Burkhardt's work are presented, together with certain generalizations and extensions (in particular, to the R^{-4} law of interaction) which prove useful in discussing the problem proposed in section 1.

II. CALCULATION OF THE INTENSITY DISTRIBUTION

3. *Introduction of the "collision time."*—It is well known[10] that, if the instantaneous circular frequency of a perturbed oscillator is written in the form

$$\omega_0(t) = \omega_0 + f(t), \tag{1}$$

a Fourier analysis of the amplitude as a function of the time yields the intensity distribution

$$J(\omega) = \left| \int_{-\infty}^{+\infty} \exp\left[i(\omega_0 - \omega)t + i\int^t f(t)\,dt \right] dt \right|^2. \tag{2}$$

[4] See Kuhn and London, *Phil. Mag.*, **18**, 987, 1934.

[5] For a detailed account of these matters see Unsöld, *Vierteljahrsschr. d. Deutsch. Astr. Gesellsch.*, **78**, 213, 1943.

[6] *Zs. f. Phys.*, **115**, 592, 1940.

[7] *Zs. f. Phys.*, **80**, 423, 1933.

[8] *Ark. Mat., Astr. och Fys.*, Vol. **32** A, No. 17, 1945.

[9] See, e.g., Unsöld, *Physik der Sternatmosphären;* also Strömgren, "On the Chemical Composition of the Solar Atmosphere," *Festschrift für Elis Strömgren* (Copenhagen, 1940).

[10] See, e.g., Lenz, *op. cit.*

The problem at hand is to evaluate the above integral for a generalized law of interaction of the Van der Waals type, i.e.,

$$f(t) = \frac{C_p}{r^p(t)} = \Delta\omega, \tag{3}$$

where C_p denotes the appropriate Van der Waals constant, measured in c.g.s. units of circular frequency. For convenience we shall make the customary change of variable

$$r^2 = v^2t^2 + \rho^2, \tag{4}$$

where ρ is the minimum value of r for a given trajectory (assumed to be linear) and v is the relative velocity of the perturbing particle along it.

Consider the phase integral appearing in the exponent, namely,

$$\Theta(t) = \int_{-\infty}^{t} f(t)\,dt = C_p \int_{-\infty}^{t} (v^2t^2 + \rho^2)^{-p/2} dt. \tag{5}$$

TABLE 1

p	$\psi(\beta)$	$\psi(\infty)$
2....	$\tan^{-1}\beta + \frac{\pi}{2}$	π
3....	$\frac{\beta}{(1+\beta^2)^{1/2}} + 1$	2
4....	$\frac{\beta}{2(1+\beta^2)} + \frac{1}{2}\tan^{-1}\beta + \frac{\pi}{4}$	$\frac{\pi}{2}$
6....	$\frac{\beta}{4(1+\beta^2)^2} + \frac{3\beta}{8(1+\beta^2)} + \frac{3}{8}\tan^{-1}\beta + \frac{3\pi}{16}$	$\frac{3\pi}{8}$

Let

$$\beta = \frac{vt}{\rho}; \qquad d\beta = \frac{v\,dt}{\rho}. \tag{6}$$

Then $\Theta(t)$ becomes

$$\Theta(\beta) = \frac{C_p}{v\rho^{p-1}} \int_{-\infty}^{\beta} (1+\beta^2)^{-p/2} d\beta = \frac{C_p}{v\rho^{p-1}} \psi_p(\beta). \tag{7}$$

The functions $\psi_p(\beta)$ are given in Table 1 for those values of p which are most important in practice. Now, the fundamental assumption made by Lenz and Burkhardt (and later also by Lindholm) is that the function $\psi_p(\beta)$, describing the phase change during the collision, can be adequately represented in the vicinity of $\beta = 0$ by a straight line, whose slope we shall call γ_p. This means that we are replacing the infinitely long collision, in which the frequency change varies according to equation (3), by one of finite duration, in which the frequency change is constant.

The functions $\psi_p(\beta)$ are plotted in Figure 1, together with the straight lines which appear to represent them best. For $p = 6$ the straight line drawn has the slope 0.76, which was adopted by Lenz and Burkhardt in their calculations.[11] It is obvious that

[11] Lindholm (*op. cit.*) feels that these slopes should be lower, which would, of course, increase the asymmetry to some extent.

the straight-line approximation is worse, the lower the value of p. From the figures we find the following values of γ:

$$\left.\begin{aligned} &p=2\,, \quad \gamma\simeq 0.54\,; \quad && p=4\,, \quad \gamma\simeq 0.73\,;\\ &p=3\,, \quad \gamma\simeq 0.69\,; \quad && p=6\,, \quad \gamma\simeq 0.76\,. \end{aligned}\right\} \tag{8}$$

Accordingly, $\Theta(\beta)$ takes the form

$$\Theta(\beta) = \left\{\begin{array}{ll} 0 & \beta < -\frac{1}{2}\dfrac{\psi(\infty)}{\gamma}\,, \\ \dfrac{C_p}{v\rho^{p-1}}\left[\gamma\beta+\tfrac{1}{2}\psi(\infty)\right] & -\dfrac{1}{2}\dfrac{\psi(\infty)}{\gamma} < \beta < +\dfrac{1}{2}\dfrac{\psi(\infty)}{\gamma}\,, \\ \dfrac{C_p}{v\rho^{p-1}}\psi(\infty) & \beta > +\dfrac{1}{2}\dfrac{\psi(\infty)}{\gamma}\,. \end{array}\right\} \tag{9}$$

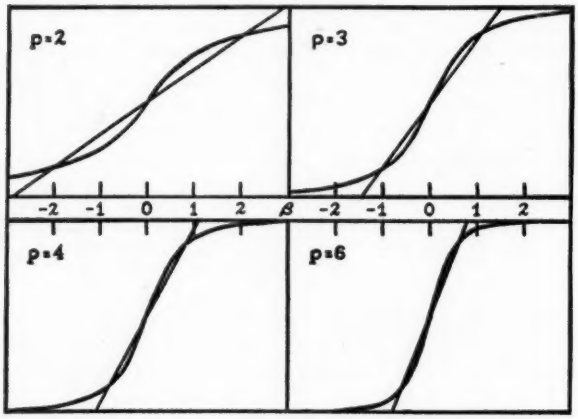

FIG. 1.—The phase functions $\psi_p(\beta)$ and their straight-line approximations. The abscissa in each case is β; the ordinates are, of course, all different.

In terms of t this becomes

$$\Theta(t) = \left\{\begin{array}{ll} 0 & t < -\frac{1}{2}\tau_s\,, \\ \dfrac{C_p}{v\rho^{p-1}}\gamma\dfrac{v}{\rho}(t+\tfrac{1}{2}\tau_s) & -\frac{1}{2}\tau_s < t < +\frac{1}{2}\tau_s\,, \\ \dfrac{C_p}{v\rho^{p-1}}\psi(\infty) & t > +\frac{1}{2}\tau_s\,, \end{array}\right\} \tag{10}$$

where the "collision time" τ_s is defined by

$$\tau_s = \frac{\rho}{v}\frac{\psi_p(\infty)}{\gamma} = k_p\frac{\rho}{v}\,. \tag{11}$$

The values of k_p are

$$\left.\begin{aligned} &k_2 = \frac{\pi}{0.54} = 5.8\,, \quad && k_4 = \frac{\pi}{2\times 0.73} = 2.15\,,\\ &k_3 = \frac{2}{0.69} = 2.9\,, \quad && k_6 = \frac{3\pi}{8\times 0.76} = 1.55\,. \end{aligned}\right\} \tag{12}$$

The constant value of $\Delta\omega$, which acts during the finite time τ_s, thus is

$$\Delta\omega = \frac{\gamma C_p}{\rho^p}, \tag{13}$$

instead of the value $\Delta\omega = C_p/r^p$ for an infinite time.

With these changes the expression for $J(\omega)$ (eq. [2]) breaks up into two types of integrals:

$$J(\omega) = \left| \sum_i \int_{\tau_{f,\,i}} e^{i(\omega_0-\omega)t}dt + \sum_j \int_{\tau_{s,\,j}} e^{i(\omega_0-\omega+\Delta\omega_j)t}dt \right|^2, \tag{14}$$

the former being extended over the various intervals of time, τ_f, during which the atom is not being disturbed, and the latter over the intervening collision times, τ_s, during which there is a constant frequency change, $\Delta\omega$.

Under suitable conditions, that is, if the phase changes produced during the collision times are large enough, the above expression can be decomposed into the sum of the squares of the individual terms.[12] It is customary to exclude temporarily all the "weak" collisions by adopting the Weisskopf condition that $\Theta \gtrsim 1$.[13] (The effect of the weak collisions will be considered in a later paragraph.) With this condition we have

$$J(\omega) = J_f(\omega) + J_s(\omega), \tag{15}$$

where

$$J_f(\omega) = \sum_i \left| \int_{\tau_{f,\,i}} e^{i(\omega_0-\omega)t}dt \right|^2 \tag{16}$$

and

$$J_s(\omega) = \sum_j \left| \int_{\tau_{s,\,j}} e^{i(\omega_0-\omega+\Delta\omega)t}dt \right|^2. \tag{17}$$

4. *The symmetric portion of the line.*—The first of these terms, $J_f(\omega)$, simply represents the Fourier analysis of an interrupted, but otherwise undisturbed, wave train—which is precisely the idea underlying the Lorentz-Weisskopf theory of collision broadening. As is well known, we have

$$\int_{\tau_{f,\,i}} e^{i(\omega_0-\omega)t}dt = \frac{e^{i(\omega_0-\omega)\tau_{f,\,i}} - 1}{i(\omega_0-\omega)}, \tag{18}$$

whence

$$J_f(\omega) = \sum_i 2\,\frac{1-\cos(\omega_0-\omega)\,\tau_{f,\,i}}{(\omega_0-\omega)^2}. \tag{19}$$

In order to average over all types of collisions we must define the quantity $\bar{\tau}_f$, the mean duration of an undisturbed wave train, by the equation

$$\bar{\tau}_f = \bar{\tau} - \bar{\tau}_s. \tag{20}$$

The quantity $\bar{\tau}$ is the mean time between collisions, and we shall see later how to determine the average $\bar{\tau}_s$. Upon multiplying the right-hand side of equation (19) by

[12] For a detailed discussion of this question see Burkhardt's paper.

[13] In his dissertation, *Über die Verbreiterung und Verschiebung von Spektrallinien* (Uppsala, 1942), Lindholm has shown how this type of assumption can be improved.

$(1/\bar{\tau}_f)e^{-\tau_f/\bar{\tau}_f}$, a factor giving the relative number of undisturbed wave trains of length τ_f, and, integrating over τ_f, we obtain, finally,

$$J_f(\omega) = \frac{c_f}{(\omega_0 - \omega)^2 + (1/\bar{\tau}_f)^2}. \tag{21}$$

This is the usual dispersion-type formula obtained for collision broadening. The proportionality factor c_f is to be determined later. As usual, the mean time between collisions is given by the relation

$$\frac{1}{\bar{\tau}} = \pi N \bar{v} \rho_0^2, \tag{22}$$

the relative velocity $\bar{v}$ by

$$\bar{v} = \sqrt{\frac{8RT}{\pi} \frac{\mu_1 + \mu_2}{\mu_1 \mu_2}}, \tag{23}$$

and ρ_0 is the "effective optical radius," which, according to the Weisskopf condition, is

$$\rho_0 = \left[\frac{C_p \psi_p(\infty)}{\bar{v}}\right]^{1/(p-1)}. \tag{24}$$

5. *The asymmetric portion of the line.*—The second term, $J_s(\omega)$, represents the Fourier analysis of those parts of the wave train during which the phase change Θ is increasing linearly with the time and there is a perturbation of constant amount $\Delta\omega$ acting. This term leads to the asymmetric portion of the line and corresponds closely to the Holtsmark or "statistical" type of broadening. Indeed, the Fourier analysis of wave trains, in which the phase change is represented by an infinite straight line, must lead to the Holtsmark expression;[14] for the infinity of the line implies that the configuration of particles is stationary—which is precisely the assumption underlying the formulation of the statistical theory.

Now, $J_s(\omega)$ can be written in the form (cf. eq. [19])

$$J_s(\omega) \propto \sum_i \frac{1 - \cos(\omega_i' - \omega)\tau_{s,i}}{(\omega_i' - \omega)^2}, \tag{25}$$

where

$$\omega_i' = \omega_0 + \Delta\omega_i. \tag{26}$$

This expression must now be averaged over all lengths of collision τ_s, that is, over all values of ρ and v (see eq. [11]).

Let us consider, first, all collisions having a given value of ρ, that is, we average, first, over the velocity distribution. This is taken from Fowler,[15] and may be stated as follows: Of the particles which pass, per second, at a distance ρ, the fraction having velocities between v and $v + dv$ is proportional to

$$v\, e^{-(v/v_0)^2} v^2 dv, \tag{27}$$

where

$$v_0 = \frac{\sqrt{\pi}}{2} \bar{v}. \tag{28}$$

[14] For a derivation of this formula see Unsöld, *Vierteljahrschr. d. Deutsch. Astr. Gesellsch.*, **78**, 213, 1943.

[15] *Statistical Mechanics* (Cambridge, 1936).

Hence the contribution to $J_s(\omega)$ of all collisions having a certain value of ρ is

$$j_s(\rho, \omega) \propto \int_0^\infty \frac{1-\cos(\omega'-\omega)\left(\frac{v_0}{v}\right)\tau_{s,0}}{(\omega'-\omega)^2} v\, e^{-(v/v_0)^3} v^2 dv, \tag{29}$$

where

$$\tau_{s,0} = \frac{2k_p}{\sqrt{\pi}} \frac{\rho}{\bar{v}}. \tag{30}$$

Burkhardt shows that the integral in equation (29) can be very well approximated by the dispersion formula, thus

$$j_s(\rho, \omega) \propto \frac{c_s}{(\omega'-\omega)^2 + 2/\tau_{s,0}^2}, \tag{31}$$

where c_s is a proportionality factor to be determined later. Thus the contribution to the line form of all collisions having the parameter ρ is a dispersion-curve of half-width $\sqrt{2}/\tau_{s,0} = (\sqrt{2\pi}\,\bar{v})/2k_p\rho$, which is displaced from the position ω_0 by the amount $\Delta\omega = \gamma C/\rho^p$.

The resultant value of $J_s(\omega)$ is obtained by averaging, in an appropriate manner, over-all the j_s distributions for all values of ρ between 0 and ρ_0.[16] That is, the distribution $j_s(\rho, \omega)$ must first be multiplied by a weight factor giving the relative number of collisions having the parameter ρ, and then be integrated from 0 to ρ_0. Thus we shall have

$$J_s(\omega) = c_s \int_0^{\rho_0} \frac{W(\rho)\, d\rho}{[\omega'(\rho) - \omega]^2 + [\sqrt{2}/\tau_{s,0}(\rho)]^2}. \tag{32}$$

To obtain the function $W(\rho)$, let the probability that a perturbing particle has a parameter between ρ and $\rho + d\rho$ be $2\pi\rho d\rho$. Then the probability that the nearest perturbing particle has a parameter between ρ and $\rho + d\rho$ must be $2\pi\rho d\rho$ times the probability that no particle is within the distance ρ, or

$$W(\rho)\, d\rho = K\rho d\rho \times e^{-(4\pi/3)N\rho^3}. \tag{33}$$

N is the number of perturbing particles per cubic centimeter, and the constant K is found from the normalizing condition to be

$$K = \frac{3}{(-\frac{1}{3}, y)!}\left(\frac{4\pi}{3} N\right)^{2/3}, \tag{34}$$

where

$$y = \frac{4\pi}{3} N\rho_0^3 \tag{35}$$

and

$$(-\tfrac{1}{3}, y)! = \int_0^y e^{-t} t^{-1/3} dt = \tfrac{3}{2} y^{2/3}\left(1 - \tfrac{3}{5}y + \tfrac{1}{8}y^2 + \ldots\right). \tag{36}$$[17]

[16] It will be recalled that larger values of ρ were excluded by the Weisskopf condition. Only a slight error is produced in the final contour by neglecting these values in calculating the asymmetric portion of the line, since their only effect occurs in the center of the line, where the collision broadening is the dominant factor in any case (cf. Fig. 3). The normalization of the asymmetric portion will, however, be affected.

[17] See Jahnke and Emde, *Funktionentafeln* (Leipzig and Dover, 1943), p. 22.

In many practical cases, y is a small quantity compared to unity, and the following approximations are sufficient:

$$(-\tfrac{1}{3}, y)\,! \simeq \tfrac{3}{2} y^{2/3}, \tag{37}$$

$$K \simeq \frac{2}{\rho_0^2}. \tag{38}$$

It may be noted that, by defining $W(\rho)$ in this fashion, the quantity

$$i_s(\rho)\, W(\rho)\, d\rho = W(\rho)\, d\rho \int_{-\infty}^{+\infty} j_s(\rho, \omega)\, d\omega = \text{const} \times \rho W(\rho)\, d\rho\,, \tag{39}$$

which represents the total intensity contributed by collisions having the parameter ρ, has been put equal (apart from the normalizing factor) to the statistical probability for ρ, which leads to the Holtsmark formula. Thus the essential difference between the asymmetric distribution obtained here and the Holtsmark distribution is that in the latter the relation between the displacement in the line and the value of ρ is strictly one to one, while in the present case a collision at the distance ρ can produce intensity anywhere in the spectrum. Thus, for example, a negative wing is to be expected for the asymmetric distribution. In the outer portions of the positive wing, however, the half-width of the $j_s(\rho, \omega)$ distributions becomes very small with respect to their displacements $\Delta\omega$, and thus we do approach the one-to-one relation and the Holtsmark distribution.

The integration indicated in equation (32) will be discussed in section 7.

6. *The normalization of* J(ω).—To normalize the final intensity distribution properly, we must add the symmetric and asymmetric distributions and normalize their sum to unity. Thus one condition on the constant factors c_f and c_s (eqs. [21] and [32], respectively) is

$$\int_{-\infty}^{+\infty} (J_f + J_s)\, d\omega = 1\,. \tag{40}$$

Now,

$$I_f = \int_{-\infty}^{+\infty} J_f(\omega)\, d\omega = c_f \bar{\tau}_f \pi\,, \tag{41}$$

and

$$I_s = \int_{-\infty}^{+\infty} J_s(\omega)\, d\omega = c_s \int_0^{\rho_0} \int_{-\infty}^{+\infty} j_s(\rho, \omega)\, W(\rho)\, d\rho\, d\omega = c_s \sqrt{2\pi}\, \bar{\tau}_s\,, \tag{42}$$

where the mean collision time, $\bar{\tau}_s$, is given by

$$\bar{\tau}_s = k_p \frac{1}{\bar{v}} \int_0^{\rho_0} \rho W(\rho)\, d\rho = k_p \frac{\bar{\rho}}{\bar{v}}\,. \tag{43}$$

The quantity $\bar{\rho}$ as defined in this way has the value

$$\bar{\rho} = -\frac{e^{-y} - 1}{(-\tfrac{1}{3}, y)\,!} \left(\frac{4\pi}{3} N\right)^{-1/3} \tag{44}$$

or, for small y,

$$\bar{\rho} \simeq \tfrac{2}{3} \rho_0\,. \tag{45}$$

Thus, in terms of the constants c_f and c_s, equation (40) becomes

$$1 = c_f \bar{\tau}_f \pi + c_s \sqrt{\frac{2}{\pi}}\, \bar{\tau}_s\,. \tag{46}$$

The second condition on c_f and c_s is that

$$\frac{I_s}{I_f}=\frac{\bar{\tau}_s}{\bar{\tau}_f}, \tag{47}$$

whence, combining equations (46) and (47),

$$c_f=\frac{1}{\pi\bar{\tau}} \quad \text{and} \quad c_s=\frac{1}{\sqrt{2\pi}\,\bar{\tau}}. \tag{48}$$

When these values for c_f and c_s are used in equations (21) and (32), the resultant intensity distribution will be normalized to unity.

An important quantity appearing in the above calculation is the ratio $\bar{\tau}_s/\bar{\tau}_f$. By means of this ratio the relative contributions of the collision and asymmetric broadening to the total intensity can be readily calculated. Because the *sum* of the intensity distributions has been normalized to unity, we may just as well consider the ratio $\bar{\tau}_s/\bar{\tau}$, which shows in a simple way how the relative importance of the asymmetric portion of a given line is uniquely determined by the temperature and pressure of the atmosphere, for we have from equations (43) and (22)

$$\frac{\bar{\tau}_s}{\bar{\tau}}=\pi N\bar{v}\rho_0^2 k_p\frac{\bar{\rho}}{\bar{v}}. \tag{49}$$

For small y this reduces simply to

$$\frac{\bar{\tau}_s}{\bar{\tau}}=\frac{2\pi}{3}k_p\frac{NC_p^{3/(p-1)}}{\bar{v}^{3/(p-1)}}; \tag{50}$$

for large y the relation will differ slightly but is still dependent explicitly on N and $\bar{v}$. Thus we have the result (the general nature of which was to be expected) that the relative contribution to the atomic absorption coefficient by the asymmetric broadening is directly proportional to the density of perturbing particles and inversely proportional to the $3/2(p-1)$ power of the temperature.

7. *The calculation of the asymmetric distribution* (32).—The expression for $J_s(\omega)$ becomes, in full,

$$J_s(\omega)=c_sK\int_0^{\rho_0}\frac{\rho\, e^{-(4\pi/3)N\rho^3}d\rho}{(\omega_0+\Delta\omega-\omega)^2+(\sqrt{2}/\tau_{s,0})^2}. \tag{51}$$

In the following, for the sake of generality, we may let

$$\left.\begin{aligned}
&\omega_0-\omega=d, \quad \Delta\omega=-\Delta=\frac{\gamma C}{\rho^p}, \quad \Delta_0=\frac{\gamma|C|}{\rho_0^p} && \text{if } C \text{ is negative;}\\
&\omega-\omega_0=d, \quad \Delta\omega=\Delta=\frac{\gamma C}{\rho^p}, \quad \Delta_0=\frac{\gamma C}{\rho_0^p} && \text{if } C \text{ is positive.}
\end{aligned}\right\} \tag{52}$$

The formal results of the two cases are the same; if C is negative, the asymmetry is to the red; and if C is positive, it is to the violet. Thus,

$$\rho^p=\frac{\gamma C}{\Delta}; \qquad \rho=(\gamma C)^{1/p}\Delta^{-1/p}; \; d\rho=-\frac{1}{p}(\gamma C)^{1/p}\Delta^{-(p+1)/p}d\Delta. \tag{53}$$

Making this change of variable, we find for $\tau_{s,0}$ the value

$$\tau_{s,0} = \frac{2k_p}{\sqrt{\pi}\,\bar{v}} (\gamma C)^{1/p} \Delta^{-1/p}, \tag{54}$$

whence it readily follows that

$$\frac{2}{\tau_{s,0}^2} = \frac{\Delta^{2/p}}{\epsilon^2}, \tag{55}$$

where, by definition,

$$\frac{1}{\epsilon^2} = \frac{\pi \bar{v}^2}{2k_p^2 (\gamma C)^{2/p}}. \tag{56}$$

Upon substituting equations (52), (53), and (55) in equation (51), we obtain, finally,

$$J_s(d) = c_s K \frac{1}{p} (\gamma C)^{2/p} \int_{\Delta_0}^{\infty} \frac{e^{-(4\pi/3)N(\gamma C/\Delta)^{3/p}} d\Delta}{[(d-\Delta)^2 + \Delta^{2/p}/\epsilon^2]\,\Delta^{1+2/p}}. \tag{57}$$

It is useful in the following discussion to measure the displacements d and Δ in units of $1/\epsilon^{p/(p-1)}$, that is, we introduce the dimensionless quantities b and β, where

$$d = \frac{b}{\epsilon^{p/(p-1)}} \quad \text{and} \quad \Delta = \frac{\beta}{\epsilon^{p/(p-1)}}. \tag{58}$$

With these substitutions, equation (57) becomes

$$J_s(b) = c_s K \frac{1}{p} (\gamma C)^{2/p} \epsilon^{(2p+2)/(p-1)} \int_{\mu}^{\infty} \frac{e^{-y(\mu/\beta)^{3/p}} d\beta}{[(b-\beta)^2 + \beta^{2/p}]\,\beta^{1+2/p}}, \tag{59}$$

where we have written

$$\mu_p = \left(\frac{2}{\pi}\right)^{p/(2[p-1])}; \tag{60}$$

and it will be recalled that

$$y = \frac{4\pi}{3} N \rho_0^3. \tag{35}$$

It is immediately apparent from equation (59) that, for all lines having $y << 1$, the dependence of $J_s(b)$ on b is the same, apart from a multiplying factor,

$$A = c_s K \frac{1}{p} (\gamma C)^{2/p} \epsilon^{(2p+2)/(p-1)}. \tag{61}$$

(This remark applies, of course, only to lines having the same value of p.) Moreover, the integral depends on the constant of interaction C_p only through the quantity y in the exponential term, the maximum range of which is only from 1 to e^{-y}. This fact greatly simplifies the calculation of the line forms, as for such cases the integral can be evaluated once and for all for a continuous set of b-values. Accordingly, we can write

$$J_s(b) = A\,\mathfrak{I}_s(b), \tag{62}$$

in which A is a factor depending only on the particular line, and

$$\mathfrak{I}_s(b) = \int_{\mu}^{\infty} \frac{e^{-y(\mu/\beta)^{3/p}} d\beta}{[(b-\beta)^2 + \beta^{2/p}]\,\beta^{1+2/p}} \tag{63}$$

is a function of b which is the same for all lines, provided that their value of y is small. It must be noted, however, that each line has its own scale factor, since the constant C_p occurs in the unit $1/\epsilon^{p/(p-1)}$. Thus in different lines the same value of b will correspond to different values of the distance from the line center, d.

In order to evaluate the integral $\Im_s(b)$, we make, following Burkhardt,[18] the approximation that the function

$$f(b-\beta) = \frac{1}{(b-\beta)^2+\beta^{2/p}} \tag{64}$$

(which is really the dispersion distribution [31]) can be adequately represented beyond $|b-\beta| = \frac{3}{2}\beta^{1/p}$ by the inverse-square function, and between $|b-\beta| = \frac{3}{2}\beta^{1/p}$ and $|b-\beta| = 0$ by the straight line passing through the points $(0, \beta^{-2/p})$ and $(\beta^{1/p}, \beta^{-2/p}/2)$. Thus, we let[19]

$$\left.\begin{aligned} f(b-\beta) &= \frac{1}{(b-\beta)^2} \qquad \text{for} \quad |b-\beta| > \tfrac{3}{2}\beta^{1/p} \\ \text{and} \\ f(b-\beta) &= \frac{1}{\beta^{2/p}} - \frac{1}{2}\frac{1}{\beta^{3/p}}|b-\beta| \qquad \text{for} \quad |b-\beta| \leq \tfrac{3}{2}\beta^{1/p}. \end{aligned}\right\} \tag{65}$$

Accordingly, the integration for $\Im_s(b)$ breaks up into three parts:

$$\Im_s(b) \simeq P+Q+R\,, \tag{66}$$

where

$$P = \int_{\mu}^{\beta_1} \exp\left[-y\left(\frac{\mu}{\beta}\right)^{3/p}\right]\beta^{-(p+2)/p}(b-\beta)^{-2}d\beta\,, \tag{67}$$

$$Q = \int_{\beta_1}^{\beta_2}\left(\frac{1}{\beta^{2/p}} - \frac{1}{2}\frac{1}{\beta^{3/p}}|b-\beta|\right)e^{-y(\mu/\beta)^{3/p}}\beta^{-(p+2)/p}d\beta\,, \tag{68}$$

and

$$R = \int_{\beta_2}^{\infty} \exp\left[-y\left(\frac{\mu}{\beta}\right)^{3/p}\right]\beta^{-(p+2)/p}(b-\beta)^{-2}d\beta\,. \tag{69}$$

The limits of integration β_1 and β_2 vary with the particular value of b; they are the two solutions of the equation

$$b-\beta = \mp\tfrac{3}{2}\beta^{1/p}. \tag{70}$$

Figure 2 shows β plotted as a function of b, for several values of p. When, for any value of p, the curves cross below the lines $\beta = \mu_p$, the value μ is to be used.

When the values of β_1 and β_2 are known, for any particular value of b, they can be used in the expressions for P, Q, and R which are summarized in Table 2. Now the integral Q becomes, after some minor transformations,

$$\left.\begin{aligned} Q = \frac{p}{3}\mu^{-4/p}\left(\frac{1}{y}\right)^{4/3}[(\tfrac{1}{3}, u_1)! - (\tfrac{1}{3}, u_2)!] + \frac{p}{6}\mu^{(p-5)/p}\left(\frac{1}{y}\right)^{(5-p)/3}\left[\left(\frac{2-p}{3}, u_1\right)!\right. \\ \left. + \left(\frac{2-p}{3}, u_2\right)! - 2\left(\frac{2-p}{3}, u_b\right)!\right] - \frac{p}{6}\mu^{-5/p}\left(\frac{1}{y}\right)^{5/3} b[(\tfrac{2}{3}, u_1)! \\ + (\tfrac{2}{3}, u_2)! - 2(\tfrac{2}{3}, u_b)!]\,, \end{aligned}\right\} \tag{71}$$

[18] See, in particular, Fig. 4 of Burkhardt's paper.

[19] An error of 2 per cent in the normalization of the dispersion distribution (64) or (31) is introduced in replacing it by eq. (65).

where

$$u = y\left(\frac{\mu}{\beta}\right)^{3/p}, \tag{72}$$

and

$$\left.\begin{aligned} u_b &= y\left(\frac{\mu}{b}\right)^{3/p} \quad \text{if } b > \mu, \\ u_b &= y \qquad\qquad\quad \text{if } b \le \mu. \end{aligned}\right\} \tag{73}$$

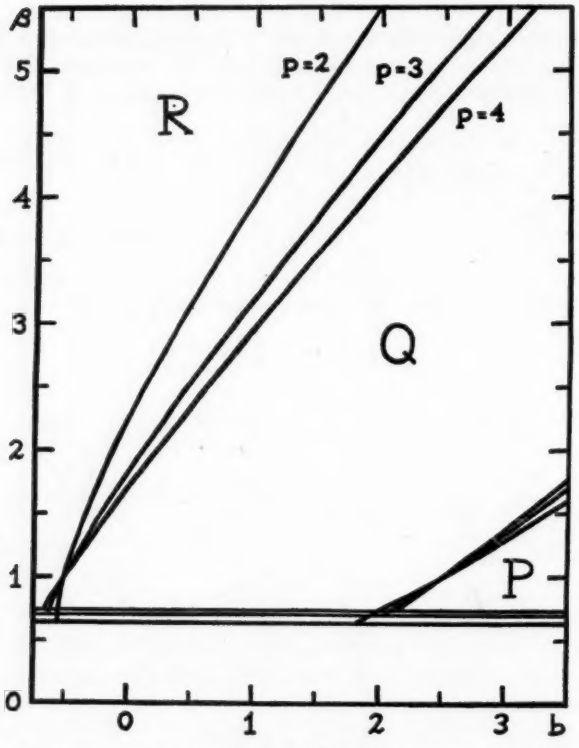

FIG. 2.—The limits of integration β_1 (*lower curves*) and β_2 (*upper curves*) as a function of b. The horizontal lines represent the different values of μ_p, the lower limit of integration. The areas marked P, Q, and R show the regions in which the integrals P, Q, and R (eqs. [67]–[69]) are to be used.

Expressions of the type $(x, u)!$ denote the incomplete gamma function (see n. 17)

$$(x, u)! = \int_0^u e^{-t} t^x dt. \tag{74}$$

Unless p is of the form $2 + 3n$, where n is a positive integer, the incomplete gamma functions occurring in the second term of Q may be expanded in terms of u_1, etc. For most of the practical cases, namely, those in which y and therefore u are very small compared to unity, the first terms in the expansions will suffice, and we obtain, finally,

$$\left.\begin{aligned} Q_{y<<1} = \frac{p}{4}\left[\beta_1^{-4/p} - \beta_2^{-4/p}\right] + \frac{p}{2(5-p)}\left[\beta_1^{-(5-p)/p} + \beta_2^{-(5-p)/p} - 2\left\{\frac{b}{\mu}\right\}^{-(5-p)/p}\right] \\ - \frac{p}{10}\, b\left[\beta_1^{-5/p} + \beta_2^{-5/p} - 2\left\{\frac{b}{\mu}\right\}^{-5/p}\right]. \end{aligned}\right\} \tag{75}$$

Equation (75) is the expression for Q to be used when $p = 2, 3, 4, 6$.

With regard to the integration of P, it is clear from Figure 2 that in this region b is always greater than β. Hence we may make the expansion,

$$(b-\beta)^{-2} = b^{-2}\left(1+2\frac{\beta}{b}+3\frac{\beta^2}{b^2}+4\frac{\beta^3}{b^3}+\dots\right), \tag{76}$$

and use as many terms as prove necessary. With this substitution and the change of variable (72), P becomes

$$\left.\begin{aligned} P=&\frac{p}{3}\,b^{-2}\mu^{-2/p}y^{-2/3}\left[\left(-\tfrac{1}{3},\,y\right)!-\left(-\tfrac{1}{3},\,u_1\right)!\right]\\ &+\frac{2p}{3}\,b^{-3}\mu^{(p-2)/p}\left(\frac{1}{y}\right)^{(2-p)/3}\left[\left(-\frac{p+1}{3},\,y\right)!-\left(-\frac{p+1}{3},\,u_1\right)!\right]+\dots\end{aligned}\right\} \tag{77}$$

If y is small, then for all values of p which are not expressible in the form $p = 3n - 1$, the first two terms of equation (77) become

$$P_{y<<1}=\frac{p}{2}\,b^{-2}\left(\mu^{-2/p}-\beta_1^{-2/p}\right)+\frac{2p}{p-2}\,b^{-3}\left(\beta_1^{(p-2)/p}-\mu^{(p-2)/p}\right)+\dots. \tag{78}$$

The third and higher terms are usually not necessary. For $p = 2$ the second term of equation (78) must be replaced by the expression

$$2d^{-3}\log_e\left(\frac{\beta_1}{\mu}\right). \tag{79}$$

Finally, it should be noted that $P = 0$ if $b < \mu + (3/2)\mu^{1/p}$ (cf. Fig. 2 and eq. [70]).

For the integration of R we note that in the positive line wing and in a small portion of the negative-line wing, β is always greater than $|b|$. For such cases we may write

$$(\beta-b)^{-2}=\beta^{-2}+2b\beta^{-3}+3b^2\beta^{-4}+\dots, \tag{80}$$

and, proceeding exactly as in the case of P, we find that

$$R_{y<<1}=\frac{p}{2p+2}\,\beta_2^{-(2p+2)/p}+\frac{2p}{3p+2}\,b\beta_2^{-(3p+2)/p}+\frac{3p}{4p+2}\,b^2\beta_2^{-(4p+2)/p}+\dots. \tag{81}$$

In the major portion of the negative wing (where R is, incidentally, quite small), R may be conveniently transformed by making the substitution

$$\beta=-b\frac{x}{1-x}. \tag{82}$$

Thus,

$$R=(-b)^{-(2p+2)/p}\int_{\mu/\mu-b}^{1}\exp\left[-y\left(\frac{\mu}{-b}\,\frac{1-x}{x}\right)^{3/p}\right]\left(\frac{1-x}{x}\right)^{1+2/p}dx. \tag{83}$$

This integral may be fairly easily evaluated by graphical means. If $y \ll 1$, the exponential term is very nearly unity, and the value of the integral depends only on the lower limit of integration.

8. *The asymptotic forms for the line wings.*—In the extreme wings of the line (where the asymmetric distribution eventually dominates, except if $p = 2$), the calculation of $J_s(b)$ is simplified and extended by the use of the following asymptotic relations:

Consider equation (62), namely,

$$J_s(b)=A\int_{\mu}^{\infty}\frac{\exp\left[-y\,(\mu/\beta)^{3/p}\right]d\beta}{\left[(b-\beta)^2+\beta^{2/p}\right]\beta^{1+2/p}}. \tag{62}$$

Now, for very large positive values of b, that is, at great distances from the line center, only the regions in which β is comparable in magnitude to b will contribute appreciably to the integral, for the integrand can differ from zero only when $\beta \simeq b$. Further, when β is very large, the exponential term approaches unity. Accordingly, the integral may be replaced by

$$\frac{1}{b^{(p+2)/p}} \int_{-\infty}^{+\infty} \frac{dx}{x^2 + b^{2/p}} = \frac{1}{b^{(p+2)/p}} \times \frac{\pi}{b^{1/p}}; \tag{84}$$

and equation (62) becomes

$$J_s(b) = A \frac{\pi}{b^{(p+3)/p}}. \tag{85}$$

As was anticipated in section 5, this limiting form for J_s in the positive wing is identical in form with that for the usual Holtsmark formula. They both follow the inverse $(p+3)/p$ law; and the difference in the coefficients is due only to the difference in the normalizations—the Holtsmark distribution has itself been normalized to unity, whereas here the total $J(\omega)$ has been so normalized.

It is readily seen from Figure 2 that, in most of the negative-line wing, $J_s(\omega)$ may be represented simply by the function

$$J_s(b) \simeq AR = A \int_{\mu}^{\infty} \frac{\exp\left[-y\,(\mu/\beta)^{3/p}\right] \beta^{-(p+2)/p} d\beta}{(b-\beta)^2}. \tag{86}$$

To discuss equation (86) it is convenient to make the change of variable (72), whence we obtain

$$J_s(b) \simeq A \frac{p}{3} \mu^{-2/p} y^{-2/3} \int_0^v \frac{e^{-u} u^{-1/3} du}{(b-Q)^2}, \tag{87}$$

where

$$Q = \mu \left(\frac{y}{u}\right)^{p/3}. \tag{88}$$

Now, when the magnitude of b is very large, Q may be neglected in comparison with it, except in the region of $u \simeq 0$, which contributes very little to the integral anyhow. Hence we may write

$$J_s(b) \simeq A \frac{p}{3} \mu^{-2/p} y^{-2/3} \frac{1}{b^2} \int_0^v e^{-u} u^{-1/3} du, \tag{89}$$

which becomes, for small values of y,

$$J_s(b) \simeq A \mu^{-2/p} \frac{p}{2} \frac{1}{b^2}. \tag{90}$$

Equations (89) and (90) show that in the negative-line wing the decrease of intensity in the asymmetric distribution follows the inverse-square law exactly as does the symmetric distribution. This is because the negative wing is just a superposition of many dispersion-curves.

Table 2 summarizes the principal results of sections 7 and 8, showing how the curve $\mathfrak{J}_s(b)$ $(y \ll 1)$ is to be constructed for the different values of b. The curve $\mathfrak{J}_s(b)$ for $p = 4$ is shown in Figure 3. In order to find $J_s(d)$ for any specific line, it is only necessary to find b by means of the relation $b = d\epsilon^{p/(p-1)}$, read off the value of $\mathfrak{J}_s(b)$, and multiply by A. This quantity, when added to the quantity $J_f(d) = c_f(d^2 + 1/\bar{\tau}_f^2)^{-1}$, gives the desired value of J for the point d.

TABLE 2

b	$\Im_a = P+Q+R$
$+$ wing.....	$\Im \to \dfrac{\pi}{b^{1+p/3}}$
$b > \mu + \frac{3}{2}\mu^{1/p}$.....	$P = \dfrac{p}{2} b^{-2}[\mu^{-2/p} - \beta_1^{-2/p}] + \dfrac{2p}{p-2} b^{-3}[\beta_1^{1-2/p} - \mu^{1-2/p}] + \ldots.$* $Q = \dfrac{p}{4}[\beta_1^{-4/p} - \beta_2^{-4/p}] + \dfrac{p}{2(5-p)}[\beta_1^{1-5/p} + \beta_2^{1-5/p} - 2b^{1-5/p}] - \dfrac{p}{10} b[\beta_1^{-5/p} + \beta_2^{-5/p} - 2b^{-5/p}]$† $R = \dfrac{p}{2p+2}\beta_2^{-(2+2/p)} + \dfrac{2p}{3p+2} b\beta_2^{-(3+2/p)} + \dfrac{3p}{4p+2} b^2\beta_2^{-(4+2/p)} + \ldots.$
$\mu < b < \mu + \frac{3}{2}\mu^{1/p}$..	$P = 0$ $Q = \dfrac{p}{4}[\mu^{-4/p} - \beta_2^{-4/p}] + \dfrac{p}{2(5-p)}[\mu^{1-5/p} + \beta_2^{1-5/p} - 2b^{1-5/p}] - \dfrac{p}{10} b[\mu^{-5/p} + \beta_2^{-5/p} - 2b^{-5/p}]$† $R = \dfrac{p}{2p+2}\beta_2^{-(2+2/p)} + \dfrac{2p}{3p+2} b\beta_2^{-(3+2/p)} + \dfrac{3p}{4p+2} b^2\beta_2^{-(4+2/p)} + \ldots.$
$-0.5 < b < \mu$.....	$P = 0$ $Q = \dfrac{p}{4}[\mu^{-4/p} - \beta_2^{-4/p}] + \dfrac{p}{2(5-p)}[\beta_2^{1-5/p} - \mu^{1-5/p}] - \dfrac{p}{10} b[\beta_2^{-5/p} - \mu^{-5/p}]$† $R = \dfrac{p}{2p+2}\beta_2^{-(2+2/p)} + \dfrac{2p}{3p+2} b\beta_2^{-(3+2/p)} + \ldots.$
$b < -0.75$.....	$P = 0$ $Q = 0$ $R = (-b)^{-(2+2/p)} \int_{\mu/\mu-b}^{1} \left(\dfrac{1-x}{x}\right)^{1+2/p} dx$
$-$ wing.....	$\Im \to \dfrac{p}{2}\mu^{-2/p}\dfrac{1}{b^2}$

* $p \neq 3n-1$.

† $p \neq 2+3n$.

From a figure such as Figure 3 it is possible to determine the point in the positive line wing at which the "statistical distribution" overtakes the damping distribution, for in the wing we may write $J_f(\omega)$ in the form

$$J_f(d) \simeq \frac{1}{\pi \bar{\tau} d^2}; \tag{91}$$

or, expressing d in units of $1/\epsilon^{p/(p-1)}$, we find, after some minor transformations,

$$J_f(b) \simeq A \frac{p}{\sqrt{2\pi}} \left(\frac{\pi}{2}\right)^{1/(p-1)} \frac{1}{b^2}. \tag{92}$$

Now the curve

$$J_f(b) = \frac{4}{\sqrt{2\pi}} \left(\frac{\pi}{2}\right)^{1/3} \frac{1}{b^2}, \tag{93}$$

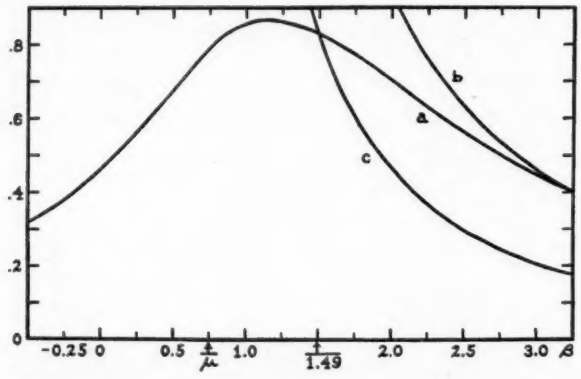

FIG. 3.—*a*, The curve $\mathfrak{I}_s(b)$ for $p = 4$. *b*, The asymptotic curve $\pi/b^{(p+3)/3}$ (eq. [85]), which holds for large values of b. *c*, The wing of the damping distribution (eq. [93]).

representing the wings of the damping curve, is plotted in Figure 3. Thus we find that for $p = 4$ the asymmetric curve overtakes the damping curve at the distance

$$d_g = \frac{1.49}{\epsilon^{4/3}}. \tag{94}$$

9. *Concluding remarks on the application of the Burkhardt theory.*—Before the foregoing procedure can be applied to the calculation of actual lines, there are three factors to be considered. In the first place, it will be recalled that the effect of collisions taking place beyond the Weisskopf radius ρ_0 has been neglected. The net effect of such "weak" collisions is to produce a slight shift of the damping portion of the line.[20] Consistent with the adoption of the Weisskopf radius as the dividing line between "effective" and "weak" collisions, the magnitude of the line shift is given as the average frequency displacement during the "weak" collisions. Thus,

$$\bar{\Delta} = \frac{\int_0^{\Delta_0} \Delta \tau_s(\Delta) W(\Delta)\, d\Delta}{\int_0^{\Delta_0} \tau_s(\Delta) W(\Delta)\, d\Delta}; \qquad \Delta = \gamma \frac{C_p}{\rho^p}; \tag{95}$$

[20] For a detailed discussion of the origin and amount of this shift, see Unsöld, *Vierteljahrschr. d. Deutsch. Astr. Gesellsch.*, **78**, 213, 1943, or Lindholm, *Über die Verbreiterung und Verschiebung von Spektrallinien*. The latter author has made a careful investigation of this problem.

and, upon carrying out the necessary substitutions and integrations, we find, in particular, that, if $p = 4$ and $y \ll 1$,

$$\bar{\Delta}_4 = \frac{1.86}{\bar{\tau}}. \tag{96}$$

While this value of the line shift must undoubtedly be of the right order of magnitude, it is not felt that its exact value should be taken too seriously, because of the rather perfunctory manner in which it has been obtained.

In calculating the present intensity distribution, it has been tacitly assumed that we are dealing with a single collision, that is, that the density is small enough so that it is sufficient to consider the effect of the nearest neighbor. This assumption can be expressed more precisely by the statement that the fundamental distance considered in this problem, namely, the collision radius ρ_0, should be small compared to the mean distance between the radiating atom and the perturbing particles, which we may call r_0. When the density of the perturbing particles is much greater than that of the perturbed atoms, we have, simply,

$$r_0 = 0.554 N^{-1/3}. \tag{97}$$

Thus we may regard the quantity ρ_0/r_0 as a measure of the relative importance of the effect of multiple collisions. It is easily seen from equations (24) and (97) that the dependence of ρ_0/r_0 upon the physical conditions is given by

$$\frac{\rho_0}{r_0} \propto \frac{N^{1/3} C^{1/(p-1)}}{\bar{v}^{1/(p-1)}}. \tag{98}$$

It is interesting to note that ρ_0/r_0 depends upon the pressure and temperature in exactly the same ratio as does $\bar{\tau}_s/\bar{\tau}$ (cf. eq. [50]), except that in the present case the variation is as the cube root and is therefore much slower. As a practical upper limit for the validity of the single-collision approximation we shall adopt the value $\rho_0/r_0 \sim \frac{1}{2}$, which was suggested by Unsöld[5] and does not seem too large, as the effect of multiple collisions must fall off exponentially.

There is one final question to be settled, namely, the method of determining the proper constant of interaction to be used for any given line. The physical problem of calculating this quantity necessarily has a different solution for each value of the orientation of the perturbed atom with respect to the perturber, that is, for all values of the magnetic quantum number m. Therefore, to calculate the amount of broadening of any line, it is necessary to know whether or not these interactions should be averaged and, if so, in what manner. Thus it must be determined whether the broadening collisions take place adiabatically (preserving the relative orientation of atom and perturber) or nonadiabatically. In the former case we should have to calculate the broadened contour for each orientation of atom and perturber and then average over them, whereas in the latter case we should calculate one broadened contour, using the average value of the interactions.

This question was investigated by Lindholm and is discussed at some length by Unsöld. The principal result is that, roughly speaking, collisions which take place within the Weisskopf radius ρ_0 are adiabatic, while the more distant collisions are nonadiabatic, and the different quantum states will tend to be "shuffled" during any collision. Thus in the region of the statistical theory the adiabatic calculation is the correct one, while, in calculating the proper value of ρ_0 to be used in the damping theory, we are considering regions in which the collisions are not strictly adiabatic, and we must therefore use the average value of the C_p's.[21]

[21] These are the results obtained by considering only the upper state of each line, which is mostly responsible for the size of the perturbation. Also, in performing the averages mentioned, the various interaction energies must, of course, be weighted according to their relative probability of occurrence.

These results have the following application to the present problem of calculating the broadening of the helium lines by protons. The interaction energies for various lines have been calculated in an earlier paper[22] and are listed in Table 2 of that paper. Correct to terms in R^{-4} (which is sufficient for the order of distances which will be considered here), they consist of two terms, the R^{-4} term plus a nonhomogeneity term in R^{-3}. Upon taking for any permitted line the properly weighted average of the interactions for use in calculating ρ_0, it is found that the R^{-3} terms drop out, and thus the collision broadening is determined by the R^{-4} law, with an average C_4.

In the region of the statistical theory we should, strictly speaking, calculate line contours for each orientation separately, a procedure in which both the R^{-3} and the R^{-4} terms would have to be used. However, our primary interest in this connection is in distances less than ρ_0, and it may be shown that for each line considered the interaction energy at the distance ρ_0 is due principally to the R^{-4} term. Hence, as a first approximation, the effect of the R^{-3} terms has been neglected in these calculations. A further simplification which has been made is to replace the separate calculations for each orientation by one calculation, using the average of the three-fourths powers of the values of C_4, that is,

$$C_4' = \overline{(C_4^{3/4})}^{4/3}. \tag{99}$$

Such a procedure would be correct for the wing of the line, as it may be seen from equations (85), (61), and (58) that in the wing the dependence of $J_e(d)$ on C_p is proportional to $C^{3/p}$. The use of two different values of C_4 in calculating the different parts of the line contour may, quite correctly, be expected to affect the normalization which was made in section 6. In practice, however, it is found that in all but one case (λ 5876) the difference between the straight average of C_4 and the average calculated by means of equation (99) amounts to less than 1.5 per cent, so that the generalized Burkhardt theory has been used with no change.

III. APPLICATION TO THE HELIUM LINES IN τ SCORPII

10. *Calculation of the stellar-line contours.*—Using the methods of Section II, we have calculated the effect of proton interactions on the broadening of helium lines for the physical conditions existing in the atmosphere of the B0 star, τ Scorpii.[23] The necessary physical data for the calculation of the atomic absorption coefficients (considering only the pressure broadening) are the density of protons, $\log N_P = 14.48$, from which we derive $r_0 = 8.25 \times 10^{-6}$ cm, and the temperature, $T = 28{,}150°$, from which we find $\log \bar{v} = 6.4330$. Knowing these quantities, together with the proper values of the interactions which were discussed in section 9, we are able to calculate the intensity distributions $J(\nu)$.

The calculation of the form of the stellar absorption lines was made by using Unsöld's semiempirical relation

$$\frac{1}{R} = \frac{1}{R_c} + \frac{1}{\kappa_\nu}, \tag{100}$$

in which R_c denotes the observed central "intensity," and κ_ν is the line-absorption coefficient at the frequency ν; thus

$$\kappa_\nu = \frac{2\pi^2 e^2}{m c} N H f J(\nu). \tag{101}$$

[22] Krogdahl, *Ap. J.*, **102**, 64, 1945.

[23] A. Unsöld, *Zs. f. Ap.*, **21**, 22, 1941.

It is well established that, with the possible exception of the very center of the line, this formula gives fairly accurate results over a large range of cases.[24] Further, it was felt that, in view of the present approximations to the calculation of $J(\nu)$, a more rigorous discussion of the manner in which the lines are formed is not justified at this stage. For the same reason the effects of natural line damping and Doppler broadening have been neglected. That the natural damping is very small compared to the collisional damping may be seen from the fifth column of Table 3. The neglect of Doppler effect could be serious only for weak lines.

Line contours have been calculated in this manner for eight of the more interesting helium lines observed in τ Scorpii. Table 3 lists them and contains the necessary observed and derived quantities pertaining to each. It is at once apparent from the table that we are dealing here with much larger collision cross-sections and damping constants than have heretofore been encountered in astrophysical problems. The values of ρ_0, for example, are of the order of a hundred times the first Bohr radius, and the quantities in the fifth column of Table 3 should be compared with $1.24 \times 10^{-22} \nu_0^2$, the half half-width for natural line damping (thus, 5.56×10^7 for λ 4471!).

TABLE 3

λ	Line	$\rho_0 \times 10^6$	$\bar{\tau} \times 10^{11}$	$\frac{1}{\bar{\tau}_f} \times 10^{-10}$	$\bar{\tau}_s \times 10^{12}$	$\frac{\bar{\tau}_s}{\bar{\tau}_f}$	$\frac{\rho_0}{r_0}$	y	Δ(A°)	d_ϱ(A°)	log NH	f	R_c
5876..	2p−3d	0.47	177.	.....	.....	.....	0.06	.....	.....	>8.	14.95	0.553	0.33
4471..	2p−4d	2.92	4.56	2.27	1.55	0.035	.35	0.03	−0.04	0.95	14.95	.129	.48 or .30
4026..	2p−5d	5.40	1.33	9.54	2.86	0.27	.65	.20	− .12	0.42	14.95	.0512	.42
4713..	2p−4s	0.93	45.09	0.22	0.49	0.001	.11	.001	− .005	3.3	14.95	.0052	(.16)
4121..	2p−5s	1.59	15.29	0.66	0.84	0.006	.19	.005	− .011	1.5	14.95	.0001	.26
4921..	2P−4D	3.32	3.53	2.99	1.76	0.053	.40	.05	− .07	1.0	14.42	.118	(.16)
4388..	2P−5D	7.61	0.67	37.2	4.03	1.50	.92	.56	− .28	0.35	14.42	.0416	.26
3965..	2S−4P	2.07	9.04	1.12	1.09	0.012	0.25	0.01	+0.017	1.1	14.06	0.057	(0.24)

It will be seen that for most of the lines the ratio $\bar{\tau}_s/\bar{\tau}_f$ is quite small, meaning that for these lines the collision damping accounts for by far the greater portion of the atomic absorption coefficient. It does not necessarily follow from this, however, that such lines will show no asymmetry in the stellar spectrum, for, no matter how small a part the asymmetric distribution plays, if we consider distances far out in the positive wing, it will eventually overtake the damping curve, in fact, at the distance d_ϱ (eq. [94]). Now it is known from the theory of line formation that beyond a certain stage the addition of more absorbing atoms fills out the wings of an absorption line, so that, no matter how small the ratio $\bar{\tau}_s/\bar{\tau}_f$ might be for a given line, if it were formed by enough absorbing atoms the asymmetry would eventually show up. This is precisely the situation encountered here, as some of the lines are fairly strong. For this reason the quantity d_ϱ, in the eleventh column, gives a better indication than does $\bar{\tau}_s/\bar{\tau}_f$ as to how much asymmetry will be present in a stellar line.

As was anticipated in section 9, the variation of ρ_0/r_0 for these lines is very similar to that of $\bar{\tau}_s/\bar{\tau}_f$. In fact, it appears that, as soon as $\bar{\tau}_s/\bar{\tau}_f$ becomes of the order of 0.1, we are also entering the region where the nearest-neighbor approximation may no longer be strictly correct.

The quantities log NH and R_c, used in computing the stellar lines, are taken from Unsöld's work. The f-values, with the exception of those for λ 4713 and λ 4121 (Hylleraas), are due to Goldberg.

[24] See, e.g., Unsöld, *Physik der Sternatmosphären*.

11. *Description of the individual lines.*—We shall now discuss the general appearance of the stellar lines. Because of the approximations made in regard to both the theory of the pressure broadening and the mechanism of line formation, it is not to be expected that the line contours given here are necessarily final. It seems clear, however, that the general features found by this method must be real.

In the line contours illustrated in Figures 4–8 the shifts $\overline{\Delta}$ have been neglected, as their effect on the equivalent widths (sec. 12) is extremely small. This is justified as long as $\overline{\Delta} \ll d_v$.

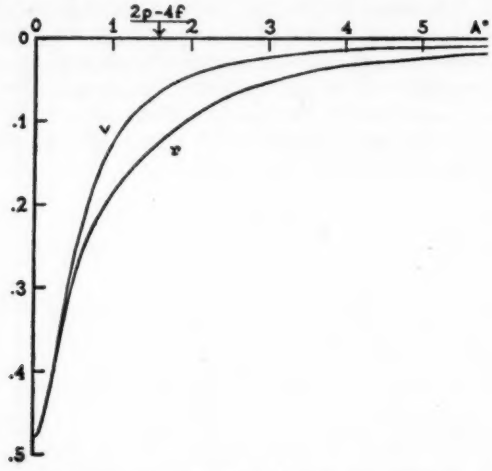

FIG. 4.—λ 4471, with R_c = 48 per cent. The letters r and v denote the red and violet wings, respectively. The arrow indicates the zero-field position of the $2p$–$4f$ line, which lies, of course, to the violet of λ 4471.

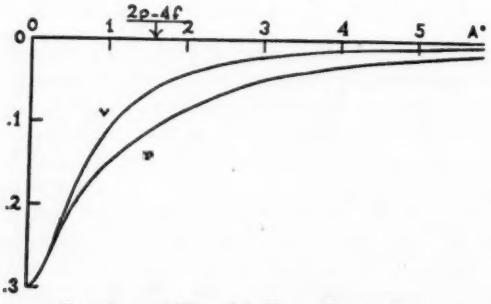

FIG. 5.—λ 4471, with R_c = 30 per cent

λ *4471.*—Unsöld lists two rather different values for the central depth of this line, namely, 48 and 30 per cent. Contours have been calculated for each case and are shown in Figures 4 and 5. For the sake of better comparison, both the red and the violet wings are plotted on the same side of the center. We see that, because of the great strength of the line, it does show asymmetry, despite the fact that $\overline{\tau}_s/\overline{\tau}_f$ is very small.

Perhaps the most interesting feature of the line, however, is the comparative strength and extent of the violet wing, which is due almost entirely to the collisional broadening. Thus, at the zero-field position of the 2p–4f line, which is indicated on the diagrams, the residual intensity in the 2p–4d line amounts to as much as 6 per cent and only drops below 1 per cent at a distance of 4.5 A from the line center. That this result is practically independent of R_c is seen from a comparison of Figures 4 and 5.

λ *4921.*—Because the constants of interaction for this line (2P–4D) are practically the same as for λ 4471, the features of the line are qualitatively the same, except that the whole line is weaker. The residual intensity in the violet wing at the 2P–4F position is 3 per cent, and it drops to 1 per cent at 3.2 A from the center.

λ *4026.*—This is the strongest helium line observed in τ Scorpii; and, while the value of r_0/r_0 is as much as 0.65, it is not felt that this is too much greater than the arbitrarily chosen limit 0.5 but that the present methods may be applied with profit. It is clear, however, that the possible effect of multiple collisions should be considered.

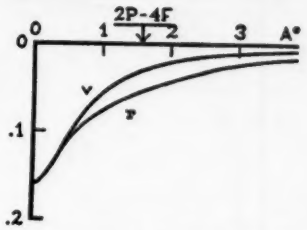

FIG. 6.—λ 4921, R_c = 16 per cent

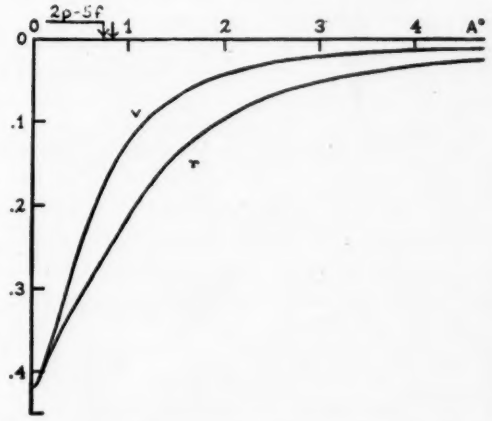

FIG. 7.—λ 4026, R_c = 42 per cent. The unmarked arrow indicates the approximate position of forbidden $2p$–$5g$.

For this line $\bar{\tau}_s/\bar{\tau}_f$ is of an appreciable size, namely, 0.27; and, because the line is also very strong, there are two reasons why its asymmetry is very much more marked than that of, say, λ 4471. The violet wing, which, however, represents the effect of the collisional broadening, has a residual intensity of nearly 18 per cent at the 2p–5f position, about 16 per cent at 2p–5g, and 1 per cent at 5.1 A from the line center, as compared with a central intensity of 42 per cent.

The profile given here is, at best, a first approximation, to the extent that we have assumed that $y = 0.20$ is negligible compared to unity. Also we have neglected $\bar{\Delta}$, which in this case amounts to two-sevenths of d_g.

λ *4388.*—Here, if the present methods were applicable, we should have an example of a line in which the asymmetric curve is dominant, as is indicated by the ratio $\bar{\tau}_s/\bar{\tau}_f$ = 1.50. At the same time, however, the value of ρ_0 is practically the same as that of r_0, which means that the use of the single-collision approximation is almost certainly no longer justifiable.

λ *3965*.—The principal interesting feature of this line is that the asymmetry is to the violet. However, it hardly shows up in the stellar line, as can be seen from the ratio $\bar{\tau}_s/\bar{\tau}_f = 0.012$ and the fact that the line is comparatively weak.

λ *4713*.—This line has an extremely small collision cross-section and degree of asymmetry, as should be expected from the fact that its upper level is a low *s*-level. Its calculated contour for τ Scorpii shows no asymmetry.

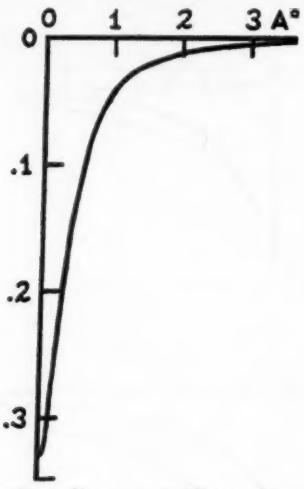

FIG. 8.—λ 5876, $R_c = 33$ per cent. The contour is symmetrical

TABLE 4

λ	Line	Equivalent Width (A) (Calculated)	Equivalent Width (A) (Observed)	R_c	Remarks
5876	2p–3d	0.402	0.562	0.33	
4471	4p–4d	1.175	0.955	.48	
		0.955	0.955	.30	
4026	2p–5d	1.135	1.259	.42	$\rho_0/r_0 = 0.65$
4713	2p–4s	0.035	0.229	(.16)	R_c uncertain
4121	2p–5s	0.008	0.288	.26	Blend; $f = 10^{-4}$
4921	2P–4D	0.484	0.831	(.16)	R_c questionable
4388	2P–5D	(0.690)	0.661	.26	$\rho_0/r_0 = 0.92$
3965	2S–4P	0.091	0.129	(0.24)	Blend; R_c uncertain

λ *4121*.—In this case also, ρ_0 and $\bar{\tau}_s/\bar{\tau}_f$ are quite small, and the resultant contour shows no asymmetry. However, the *f*-value given by Hylleraas seems incredibly small;[25] and, if it should be in error, it is possible that the asymmetry would show up.

λ *5876*.—This line is of especial interest, as it is the only one of the lines considered which is the leading member of a series. Since, for the upper state, we have $n = 3$, the interaction and therefore the collision cross-section and ratio $\bar{\tau}_s/\bar{\tau}_f$ are very small (compared to other lines of the series). As the line is not especially strong in τ Scorpii, it therefore shows no asymmetry. The shift, if any, is to the violet.

[25] Cf. Unsöld's remarks on the subject (*Zs. f. Ap.*, 21, 22, 1941).

12. *The equivalent widths of the lines.*—Perhaps the most significant result of these calculations, however, is that contained in Table 4, of which the third column gives the equivalent widths of the eight lines as determined by planimeter measurement. The two values listed for λ 4471 correspond to the two empirical values for R_c. The width given for λ 4388 is simply an estimate based on the behavior of the wings of the line and should not be taken seriously.

The fourth column contains the observed equivalent widths adopted by Unsöld from several sets of measurements. A comparison of the two columns leaves little doubt that for most of the lines the agreement is good. (To be sure, the values for λ 4713 and λ 4121 are too low—but, as has been mentioned before, the *f*-value for the latter may be questionable.) Further, the agreement between calculated and observed intensity holds over a considerable range of line strengths (at least a factor of 10), and for several distinct types of line series. Now the significance of these results for the theory of line broadening by direct proton interactions lies in the fact that they are consistent with the observed physical parameters of the atmosphere. In other words, they suggest that the direct interactions may be entirely capable of accounting for the observed strengths of the helium lines, at the temperature and electron density to be expected from other considerations (such as the number of observable *H* lives, Stark effect of same, etc.).

To summarize the conclusions of sections 10–12, a preliminary investigation of the effect of direct proton interactions on the broadening of the helium lines in τ Scorpii leads to two results. The first is that the physical conditions in the atmosphere are such that, for most lines, collisional damping of a modified Lorentz-Weisskopf type is primarily responsible for the broadening. Secondly, it is found that broadening of this type can furnish a satisfactory explanation of the equivalent widths of the lines, no qualifying assumptions being necessary. Thus the answer to the problem proposed in the introductory section is that a consideration of the effect of direct interactions on line broadening shows it to be a most fruitful method of attack, which should be discussed, if possible, by more refined methods.

I wish to express my sincere thanks to Dr. S. Chandrasekhar for reading the manuscript and for the numerous invaluable discussions of many aspects of the problem. The present work was started at the Yerkes observatory and completed at Evanston, Illinois.

NOTES

AW PEGASI

INTRODUCTION

The light-variability of the eclipsing binary, AW Pegasi, was discovered in 1930 by Plaut. Since that time, several light-curves and photometric elements[1] have been published, but little has been done until recently on the spectroscopic characteristics of the star, beyond a preliminary classification of the spectral type of the components. About a year ago Otto Struve[2] published an analysis of spectroscopic observations which shows very clearly that this is not an ordinary binary but an additional member of that ever increasing group of objects which are unusual from the astrophysical point of view.

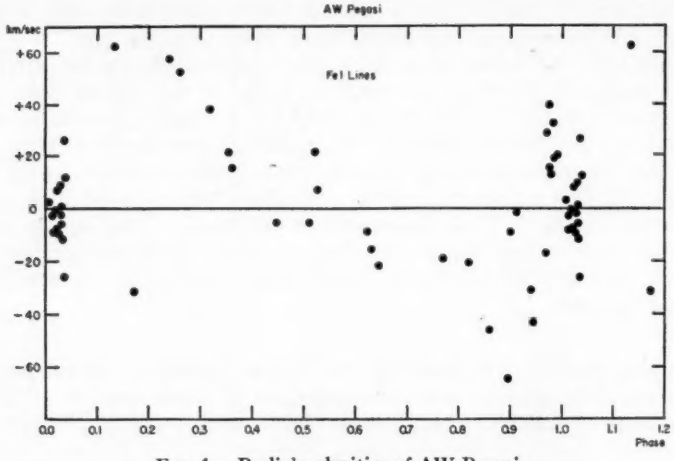

FIG. 1.—Radial velocities of AW Pegasi

Because of the complications of the spectrum, it seemed well to publish observations of the same object which were made at the Lick Observatory several years ago. These confirm very well the results reached by Struve and perhaps add a bit to his conclusions.

OBSERVATIONAL MATERIAL

The observations were made at the Lick Observatory during the years 1940 and 1941. Most of the plates were taken with a two-prism, 6-inch camera attached to the 36-inch refractor. In the neighborhood of principal eclipse a three-prism, 6-inch camera was used. These gave a dispersion of 75 A/mm and 54 A/mm, respectively, in the region of the $H\gamma$ line. The exposures range from 25 minutes for observations made outside of eclipse with the lower dispersion to 60 minutes for observations made at minimum light with the three-prism camera. Fifty-eight plates were secured, fifty-three of which were measured.

Data for the individual plates and the radial velocities for the various lines are given in Table 1. Phases were computed from the elements of Rügemer:[1]

$$\text{Principal minimum} = \text{JD}2426543.480 + 10.62228\,E\,.$$

[1] Rügemer, *Beob. Zirk.*, **14**, 74, 1932.

[2] *Ap. J.*, **102**, 120, 1945.

TABLE 1

RADIAL VELOCITIES OF AW PEGASI IN KM/SEC

Plate	Date	Phase in Period	No. of Prisms	Ca II	Fe I	Sr II	H	Fe II	Ca I
27183P....	1940 Aug. 15	0.007	3	.....	+ 3.4	+ 9.9	−13.3	.....	− 11.2
27669M...	1941 Oct. 14	.013	3	.....	− 2.3	−19.9	−22.4	− 1.4	0.0
27184Q....	1940 Aug. 15	.015	3	.....	− 8.3	.....	− 2.5	.....	− 12.0
27670N...	1941 Oct. 14	.017	3	.....	0.0	− 4.1	− 8.2	−15.5	− 12.0
27671T....	1941 Oct. 14	.020	3	.....	− 7.4	−10.6	−14.0	.....	+ 20.4
27185R...	1940 Aug. 15	.023	3	.....	+ 7.9	.....	−12.8	.....	− 26.2
27672W...	1941 Oct. 14	.024	3	− 7.8	− 9.5	−17.1	− 8.3	− 9.7	+ 10.5
27673M...	1941 Oct. 14	.027	3	.....	− 1.9	.....	−17.1	−28.6	− 30.0
27674N...	1941 Oct. 14	.028	3	.....	+ 9.2	.....	−20.5	−35.0	− 4.1
27186V....	1940 Aug. 15	.030	2	+ 4.3	+ 1.1	+46.9	−16.1	+20.6	− 25.6
27675Q...	1941 Oct. 14	.030	3	.....	− 5.8	−46.1	−31.8	−34.9	− 30.2
27676M...	1941 Oct. 14	.033	3	.....	−11.5	.....	−53.6	−57.8	+ 15.3
27602M...	1941 Sept. 23	.034	2	.....	+26.7	.....	−42.0	.....	.....
27132M...	1940 July 25	.035	2	−33.7	−26.0	.....	−11.0	− 7.6	− 29.5
27603N...	1941 Sept. 23	.036	2	.....	+12.4	+23.3	−31.2	.....	.....
27137Q...	1940 July 26	.133	2	.....	+62.0	+ 2.2	−10.0	.....	.....
27650M...	1941 Oct. 6	.171	2	.....	.....	.....	−22.2	+13.4	.....
27651N...	1941 Oct. 6	.173	2	.....	−30.9	.....	−30.3	+64.1	+ 39.3
27138M...	1940 July 27	.237	2	.....	+57.4	.....	+ 5.6	.....	.....
27175T...	1940 Aug. 7	.260	2	.....	+52.1	.....	+ 9.7	.....	.....
27142Q...	1940 July 28	.317	2	.....	+37.4	.....	−37.1	.....	.....
27178W...	1940 Aug. 8	.354	2	.....	+21.3	+11.5	−22.7	−15.1	− 7.8
27656M...	1941 Oct. 8	.359	2	.....	+15.5	.....	−25.5	−39.2	.....
27657N...	1941 Oct. 8	.360	2	.....	.....	.....	−12.4	−18.4	+ 21.6
27233P....	1940 Oct. 22	.441	2	.....	.....	.....	+13.3	−14.5	+ 27.0
27234Q...	1940 Oct. 22	.446	2	.....	− 5.3	.....	− 0.7	+17.6	.....
27153Q...	1940 July 30	.510	2	.....	− 5.2	.....	−13.6	+14.9	− 43.5
27696Q...	1941 Oct. 30	.520	2	.....	+21.3	.....	− 3.5	.....	.....
27697T...	1941 Oct. 31	.524	2	.....	+ 6.9	.....	+31.0	−43.0	.....
27566S....	1941 Sept. 8	.624	2	.....	− 8.8	−31.6	−53.6	−32.4	.....
27567T...	1941 Sept. 8	.631	2	.....	−15.8	− 3.2	−20.3	.....	− 13.0
27180N...	1940 Aug. 11	.646	2	−10.7	−21.6	.....	− 7.4	+ 4.1	− 38.5
27181M...	1940 Aug. 12	.726	2	.....	.....	−41.4	−16.3	−13.0	−133.7
27126Q...	1940 July 22	.760	3	.....	.....	.....	−14.4	.....	.....
27192R...	1940 Aug. 23	.765	2	.....	.....	.....	−39.3	+52.4	−113.8
27193S....	1940 Aug. 23	.770	2	.....	−18.9	.....	−20.8	+10.8	.....
27182T...	1940 Aug. 13	.820	2	.....	−20.7	+20.2	−69.5	+46.1	.....
27194N...	1940 Aug. 24	.861	2	− 2.8	−45.8	.....	−41.5	− 7.8	.....
27160M...	1940 Aug. 3	.896	2	.....	−64.3	.....	−31.8	−28.3	−111.2
27161N...	1940 Aug. 3	.900	2	.....	− 8.9	.....	−63.8	−30.7	− 91.7
27580O...	1941 Sept. 11	.910	2	+ 8.5	− 1.6	.....	−25.9	−93.6	.....
27581P....	1941 Sept. 11	.910	2	+37.0	.....	−40.8	−15.3	+25.9	− 41.0
27129S....	1940 July 24	.940	2	−27.9	−30.9	.....	−22.0	−11.8	− 73.3
27195W...	1941 Aug. 25	.946	2	+11.8	−42.4	.....	−29.6	−51.3	− 24.1
27162P....	1940 Aug. 4	.970	2	.....	−16.6	.....	−45.0	−34.4	.....
27642N...	1941 Oct. 3	.972	3	.....	+28.4	.....	+ 8.4	+ 4.0	+ 15.4
27643T...	1941 Oct. 3	.975	3	.....	+39.2	.....	+15.8	+20.3	+ 5.6
27163Q...	1940 Aug. 4	.975	3	.....	.....	.....	− 7.4	−15.0	.....
27644M...	1941 Oct. 3	.976	3	+ 7.8	+15.6	+ 3.9	+ 7.4	+39.9	+ 10.4
27164R...	1940 Aug. 4	.981	3	.....	+12.7	.....	− 9.2	+17.2	+ 10.8
27645N...	1941 Oct. 3	.982	3	+19.2	+32.5	+23.0	+10.7	+46.2	+ 34.5
27165S....	1940 Sept. 4	.985	3	.....	+19.6	−10.3	−20.3	−36.0	.....
27166T...	1940 Aug. 4	0.990	3	.....	+20.2	− 4.1	−15.0	+18.2	+ 13.7

DISCUSSION

The two components are classified as belonging to spectral types A2 and F0. The F0 star is in front at principal eclipse, and spectroscopically it is as bright as the A2 star, although photometrically there is a drop of 1.26 mag.[1] at principal eclipse. The lines corresponding to low-excitation energies belong chiefly to the F0 star.

In general, the velocity-curves agree very closely with those found by Struve.[2] The curve derived from the *Fe* I lines has a definite maximum at 0.25 *P*, a minimum at 0.75 *P*, and a range of about 100 km/sec. The other curves are much less pronounced. All the low-excitation lines show a distortion in the velocity-curve at principal eclipse which extends from about 0.97 *P* through central eclipse to 0.04 *P* (see Fig. 1 for *Fe* I lines). This includes not only totality, which lasts, according to Dugan,[3] about 10 hours, but also the partial phase. Before totality the curve is distorted by excessive velocity of recession and after totality by excessive velocity of approach. If the eclipse is at all total, as is claimed by the photometric observers, the light from the A2 star will be completely blotted out. The displacement of the lines might then be produced by the light of the A2 star shining through the atmosphere of the F0 star, in other words, by the ζ Aurigae effect.

An interesting feature of the system of AW Pegasi, as contrasted with that of ζ Aurigae, would be the fact that, while in the latter the early-type star can be treated as a point source, this is certainly not the case in AW Pegasi. The duration of the observed anomaly would be due not so much to the great extent of the atmosphere of the F0 star as to the duration of the passage of the fairly large A2 star beyond the reversing layer of the F0 star. It is not necessary to endow the F0 star with an atmosphere of exceptional extent, such as is normally observed only in the case of supergiants; probably an ordinary giant reversing layer would be sufficient.

This is presented only as a possible interpretation of this phenomenon. It may be that further observations of this or other stars of the same general type will disclose other facts, which may indicate a different explanation.

I wish to express my sincerest appreciation to the following persons for making possible this investigation: to Drs. W. H. Wright and J. H. Moore, who kindly granted me use of the facilities of the Lick Observatory; to Dr. Neubauer and the late Dr. Wyse for their help in planning and executing the observing program; and to Dr. Struve for advice in the interpretation of the results.

LOIS T. SLOCUM

WILSON COLLEGE
September 1946

ERRATUM

On page 263, Volume **104**, for "P Leonis Minoris" read "T Leonis Minoris."

[3] *Contr. Princeton U. Obs.*, No. 15, 1934.